

Université de Lille

Ecole Doctorale Biologie Santé

Thèse de DOCTORAT

En vue de l'obtention du grade de Docteur en Science de l'Université de Lille

Présentée par

Khalil Mallah

**In Depth Systemic Biology Analysis of Central Nervous
System Injuries**

Soutenue à Lille le 13 Décembre 2018

Devant le jury composé de :

Rapporteur	Pr Lut Arckens	KU Leuven
Rapporteur	Pr Christophe Hirtz	Université de Montpellier
Examineur	Pr Bernard Sablonniere	Université de Lille
Examineur	Pr Philippe Marin	Université de Montpellier
Examineur	Ass. Pr Firas Kobeissy	American University of Beirut
Examineur	Pr Michel Salzet	Université de Lille
Directrice de Thèse	Pr Isabelle Fournier	Université de Lille
Co-directeur	Pr Kazem Zibara	Université Libanaise

*“Impossible is just a big word thrown around
by small men who find it easier to live in
the world they’ve been given than
to explore the power they have to change it.
Impossible is not a fact. It’s an opinion.
Impossible is not a declaration. It’s a dare.
Impossible is potential. Impossible is temporary.
Impossible is nothing.”*

- Muhammad Ali

Acknowledgment

I would like to express my gratitude to everyone who contributed to my work:

Prof. Isabelle Fournier (my thesis director) for her continuous guidance, keenness, motivation, and support during my studies. I have gained a lot of knowledge from her expertise, especially in the mass spectrometry and proteomics branches of my project. Also, I would like to express my appreciation for Prof. Michel Salzet (Director of PRISM laboratory) for welcoming me into the lab and always carrying out discussions when I faced a dead-end in some parts of the project. Your ideas and coordination paved the path that I used during my studies in your lab. You both were always a source of inspiration to me in these few years that I spent in your lab. I am truly honored to have started my research career under the mentoring of two pioneer scientists in the MS and proteomics domain, who have dedicated their entire lives to Science.

Prof. Kazem Zibara (my thesis co-director) for the continuous support and discussions during my studies. You were of major assistance for me starting my PhD, and for this I am thankful to you. To Dr. Firas Kobeissy, who introduced me to the field of brain injury, and welcomed me in his lab. I have gained a lot from your expertise in systems biology and neuroproteomics, and for that I am grateful to you. Dr. Nabil El-Zein for always giving me the best advice, when I was truly in need of it.

My thesis reporters, Prof. Lut Arckens, and Prof. Christophe Hirtz for kindly accepting to evaluate my work. My thesis examiners, Prof. Bernard Sablonniere and Prof. Philippe Marin, for accepting to judge my work.

To Dr. Jusal Quanico, who was directly implicated in my project, and worked side-by-side to reach the goals we set out. For training me and introducing me to all the MS techniques used in the lab. To the endless help and follow-through on all the ideas we always came up with. It was a privilege to work with you.

Dr. Julien Franck and Dr. Maxence Wisztorski for all the assistance you provided me with during my studies and all the light-hearted moments and conversations we had. Also, Dr. Stephanie Devaux for guiding me through the first few months of my studies and showing me the commonly used techniques in the lab, and Dr. Marie Duhamel for always being there when I needed advice.

Friends and colleagues at PRISM laboratory: Tanina, Antonella, Tristan, Quentin, Phillippe, Adriana, Zahra, Melanie, Lauranne, Flore, and Tony, for all the joyful moments we had.

To the personnel in PRISM lab who helped in instrumentation and conducting my experiments: Soulaïmane, Jean-Pascal, and Annie. Thank you for your contribution.

My colleagues who were previously at the American University of Beirut, Naify and Sara, for all the help in the in-vivo part and all the cheerful moments we had together.

My friends in Lille, especially Sami, I couldn't have passed the time here during my thesis without your presence and advice. Thank you for always being there when needed.

ASOS association for providing me with the funding.

Finally, my family, mom and dad, for the unlimited support and encouragement you have always provided me with. I couldn't have accomplished any of this without you. Thank you from the bottom of my heart. My sisters (Zahraa, Fatima, Batoul), Hassan and Aya, I love you to the moon and back.

Summary

In the context of studying biological alterations occurring post impact to the central nervous system (CNS), my thesis was focused on studying the proteomic and lipid changes occurring post injury to the brain and spinal cord. A fundamental spatio-temporal study was conducted on an open-head rat TBI model to identify potential injury-specific markers. Using MALDI MSI, we performed 3D reconstruction of the injured brain at 3 days after injury and depicted lesion-specific m/z lipid molecules. After, MALDI MSI was applied on the acute/sub-acute time frame post impact: 1 day, 3 days, 7 days, and 10 days. In parallel, a microproteomic analysis was carried out on tissue segments directly consecutive to the imaged ones in an approach to correlate both lipid and protein changes. Our results yielded the identification of a family of lipids, acylcarnitines, which are expressed within the injured cortex with maximum intensity 3 days post impact. These lipid molecules also were found to be expressed in the Substantia nigra and microproteomics data showed an upregulation in expression of Parkinson's related proteins. Taken altogether, our results depict a role of link between mild-TBI and Parkinson's disease as early as 3 days post impact, with a possible role of acylcarnitine.

Key words: Mass spectrometry, MALDI-MSI, microproteomics, Traumatic Brain Injury, Spinal Cord Injury, Parkinson's disease, acylcarnitine, 3-dimensional.

Résumé

Dans un contexte d'étude des altérations biologiques survenant après un impact au niveau du système nerveux central (SNC), ma thèse porte sur l'étude des modifications protéomiques et lipidiques survenant après lésion. Une étude spatio-temporelle a été menée sur un modèle de traumatisme crânien moyen de rat afin d'identifier des marqueurs spécifiques suite à la lésion. En utilisant la technique d'imagerie MALDI nous avons effectué une reconstruction 3D du cerveau lésé 3 jours post-lésion et avons identifié les molécules lipidiques spécifiques de la lésion. Une étude spatio-temporelle a ensuite été réalisée 1, 3, 7 et 10 jours suivie d'une analyse microprotéomique à partir de coupes de tissus ayant pour but de corréler les modifications lipidiques et protéiques. Nos résultats ont permis d'identifier une famille de lipides, les acylcarnitines, exprimant dans le cortex lésé avec une intensité maximale à 3 jours post-lésion. Les données de protéomiques ont montré une régulation positive de l'expression des protéines liées à la maladie de Parkinson. Dans l'ensemble, nos résultats décrivent un lien entre le traumatisme crânien et la maladie de Parkinson dès 3 jours après impact, avec un rôle possible de les acylcarnitines.

Mots clés : spectrométrie de masse, MALDI-MSI, microprotéomique, lésion cérébrale traumatique, lésion de la moelle épinière, Parkinson's disease, acylcarnitine, 3-dimensional.

Table of Contents

Acknowledgment	3
Summary	5
Résumé	6
Publications.....	9
List of Figures:	12
List of Tables:	14
List of Abbreviations	15
Introduction	17
Bibliography	20
Central nervous system anatomy	20
Severity and Classification	25
Types of Injury.....	27
Animal Models of Injury.....	29
TBI injury models:	29
SCI injury models:.....	31
Cells of the Central Nervous System.....	33
Nerve cells (neurons)	33
Microglia:	35
Astrocytes	37
Oligodendrocytes.....	38
Pathophysiology of CNS injury	39
DAMPs:.....	40
Neutrophils:	42
Infiltrating (macrophages) and resident (microglia) myeloid cells	42
Astrocytes:	43
T-Cells/Adaptive immunity:	44
Mass Spectrometry Imaging	45
Secondary ion mass spectrometry (SIMS) imaging.....	47
Desorption electron spray ionization (DESI) imaging	48
Matrix-assisted laser desorption ionization (MALDI) imaging.....	49

Proteomics	53
Laser Capture Microdissection (LCM)	56
Parafilm Assisted Microdissection (PAM):	57
Liquid Microjunction Extraction (LMJ):	58
Hypothesis:	60
Objectives:	60
Chapter 1: 3D high-spectral resolution MALDI MSI applied to Traumatic Brain Injury	62
Introduction	62
Article 1: Lipid Changes Associated with Traumatic Brain Injury Revealed by 3D MALDI-MSI	63
Conclusion – Chapter 1	86
Chapter 2: Spatially and Temporally Resolved Omics Approach applied to Traumatic Brain Injury	87
Introduction	87
Article 2: Systemic Biology Study of Mild-TBI Unveils the Role of Long Chain Acylcarnitines	89
Conclusion – Chapter 2	143
Chapter 3: Proteomic Analysis of RhoA Inhibitor Effect on Rat Model of SCI.	147
Introduction	147
Article 3: RhoA inhibitor treatment at acute phase of spinal cord injury may induce neurite outgrowth and synaptogenesis	149
Conclusion – Chapter 3	172
Discussion.....	174
References	178
ANNEX	191

Publications

Accepted Publications

- **Mallah K**, Quanico J, Trede D, Kobeissy F, Zibara K, Salzet M, Fournier I. **Lipid Changes Associated with Traumatic Brain Injury Revealed by 3D MALDI-MSI**. Analytical Chemistry. 2018 Aug 2. DOI: 10.1021/acs.analchem.8b02682.
- Zibara K, Zeidan A, **Mallah K**, Kassem N, Awwad A, Mazurier F, Badran B, El-Zein N. **Signaling pathways activated by PACAP in MCF-7 breast cancer cells**. Cellular Signalling. 2018 Jun 20;50:37-47. DOI: 10.1016/j.cellsig.2018.06.009.
- Devaux S•, Cizkova D•, **Mallah K•**, Karnoub M, Laouby Z, Kobeissy F, Blasko J, Nataf S, Pays L, Mériaux C, Fournier I, Salzet M. **RhoA inhibitor treatment at acute phase of spinal cord injury may induce neurite outgrowth and synaptogenesis**. Molecular and Cellular Proteomics. (• = co-first author/equal contribution) 2017 Aug; 16(8):1394-1415 DOI: 10.1074/mcp.M116.064881.
- Abou-Abbass H, Bahmad H, Abou-El-Hassan H, Zhu R, Zhou S, Dong X, Hamade E, **Mallah K**, Zebian A, Ramadan N, Mondello S, Fares J, Comair Y, Atweh S, Darwish H, Zibara K, Mechref Y, Kobeissy F. **Deciphering glycomics and neuroproteomic alterations in experimental traumatic brain injury: Comparative analysis of aspirin and clopidogrel treatment**. Electrophoresis. 2016 Jun; 37(11):1562-76. DOI: 10.1002/elps.201500583.

Proceedings

- **Mallah K**, Quanico J, Raffo-Romero A, Aboulouard S, Kobeissy F, Zibara K, Salzet M, Fournier I. **Systemic Biology Study of Mild-TBI Unveils the Role of Long Chain Acylcarnitines**. (submitted)
- Murgoci AN, **Mallah K**, Aboulouard S, Lefebvre C, Kobeissy F, Fournier I, Cizek M, Ciskova D, Salzet M. **The origin of microglia determines the content of exosomes and biological function**. (in revision)

Oral Presentations

- **Mallah K**, Quanico J, Kobeissy F, Zibara K, Salzet M, Fournier I. **Temporally- & Spatially-Resolved Microproteomics & MSI Analysis for Traumatic Brain Injury**

Biomarker Identification. Plenary talk (30 min) at European Biotechnology Congress, Athens-Greece, 26-28 April 2018.

- **Mallah K, Quanico J, Kobeissy F, Zibara K, Salzet M, Fournier I. Can 3D MALDI-MS Imaging be the Missing Piece for Understanding the Traumatic Brain Injury Puzzle?** XXIIIème Rencontres et Ecole de Printemps de la SFSM, Saint-Martin-de-Londres, Montpellier-France, 26-30 March 2018.
- **Mallah K, Quanico J, Kobeissy F, Zibara K, Salzet M, Fournier I. New Insight to Traumatic Brain Injury: Temporally- & Spatially-Resolved Microproteomics and Lipid MALDI MS Imaging Analysis. Elevator Pitch Prize (3rd place).** 19th Euron PhD Student Meeting, Kerkrade-Netherlands, 25-26 October 2017.
- **Mallah K, Quanico J, Kobeissy F, Zibara K, Salzet M, Fournier I. Temporally & Spatially-Resolved Microproteomics Analysis for Traumatic Brain Injury Biomarkers Identification.** Club Jeunes de la Société Française d'Electrophorèse et d'Analyse Protéomique, Montpellier-France, 5-7 April 2017.
- **Mallah K, Quanico J, Kobeissy F, Zibara K, Salzet M, Fournier I. Temporally- & Spatially-Resolved Microproteomics & MSI Analysis for Traumatic Brain Injury Biomarker Identification.** Rencontres du Club Jeune de la SFSM, Trelon-France, 20-24 March 2017.

Poster Presentations

- **Mallah K, Quanico J, Kobeissy F, Zibara K, Salzet M, Fournier I. New Insight to Traumatic Brain Injury: Temporally- & Spatially-Resolved Microproteomics and Lipid MALDI MS Imaging Analysis.** 19th Euron PhD Student Meeting, Kerkrade-Netherlands, 25-26 October 2017.
- **Mallah K, Quanico J, Kobeissy F, Zibara K, Salzet M, Fournier I. Temporally- & Spatially-Resolved Microproteomics & MSI Analysis for Traumatic Brain Injury Biomarker Identification.** SMMAP conference 2017, Disneyland, Paris-France 2-5 October 2017.
- **Mallah K, Quanico J, Kobeissy F, Zibara K, Salzet M, Fournier I. Utilizing Lipid MALDI MSI and Microproteomic Profiling for Traumatic Brain Injury Biomarker Identification.** OurCon V – Mass Spectrometry Imaging Conference- Doorn-Netherlands, 25-28 September 2017.

- **Mallah K**, Quanico J, Kobeissy F, Zibara K, Salzet M, Fournier I. **Temporally- & Spatially-Resolved Microproteomics & MSI Analysis for Traumatic Brain Injury Biomarker Identification**. 16th Human Proteome Organization World Congress, Dublin-Ireland, 17-21 September 2017.
- **Mallah K**, Quanico J, Kobeissy F, Zibara K, Salzet M, Fournier I. **Temporally- & Spatially-Resolved Microproteomics & MSI Analysis for Traumatic Brain Injury Biomarker Identification**. Journe Andre Verbret 2017. Lille1 University, Lille-France, 14 September 2017.
- **Mallah K**, Devaux S, Cizkova D, Mansy D, Blasko J, Kobeissy F, Nataf S, Pays L, Fournier I, Salzet M. **RhoA inhibitor treatment of spinal cord injury: A temporal therapeutic recommendation and deep inside mechanism understanding**. 18th EURON RESEARCH and STUDENT DAYS, Universite de Lille, Lille-France. October 13-14, 2016.
- **Mallah K**, Abou-Abbass H, Bahmad H, Abou-El-Hassan H, Zhu R, Zhou S, Dong X, Hamade E, Zebian A, Ramadan N, Mondello S, Fares J, Comair Y, Atweh S, Darwish H, Zibara K, Mechref Y, Kobeissy F. **Deciphering glycomics and neuroproteomic alterations in experimental traumatic brain injury: Comparative analysis of aspirin and clopidogrel treatment**. Sixth Annual AUB Biomedical Research Day, Beirut-Lebanon. February 27, 2016.

List of Figures:

Figure 1: Anatomy of the human brain.	21
Figure 2: A drawing of blood capillary with BBB components.	23
Figure 3: Anatomy of the human spinal cord showing the 31 complete spinal segments..	24
Figure 4: Drawing representation of both open head injury and closed head injury in TBI.	28
Figure 5: Representative scheme of complete and incomplete spinal cord injury along with the different paraplegia and tetraplegia/quadruplegia cases in both types of injury.	29
Figure 6: Different animal injury models used in brain injury including FPI, CCI, and Blast injury	31
Figure 7: A) Photograph of the injury tool used in clip compression. B) Drawing of the mechanical procedure of calibrated forceps injury model. C) Photograph of the balloon compression device showing the balloon tip along with the tubing and syringe used for inflation of the balloon with saline solution.	32
Figure 8: Structure of a neuron along with close-up representation of a synapse.	34
Figure 9: Representative drawing of neuron and its interaction with glial cells of the CNS.	35
Figure 10: Activation states of Microglia in the Brain.	36
Figure 11: Micrograph of a protoplasmic astrocyte (green) enwrapping the cell body of a neuron (red).	37
Figure 12: Kinetics and order of involvement of molecular and cellular immune cells to CNS injury in time order.	40
Figure 13: Mechanism of inflammasome activation through NLRP3.	41
Figure 14: Neuroprotective modes of action of T-cell in CNS injury	45
Figure 15: Ion images at m/z 6765 of serial sectioned mouse brain (cerebellum region) acquired at different spatial resolutions (200, 100, 50, and 25 μm) using MALDI MSI.	47
Figure 16: Different ionization methods used in MSI, mainly MALDI-MS, SIMS, and DESI-MS. ..	48
Figure 17: Schematic representation of DESI experimental setup	49
Figure 18: MALDI-MSI workflow	50
Figure 19: A) Average spectrum of acquired ion image on rat cerebellum. B) MALDI TOF ion image of rat cerebellum showing m/z 788 (green) and m/z 820 (red). The matrix was deposited using sublimation and spatial resolution was at 30 μm.	53
Figure 20: Proteomic approaches most commonly used: bottom-up and top-down.	55
Figure 21: Principle of Laser capture microdissection	57
Figure 22: A) Schematic drawing of PAM approach to manually dissect region of interest. B) Optical image of a rat brain where several regions of interest were extracted. C) Atlas figure of rat brain along with the theoretical position of extracted region of interest.	58
Figure 23: Workflow of LMJ	59
Figure 24: 3D Model representation of interaction between human galectin 3 and acylcarnitine (octanoylcarnitine) obtained by surface docking analysis	144
Figure 25: Docking generate by ClusPro 2.0 HmGB1-Synuclein_ITasser corresponding to α synuclein (blue) and HMGB1 (Red).	145
Figure 26: Heat Map based on LFQ value of detected proteins within the cortex ipsilateral by comparing time point (2 and 7 days) and number of hits (1 and 3 hits) with a control sham at 2 days	146

Figure 27: Immunofluorescence performed with anti-IgG coupled to fluorescein and anti-GFAP coupled to Texas Red on primary culture of astrocytes extracted either from Cortex or spinal cord of rat pups (P3) after LPS treatment or not. Inserted pictures correspond to spinal cord astrocytes stimulated by LPS at 63X..... 173

List of Tables:

Table 1: Glasgow Coma Scale for TBI severity assessment.....26

List of Abbreviations

3D	3 Dimensional
ABI	Acquired Brain Injury
ASIA	American Spinal Injury Association
BBB	Blood-Brain-Barrier
BDNF	Brain-derived neurotrophic factor
BMP	bis(monoacylglycero)phosphate
BSCB	Blood-Spinal-Cord-Barrier
CCI	Controlled Cortical Impact
CD	Cluster of Differentiation
CDC	US Center of Disease Control and Prevention
CHCA	α -Cyano-4-hydroxycinnamic acid
CM	Conditioned medium
CSF	Cerebrospinal Fluid
CSPGs	Chondroitin sulfate proteoglycan
DAMP	Damage-associated molecular pattern molecules
DESI	Desorption electrospray ionization
DHB	2,5-dihydroxybenzoic acid
DRG	Dorsal root ganglion
ECM	Extracellular matrix
ESI	Electron spray ionization
EVs	Extracellular vesicles
FPI	Fluid Percussion Injury
GCS	Glasgow Coma Scale
GFAP	Glial fibrillary acidic protein
HMGB1	High mobility group box 1 protein
IF	Infrared
IFN	Interferon
Ig	Immunoglobulins
IL	interleukin
ISNCSCI	International Standard for Neurological Classification of Spinal Cord Injury
LCM	laser capture microdissection
LFQ	Label Free Quantification
LMJ	Liquid Microjunction Extraction
LOC	Loss of consciousness
LPS	Lipopolysaccharide
MALDI	Matrix Assisted Laser Desorption Ionization
MHC	Major Histocompatibility Complex
MRI	Magnetic resonance imaging
MSCs	Mesenchymal stem cells
MSI	Mass Spectrometry Imaging

MyD88	Myeloid differentiation primary response 88
NLRs	NOD-like receptors
PAM	Parafilm assisted microdissection
PAMP	Pathogen-associated molecular pattern molecules
PRR	Pattern recognition receptors
PTA	Posttraumatic amnesia
PTMs	Post-translational modifications
RAGE	Receptor for advanced glycation endproducts
ROI	Region of interest
ROS	Reactive oxygen species
SA	Sinapinic acid
SBDP	Spectrin Breakdown Products
SCI	Spinal Cord Injury
SIMS	Secondary ion mass spectrometry
SN	Substantia Nigra
TBI	Traumatic Brain Injury
TGF- β	transforming growth factor β
TLRs	Toll-like receptors
TNF	Tumor necrosis factor
TOF	Time-of-flight
UCH-L1	Ubiquitin C-terminal hydrolase-L1
UV	Ultraviolet

Introduction

The central nervous system (CNS) is the elemental part of the nervous system consisting of the brain and spinal cord. From its name, “Central”, this system is responsible for gathering information from the whole body, processing this information, and then controlling the responding action throughout the organism. While the brain is responsible for controlling most of the body functions, including movement, memory, awareness, breathing, coordination, precision, etc., the spinal cord functions in the communication between the brain and peripheral nervous system. Most actions/movements of the body are controlled by the brain. However, some actions that occur in response to an external force, including non-voluntary reflex movements, occur via the spinal cord with no participation of the brain. Due to such main functions of the CNS, any change in the normal state of this system, such as an injury, could lead to devastating consequences. In fact, injury to the CNS comes in many forms including: stroke, infection, and hemorrhage, but the most recognizable are traumatic brain injury and spinal cord injury (Miller et al. 2009).

Traumatic brain injury (TBI) an alteration in the mental state of an individual due to an impact or rapid movement of the brain within the skull caused by collision with an external force, which could be a penetrating one or not. Our daily routine actions, such as driving and sports, along with the surrounding environment, make us susceptible to injury and thus TBI related deaths are in continuous increase. In fact, at the current rate of global incidence for TBI, this form of brain injury is expected to become the third leading cause of death worldwide by the year 2020 (Meaney et al. 2014). The worldwide epidemiology evaluation of TBI is a challenging task and very rare studies have focused on the statistics with respect to TBI in a worldwide perspective, but rather each country or continent alone. This is due to many reasons, but mainly because of the different assessment and classification systems which vary from one country to another. For example, in the USA, the “Center of Disease Control and Prevention (CDC)” is responsible for the data collection and epidemiological monitoring of TBI. Thus, the CDC provides a standard classification system and obliges all hospitals on US territory to use the same criteria for assessment of TBI related injuries. However, in Europe, the situation is more complicated due to the differences in diagnostic criteria and case ascertainment between the different countries. On average, approximately 235 people per 100,000 sustain a TBI within Europe (Tagliaferri et al. 2006), while in the USA, 100 people per 100,000 have a TBI (Roozenbeek et al. 2013). According

to a recent statistical study by the CDC based on data between the years of 2007 and 2013 in the USA, 2.8 million TBI's occur in the USA every year. Of these 2.8 million, 2.5 million cases are treated directly in the emergency room and released, 282,000 people are administered into the hospital, and 56,000 die (Taylor et al. 2017). Thus, on a daily basis, 153 people die in the USA from TBI related injuries. Although the incidence by gender is more common to all worldwide countries, with the males more likely to sustain an injury than females, factors like age vary. For instance, the annual incidence of TBI among adolescents (age between 15-30 years) is between 154 and 415 people per 100,000 in the US, while it is approximately 535 people per 100,000 in France. In adults, the number decreases in both countries to reach 93 per 100,000 persons in the US and 190 per 100,000 in France (Popescu C et al. 2015).

Spinal cord injury (SCI) is defined as a damage to any segment of the spinal cord which leads to changes, often permanent, in the strength, sensation, and functions/roles of the body below the injured area. According to a recent published fact sheet in 2015 regarding the epidemiology of SCI, 40 cases per million population in the USA sustain a SCI. With 80% of the new cases being males, the average age of injury is around 42 years, showing a dramatic increase since the 1970s where it was 29 years (The national SCI statistical center. 2012). In France, the latest study performed on epidemiology of spinal cord injury was performed in 2015, and showed that 40,000 patients are paraplegic or tetraplegic due to SCI lesion. With regard to Europe, based on data collected from 22 different European countries, a total of 1840 traumatic SCI-related deaths were detected in the year of 2012, 59% of whom were males (Majdan et al. 2017). As the case in TBI, the number of SCI affected persons worldwide is in continuous increase and the need for a therapeutic approach to both injury types is becoming more essential.

The impact of both TBI and SCI on the patient, close family, and society is becoming a major burden on both the health and socio-economical systems worldwide. For TBI, the major effects include: psychological effects on the families who have injured persons (Brooks et al. 1986), economic problems for these families who care for the cost of the injury (Humphreys et al. 2013), close-relationship breakdowns or divorces for the injured ones resulting in problems such as social isolation (Wood & Yurdakul 1997), and mood change disorders that lead to an increased risk of suicide (Fleminger et al. 2003). In the year of 2010, TBI estimated cost on the US economy was \$76.5 billion dollars (Alali et al. 2015). The cost associated with spinal cord injury, is mainly

controlled by the severity of the injury and the localization within the spinal cord thus resulting in different physiological outcomes. The cost is also associated with the period post injury and if there is a possible cure and progression or not. In fact, and in the year of 2011, the average yearly expense of an incomplete spinal cord injury was around \$334,170 for the first year, and almost \$40,589 for every subsequent year per person. On the contrast, for individuals suffering from C1-4 tetraplegia, the first year cost approximately \$1,023,924, and \$177,808 for the subsequent years per person (DeVivo et al. 2011). The major causes of TBI and SCI are more or less the same, which involve sources that all individuals are susceptible to in their daily routine actions. These include: motor-vehicle accidents, sports, violence, and random falls (Clairmont & Matkovic 2005). For the brain, another form of brain injury can be obtained and is classified as Acquired Brain Injury (ABI). ABI is a result of several possible internal causes within the body such as strokes, tumors, chemical or toxic substances, hypoxia, and choking or drowning.

Injuries occurring to the CNS, especially TBI and SCI, are characterized by 2 main phases post impact. Phase one, primary injury, is due to the direct mechanical insult from a foreign object to the brain or spinal cord. This leads to neurodegeneration and cell death within the trauma site. Just after the primary injury, a series of inflammatory responses are initiated, mainly by the recruitment of microglia and astrocytes towards the lesion site, and followed by the infiltration of peripheral immune cells including macrophages, neutrophils, and lymphocytes. This inflammatory cascade remains for several days/weeks post injury and has a dual controversial role. In one perspective, it is believed to be implicated in debris removal and aiding neuronal regeneration, while on the other hand, it is believed that this inflammatory process leads to release of neurotoxic factors and continuous damage to cells within the lesion site. There remains a lack of understanding of the molecular and cellular communication between the cells and the infiltrating immune cells within the micro-injured environment, along with the involved underlying global biological processes. Such a study, especially at several molecular levels, including lipids and proteins, will allow the better characterization of the micro-injured area and open the possibility for molecular targets for a therapeutic approach based on time post injury and different affected regions within the CNS.

Bibliography

Central nervous system anatomy

The central nervous system is composed of more than 100 billion individual nerve cells all gathered in a network, that communicate and function together to control our actions, help us understand our surrounding environment, and react to environmental changes (Ballios et al. 2011). The brain is divided into 3 main structures: the cerebrum, the cerebellum, and the brainstem (**Figure 1**). The complete brain is surrounded by the skull, a bone layer designed for protection.

- a) **The cerebrum** or referred to as the telencephalon, is the largest and uppermost component of the brain. It is the most highly developed and has several roles including thinking, perceiving, and language understanding. The cerebrum is divided equally into two hemispheres (left and right), which are connected by a bundle of nerve fibers annotated as the corpus callosum (also known as the main constituent of the white matter of the brain). The corpus callosum mainly functions as a bridge of communication between both right and left hemispheres. The outermost layer of the cerebrum consists mainly of grey matter (cell bodies) and is designated as the cerebral cortex. It is constituted of folded lumps called gyri which form grooves in the cortex called sulci. The cerebral cortex is divided into four main lobes: frontal, parietal, temporal, and occipital. As its name, the frontal lobe is in the frontal part of the brain and is responsible of voluntary movement, along with mood, memory, and other functions. The parietal lobe is just in between the frontal lobe and the occipital lobe and is mainly involved in sensory information processing including functions such as: pain, touch, and temperature. The temporal lobes are located on both sides of the brain and function in processing auditory information and language. Finally, the occipital lobe is in the rear part of the brain and plays a role in processing visual information.

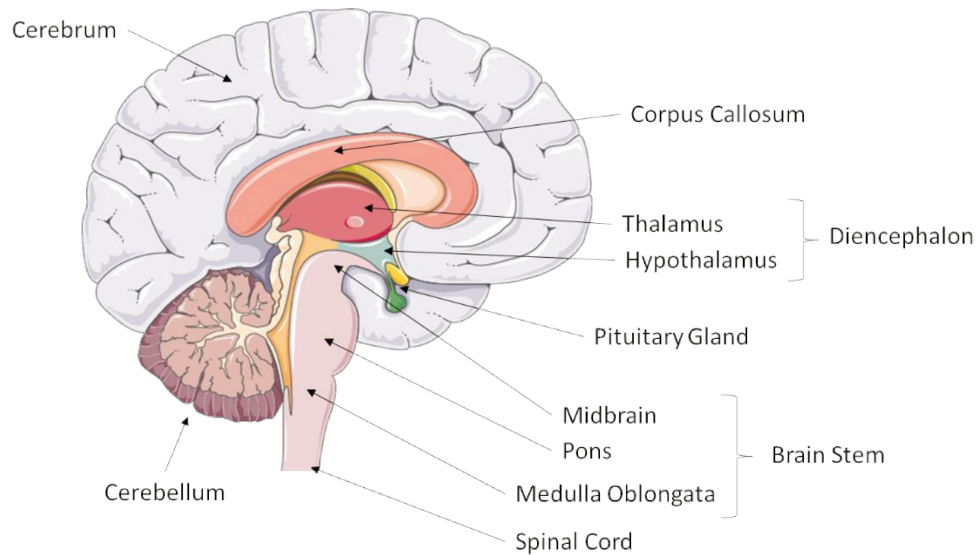


Figure 1: Anatomy of the human brain. This figure shows the different compartments of the brain in a sagittal view, with labelling of the different structures which together form the brain. Source: Khalil Mallah (Figure was created using Servier Medical Art).

Inward towards the center of the brain, different structures exist including the hippocampus, pituitary gland, thalamus, and hypothalamus. While the hippocampus plays an essential role in memory (both declarative memory and spatial relationships), the pituitary gland functions in hormone production and secretion which control body functions such as metabolism and sexual response. The thalamus is positioned between the brain stem and the cortex and functions in relaying sensory and motor information to the cortex. Just below the thalamus, the hypothalamus is responsible for regulating automatic tasks such as appetite and thirst. Along with the pituitary gland, the hypothalamus functions in hormone production and secretion to control actions such as thirst, hunger, mood, and sleep. The thalamus and hypothalamus together, along with the subthalamus and epithalamus, form what is known as the diencephalon of the brain.

- b) **The cerebellum** is found in the basal part of the brain. It also consists of two lateral hemispheres which are joined by the vermis. It mainly functions controlling movement and equilibrium. In addition, it has been believed to be involved in memory skills, for example, mathematical skills.

- c) **The brainstem** consists of three main parts: the midbrain, the pons, and medulla oblongata and is located just below the hypothalamus. It is responsible for the communication and signal transfer between the brain and the spinal cord. Several cranial nerves involved in eye muscle control are associated with the midbrain and thus its main functions are involved in eye sight and movement, along with hearing. Just after the midbrain, and before the medulla oblongata, the pons is located and serves as a connecting bridge of both the midbrain and medulla oblongata. In this structure, several other nerves and fibers involved in eye sight and facial movement can be found. Another important role for the pons is that it serves in relay of sensory information from the cerebrum to the cerebellum, and vice versa. The medulla oblongata lies in the bottom of the brainstem and is in direct and continuous connection with the spinal cord. As well as its main function of relaying nerve signals between the brain and spinal cord, the medulla oblongata helps control involuntary functions such as heart rate and respiration.

Both the brain and spinal cord are covered and protected by three layers of tissue, the meninges. They are the dura mater, arachnoid mater, and pia mater with the dura mater being the most exterior layer and the pia mater being the most interior. While the dura matter is the strongest, thickest, and closest to the skull, the arachnoid mater is a thin web-like membrane, and the pia mater is the layer directly covering the brain. The space between the arachnoid and pia mater is called the subarachnoid space, where the cerebrospinal fluid furnishes. In fact, the cerebrospinal fluid (CSF) surrounds both the spinal cord and brain, and flushes through the ventricular system of the brain thus providing a possible mode of trafficking and exchange between the spinal cord and brain. In addition, it has been long known that the brain and spinal cord have no vascularization system integrated within the neuronal tissue. However, the major site where the blood and the CNS exchange and/or traffic molecules to and out of the brain is the blood-brain-barrier (BBB) (Abbott et al. 2010). The BBB was first described by Erlich in 1904, while using several animal models, he injected a blue dye into the circulatory system and found that this dye moves to most organs of the body, except the brain. On the contrary, one of his students, Goldmann in 1913, injected the dye into the CSF and found that all cells of the brain were stained and none of the peripheral organs (Carvey et al. 2009). These sets of experiments led to the conclusion that the BBB separates the CNS from the peripheral organs. Precisely, the BBB separates the brain from the periphery and

prevents the infiltration of immune cells and blood-borne molecules into the brain (Muldoon et al. 2013). The BBB also extends from the brain to cover the spinal cord but is sometimes referred to as the blood spinal cord barrier (BSCB). The BSCB has the same function as the BBB regarding protection and communication with the surrounding, and isolation of the spinal cord from blood-related molecules. The BBB is constituted of brain endothelial cells along with pericytes surrounding the blood capillaries which pass through and just near the CNS. This structure is then in direct contact with cells such as astrocytes and neurons where transfer and exchange with the surrounding occurs using mechanisms such as diffusion (**Figure 2**). In addition, these astrocytic processes help in protection from biochemical fluctuations that occur in the periphery (Shoichet et al. 2008).

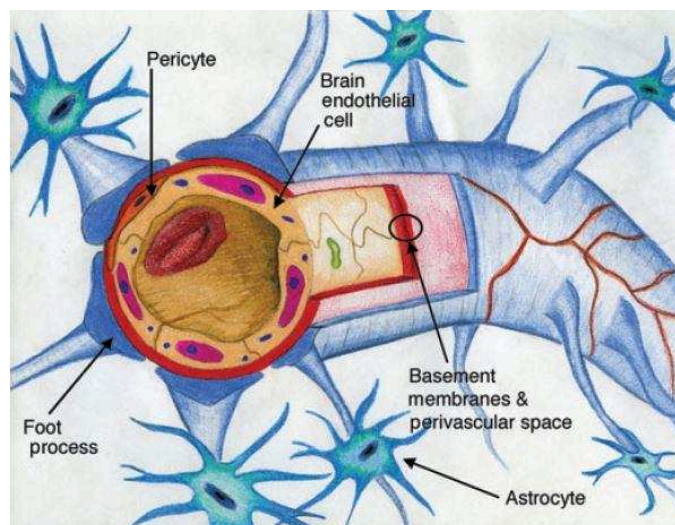


Figure 2: A drawing of blood capillary with BBB components. This figure shows the presence of a blood capillary surrounded by astrocytes and foot processes. Reprinted/Reused from (Carvey et al. 2009), “The blood–brain barrier in neurodegenerative disease: a rhetorical perspective”, *Journal of Neurochemistry*, Copyright (2009), with permission from John Wiley and Sons.

Starting just after the medulla oblongata, the spinal cord descends through the vertebral canal and backbone. The complete spinal cord is divided into different segments fixed one over the other in an ascending manner. All body movement is controlled by the signals that pass through these segments to and from the brain. On average, the adult human spinal cord is 2 cm thick and 45 cm long and divided into 31 segments. Depending on the location, and the different organs which are controlled by these segments, the entire spinal cord segments are divided into (**Figure 3**):

- 8 cervical segments: These are responsible for signal transmission and control of the areas of head, neck, shoulders, arms, and hands. These are designated from C1 to C8.
- 12 Thoracic segments: Transmit signal to part of the arms, but also the anterior and posterior parts of the chest and abdominal area. These are designated from T1 to T12.
- 5 lumbar segments: Transmit signal to the legs and feet. These are designated from L1 to L5.
- 5 Sacral Segments: These transmit signal to the lower back, along with the genital organ areas and pelvic ones. These are assigned from S1 to S5.
- 1 coccygeal remnant segment in the tailbone region, Co.

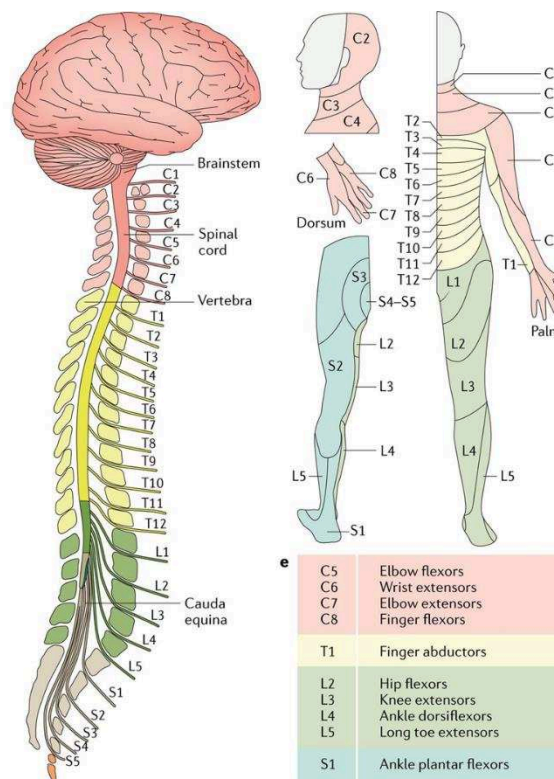


Figure 3: Anatomy of the human spinal cord showing the 31 complete spinal segments. Reprinted by permission from Springer Nature Customer Service Centre GmbH, Springer Nature, Nature Reviews Disease Primers, “Traumatic spinal cord injury”, (Ahuja et al. 2017), Copyright (2017).

Each segment has 1 nerve pair, thus yielding 31 total spinal nerve pairs lying within the vertical column. These nerve pairs function in transmitting sensory information from the body to the spinal cord and then finally to the brain, and in parallel, send motor commands from the brain and spinal cord to the body organs. These spinal nerves are only about 1 cm long, and after, they

interconnect with the different peripheral nerves. In addition, each segment has a ventral and dorsal root where these spinal nerves are connected. The ventral root contains axons of motor neurons and the dorsal root contains axons implicated in sensory neurons. The spinal cord, as the brain, is also divided into both gray and white matter. While the grey matter is mainly consisting of the neuronal cell bodies, dendrites, axons, and nerve synapses, the white is mainly composed of bundles of myelinated axons. As previously mentioned, the spinal cord as the brain, is covered by the three layers of meninges and the cerebrospinal fluid which together, provide protection and isolation of the spinal cord and spinal roots, along with the brain.

The anatomy of the CNS of the human and rat are very similar. In fact, with regard to the spinal cord, the main difference is the number of segments and therefore the number of nerve pairs. While the human spinal cord is made of 31 segments and thus 31 nerve pairs, the rat spinal cord is made of 34 segments and thus 34 nerve pairs. The anatomical features of the brain and its organization are also very similar in both human and rat. Such similarity, along with the easy handling/manipulation, accessibility, and expense of experiments, have all yielded the development of animal CNS injury models, especially rodents (rats and mice). For this, several injury models have been realized and some are mentioned in the following parts of this chapter. In addition, access to human samples for performing research is not an easy task, especially with the different governmental restrictions, paperwork, and approval of the close relatives of patients.

Severity and Classification

In order to receive the most appropriate preliminary treatment, surgeons must give the most accurate diagnosis and injury classification of an injury upon arrival of the patient to the emergency room. This assessment will also be used to indicate the type of treatment and severity of the impact. For this, several worldwide classification systems have been developed for TBI, but mainly Glasgow Coma Scale (GCS) is being used nowadays. Since its introduction in 1974 (Teasdale & Jennett 1974), it has been the most widely used worldwide scale for assessment of TBI because of its simplicity and precise assessment of severity when compared to the other classification systems.. The GCS classifies the injury based on the combined sum of scores for three responses: eye response (from 1 to 4 points), motor response (from 1 to 6 points), and verbal response (from 1 to 5 points) (**Table 1**). A combined score of all three factors from 3 to 8 is considered as severe, from 9 to 12 is classified as moderate, and from 13 to 15 is classified as mild.

Glasgow Coma Scale		
Response	Scale	Score/Point
Eye Response	Eyes open spontaneously	4
	Eyes open to surrounding noise (Speech, shout)	3
	Eyes Open to Pain	2
	Does not Open Eyes	1
Verbal Response	Oriented	5
	Confused (able to answer but with disorientation)	4
	Innapropriate Response/Words	3
	Incomprehensible sounds	2
	No verbal response	1
Motor Response	Obeys Commands for movement	6
	Purposeful movement to painful stimulus	5
	Withdrawal from pain	4
	Decorticate posturing accentuated by pain	3
	Decerebrate posturing accentuated by pain	2
	No motor response	1

Table 1: Glasgow Coma Scale for TBI severity assessment. This table shows the different possible scores which can be assigned to each of the different GCS factors (eye response, verbal response, and motor response) based on injury condition.

In addition to the GCS, another commonly used system for the clinical classification of TBI is the duration of loss of consciousness (LOC). Depending on the time that the patient needs to recover consciousness, or change the current mental state, the injury is classified as mild (less than 30 min), moderate (between 30 min and up to 6 hours), or severe (more than 6 hours). Another classification system is based on the duration of posttraumatic amnesia (PTA) which classifies the injury based on the time between moments of injury, until the patient can obtain a continuous memory of the occurring events which are surrounding him/her. The classification is as follows: mild (less than 1 hour), moderate (1 hour to 24 hours), severe (1 day to 7 days), or very severe (more than 7 days) (RUSSELL & SMITH 1961). When comparing between classification systems, we can see that the GCS system allows classification upon arrival to emergency room (mainly within the first minutes to hours), while systems such as PTA allow a more predictive outcome in later time of injury.

The classification of a spinal cord injury is also a universally applied procedure developed by the International Standard for Neurological Classification of Spinal Cord Injury (ISNCSCI). This examination takes into consideration three main scores developed by the American Spinal Injury Association (ASIA). The scores are ASIA motor score (dealing with movement), ASIA sensory score (dealing with light touching), and the ASIA impairment scale (if the injury is

complete or not). This exam occurs directly within the first 72 hours post injury and the given grade ranges from grade A to grade E with A being the most severe (complete sensory and/or motor dysfunction below injury level) and grade E being the least severe (normal sensory and motor function).

Types of Injury

TBI is a changed in mental state as a result of an external force to the head, which can be in several shapes and forms. Based on the mechanism of injury of this external force, TBI's can be divided into two main types: open head and closed head (**Figure 4**). The open head injury involves the penetration of the skull by an external object, such as a knife, bullet, or any other sharp object. This penetration leads to direct damage to the underlying tissue and results mainly in cell death or non-reversible damage. On the other hand, closed head injury involves no penetration or breaking of the skull, but rather an impact of an external force leading to the movement of the brain within the skull. This rough movement of the brain results in damage of the external layers of the brain such as cell shearing due to the contact between the outer layers of the brain with the interior part of the skull. An example of closed head injury is a concussion which is a result of a blow to the head, violent shaking of the head, or even motor-vehicle accidents. Others types of brain injury exist such as hypoxia (deprivation of oxygen in the brain), stroke, chemical/toxic damage, or infection, but they are termed as Acquired Brain Injuries (ABI) since they are not a result of an external force as in the case of TBI, but rather due to internal reasons.

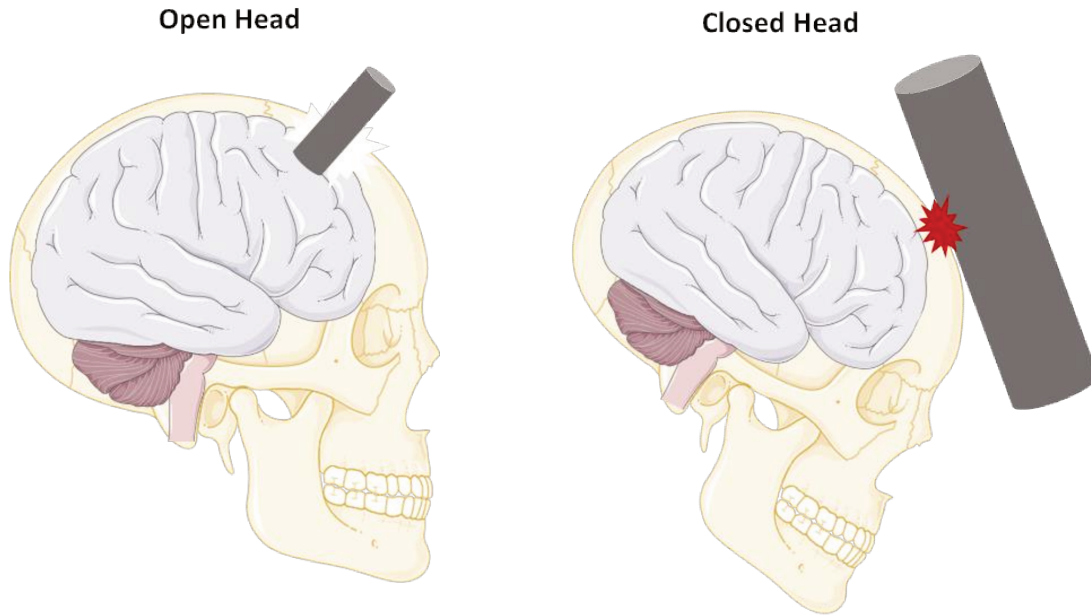


Figure 4: Drawing representation of both open head injury and closed head injury in TBI. As visualized in the figure, the open head injury involves the penetration of the skull by a foreign object and damage of the underlying brain tissue, while closed head injury involves the the impact of the brain by the exterior part of the brain with no penetration. Source: Khalil Mallah (Figure was created using Servier Medical Art).

As previously mentioned, the clinical assessment of a SCI is given based on the extent of damage within the segments of the spinal cord. Based on this, all SCI's are categorized into two main groups: complete or incomplete. Based on the standards set by the ASIA, a complete injury is defined as an injury where no preservation of motor and/or sensory function is found more than 3 segments below the neurological level of injury, contrary to incomplete injury, where some preservation of sensory and/or motor function exists in the neurological level of injury (Waters et al. 1991). A more recent injury definition by the ASIA states that a complete injury is one where the sensory and motor function are lost in the lowest sacral segment (S4-S5) (Kirshblum et al. 2011). In both types of injury, a sub-type of injury, either a paraplegia or tetraplegia/quadriplegia can exist (**Figure 5**). Paraplegia is the case were the patient loses function in their lower limbs (legs) but keep the function of their hands. This is mainly due to an injury below the thoracic spinal levels (from T1 to L5). However, tetraplegia/quadriplegia results in the paralysis of all four limbs which is caused by an impact/damage above the first thoracic cerebra, or within the cervical sections (from C1 to C8). Not all SCI result in paraplegia and tetraplegia/quadriplegia, although they are the most common and incidental after injury. For example, Cauda equina syndrome, is a

condition that occurs post SCI resulting in bladder dysfunction, lower-back pain, and bilateral sciatica (Orendáčová et al. 2001).

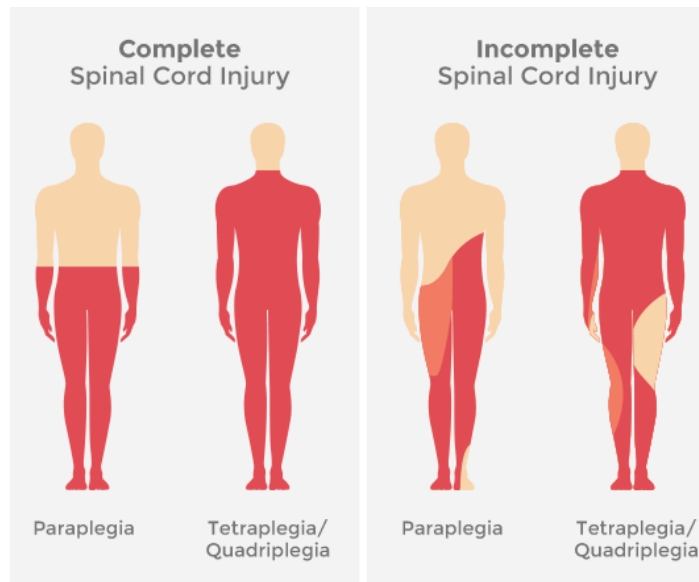


Figure 5: Representative scheme of complete and incomplete spinal cord injury along with the different paraplegia and tetraplegia/quadruplegia cases in both types of injury. (Adapted from wongmedicalcentreipohmalaysia.blogspot.com on October 17 2018).

Animal Models of Injury

For both TBI and SCI injuries, several animal models have been developed in order to mimic the real-life possible previously mentioned types of injury. By using such animal injury models, we obtain the practicability to better understand the anatomical and biological consequences and molecular changes occurring post injury. Availability of such animals, low cost, numerous rodent models, including rats and mice, have been factors leading to their use in studying CNS injuries (Marklund 2016). Since TBI is not only one single disease, and rather exists in many forms and conditions, several TBI animal injury models have been developed.

TBI injury models:

- a) **Fluid percussion injury model (FPI):** this model involves the injection of fluid to the underlying intact dura through a cranial cavity (Dixon et al. 1987) (**Figure 6**). The speed and pressure of the entering fluid induce severity and deformation within the brain tissue. This injury model mimics a TBI with no involvement of skull fracture, but rather replicating an intracranial hemorrhage or brain swelling (Xiong et al. 2013).

b) **Controlled Cortical impact (CCI):** this model of injury is a mechanical one which involves performing a direct impact to the cortex (LIGHTHALL 1988) (**Figure 6**). In fact, this model requires a craniotomy to the skull and direct damage with a rigid impactor to the exposed cortical tissue resulting in tissue loss, hematoma, axonal injury, concussion, BBB dysfunction, and possibly comma (Xiong et al. 2013). The main advantage of this technique is in its reproducibility between all experimental samples due to several controllable factors including reproducible coordinates of injury. Another advantage is the management of histopathological severity as the cortical deformation can be controlled by the velocity of impact and depth of injury within the cortical tissue, and thus can be adjusted for desired experimental requirements (Saatman et al. 2006). In addition, this system has been applied to a wide range of animal models including: ferrets, rats, mice, swine, and sheep (Marklund & Hillered 2011). One main disadvantage for this technique is that the price of machinery of this model is expensive. During my thesis, the chosen TBI open head injury rat model was performed using CCI.

c) **Blast Injury:** this model aims to mimic an injury due to an explosive blast in which no external mechanical damage directly affects the head, but rather shock waves are sent to the body and head of the animal (**Figure 6**). This is the case of many military personnel who have been exposed to such blasts, but are not diagnosed with TBI and show no external injury. Such soldiers can be exposed several times to blast injuries but never report such cases because they don't realize they were affected (Benzinger et al. 2009).

Several other injury models for TBI exist such as weight drop models (ex. Feeney's weight-drop model), penetrating ballistic-like brain injury, and Maryland's model. However, the ones I previously discussed are the most frequently used by many studies in TBI.

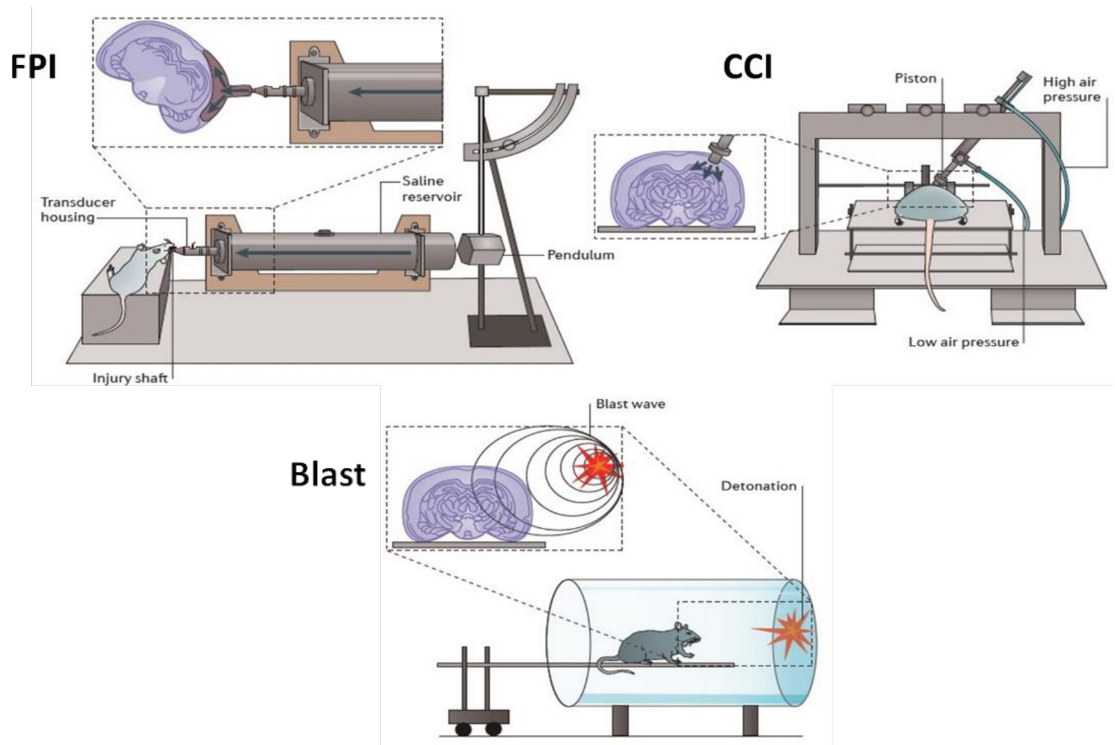


Figure 6: Different animal injury models used in brain injury including FPI, CCI, and Blast injury. Reprinted by permission from Springer Nature Customer Service Centre GmbH, Springer Nature, Nature Reviews Neuroscience, “Animal models of traumatic brain injury”, (Xiong et al. 2013), Copyright (2013).

With regard to SCI, this injury type can be a result of 3 main physical mechanisms: compression of spinal discs, destruction by an external force, or ischemia (a reduction in blood flow). Thus, all animal injury models have been developed to mimic these three causes, however all three can be categorized as part of either one of the previously mentioned injury types: complete or non-complete injury.

SCI injury models:

- a) **Transection:** This injury model mimics the complete SCI injury. Although this type of injury is considered rare in the human SCI, it provides researches with a possibility to study processes such as regeneration and plasticity at the axonal level (Sharif-Alhoseini & Rahimi-Movaghar 2014). The procedure uses spring scissors after laminectomy to completely cut the spinal cord at a designated segment for the study (Nakae et al. 2011).

b) **Compression:** This injury model is a result of constant compression and pressure applied to the spinal cord of the animal. Several compression models have been developed including clip, balloon, spacer, and forceps compression. Designed in 1979 (Dolan & Tator 1979), the clip compression model is a non-transsection model that applies consistent force to the dura matter of the spinal cord. After laminectomy, the calibrated clip applies a specific controlled force to the spinal cord (Bruce et al. 2002) (**Figure 7a**). The calibrated forceps compression allows to induce a lateral injury model. By inserting both sides of the forceps on both hemispheres of the spinal cord, a pressure is exerted towards the center resulting in hemorrhagic necrosis and displacement of the damaged tissue in both cranial and caudal directions (Blight 2000) (**Figure 7b**).

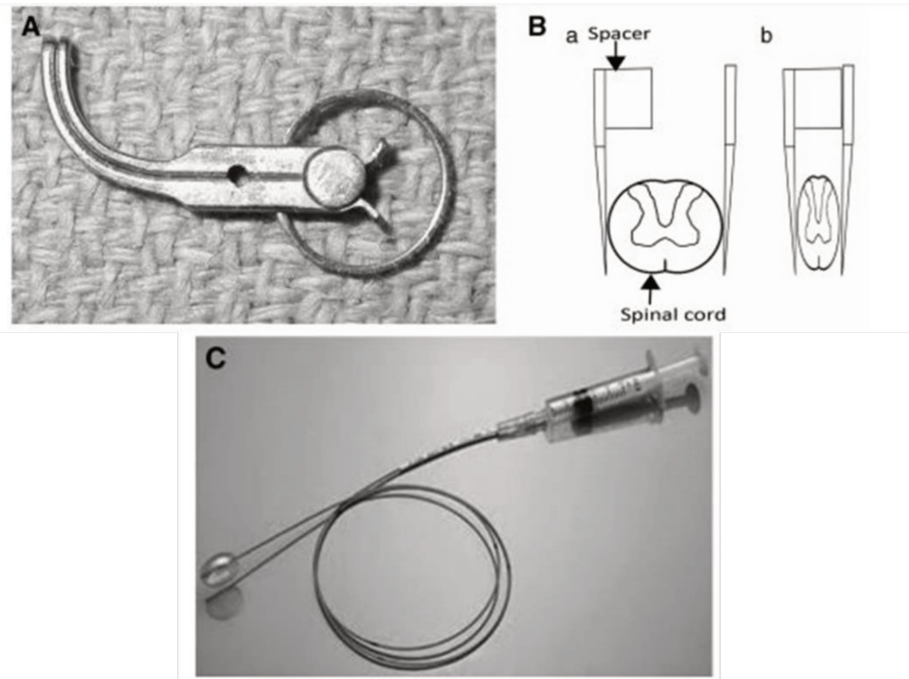


Figure 7: A) Photograph of the injury tool used in clip compression. B) Drawing of the mechanical procedure of calibrated forceps injury model. C) Photograph of the balloon compression device showing the balloon tip along with the tubing and syringe used for inflation of the balloon with saline solution. Reprinted by permission from Springer Nature Customer Service Centre GmbH, Springer Nature, Spinal Cord, “Spinal cord injury models: a review”, (Cheriyian et al. 2014), Copyright (2014).

One commonly used compression model is the “Balloon compression model” which was first developed and used on dogs in 1953 (TARLOV et al. 1953). Severity of injury and duration of compression are controllable factors in this technique which are accomplished by the volume of inflation of the balloon using a saline solution (**Figure 7c**)

and time of insertion of the balloon within the injury site. This method requires a laminectomy in which a Fogarty catheter is inserted into the dorsal epidural space through a small hole in the vertebral arch. The catheter is then advanced cranially to the desired segment of injury, and after, the balloon is inflated for a desired time and size in order to mimic different injury severities. In our experiments, we utilized this injury model and inserted the French Fogarty catheter through a small hole in the T10 vertebral arch. This was then advanced until the T8-T9 spinal level and the balloon was inflated for 5 min.

- c) **Controlled Contusion:** This model uses a computer controlled impactor device which allows to select different depths of injury within the spinal cord and thus yielding different severity. It is a blunt injury model which mimics mainly vehicle accidents (Chiu et al. 2017). Although the machinery is expensive, thus giving it some disadvantage, all its experiments are reproducible.

- d) **Photochemical model:** This model does not involve the direct mechanical damage to the spinal cord, but rather it resembles an ischemic model of injury. Introduced in 1986 (Watson et al. 1986), this model involves the excitation of an injected dye (rose Bengal as an example) by exposing the intact spinal column surface to irradiation and thus leading to side effects such as hemorrhagic necrosis of the central grey matter and vascular congestion. The resulted injury is a non-mechanical insult to the spinal cord which is considered as the main advantage of this technique. However, one great disadvantage is that the extent of injury along with the severity are both uncontrollable factor.

Cells of the Central Nervous System

The cellular composition of both the spinal cord and brain are very similar. These cells can be divided into two main types: nerve cells (neurons) and glial cells.

Nerve cells (neurons) are the building blocks of the brain and illicit an electrical impulse which is transmitted either to a consecutive neuron or other cell types by means of a synapse. A neuron is mainly constructed of cell body (soma), dendrites, axon, and axon terminals (**Figure 8**). While the soma contains the nucleus and is responsible for most of the protein synthesis, the

dendrites are processes which extend from the cell body. The axon arises from the cell body and most of axons are covered by an insulating substance, myelin. The myelin is mainly generated by myelin forming cells such as oligodendrocytes and Schwann cells and form a myelin sheath around the axon of a neuron. This accelerates the conduction of action potential along the axon of the same neuron, thus drastically increasing the speed of its propagation in function of the diameter of the axon (Hartline & Colman 2007).

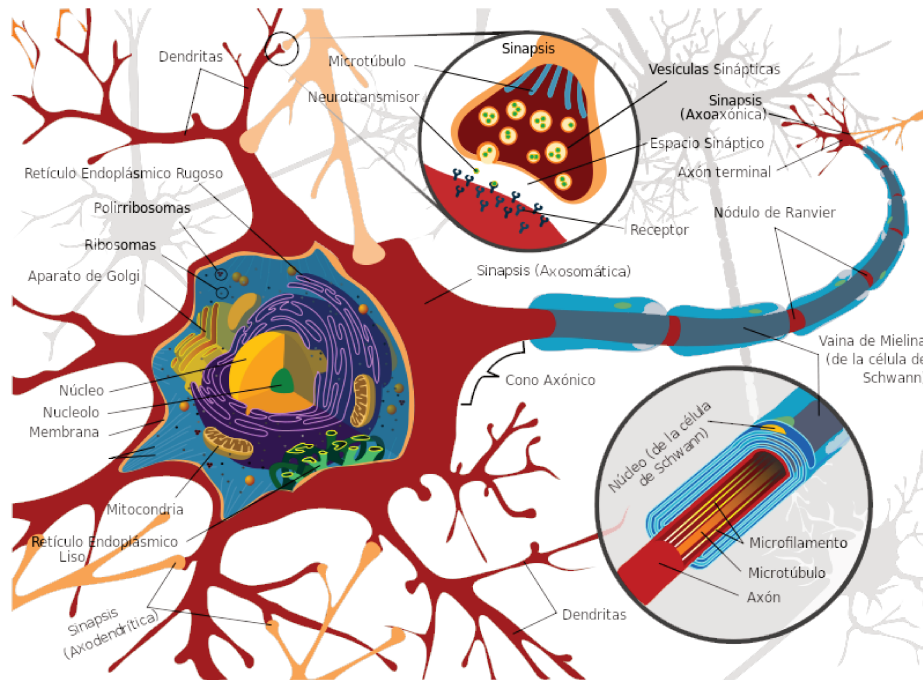


Figure 8: Structure of a neuron along with close-up representation of a synapse. This figure shows the different compartments of a single neuron including: cell body (nucleus, mitochondria, golgi, etc.), axon, dendrites, and synapse (Adapted from https://commons.wikimedia.org/wiki/File:Complete_neuron_cell_diagram_es.svg, 17 October 2018)

The synapse is the site of communication between two neurons and information is relayed from the first neuron, presynaptic neuron, to the target neuron, the postsynaptic neuron. Upon arrival of an electric potential to the terminal part of the presynaptic neuron, chemical messengers (neurotransmitters) are released and bind to the membrane receptors located on the postsynaptic cell, thus conveying either an excitatory message or an inhibitory one. According to their function, neurons are divided into sensory, motor, and interneurons.

- Sensory: carry information from the peripheral nervous system to the CNS.

- Motor: carry order information from the CNS (including both brain and spinal cord) to the remaining muscles and organs in the body.
- Interneurons: responsible for communication within the CNS and are divided into two: “Projection” interneurons that carry a signal from one brain region to the other, and “Local” interneurons that form connections with close neurons within the same region.

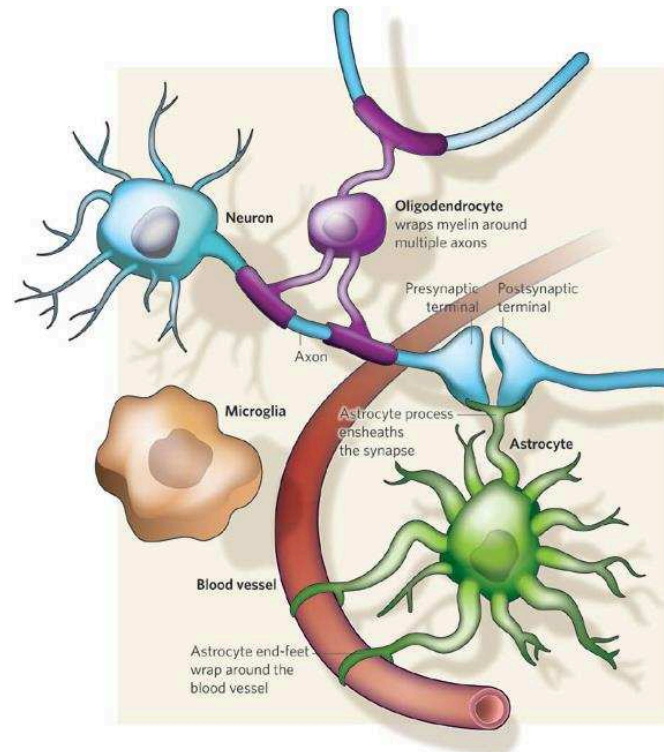


Figure 9: Representative drawing of neuron and its interaction with glial cells of the CNS which include: microglia, astrocytes, and oligodendrocytes. Reprinted by permission from Springer Nature Customer Service Centre GmbH, Springer Nature, Nature, “Neuroscience: Glia-more than just brain glue”, (Allen & Barres 2009), Copyright (2009).

Glial cells have a supportive role for neurons and provide support and protection to the environment which they exist in. These glial cells are divided into three main types: microglia, astrocytes, and oligodendrocytes (**Figure 9**) (Allen & Barres 2009).

- i) **Microglia:** As the CNS is believed to be immune deprived, the microglia are considered as the resident immune cells of the CNS. These cells mainly play a role in protection against any foreign intruder to the brain (eg: pathogens) and function in debris removal. They have a major function of continuous surveillance in the CNS by movement within their area using highly motile protrusions and communication with the localized neurons

(Nimmerjahn 2005), in a guardian-like action. Discovered by famous Spanish scientist Pio del Rio Hortega (Pérez-Cerdá et al. 2015), these cells possess a small soma, a perinuclear cytoplasm, and fine branched processes. However, the morphological structure of the microglial cells can change based on their activation state. In the brain, 4 activation states exist: ramified, hyper-ramified, bushy, and amoeboid (Crews & Vetreno 2016) (**Figure 10**).

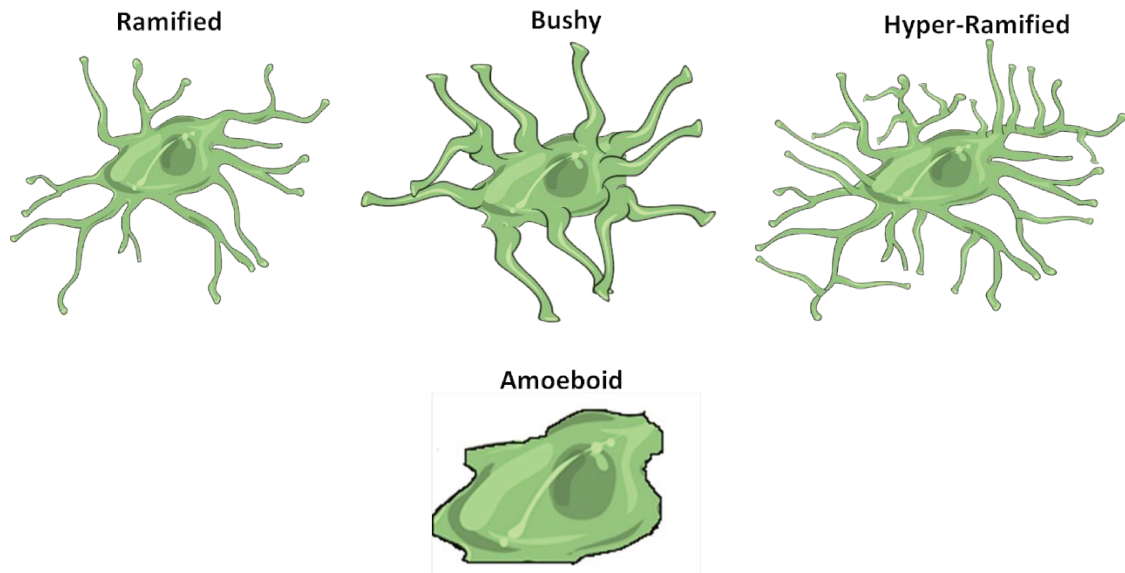


Figure 10: Activation states of microglia in the brain: Ramified, busy, hyper-ramified, and amoeboid. Source: Khalil Mallah (Figure was created using Servier Medical Art).

The morphological form which is dominantly present is the ramified one. This is the case of microglia in a resting non-pathological condition, in which they possess an M2 (anti-inflammatory) phenotype. Upon beginning of activation by a foreign pathogen or trauma, the cellular processes increase in number and the cell processes a “hyper-ramified” shape that secrete pro-inflammatory cytokines. These ramifications, especially in their hyper state, usually facilitate the contact and communication of these cells with several neuronal and non-neuronal cells in their surrounding environment (Zhao et al. 2018). In the transition phase from the ramified resting shape to a fully activated amoeboid one, the cellular components enlarge and the cells take what is known as a “bushy” structure. Finally, fully reactive microglia change their morphological structure to an amoeboid round-shaped one with little or few cellular processes (Beynon & Walker 2012). These amoeboid activated microglia possess the M1 phenotype, generally known as pro-

inflammatory. Resident microglia possess several receptors on their surface which facilitate communication with surrounding cells along with the rapid response to any trauma. These include: myeloid-monocytic markers such as Fc receptors, cluster of differentiation (CD32 and CD64), complement receptors (CD11b and CD11c), integrins, MHC class I and II, and CD45 (Tambuyzer et al. 2009). In addition to their neuro-protective role, it has recently been discussed that microglia play a role in controlling the neuronal microenvironment by participating in processes such as neuronal proliferation, differentiation, and even formation of synaptic connections (Graeber 2010). One example of this function is that the microglia are capable of removing any dysfunctioning axonal terminals, and thus preserving the intact factor of neuronal connections. Roles such as this have given the microglia greater importance than rather just “immune cells of the CNS”.

- ii) **Astrocytes** are the most abundant glial cell type in the CNS. They have an essential role in maintaining brain homeostasis and providing neurons with all required energy and substrates for neurotransmission (Allen & Barres 2009). There are two main types of astrocytes based on their location in the brain and point of contact with the neuron. The first type is “Protoplasmic” astrocytes which are located in the grey matter and in contact with the neuronal cell bodies and synapses. The second type is the “Fibrous” astrocytes which are located in the white matter and in direct association with the neuronal axons.

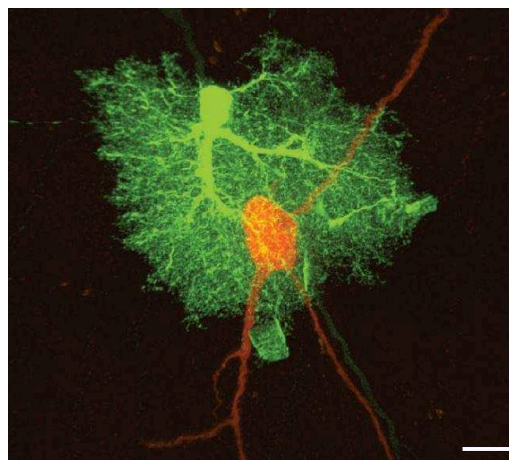


Figure 11: Micrograph of a protoplasmic astrocyte (green) enwrapping the cell body of a neuron (red). Reprinted by permission from Springer Nature Customer Service Centre GmbH, Springer Nature, Nature, “Neuroscience: Glia-more than just brain glue”, (Allen & Barres 2009), Copyright (2009).

Astrocytes have major importance in maintenance and permeability of the blood brain barrier. This is due to their presence near both the blood vessels and other CNS cells including neurons and microglia (Colombo & Farina 2016). These cells have a key role in the activation of the immune system and can control immune cell trafficking by secretion of cytokines and chemokines. Astrocytes themselves are immune-competent cells and are actively participating in innate immunity (Cordiglieri & Farina 2010). Along with resident microglia, they are the protectors of the CNS from any pathogens, and are the first responders after a trauma. Glial fibrillary acid protein (GFAP) has become a prototypical marker for immunohistochemical identification of astrocytes. Expression of GFAP post injury to the brain or spinal cord shows that reactive astrocytes accumulate at the border of the focal injured tissue and form a scar which isolates the damaged tissue from the possibly remaining live cells (Sofroniew & Vinters 2010). Although this action helps sequester the injury and stops the spreading of damage to remaining viable cells, it is also believed that this accumulation and formation of the scar participates in preventing axonal regeneration post trauma (Rudge & Silver 1990).

- iii) **Oligodendrocytes** are glial cells of the CNS responsible for myelin production (Bradl & Lassmann 2010). Myelin are lipid-rich structures that extend from oligodendrocytes and surround the axons of neurons. Myelin functions in providing support and insulation to axons, in addition to acceleration of the action potential propagation when compared to non-myelinated neurons. Oligodendrocytes have very small cytoplasm and possess few short processes. In the white matter, they are myelin-forming cells, while in the grey matter they are satellite cells found around neurons. Similar to the oligodendrocytes, the Schwann cells are myelin forming cells in the peripheral nervous system.

Communication and interaction between neurons and glial cells is essential for information processing and trafficking to and from the CNS. This is maintained in two basic manners: the first is through soluble factors such as neurotransmitters and neuromodulators, and the second is by cell-cell contact and exchange of factors. One example of this interaction is that of microglia with neurons. In fact, neurons control microglia in an “On” or “Off” manner (Biber et al. 2007). “Off” signals keep the microglia in their resting state and block any pro-inflammatory action through factors such as transforming growth factor β (TGF- β), CD22, CX3CL1, and several other

neurotransmitters. This helps in maintaining homeostasis and preventing damage to the healthy tissue, which can be normally caused by microglial cells. However, “On” signals such as CCL21 and CXCL10 are released from apoptotic or damaged neurons to activate the pro-inflammatory state of microglia (Chavarría & Cárdenas 2013). In another example of communication in the CNS, the neuronal contact with the cerebrovasculature is maintained by interaction between the neuron and astrocyte. Due to the close contact of astrocytes with synapses occurring between neurons, the activation of glutamatergic synapses stimulates receptors found on the surface of astrocytes (mainly glutamate and purinergic receptors) through neurotransmitters. This in turn leads to an increase in calcium signaling within the astrocyte through a phospholipase C dependent manner. The calcium will then move towards the end foot of the astrocyte near the vasculature where it can lead to changes in vasodilatory and cause vasoconstrictive actions (Haydon & Carmignoto 2006).

Pathophysiology of CNS injury

According to the events that occur post injury to the CNS, there is not substantial difference in the response of the immune system to the injured brain or any peripheral tissue (Gadani et al. 2015), including the spinal cord. The pathophysiological events taking place post injury are based on the nature of interaction between the CNS and the immune system. As previously mentioned, it is believed that the CNS, including brain and spinal cord, is immune privileged due to the presence of barriers such as BBB and BSCB. Thus, the infiltration of peripheral immune cells to the CNS post damage to the BBB controls the outcomes and response within the injured environment. It is believed that the involvement of the immune system in the CNS injury has dual contrary roles: beneficial in regeneration and healing, and detrimental in the continuous destruction post mechanical impact. For example, Walsh et al. demonstrated IL-4 producing T cells lead to protection and recovery of injured neurons through activation of their IL-4 neuronal receptors, mediated through MyD88 signaling dependent process (Walsh et al. 2015). On the contrary, macrophages are suggested to participate in damage to neurons and glial cells, as the depletion of these cells in a rat spinal cord model helped improve hindlimb usage during motion (Popovich et al. 1999). The events occurring post injury divided into two phases based on time post insult: primary phase and secondary phase. The primary injury is a result of the mechanical impact that occurs to the CNS, either brain or spinal cord. This results in direct cellular death along with damaging of the local blood vessels and infiltration of blood and peripheral immune cells to the injured area. This is accompanied with shearing of axons and neuronal connections.

Secondary injury is known as the cellular and tissue destructive biological changes that lead to dysfunction or death in the time of hours to weeks after the primary injury (Borgens & Liu-Snyder 2012). It is mainly known for the inflammatory response caused by the infiltration of immune cells to the site of injury along with continuous diffuse axonal injury (Das et al. 2012). Several factors including DAMPs and immune cells including neutrophils, microglia, macrophages, and T-cell are implicated in the secondary injury and will be discussed in this part. The kinetics of recruitment of immune factors and immune cell involvement with time is found in the **Figure 12**.

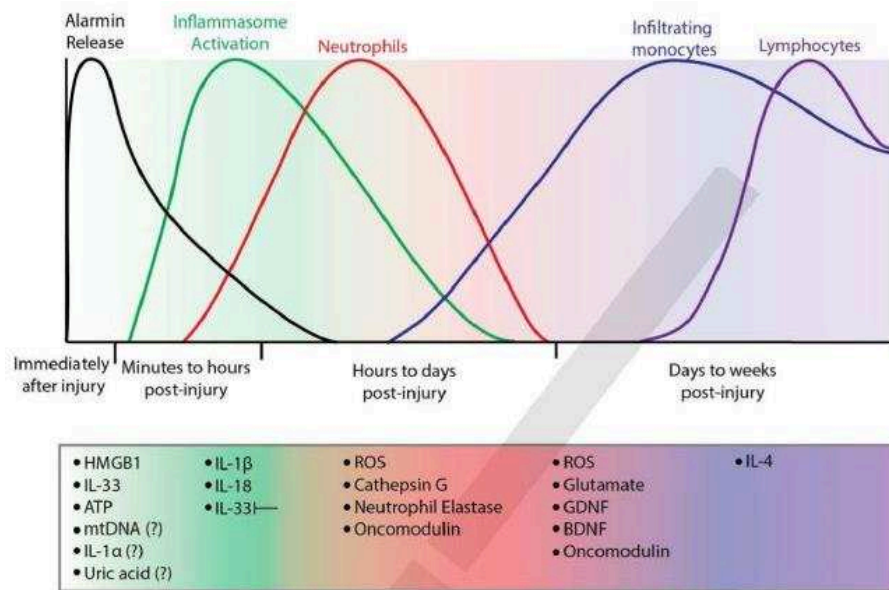


Figure 12: Kinetics and order of involvement of molecular and cellular immune cells to CNS injury in time order. Reprinted from Neuron, Vol. 87, (Gadani et al. 2015), “Dealing with Danger in the CNS: The Response of the Immune System to Injury”, Copyright (2015), with permission from Elsevier.

DAMPs: Just after impact, and within the first few minutes of injury, several factors designated as “Danger Signals” are released into the injured environment. Depending on their origin, these danger signals are either released from damaged cells and are annotated as damage-associated molecular pattern molecules (DAMPs) or from pathogens and are therefore named pathogen-associated molecular pattern molecules (PAMPs) (Tang et al. 2012). More precisely, DAMPs are considered as a larger group which contains signals that are either endogenous “alarmins” or exogenous “PAMPs” (Bianchi 2007). ATP, DNA, ROS species, HMGB1, and il-33 are considered as the main endogenous alarmins which are secreted post injury and stimulate the

immune response. These secreted alarmins bind to several family members of pattern recognition receptors (PRR) which are either transmembrane such as Toll-like receptors (TLRs), or cytoplasmic such as NOD-like receptors (NLRs) (Takeuchi & Akira 2010). The PRR, along with the enzyme caspase1, and the adaptor protein apoptosis associated speck-like protein containing a caspase activation and recruitment domain (ASC), all together form an inflammasome (Sharma & Kanneganti 2016).

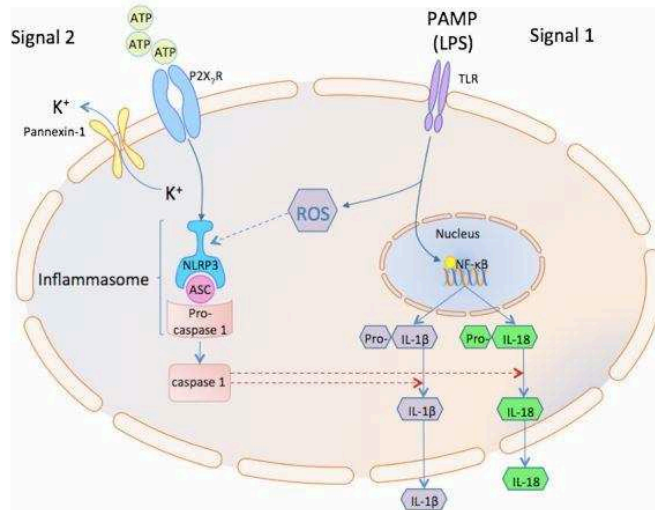


Figure 13: Mechanism of inflammasome activation through NLRP3 in myeloid cells.
 Reprinted from (Turner et al. 2014), BMC Nephrology, Licensee BioMed Central Ltd., 2014.

One example of the activation of an inflammasome is the NLRP3 inflammasome, a cytoplasmic NLR. The stimulation of TLR induces an NFκB-dependent signaling pathway resulting in the production of pro-IL-1β and pro-IL-18 in myeloid cells (Turner et al. 2014) (**Figure 13**). In parallel, the damage leads to an increase in ATP release into the extracellular space and thus stimulates the P2X₇ receptor (Sperlágh & Illes 2014). This receptor will then aid the assembly of the NLRP3 inflammasome and activate caspase 1 after auto-cleavage and activation of pro-caspase-1. Activated caspase-1 will then cleave pro-IL-1β and pro-IL-18 to their active forms. This could also be activated by the NF-κB pathway and the release of IL-1β and IL-18 due to binding of tumor necrosis factor (TNF) or IL-1α which are expressed post injury. Another alarmin example is High-Mobility Group Protein B1 (HMGB1), a nuclear DNA-binding protein found in all cell types of the CNS and functions in processes as DNA replication and transcription (Hong et al. 2013). Post injury, HMGB1 is released into the extracellular area, where it functions as a cytokine

and stimulates activation and signaling through the TLR4 and RAGE receptors to induce migration, proliferation, and differentiation of immune cells (Martinotti et al. 2015). In the CNS, the HMGB1 has a major impact on chemokine production in astrocytes, especially neutrophil chemo-attractants such as CXCL1, CXCL2, and CCL3 and T-cell chemo-attractants such as CCL2, CCL5, and CX3CL1.

Neutrophils: Post injury, neutrophils are considered as the first leukocytes to arrive on scene in order to kill pathogens and remove cellular debris (Rosales et al. 2016). These neutrophils appear within the first few hours post injury. In TBI, neutrophils enter in the parenchyma of the brain with highest recruitment at 24 hours post injury (Soares et al. 1995). Same observation was seen in SCI, as neutrophils enter the SCI and phagocyte cellular debris with maximum activation and infiltration at 24 hours post injury (Taoka et al. 1997). As previously mentioned, one main cause of recruitment of neutrophils is the release of DAMPS and activation of inflammasomes. Neutrophils, especially distant ones, are attracted via CXCL-chemokines, mainly CXCL8 (or IL-8) which binds to CXCR2 receptor found on neutrophils (de Oliveira et al. 2013). More recently, Sawant et al. showed that the chemokine CXCL1 can also be implicated in neutrophil recruitment and not only CXCL8 (Sawant et al. 2016). Within the injury site, the neutrophils have three mode of actions in an aim to compensate the consequences of trauma and aid in promoting tissue repair: a) phagocytosis of cellular debris and necrotic cells, b) release of effector molecules that will help in angiogenesis and regeneration, and c) become apoptotic neutrophils, to be phagocytized by cells such as macrophages in order to release reparative cytokines such as TGF- β and interleukin-10 (IL-10) (Wang 2018). Neutrophils also play a role in the recruitment of other immune system cells to the injury site via secretion of immunoregulatory cytokines such as interferon (IFN)-gamma, which is responsible for the recruitment of macrophages (Mantovani et al. 2011).

Infiltrating (macrophages) and resident (microglia) myeloid cells: Within the first few hours post trauma, monocytes infiltrate the injured environment and last for up to few days. It has been long believed that the microglia are the immune cells of the CNS. In fact, within studies regarding the CNS, there was never any differentiation between macrophages and microglia. They are always considered as the same population of cells, except that the microglia are the resident cells, and macrophages are the infiltrating ones. Microglia, along with perivascular macrophages, meningeal macrophages, macrophages of the choroid plexus, and macrophages of the

circumventricular organs are all considered as the macrophage population of the CNS (Perry & Teeling 2013). Macrophages exhibit what is known as M1 (pro-inflammatory) and M2 (anti-inflammatory) phenotypes. While M2 is induced by cytokines IL-4 or IL-13, the M1 phenotype is induced by IFN-gamma and factors such as lipopolysaccharide (LPS) or TNF (Ferrante & Leibovich 2012). Upon injury, the resident microglia are among the first responders to enter and accumulate in the damaged area. As previously discussed, after injury, microglia become activated and are amoeboid round-shaped with an enlarged cell body and accumulate with increased numbers within the injured site. This accumulation results in release of several various bioactive molecules which are either cytotoxic (pro-inflammatory) or regenerative. Such factors, along with the BBB damage, facilitate the entrance of macrophages into the injured environment. Both active microglia and infiltrating macrophages can contribute to the continuous damage within the injury site. For example, the increase in TNF expression stimulates the present microglia to produce glutamate. The excessive amount of glutamate leads to an excitotoxicity death of neurons (Maezawa & Jin 2010). Other mechanisms by which microglia can kill neurons include: release of TNF α , release of cathepsin, and phagocytosis of stressed neurons (Brown & Vilalta 2015). In addition, macrophages are believed to cause death to neurons post injury by releasing molecules such as iNOS and free radicals which in turn contribute to secondary injury and neuronal death (O'Connell & Littleton-Kearney 2013). The CX3CR1 signaling cascade in microglia and macrophages leads to intensive inflammation and harm post SCI. Blocking of the CX3CR1 signaling cascade led to an anti-inflammatory effect by reducing inflammatory signaling in microglia and monocyte derived macrophages which are involved in a mouse spinal cord injury model (Donnelly et al. 2011). On the contrary, microglia/macrophages have also been shown to be implicated in tissue protection and regeneration post CNS injury. Colton discussed the crucial immune role of macrophages/microglia in the clearance of cellular debris post trauma, in addition to reduction of self-toxicity and reconstruction of the damaged extracellular matrix within the brain (Colton 2009). Macrophages were also shown to secrete growth promoting molecules such as oncomodulin, which is implicated in axon regeneration (Yin et al. 2006).

Astrocytes: Astrocytes are activated and implicated in the subacute phase of the injury, the period starting just after impact and lasting until almost a week after. In an aim to limit the inflammatory consequences, astrocytes function in two general mechanisms: forming a “physical” barrier around the injury, and generating a “molecular” barrier by communicating and regulating

the action of infiltrating immune cells (Cekanaviciute & Buckwalter 2016). The physical barrier is achieved by forming a wall constituted of bundles of reactive astrocytes, which together along with the extracellular matrix (ECM) components physically surround the injured tissue (Wanner et al. 2013). Also, the astrocytes upregulate the expression of ECM proteins such as vimentin. But one main ECM protein, chondroitin sulfate proteoglycan (CSPGs), works together with the polarized astrocytes to form a tight barrier that restricts the physical communication of cells within the injury site, and the surrounding. Although the physical barrier (astrocytic barrier) has an important role in controlling the inflammation by sequestering the injured area and not allowing the spread of injury to remaining viable cells, it is also believed that the long-term persistence of this scar is disadvantageous by preventing axonal regrowth and neuronal regeneration. This is mainly observed in the role of CSPG which contributes to inhibiting neurite outgrowth (Monnier et al. 2003).

The molecular barrier produced by astrocytes post injury is accomplished by communication and interaction with cells such as resident microglia and infiltrating macrophages through chemokine and cytokine secretion. Due to their ability to sense and react with neuronal disruption and immune response at the same time, astrocytes have become major determinants of the size and extent of immune response post injury. The role of these secretions are quite contradicting in the sense that some cytokines released by astrocytes have a pro-inflammatory role, while others have an anti-inflammatory one. For example, activated astrocytes, release high levels of TNF- α , which in turn stimulates the pro-inflammatory activation of microglia to phagocyte neurons and induce neuronal death (Neniskyte et al. 2014). On the contrary, and under same injury conditions, astrocytes also have the ability to secrete anti-inflammatory cytokines such as IL-10 (Kelly et al. 2001) and TGF- β . This impact of astrocytes on chemokine and cytokine secretion may be in an indirect manner, meaning that the effect may not be on the astrocytes themselves. For example, astrocytes can result in an activation state of microglia, which then have the possibility to release several chemokines such as CCL2 and CXCL1.

T-Cells/Adaptive immunity: Few days post trauma, and lasting up to weeks, lymphocytes infiltrate into the injury site. CD2 and CD8 positive T-lymphocytes, essential constituents of the adaptive immune system, were shown to infiltrate into the injury site of a rodent SCI model (Gattlen et al. 2016)(Sroga et al. 2003). In 1996, Popovich et al. showed that these cells have a

detrimental role after their infiltration into the injury area such as autoimmune reactions to myelin proteins (Popovich et al. 1996). However, they also can have a beneficial role, as seen in their communication and interaction of T-cells with injured neurons, leading to a neuroprotective effect after injury. Also, the stimulation of T cells in-vitro lead to an increase in the production of several endogenous neurotrophins, including BDNF which is implicated in neuroprotection (Kerschensteiner et al. 1999) (Linker et al. 2010). In addition, CD4+ T cells have the potential to interact with myeloid cells infiltrating in the injury. They can promote the acquiring of an M2 anti-inflammatory phenotype by the secretion of IL-4 and IL-13 to the myeloid cells (Walsh et al. 2014). These myeloid cells can then produce neuroprotective molecules such as TGF- β to stimulate protection in neurons (Figure 14).

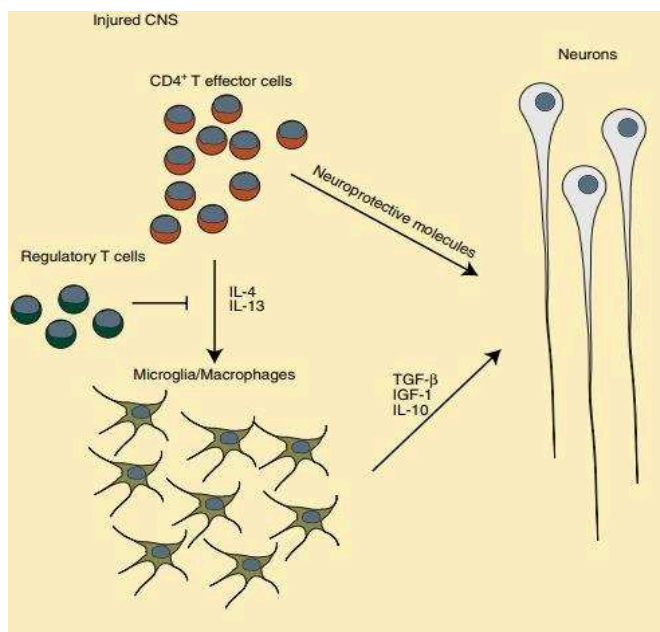


Figure 14: Neuroprotective modes of action of T-cell in CNS injury. Reprinted/Reused from (Walsh et al. 2014), “T cells in the central nervous system: messengers of destruction or purveyors of protection?”, Immunology, Copyright (2014), with permission from John Wiley and Sons.

Mass Spectrometry Imaging

Mass spectrometry imaging (MSI) is a technique used to visualize the spatial distribution of molecules along with their expression intensities collected within spectra. MSI allows to simultaneously measure hundreds of molecules within one single experiment. Several ionization sources are used by MSI setups, but mainly laser and secondary ionization are the dominant. Briefly, the laser will raster throughout a manually designated area covering the region of interest

(ROI) within a tissue and with specified spatial resolution. Within each raster point in the ROI, a mass spectrum and corresponding coordinates are simultaneously collected and then processed to what is known as a pixel. Each spectrum will contain a wide distribution of peaks within a previously specified mass range corresponding to several species of different analytes such as metabolites, lipids, peptides, and proteins (Julien Franck et al. 2009). The collection of pixels yields a molecular ion image in which the spatial distribution of molecules can be detected across the complete ROI. Post imaging, the ions are detected from the collected pixels based on their corresponding mass-to-charge (m/z) ratio. Within each pixel containing a spectrum, all m/z values are plotted along the x-axis, and the relative intensity of the m/z are plotted against the y-axis. For each m/z value, the intensity distribution corresponding to this m/z within the ROI can be visualized across all mass spectra from all collected pixels as a pseudo colored image, or m/z image (Alexandrov et al. 2013). Each pixel is colored based on the intensity of this m/z value within the spectrum, and thus it is considered that the MS data are a hyperspectral image of thousands of spectral channels. An MSI instrument is mainly constituted of the following: ion source, mass analyzer, detector, and software analyzer (Cameron 2012).

The quality of the generated images is controlled by several parameters which differ from one MS setup to another: mass accuracy, mass resolution, and spatial resolution. Mass accuracy is the extent of accordance between the measured mass of an m/z ion with its theoretical mass. Mass resolution is the minimum difference that allows to separate between two mass peaks of equal height and width (G Marshall et al. 2013). This parameter is essential in proteomic studies, especially shotgun proteomics, where tens of thousands of peptides are analyzed in consecutive chromatographic elutions. If instruments with low resolution are used, then peptides with similar m/z , which co-elute at the same time, will be overlapped in the MS analysis and thus prevent from accurate mass analysis, accurate charge state determination, and accurate quantitation (Mann & Kelleher 2008). This could mask the identification of peptides and thus result in the non-identification of the corresponding proteins which are involved in a studied biological case. Finally, spatial resolution or lateral resolution, is the center-to-center distance between two consecutive pixels while acquiring of an image. The spatial resolution can be of major importance for the nature of molecular information which can be obtained, along with the histological annotation, especially when dealing with blind sample experimentations or cancer tissue margins. This spatial resolution depends on the sample preparation and type of ion source used. One

example on the impact of spatial resolution on the quality of m/z ion images is found in **Figure 15**.

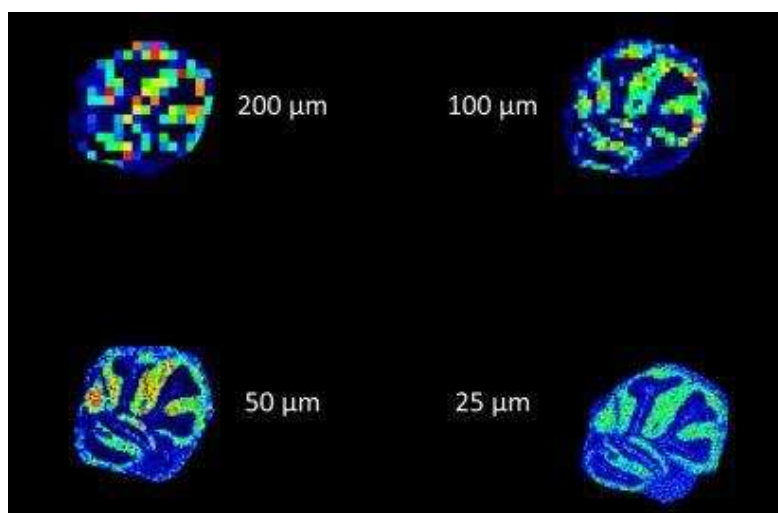


Figure 15: Ion images at m/z 6765 of serial sectioned mouse brain (cerebellum region) acquired at different spatial resolutions (200, 100, 50, and 25 μm) using MALDI MSI. Reprinted (adapted) from (Norris & Caprioli 2013), with permission from Chemical Reviews, Copyright 2013, American Chemical Society.

Based on sample preparation, and criteria previously discussed, along with others such as sensitivity and mass range, several ionization methods have been developed with wide application in different fields of study. The three main ionization methods used in MSI are: SIMS, DESI, and MALDI (Gemperline et al. 2014) .

Secondary ion mass spectrometry (SIMS) imaging is considered as the “oldest” mass spectrometry imaging technique and was first applied on imaging of surface metals in 1962 (Castaing & Slodzian 1962). Briefly, under vacuum conditions, a primary beam of ions bombard the surface of the tissue yielding the ejection of molecules and atoms. While most of the ejected population is neutral, many are ionized and poses either a positive or negative charge and are thus termed as secondary ions or droplets (Gamble & Anderton 2016) (**figure 16**). Several primary ions exist but most used are noble gases and oxygen. These secondary ions are then analyzed in the mass analyzer based on their m/z ratio. Although modern advancement in SIMS such as nano-SIMS imaging has allowed to perform images with high lateral resolution (< 100 nm), this imaging technique is considered as a harsh ionization technique (Boughton et al. 2016). Due to the high energy which is transferred during the impact of the primary ion beam, the analytes can undergo

fragmentation and loss, resulting in a decrease in chemical specificity and distribution. In other means, this technique is not suitable for analysis of biological macromolecules because of the high energy beam which can dissociate such analytes before being analyzed in the MS instrument. SIMS is mainly used for the detection of lipids, biologically small particles (such as drugs), and elemental ions (Bodzon-Kulakowska & Suder 2016).

Although, no additional sample preparation is needed in SIMS, several optional methods have been developed in an approach to extend the detection mass range of the SIMS, along with the improvement of signal intensity. Altelaar et al., showed that modifying the surface to be analyzed either by addition of matrix, matrix-enhanced SIMS (ME-SIMS), or by adding a layer of metal such as gold (MetA-SIMS) leads to the improvement signal intensity in images conducted at single-cell and tissue levels (Altelaar et al. 2006). There is two main modes of action for SIMS: dynamic and static. Dynamic SIMS uses high energy in the primary ion beam yielding large amount of secondary ions, and leading to total destruction of the sampling area. This is mainly used while analyzing elements in minerals to obtain compositional information with respect to depth. On the other hand, static SIMS uses lower energy ion beams such as Ga or Cs, and is mainly used for analysis of atomic monolayers.

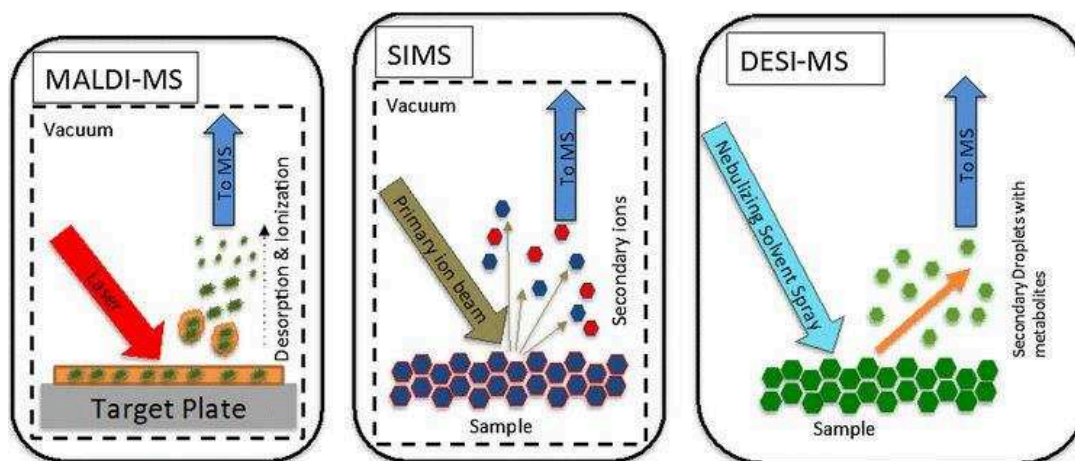


Figure 16: Different ionization methods used in MSI, mainly MALDI-MS, SIMS, and DESI-MS. Reprinted by permission from Springer Nature Customer Service Centre GmbH, Springer Nature, Phytochemistry Reviews, “The potential of mass spectrometry imaging in plant metabolomics: a review”, (Heyman & Dubery 2016), Copyright (2015).

Desorption electron spray ionization (DESI) imaging is one of the most used mass spectrometry setups that function under ambient conditions. Introduced in 2004, this technique

induces ionization by moving electrosprayed charged droplets onto the tissue surface to be analyzed (Takats 2004). The analytes are then dissolved within the thin liquid film that is produced over the surface. Secondary droplets which contain ionized analytes are then transported from the surface into the MS inlet (Figure 17). This setup is considered as a “soft” ionization method and is capable of producing multiple-charged ions of molecules such as proteins which fall in the higher mass range. In fact, DESI is believed to be best functioning in a mass range limited to 2000 Da (Bodzon-Kulakowska & Suder 2016).

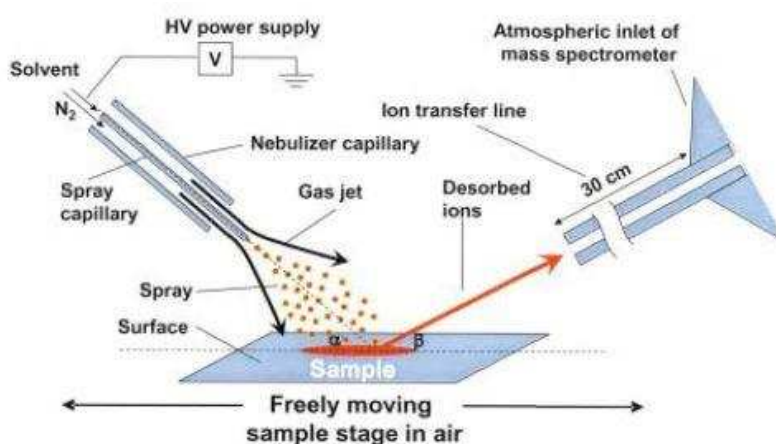


Figure 17: Schematic representation of DESI experimental setup.(Reprinted/Reused with permission from (Takats 2004)).

Although the considered normal spatial resolution of the DESI is approximately 200 μm (Wu et al. 2013), some groups have shown the possibility to optimize and obtain a resolution of 35 μm in biological samples by optimizing factors such as emitter capillary size, solvent flow rate, and step-size (Campbell et al. 2012). Several solvents can be used during DESI imaging including mixtures such of methanol:water and acetonitrile:water. One main advantage of this technique is the little amount of sample preparation required and all experiment procedures are performed under ambient conditions. Another main advantage, is that for molecules such as lipids, molecules may be directly identified by performing direct MS/MS fragmentation, along with their intensity measurement and spatial distribution (Bodzon-Kulakowska et al. 2015).

Matrix-assisted laser desorption ionization (MALDI) imaging was developed and applied on tissue by Richard Caprioli in 1997 (Caprioli et al. 1997) and is used in detection of molecules directly from the surface of samples (Fournier et al. 2003). The sample ionization does not lead to the direct fragmentation of molecules on the tissue surface, and is thus considered as a

“soft” ionization technique allowing to detect molecules with wide range of molecular weight, from hundreds of Da to more than 100 kDa (Franck et al. 2010; van Remoortere et al. 2010). This technique is characterized by depositing a matrix coat on the surface of the sample. This matrix coat, which is developed to absorb the energy from a pulsed laser beam, incorporates the targeted analytes within its formed matrix crystals. Thus, after irradiation of the surface with a laser beam, the energy is absorbed into the analyte-containing crystals which leads to their desorption and ionization. Eventually, the absorbed energy causes an explosive desorption of the matrix crystals along with all charged molecules within the irradiated area and these in turn accelerate from the source towards the mass analyzer, all under vacuum conditions. These charged molecules include the charged analytes, their alkali metal adducts, and neutral species. Most MALDI sources use UV lasers such as N_2 or frequency-tripled neodymium-doped yttrium aluminum garnet (Nd:YAG) lasers.

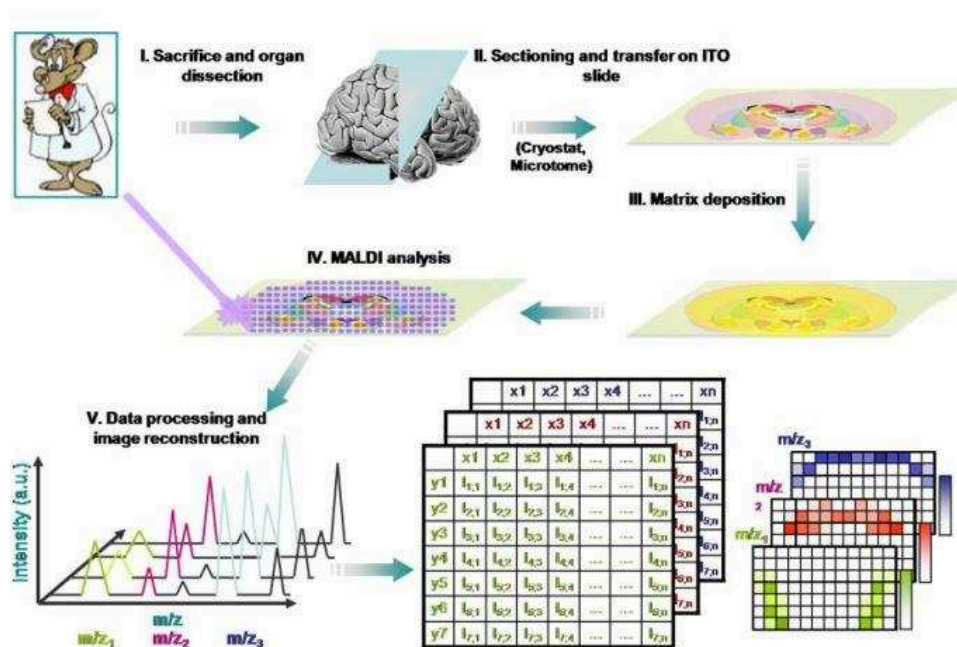


Figure 18: MALDI-MSI workflow. The complete process is presented, starting with animal sacrifice, then sectioning of the organ to be analyzed and cryosectioned on glass slides. Then, matrix is deposited on the tissue and MALDI acquisition is performed. Finally, data processing is performed and the distribution of different m/z can be visualized across all selected acquired pixels. Reprinted/Reused from (Julien Franck et al. 2009) with permission from AMERICAN SOCIETY FOR BIOCHEMISTRY AND MOLECULAR BIOLOGY, Copyright 2009.

The standard workflow of MALDI-MSI is found in (**Figure 18**). After the complete organ is collected, it is cut by means of cryosectioning in a micro-meter thickness scale using systems such as cryostat or microtome, and these sections are then mounted on glass slides (Wisztorski et al. 2010). The tissue thickness has major effect on peak intensity and signal-to-noise ratio (SUGIURA et al. 2006). Surprisingly, thinner tissue sections (<10 μm) showed an increased number of observed peaks and relevant peak intensity when compared to thicker ones (approximately 40 μm). After mounting the tissue on the slide, a layer of matrix is deposited on the tissue sample with in an aim to form an organic crystallized layer that incorporates the desired analytes to be analyzed. The crystallization step is important for analyte incorporation and resolution. Characteristics of obtained crystals (especially their size) depend on several factors including the solvent, time of incubation, and matrix concentration (Römpf & Spengler 2013; Lemaire, Wisztorski, et al. 2006; Lemaire, Tabet, et al. 2006). With the presence of conventional automated sprayers, factors such as time of incubation and spray nebulizing power are controllable. By such means, there are four main matrix deposition methods: manual spray, robotic spray, sublimation, and automated spotting (J. Franck et al. 2009; Norris & Caprioli 2013). Manual spray utilizes a pneumatic sprayer to apply a coat of matrix over the complete tissue. Although this deposition method is relevantly cheap and easy to be accessed in the laboratory, it can have several drawbacks such as inconsistency and reproducibility for matrix deposition across several tissue samples. The robotic method is a controlled automated device which can spray matrix in a repeatable and programmable manner. Several companies have commercialized devices such as the ImagePrep (Bruker Daltonics) and the TM sprayer (HTX technologies). Using such devices, parameters such as the chamber temperature, amount of deposited matrix, and others are controllable and adjustable. Sublimation was first performed to apply a uniform matrix layer for the analysis of lipids (Hankin et al. 2007; Meriaux et al. 2010), but was later on developed for the analysis of other analyte classes such as proteins (Yang & Caprioli 2011) owing the fact that common organic MALDI matrices can undergo sublimation without decaying under vacuum pressure and elevated temperature. Briefly, once the chamber is evacuated of air, heat is applied to the matrix which will lead to its transition from solid phase to a vapor one. Upon the subliming of the matrix, it will strike and condense on the surface containing the sample which is previously cooled returning to its solid state, yielding a fine and homogenous deposition of matrix across the complete tissue. The low cost of such technique, and controllable matrix thickness deposition,

which is adjusted by adjusting the time, make such a matrix deposition method very popular. Finally, automated spotters prepare samples by coating the tissue with regularly spaced droplets. Thus, by such techniques, the image resolution is controlled by the droplet deposition resolution rather than by the raster spacing. Most developed machines such as the ChIP-1000 (Shimadzu Scientific Instruments) are equipped with a scanner and software to mark the desired region of matrix deposition (J. Franck et al. 2009).

Matrix selection is of crucial importance for the successful analysis of different analyte classes. Several organic matrices have been developed including: α -Cyano-4-hydroxycinnamic acid (CHCA), sinapinic acid (SA), and 2,5-dihydroxybenzoic acid (DHB). While SA is commonly used for the MSI imaging of high molecular weight proteins, CHCA is used for lower molecular weight peptides (Schwartz et al. 2003), and DHB is routinely used for analysis of lipids in both positive and negative ionization mode (Jackson et al. 2005). Dissolving such matrices with the proper organic solvents, in addition to an acidic solution, allows the extraction of analytes from the surface of the tissue and their incorporation into the deposited matrix layer. This matrix layer, containing acid, serves to maintain the proton, cation, and electron transfer process that yields the formation of single-charged species which are detected in the MS analyzer. More recently, ionic liquid matrices have been introduced and applied in MALDI MSI with an aim to reduce the effect of non-heterogeneous deposition of matrices on tissue and thus affecting the spatial resolution. Addition of organic base 3-acetylpyridine to 2,5-DHB matrix yielded an ionic liquid matrix that was homogeneously applied on the sample, required less sample preparation time when compared to 2,5-DHB matrix alone, and successfully generated positive and negative ion mode images (Meriaux et al. 2010).

Finally, after the sample is prepared by the optimized matrix selection and deposition method, laser rastering is performed, and point by point spectra are collected across the whole sample to generate a grid of points/pixels. This grid is then converted into spatial coordinates after the complete acquisition is done. The m/z image is then generated by displaying the intensity of the ion at a selected m/z value. Example of m/z ion images of rat cerebellum are found in **figure 19**.

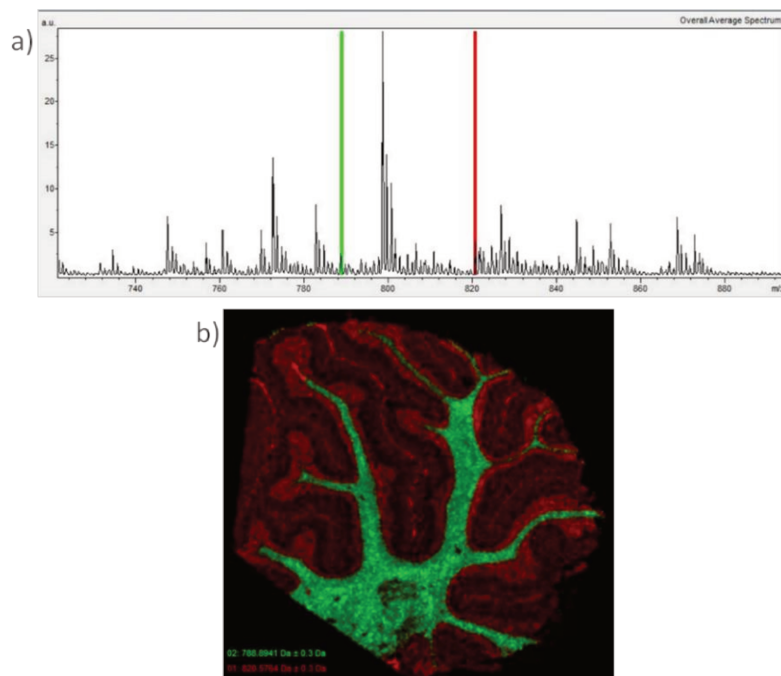


Figure 19: A) Average spectrum of acquired ion image on rat cerebellum. B) MALDI TOF ion image of rat cerebellum showing m/z 788 (green) and m/z 820 (red). The matrix was deposited using sublimation and spatial resolution was at 30 μm . Source: Khalil Mallah, experiment conducted in PRISM laboratory.

Several mass analyzers can be linked to the MALDI source mainly including the time-of-flight (TOF) and Orbitrap. For the TOF, in a drift tube placed under vacuum, the MALDI source is placed at one end of the tube, and the detector is found on the opposite end. Ions are separated based on their time to pass a defined distance within the tube from the MALDI source to the detector. The velocity of the ions is dependent on its m/z ratio and thus the later can be detected. In addition, due to its high mass resolution, MALDI orbitrap instruments have become commonly used in applications such as drug detection (Ostermann et al. 2014) , peptides (Quanico et al. 2013a) and lipidomic analysis (Moreno-Gordaliza et al. 2017).

Proteomics

Coming from the two words “**protein**” and “**genomics**”, proteomics is the field of study concerning the identification and quantification of all proteins within a proteome (Zhang et al. 2013). This also includes cellular localization, post-translational modifications (PTMs), interaction in-between proteins, and the global biological pathways in which they participate in. Advances in mass spectrometry have evolved the field of proteomics and have had major impact on several breakthrough discoveries. The use of chromatography separation systems, “soft” ionization

sources such as MALDI or electron spray ionization (ESI) (Fenn et al. 1989), and tandem mass spectrometry have yielded the identification and characterization of large biomolecules such as proteins and peptides. In fact, two main approaches have been characterized for the study of proteins: bottom-up (shotgun) and top-down (**Figure 20**). Bottom-up approach identifies proteins based on the analysis of liberated peptides post enzymatic digestion of intact proteins, usually using trypsin. When dealing with a mixture of proteins, the bottom-up approach is also annotated as “shotgun proteomics” (Yates 2004). Briefly, after protein extraction, an optional protein separation step is possible by techniques such as 2D gel electrophoresis or liquid chromatography. Although this step is not mandatory, it can be used for a targeted approach against a protein of known molecular weight. After, proteolytic digestion is applied, usually using trypsin enzyme yielding to a mixture of peptides. This mixture is then separated by liquid chromatography and subjected to tandem mass spectrometry, i.e. MS/MS fragmentation. After obtaining the tandem mass spectra, peptide identification is performed by comparing these spectra to theoretical tandem mass spectra previously obtained from *in silico* digestion of a protein database. The final step, is protein assignment based on the identified peptides. These peptide fragments are computationally matched with the complete sequences of all known proteins within the organism to obtain potential protein identities. To further confirm the identified proteins, several parameters are taken into consideration, including the number of peptides per protein, along with the peptide confidence and length.

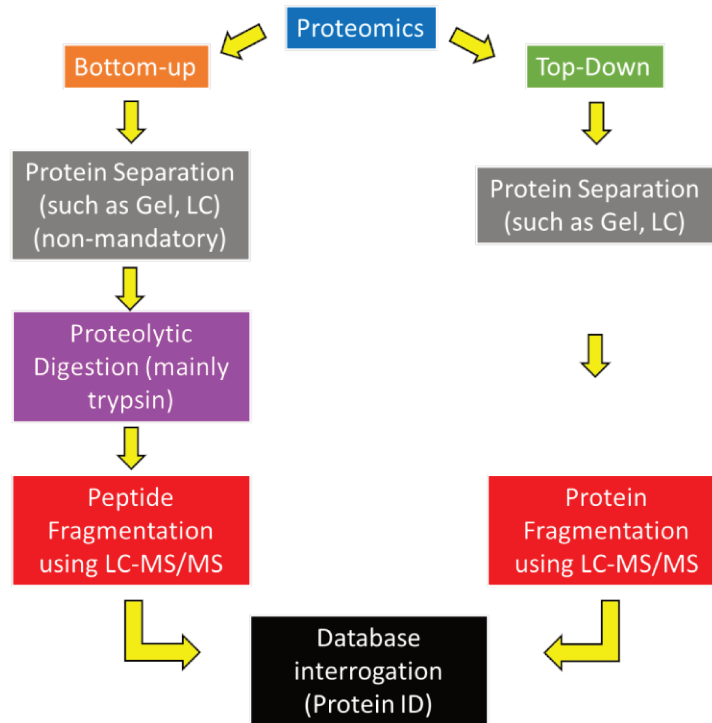


Figure 20: Proteomic approaches most commonly used: bottom-up and top-down. Source: Khalil Mallah

The top-down approach is used for the identification of intact proteins, with a main advantage of detecting and studying PTMs. However, this method is very challenging by facing difficulties such as protein fractionation, protein ionization, and fragmentation in the gas phase (Zhang et al. 2013). Briefly, the intact proteins are first separated using techniques such as gel or liquid chromatography. The separated proteins are then directly fractionated again in LC and injected into the mass spectrometer, and subjected to MS/MS analysis. The protein tandem mass spectra are then interrogated with a previously acquired database. Although bottom-up proteomics is the most commonly used approach, the obtained peptides are more or less redundant between several proteins, especially isoforms, and thus lead to difficulties in differentiation between them. In addition to such set back in bottom-up proteomics, and the difficulty of performing Top-down proteomics due to the previously mentioned reasons, more recently, middle-down proteomics has emerged in an aim to solve such problems of these two approaches. As an example, by using outer membrane protease T, we can obtain larger sized peptide fragments (>6.3 kDa), and thus decrease the redundancy of peptides between protein identification (Wu et al. 2012). In addition, such

fragments can also give information on the PTMs which are mainly obtained in top-down proteomics.

With many studies being conducted on limited tissue size or small liquid samples, microproteomic techniques have been developed. Specific tissues, as in the case of several cancer cases, are microscopically small and very heterogeneous. Thus the study of proteomic changes in such non-uniform regions of interest, requires dissection and protein extraction from very small surface area (Gutstein et al. 2008). Such developed techniques include: laser capture microdissection, liquid microjunction extraction, and parafilm-assisted microdissection.

Laser Capture Microdissection (LCM) is a technique mainly used for isolation of heterogeneous cell population and morphological criteria recognition (Mustafa et al. 2008). There are two main types of lasers used in LCM: infrared (IR) and ultraviolet (UV) (Chung & Shen 2015). Briefly, a pulse of laser will shoot at the designated target within the tissue and eject the region of interest from its position. This is then captured on a membrane/film placed just above the tissue (**Figure 21**). After obtaining the tissue extracts, one of the previously mentioned proteomic approaches (bottom, middle, or top down) can be applied for the protein identification. The main advantage of LCM is its ability to cut out and isolate up to cellular level, or even at the subcellular level as it was shown that LCM has the capability to isolate cell organelles such as the mitochondria (Pflugradt et al. 2011). In addition, the time needed for isolation is very short when compared to other dissection methods, and LCM preserves tissue morphology during the dissection process. On the contrary, the biggest disadvantage for such technique is the cost. In fact, the price of an LCM along with its corresponding microscope can exceed 1 million dollars (Chung & Shen 2015). Such high price makes this instrument very difficult to obtain in most public research facilities. Another major disadvantage is the amount of cells required to be able to conduct a proteomics investigation. Thus several captures from consecutive tissues would need to be combined in order to obtain enough protein concentration for a proteomics analysis.

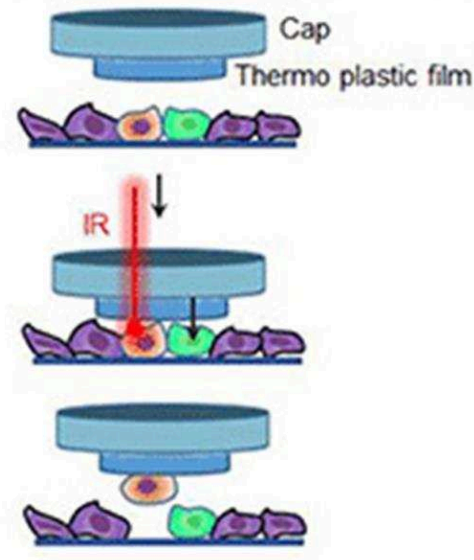


Figure 21: Principle of Laser capture microdissection. Reprinted/Adapted from (Hu et al. 2016), *Frontiers in Cell and Development Biology*.

Parafilm Assisted Microdissection (PAM): this technique was introduced in 2013 by Franck et. al., as a tissue extraction technique for small surface areas (Franck et al. 2013). Tissue sections are mounted on a previously parafilm M-covered glass slide. Then, manual dissection of a region of interest can be performed under microscope using a scalpel (**Figure 22**). Franck et al used several surface areas from three regions of interest (ROI1 = 3.4 mm², ROI2 = 2.86 mm², ROI3 = 1.77 mm²) to perform protein identification and quantification using spectral counting as label-free quantification. This quantification gave the possibility to perform protein imaging of the tissue based on the obtained results. The extracted regions can be used for digestion and obtaining a mixture of peptides which will be analyzed by LC/MS-MS and protein identification. Or, intact proteins can be extracted to study the PTMs. The main advantage of this technique is the lost cost and the rapid microdissection time. There is no need for any state-of-art tools to perform such microextraction. This technique was later used as part of a workflow for the identification of prostate cancer protein biomarkers (Quanico et al. 2015).

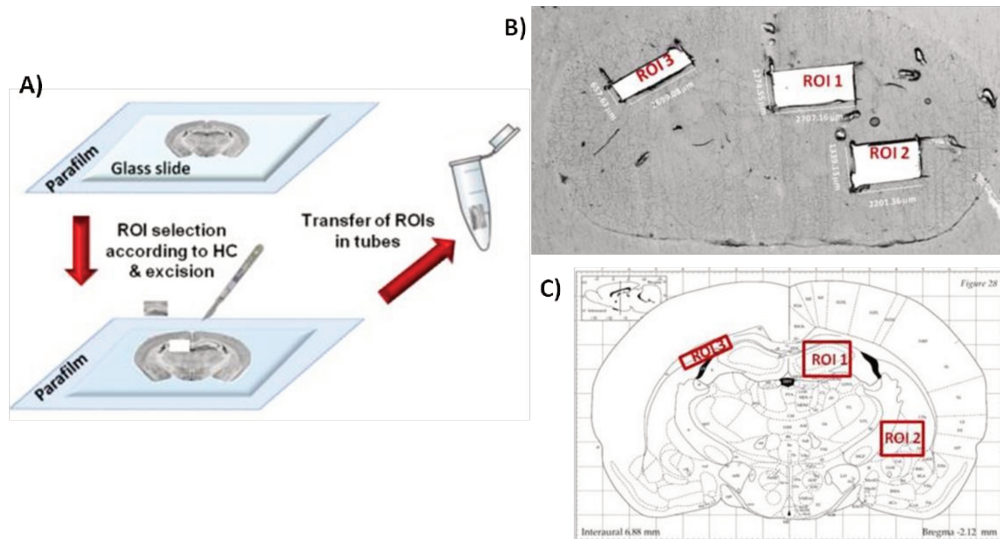


Figure 22: A) Schematic drawing of PAM approach to manually dissect region of interest. B) Optical image of a rat brain where several regions of interest were extracted. C) Atlas figure of rat brain along with the theoretical position of extracted region of interest. Reprinted (Adapted) from (Franck et al. 2013) with permission from Analytical Chemistry, Copyright 2013, American Chemical Society.

Liquid Microjunction Extraction (LMJ): Presented in 2013 by Quanico et. al, LMJ allowed the identification of proteins while maintaining their localization within the tissue (Quanico et al. 2013b). This technique yielded the identification of around 1500 proteins with high confidence from a tissue surface area of 650 μm diameter, corresponding to almost 1900 cells. Briefly, direct on-tissue digestion is performed at a targeted site, and digested peptides are then micro-extracted using a liquid micro-junction interface by depositing and aspirating several solvents including methanol, acetonitrile, and tri-fluoroacetic acid. The technique was used during my studies and the workflow is found in the figure below (**Figure 23**). After extraction, the peptides are then subjected to LC-MS/MS analysis and protein identification similar to the steps in the bottom-up approach, after obtaining a peptide mixture.

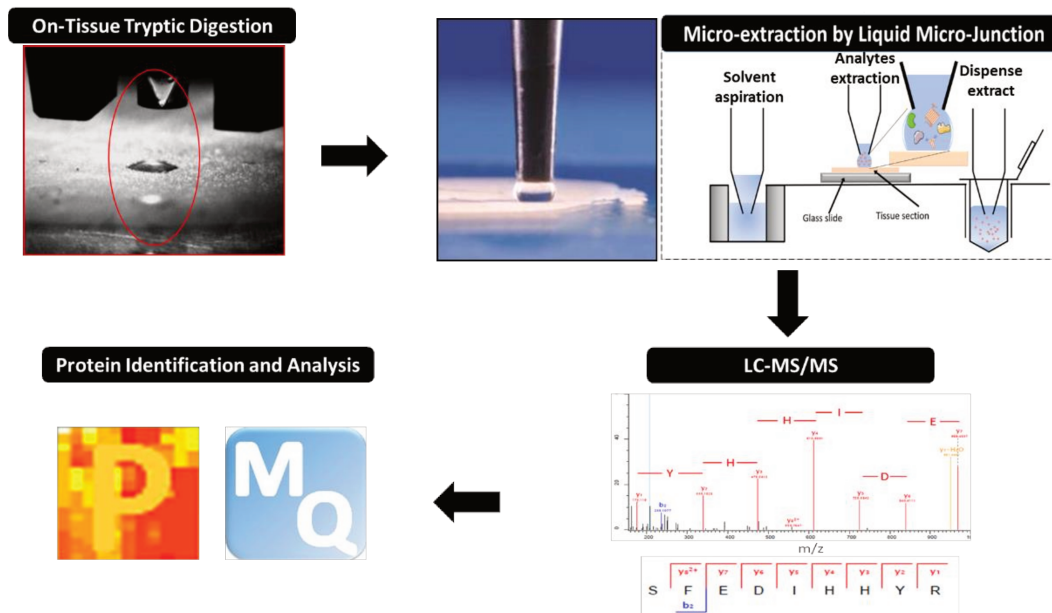


Figure 23: Workflow of LMJ. First, localized on-tryptic microdigestion is performed. Digested peptides are then collected using LESA instrumentation. Collected peptides are then subjected to LC-MS/MS analysis followed by protein identification and analysis.

This technique was later on developed and applied on FFPE tissues (Wisztorski et al. 2013). This did not involve performing on-tissue tryptic digestion, and liquid junction extraction using methanol and acetonitrile. Instead, conventional detergents such as SDS were used to extract the region of interest with millimeter resolution and the extracts in turn were compatible with other experimental approaches such as western blot, as well as MS based proteomics. Using such extraction method, almost 1400 proteins were identified from a 1 mm² surface area on rat brain tissue. However Top-down proteomic can also be conducted using LMJ and PAM technologies in order to get access to identification of intact proteins along with their PTMs (Delcourt et al. 2018; Delcourt et al. 2017).

Hypothesis:

In light of what has been mentioned, it is important to obtain a fundamental understanding of the underlying biological and molecular processes occurring in both TBI and SCI, along with the involvement of the body systems, especially the immune system, within these injuries. Such understanding is achieved by studying the different key players involved in the injury environment including lipids and proteins using novel state-of-the-art mass spectrometry (MS) technology. Studies like this open up potential therapeutic windows to help find a possible treatment to CNS injuries with an aim to restore neuron-related regeneration mechanisms such as nerve regeneration, astrocytosis, and promotion of axonal growth.

The thesis aims to respond to the following questions:

1. What are the spatio-temporal factors, including both lipids and proteins, which are involved after impact in TBI and SCI?
2. Can we find similar molecular and cellular features between TBI and SCI?
3. What type of cells are involved based on time manner post injury in both TBI and SCI? And which released factors impact such involved cells.
4. Can we find a therapeutic window or targets based on spatio-temporal lipid and proteomic data in TBI and SCI?

Objectives:

Two main objectives were set out for my thesis:

The **first** objective of my PhD focuses on understanding the underlying proteomic and lipid profile changes in the microenvironment of TBI. Using multiple omics technology, a spatial and temporal study was conducted on the acute and sub-acute phases of an open head rat injury model. In this context, high resolution MALDI mass spectrometry imaging was performed to monitor the different species of lipids distributed within the brain post injury, in addition to identifying injury specific lipids as possible biomarkers in TBI. Both 2-Dimensional and 3-Dimensional MALDI MSI were applied in order to obtain a better comprehension of the spatial distribution of such potential lipid biomarkers. In parallel, a large-scale microproteomic approach using tryptic microdigestion followed by LC-MS/MS was applied on the injured brain to detect the proteomic processes occurring within the micro-injured area. The obtained identified proteins were subjected

to systems biology protein pathway analysis to have a global picture of the involvement of such proteins in the outcome of the injured brain.

The **second** objective within my PhD studies focuses on SCI. PRISM U1192 has previously performed a spatio-temporal proteomic study on a rat model of SCI. Results yielded several potential proteomic pathways to target in therapy such as the MEMO1-RHOA-DIAPH1 which is implicated in the injury. In addition, several protein families involved in the injury were identified including immunoglobulins IgG. During my studies I aimed to study the effect of RhoA inhibitor in a therapeutic approach by studying its effect in-vitro on DRG cell lines and in-vivo on the rat injury model. Proteomic experiments were conducted followed by a systems biology analysis to visualize the protein processes involved along with their sub-cellular localization.

Chapter 1: 3D high-spectral resolution MALDI MSI applied to Traumatic Brain Injury

Introduction

Because biological samples exist in a 3D nature, it is believed that visualizing molecular distributions in 3D manner is more informative and yields results that cannot be achieved in 2D manner. 3D mass spectrometry imaging was first introduced in 2005 in an aim to visualize volumetric distribution of ions within tissue specimens, specifically in this case, protein expression in a mouse brain (Crecelius et al. 2005). This technique was based on reconstructing the 3D volume from serial sections MS imaged in 2D. While comparing with other techniques such as magnetic resonance imaging (MRI) and 3D immunohistochemistry, 3D MSI has many advantages. Mainly, 3D imaging requires no labelling, is an untargeted approach (meaning that hundreds of molecules can be detected with one single experiment), and sensitive (Palmer & Alexandrov 2015). One main disadvantage is the large size of the datasets that one 3D reconstruction requires. One MALDI-MSI image may contain up to millions of mass spectra, and thus require very challenging computational power and performance (Thiele et al. 2014).

From a biological point of view, especially in the case of model animal studies such as our TBI study, it is of high interest to be capable of determining the extent of the molecular changes without a priori in the surrounding of the injury site and not only restricting the study to morphological or histological features. Using high resolution MALDI-LTQ-Orbitrap-XL, we established, for the first time in TBI, a 3-Dimensional (3D) lipid ion image reconstruction of injured brains at 3 days post injury (Article 1). This 3D reconstruction and spatial segmentation served as a lipid molecular mirror of the injured brain. Further analysis in 3D manner allowed to depict lipid m/z ion species with common expression between the injured cortical tissue and the ventricular system of the brain, thus explaining a possible flow and transfer of lipid molecules between the injured cortical tissue and the spinal cord through the cerebrospinal fluid. In addition, certain m/z ion were unique to either the cortical tissue or the ventricular system.

**Reproduced with permission from the Journal of Analytical Chemistry. Copyright 2018.
American Chemical Society.**

**Article 1: Lipid Changes Associated with Traumatic Brain Injury Revealed
by 3D MALDI-MSI**

Authors: Khalil Mallah, Jusai Quanico, Dennis Trede, Firas Kobeissy, Kazem Zibara, Michel Salzet, and Isabelle Fournier.

Article Status: Published in Analytical Chemistry. 2018 Aug 2. DOI:
10.1021/acs.analchem.8b02682

Summary: All experimental manipulations, along with sample preparation and data analysis was performed by Mr. Mallah. He also participated in writing the paper, and participated in the revision. In detail, my contributions include:

- Performing the experimental TBI procedure and collection of tissue.
- MALDI-MSI experimentation and sample preparation including cryosectioning the tissue, matrix deposition and image acquisition on the MALDI-LTQ-XL Orbitrap instrument.
- Data processing on Scils software, including 3D image reconstruction, spatial segmentation, ROC analysis, coloc analysis, and principal component analysis.
- In terms of writing the manuscript, Mr. Mallah wrote the initial drafts which were then built upon in the subsequent writing of the final manuscript.

Lipid Changes Associated with Traumatic Brain Injury Revealed by 3D MALDI-MSI

Khalil Mallah,^{†,‡} Jusal Quanico,[†] Dennis Trede,[§] Firas Kobeissy,^{||} Kazem Zibara,[‡] Michel Salzet,^{*,†} and Isabelle Fournier^{*,†}

[†]INSERM, U1192 - Laboratoire Protéomique, Réponse Inflammatoire et Spectrométrie de Masse (PRISM), Université de Lille, F-59000 Lille, France

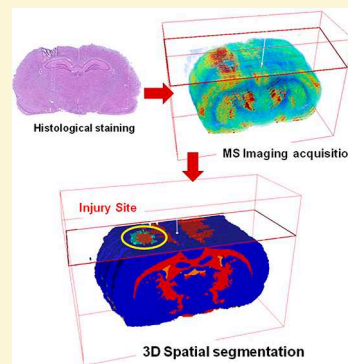
[‡]ER045, PRASE, Laboratory of Stem Cells, Department of Biology, Faculty of Sciences-I, Lebanese University, 6573-14 Beirut, Lebanon

[§]SCiLS, 28359 Bremen, Germany

^{||}Department of Biochemistry and Molecular Genetics, Faculty of Medicine, American University of Beirut, 1107 2020 Beirut, Lebanon

Supporting Information

ABSTRACT: Traumatic brain injury (TBI) is a major cause of death and disability in children and young adults worldwide according to the World Health Organization (WHO). The emergence of mass-spectrometry-based techniques, such as MALDI-MSI, has allowed the monitoring and visualization of changes post injury, providing a global picture of the impact of TBI on different classes of molecules in a single study. In this work, we show the ability to track lipid changes post-TBI by three-dimensional matrix-assisted laser desorption/ionization–mass-spectrometry imaging (MALDI-MSI). Controlled cortical impact (CCI) was induced on adult male rats resulting in direct mechanical injury to the cortical tissue on the right ipsilateral hemisphere of the brain. Images of lipid distribution in coronally sectioned injured brains were acquired using a high-resolution mass spectrometer (MALDI-LTQ-Orbitrap-XL). Results reveal unique lipid signatures for the injured cortical tissue, which further segregate into two subgroups of injury (lesion interior and lesion exterior). Although both subgroups show different profiles from that of the noninjured cortical tissue, the lesion interior is more similar to the ventricular system than the lesion exterior. For example, m/z 725.56 showed expression in both injured tissue and the ventricular system, whereas m/z 856.59 (phosphatidylcholine 42:9) is uniquely expressed in injured tissue. On the other hand, m/z 797.59 (also a phosphatidylcholine) showed unique expression to the ventricular system and not to the injured cortical tissue. Our results can help in further monitoring and identifying lesion-specific lipids in a 3D manner to obtain a better understanding and visualization of molecular and cellular events occurring post-TBI.



Traumatic brain injury (TBI) is an alteration in brain function due to the application of an external force to the brain, such as head strike, rapid acceleration or deceleration movement, or object penetration.¹ On average, the annual death rate due to TBI is 1.5 million people worldwide,² with men being at higher risk than women. TBI is not only restricted to an individual's health; it also expands to being a major financial burden for families.³

The neurological outcomes postinjury are divided into two main phases, namely, primary and secondary phases. Primary injury is due to direct mechanical insult resulting in direct damage or penetration of the underlying tissue and disruption of brain function. On the other hand, secondary injury occurs as a direct consequence of the primary injury; however, it is characterized by complex molecular mechanisms, such as altered metabolic changes, oxidative stress, ischemia, hypoxic damage, cerebral edema, and infection.⁴ This leads to cell death, inflammation due to the involvement of different

immune cells, and neurological dysfunction within injured patients.⁵

Many techniques have been used to visualize the main histological changes within the brain, aiming to follow up on patients post-TBI. For example, magnetic-resonance imaging (MRI) and computed-tomography (CT) scans allow one to visualize hemorrhages or even brain deformation.⁶ On the contrary, the lumbar-puncture method helps in analyzing the cerebrospinal fluid (CSF) when looking for molecular-signature markers. Because of a lack of information at the axonal-injury level with conventional techniques, diffusion-tensor-imaging (DTI) MRI was later introduced and applied to TBI in 2002.⁷ Although conventional MRI shows changes at the macroscopic level of the brain, DTI has the advantage of

Received: June 13, 2018

Accepted: August 2, 2018

Published: August 2, 2018

detecting microstructural changes, especially in the white matter.⁸ Indeed, the latter technique is highly sensitive to axonal-fiber injuries in the white matter of the brain, such as in the corpus callosum. However, this characteristic could also be a disadvantage because changes to other compartments of the brain with possible injury, mainly the cortex, could be difficult to visualize using such a technique. In the pursuit of a therapeutic window for TBI, protein biomarkers have been identified, mainly employing immunofluorescence (IF) techniques and other advanced proteomics-based techniques.^{9,10} However, proteins are not the only players involved in diseases and injuries. To better characterize pathophysiological outcomes post-TBI, a full understanding of the different molecules present must be considered.

With the advances of mass spectrometry in the field of mass-spectrometry imaging (MSI) such needed approaches are now possible. Among the different modalities of MSI, MALDI-MSI is currently the technology that offers the broadest panel of applications as a result of its ability to analyze a large variety of analytes, including small organics,¹¹ metabolites, and lipids^{12,13} as well as peptides and proteins in their intact forms,^{14–16} even providing cellular-level spatial resolution in routine experiments. Conventionally, MALDI-MSI is performed from a single tissue section, leading to the mapping of the analytes in the (*x*, *y*) plane. However, increases in the acquisition speed of MS instruments dedicated to MSI together with improvements in spatial resolution has led to the gradual development of 3D MSI, which corresponds to the reconstruction of 3D volumes from the 2D mapping of serial sections.¹⁷ 3D MSI is not a routine operation, because it requires a large amount of tissue sections, and thus, it is definitely not always required. However, it is very relevant in certain situations to monitor the extent of molecular changes when these cannot be gathered by other means. This is, for example, the case when studying physio-pathological situations in model organisms from which complete organs can be studied. In 2005, 3D MSI was initially performed on acquired protein-ion images of a complete mouse brain¹⁸ as a proof-of-concept, but 10 years of developments were required so that 3D MSI could be used for biological applications.¹⁹

Lipids are essential players in the central nervous system (CNS) because they support homeostasis and normal functioning of the brain.^{20,21} However, lipids and their associated metabolites are also known to be involved in inflammatory processes and are therefore of major importance in the cascade of secondary events occurring after brain injury.²² Certain lipids have been identified as drivers of inflammation, such as arachidonic acid, which is metabolized into prostaglandins (e.g., PGE2) and leukotrienes (e.g., LTA4, LTB4) and promotes the activation of the immune response. Although metabolic pathways of certain lipids have been well described for TBI, a more global picture enabling both the identification and localization of various lipids using untargeted approaches is also of interest and can help identify new targets. MALDI-MSI is particularly well-suited to monitor lipid molecular changes in the study of TBI. Previously, 2D MALDI-MSI was used to study TBI by several groups. Most studies dealt with lipid changes after brain injury using mouse and rat models subjected to controlled cortical-impact injury (CCI).^{23,24} Injured mice with sensorimotor and learning deficits showed decreased levels of cortical and cerebellar phosphatidylcholine (PC) and phosphatidylethanolamine (PE) levels, whereas hippocampal levels of PC, PE, and

sphingomyelin were elevated.²⁵ In addition, MALDI-MSI studies were used to investigate the ischemia–reperfusion injury model of TBI¹³ and showed a large increase in ion abundance at *m/z* 548.5, which corresponded to ceramide (d18:1/18:0), a lipid family known to be associated with the regulation of signaling processes including cellular apoptosis.²⁶ More recently, using a rat fluid-percussion model, Guo et al. studied lipid changes post-TBI in a time-course manner, but they used a developed liquid-extraction-ESSI device for MSI rather than MALDI-MSI.²⁷ Their findings suggest a role for docosahexaenoic acid (DHA) in brain injury, as they tracked elevated levels of DHA expression in the acute phase of injury (0 to 1 days post-trauma) and an increase of DHA-containing lipids, such as PE, in the chronic phase of injury (up to 7 days). Recently, Roux et al. used MALDI-MSI in time-course experiments post-TBI (CCI model) and revealed an increase in ceramides and a decrease in sphingomyelins, accompanied by changes in glycerophospholipids and cholesterol derivatives.²⁸ In these experiments, it was shown that each lipid class was presenting a distinct kinetics. For example, ceramides were increased as early as 1 day post injury, whereas other lipid changes were occurring between 3 and 7 days post injury.²⁸ The same research group has recently shown the advantage of using MALDI-MSI to track ceramide-related *m/z* ratios as biomarkers of injury with their potential role in monitoring the effects of injury and drug-treatment approaches.²⁹ Treatment of CCI-injured rats 3 days post injury with a dynorphin-binding “decoy peptide”, a peptide shown to prevent NMDA-mediated dynorphin neurotoxicity, leads to a significant reduction in four ceramide species (CER 34:1, 36:2, 36:1, and 38:1) when compared with the levels in non treated injured rats. This finding suggests the use of such ceramide species as lipid biomarkers in brain injury and therapeutic approaches.

In this study, 3D MALDI-MSI was applied, for the first time, to a controlled-cortical-impact (CCI)-TBI-rat-brain model, using high-resolution MS. 3D MALDI-MSI was used to assess the extension of the injury at the molecular level, which is not obtained by using conventional IHC or 2D MALDI-MSI. Indeed, we were looking for the molecular changes not only at the injury site but also at regions distant from the injury site as a result of brain plasticity. For this, adult male rats were subjected to CCI on the right cortical ipsilateral hemisphere and sacrificed 3 days post injury; 2D ion images were acquired from serially sectioned samples to reconstruct the 3D volumes. Combining this volume reconstruction with clustering was shown to be very useful in accessing changes in cell phenotypes in three dimensions and extracting the corresponding changes in lipid regulation.

■ EXPERIMENTAL SECTION

Reagents. Absolute methanol (MeOH), water (H₂O), chloroform (CHCl₃), analytical-reagent (AR)-grade trifluoroacetic acid (TFA), ethanol (EtOH), and xylene were obtained from Biosolve B. V. (Dieuze, France). 2,5-Dihydroxybenzoic acid (DHB) and a ProteoMass MALDI Calibration kit were purchased from Sigma-Aldrich (Saint-Quentin Fallavier, France). Mayer's Hemalun solution was purchased from Merck KGaA (Darmstadt, Germany), phloxine B was purchased from RAL Diagnostics (Martillac, France), and saffron was purchased from Labonor (Templemars, Belgium). EUKITT slide-mounting medium was bought from O. Kindler GmbH (Freiburg, Germany).

Animals. Procedures were performed on adult male Sprague–Dawley rats (225–250 g, 7–8 weeks old) in accordance with the National Institutes of Health Guidelines for Animal Research (Guide for the Care and Use of Laboratory Animals) and with the approval of the Institutional Animal Care and Use Committee (IACUC) at the American University of Beirut (AUB). Rats were maintained and housed under pathogen-free conditions with constant temperature and humidity control at the AUB Animal Care Facility (ACF).

Controlled-Cortical-Impact Model. Rats were anesthetized, and their cortices were exposed by craniotomy; this was followed by controlled cortical impact (CCI) to induce mechanical damage to the cortex tissue.³⁰ Briefly, after anesthesia using a ketamine (10 mg/kg)–xylazine (100 mg/kg) mix, rats were fixed on a stereotactic frame, where ear and incisor bars were used to secure the position of the rat head. Using a blade, a midline incision was performed to expose the underlying tissue, and the skin was retracted on the right hemisphere (ipsilateral). After scalping the excess tissue, a target was set halfway between the bregma and lambda using machine software (ipsilateral); this was followed by a craniotomy (5–7 mm diameter) at the target site. An impact was induced using an impactor tip of 2 mm diameter, 2 mm depth, and 4 m/s velocity at 0.8 m/s speed. After impact, the rat was sutured and kept for 3 days.

Brain Harvesting and Tissue Preparation. Three days post injury, rats ($n = 3$) were anesthetized by 5% isoflurane and sacrificed by decapitation. The complete brain was removed, snap-frozen on dry-ice-cooled isopentane, and then stored at -80 °C. Using a cryostat (Leica Microsystems, Nanterre, France), 20 μm tissue sections were collected in a coronal view and thaw-mounted on polylysine slides. Tissue sections obtained every 200–250 μm (approximately) were subjected to MSI.

Mass-Spectrometry Imaging. Tissue sections used for imaging were dried in a vacuum desiccator for 15 min prior to use. The matrix (2,5-dihydroxybenzoic acid, DHB) was prepared at a concentration of 20 mg/mL in a 70:30 (v/v) ratio of methanol–0.1% TFA in H_2O . The matrix was manually sprayed for 12 min at an air pressure of 1 bar and a matrix flow rate of 300 $\mu\text{L}/\text{h}$ using a nebulizer constructed in house.³¹ Images and full-scan data were acquired on a MALDI LTQ Orbitrap XL (Thermo Fisher Scientific, Bremen, Germany) operated by Xcalibur software version 2.0.7 (Thermo Fisher Scientific). The MALDI LTQ Orbitrap XL is equipped with a commercial N_2 laser (LTB Laser Technik, Berlin, Germany) operating at $\lambda = 337$ nm with a maximum repetition rate of 60 Hz. Spectra were obtained in positive-ion mode at a spectral-mass resolution of 30 000 (centered at m/z 400) in the mass range of 300–1000 Da. Each spectrum was acquired by averaging 10 scans with 1 microscan per step with a raster step size (lateral resolution) of 70 μm . External calibration in the normal mass range (m/z 150–2000) was performed before every acquired image using the ProteoMass MALDI calibration kit.

Data Processing. Images were converted to the vendor-neutral imzML format using the imzML converter available in ImageQuest software version 1.1.0 build S4 (Thermo Fisher Scientific). The converted files were then uploaded and processed in SCiLS Lab MVS, version 2018b Premium 3D release 6.01.10194 (SCiLS, Bremen, Germany). With this version of SCiLS Lab MVS, the baseline-removal option is not available, and the peaks are automatically imported. Normal-

ization was performed on the basis of the total-ion-count (TIC) method. The m/z intervals were also automatically set at ± 33.155 mDa. All spectra were aligned using the move-peaks-to-local-max feature with the reference-sample data set chosen arbitrarily. All ion images were plotted with the weak-denoising option. Spatial segmentation was performed using the bisecting k -means algorithm with a Euclidean-distance metric.³² Regions were specified on the basis of the results of spatial segmentation. Colocalization analysis was performed using Pearson's correlation analysis.³³ Receiver-operating-characteristic (ROC) analysis was performed to discriminate between the injury area and ventricles.³⁴

3D Image Reconstruction. A total of 16 coronal sections of 20 μm thicknesses were used to reconstruct the 3D image; images were taken consecutively every 200–250 μm interval and covered the entire area of the brain containing the cortical-impact injury. This spans the bregma -1.30 to -4.80 mm, starting from the ventral part where the third ventricle starts to appear up until the sections where the thalamus terminates. The coregistration of all images was done interactively using rigid alignment of the 2D optical scans of the tissue taken at 8 \times bit resolution using a Nikon scanner (Nikon Technologies, Tokyo, Japan). After alignment of all tissue, space filling was performed with each tissue filling a 500 μm gap.

Lipid Assignment. Preliminary assignments based on accurate mass measurements were done by interrogation of the METLIN metabolomics database (public domain: <http://metlin.scripps.edu/>) using a threshold of ± 4 ppm. MS/MS spectra, if possible, were acquired using an off-tissue approach that involved liquid–liquid extraction using the Folch method. Four 20 μm thick brain sections were suspended in 60 μL of CHCl_3 , and to this, 30 μL of MeOH and 30 μL of H_2O were added. The mixture was vortexed for 1 min, sonicated for 5 min, and then centrifuged at 10 000 rcf for 10 min. After centrifugation, the CHCl_3 extracts in the lower phase of the Eppendorf tube were collected. To ensure maximum lipid extraction, CHCl_3 extraction was performed twice. CHCl_3 extract (1 μL) was spotted on a MALDI target and combined with 1 μL of matrix (20 mg/mL DHB dissolved in 70:30 MeOH–0.1% TFA). Full scans were acquired at 100 000 resolution (centered at m/z 400) in positive mode in the same mass range used during image acquisition (m/z 300–1000) by averaging 10 scans acquired with 2 microscans at 2 microscans per step. Precursor-ion isolation was performed using an isolation window between ± 1 and 2 Da, and the fragments were scanned with a maximum accumulation time between 120 and 200 ms. The normalized collision energy (NCE) was optimized for the individual precursor ions.

HPS Staining. After MALDI-Orbitrap acquisition, the matrix was removed by dipping the slide in methanol for 30 s. After drying in the desiccator, the tissue was treated with hematoxylin solution for 1 min and rinsed with tap water. The tissue section was then stained with phloxine (0.1% aqueous solution) for 10 s and rinsed with tap water. Then, a dehydration step in 70 and 100% ethanol was performed. The tissue was then dipped in saffron for 5 s, rinsed twice in alcohol, and given a final rinse in xylene before the mounting with the EUKITT slide-mounting medium and the addition of a coverslip.

RESULTS AND DISCUSSION

Unsupervised Spatial Segmentation and 3D Image Reconstruction. Spatial segmentation was employed to

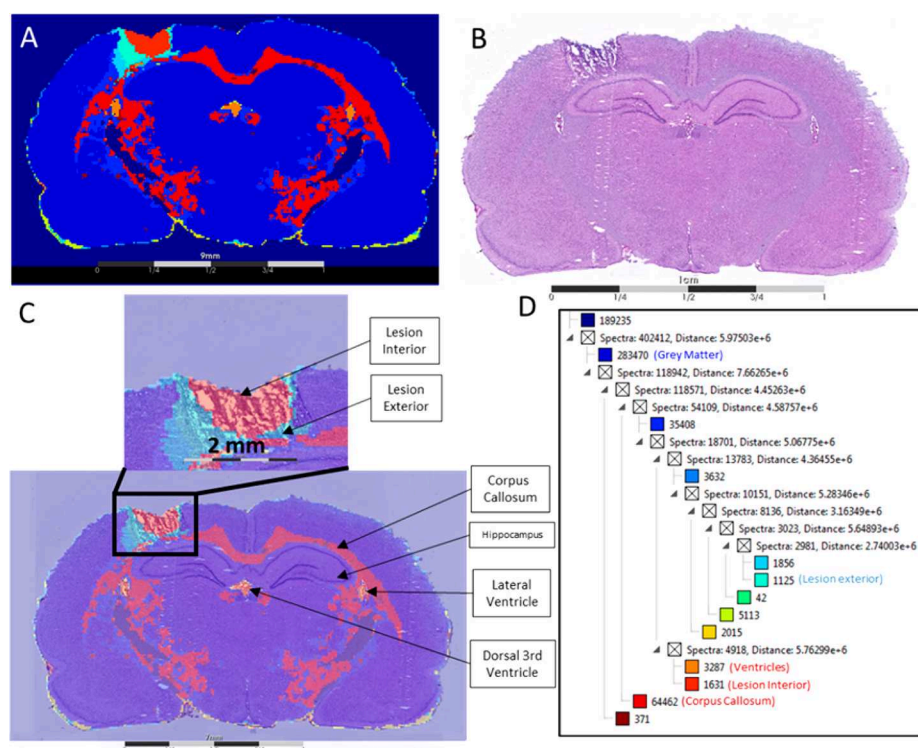


Figure 1. (A) Spatially segmented cluster image obtained after processing of MALDI-MSI lipid data of a rat brain 3 days post injury. (B) HPS staining of the same tissue section MALDI imaged previously. (C) Coregistration of spatial-segmentation and HPS-staining images revealing the depth of injury induced by controlled cortical impact (zoom). (D) Cluster tree corresponding to the same tissue slice after segmentation based on the Euclidean-distance-calculation method.

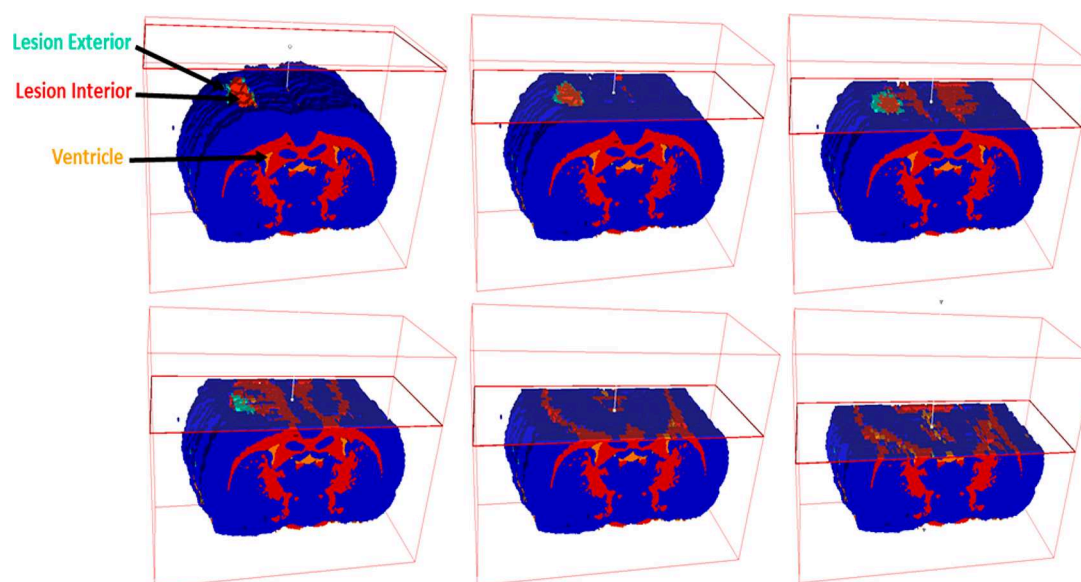


Figure 2. 3D representation of the spatial-segmentation results after superposing all consecutive MS-imaged tissues. Images show a series of clippings made at various depths with the plane perpendicular to the coronal axis. Clusters pertaining to regions with no tissue (i.e., only matrix present) were hidden for clarity.

visualize regions sharing similar molecular profiles within the tissue (Figure 1a). The depth of the cluster was chosen interactively such that the anatomical features of the rat brain could be discerned by comparison with the HPS-stained section as reference (Figure 1b). The resulting segmentation maps were then superimposed on the optical scans of the HPS-stained tissue section to verify the colocalization of individual clusters to their corresponding anatomical regions (Figure 1c).

In this manner, it can be shown that the white matter (corpus callosum, red, corresponding to 64 462 spectra) can be distinguished from the gray matter (cortical tissue, blue, corresponding to 283 470 spectra). More importantly, spatial segmentation reveals that the injured cortical tissue in the right hemisphere clearly clusters distinctly from the rest of the brain (Figure 1a). In fact, spectra corresponding to the injured tissue cluster into two different groups (one colored light blue and

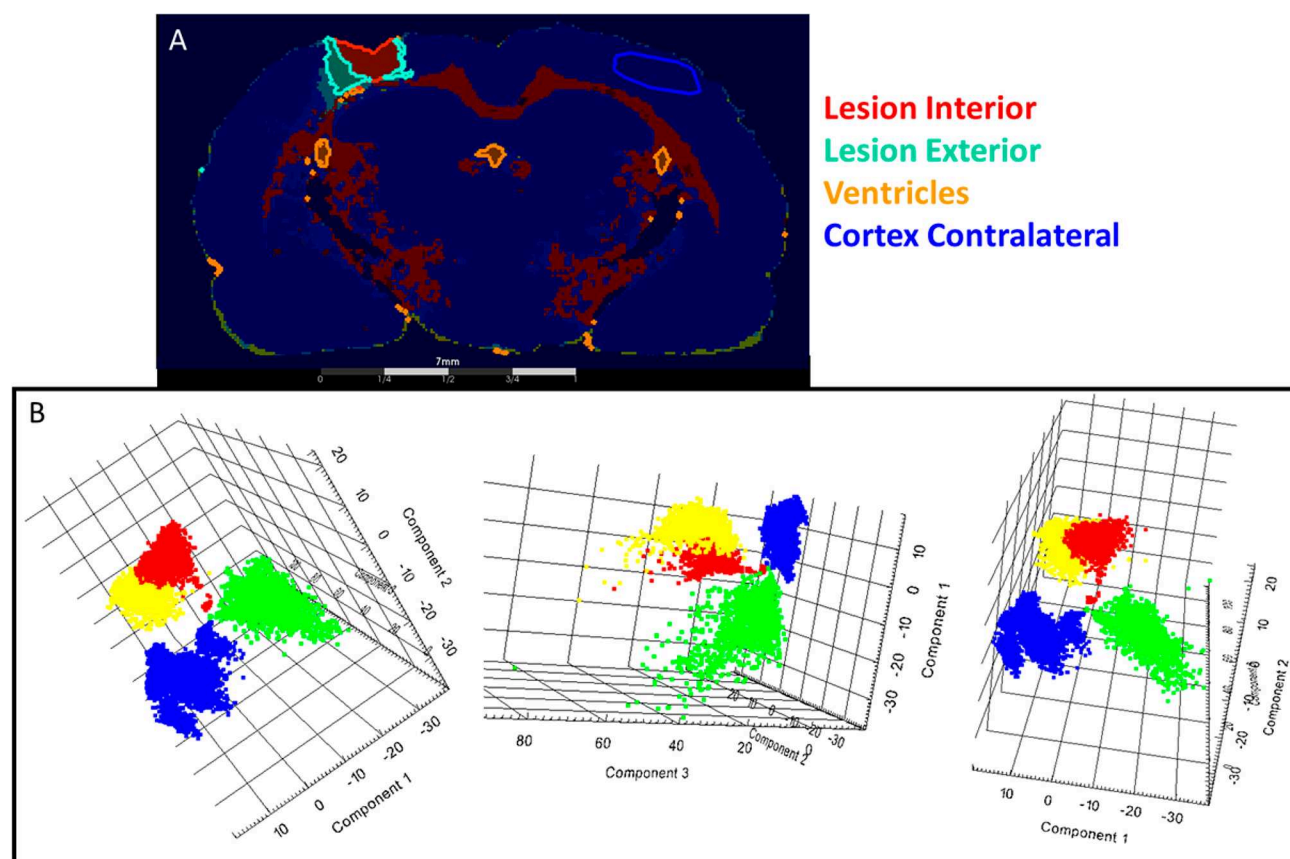


Figure 3. (A) 2D image of spatial-segmentation result with the regions of interest (lesion interior, lesion exterior, ventricles, and cortex contralateral) that were selected for further statistical analysis highlighted. (B) Scores plot of the first three components of the PCA of the selected regions: cortex contralateral (blue), lesion interior (red), lesion exterior (yellow), and ventricles (green).

corresponding to 1125 spectra and the other colored light red and corresponding to 1631 spectra, annotated as lesion exterior and lesion interior, respectively; Figure 1d), with each group separated clearly from the other and at different depths in the clustering tree. The surface area of the region covered by the two clusters is in agreement with the approximate area of the impact region expected on the basis of the diameter of the impactor tip (2 mm, Figure 1c, zoom). The underlying hippocampus shows no physical evidence of damage, as confirmed by the spatial-segmentation result and HPS staining. The two clusters can be further discerned from each other when the 3D volume image is rebuilt by superposing the spatial-segmentation images of all sections and taking cross-sections of the 3D volumes at different depths (Figure 2). The surface of the cortex at the site of the impact is dominated by the light-red cluster, and the impact site is bordered by the light-blue cluster. At deeper depths of the cross-section, the size of the red cluster reduces whereas that of the light-blue cluster increases until only the latter can be observed at cross-section depths closer to the corpus callosum.

The segmentation results also revealed a cluster whose distance was close to that of the lesion exterior but which was not present in the injured tissue region. Comparison with the rat-brain atlas shows that this cluster corresponds to the left and right lateral ventricles and the third dorsal ventricle. Spectra from these regions all group in the same cluster (light brown, 3287), thus showing the same molecular profile for the three ventricles (Figure 1d). The localization of the ventricles and their progression deeper in the tissue is clearly shown in a

coronal view of the brain when the cluster corresponding to the ventricle regions is 3D-rendered separately (Supplementary Figure 1). The evolution of the ventricle cluster within the brain, from the frontal part close to the olfactory bulbs toward the rear part close to the cerebellum, is in coherence with the shape of the ventricle expected on the basis of the rat-brain atlas.³⁵ In the same 3D plots, the images of the clusters corresponding to the lesion interior and exterior are also shown.

Differential Lipid Expression within Different Regions of the Injured Brain. Data from unsupervised spatial segmentation were used to select regions of interest (i.e., lesion interior, lesion exterior, ventricles, and contralateral cortex; Figure 3a). Spectra from these regions were then subjected to principal-component analysis (PCA) to create a model that would explain the observed differences in the spectral profiles between the lesion interior and exterior, between the injured cortical tissue and the uninjured cortical tissue in the opposite hemisphere of the brain (contralateral cortex), and among the three ventricles (left lateral, right lateral, and third dorsal ventricles). The first principal component explains 7.125% of the variance observed across the groups, and the second and third components explain 6.659 and 4.878%, respectively. From the scores plot of the first three PCs, it can be observed that the clusters are distinctly separated from each other (Figure 3b). The contralateral-cortex group (blue) is clearly separated from the lesion interior (red), the lesion exterior (yellow), and the ventricles (green). On the other hand, although the lesion-interior and -exterior clusters were very

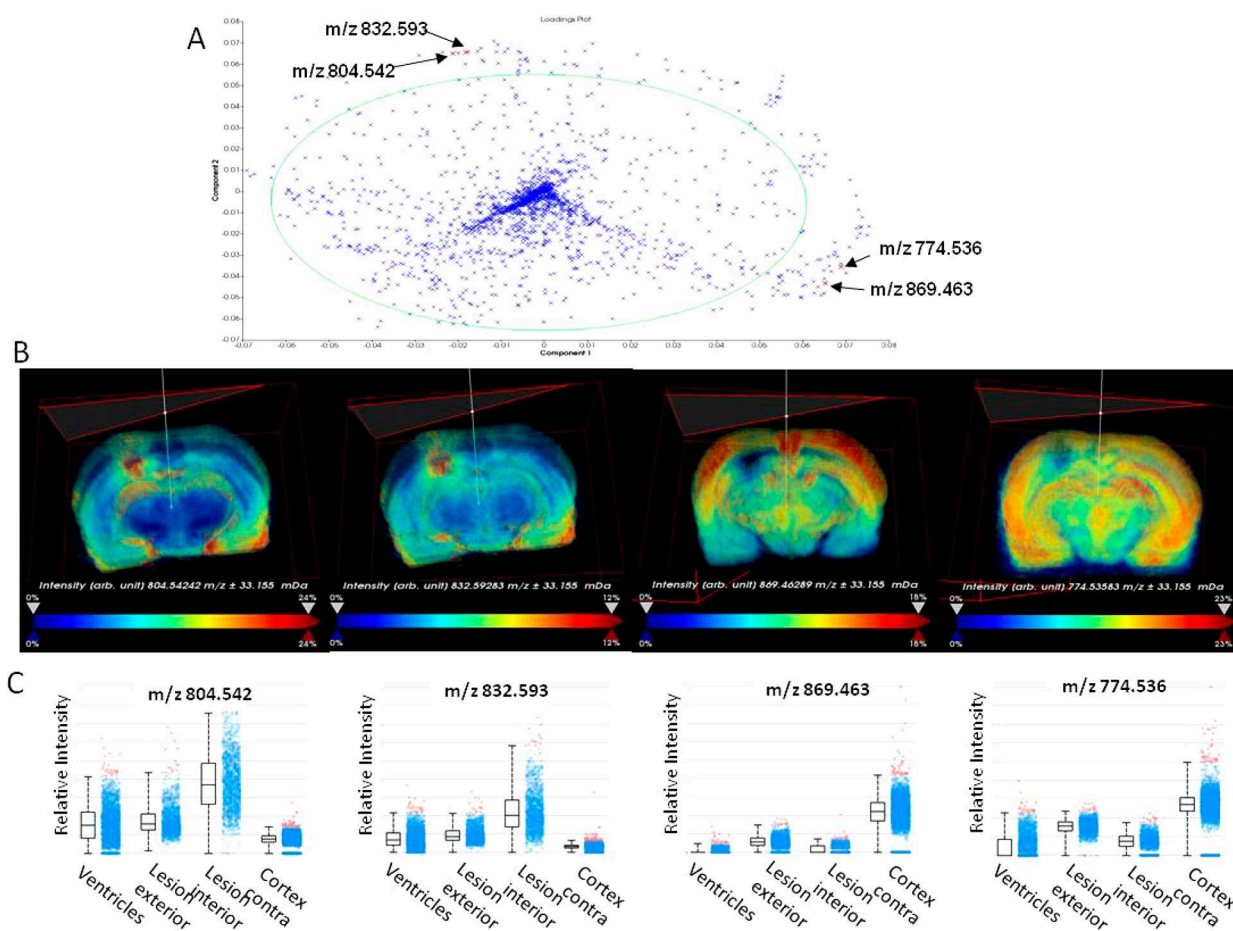


Figure 4. (A) Scatter plot of the loadings for the first two PCs with the selected m/z ratios highlighted. (B) 3D representation of m/z 804.542, 832.593, 869.463, and 774.536. (C) Box plot of the intensity variation of the selected regions (ventricles, lesion interior, lesion exterior, and cortex contralateral) for each of the chosen m/z values in (B).

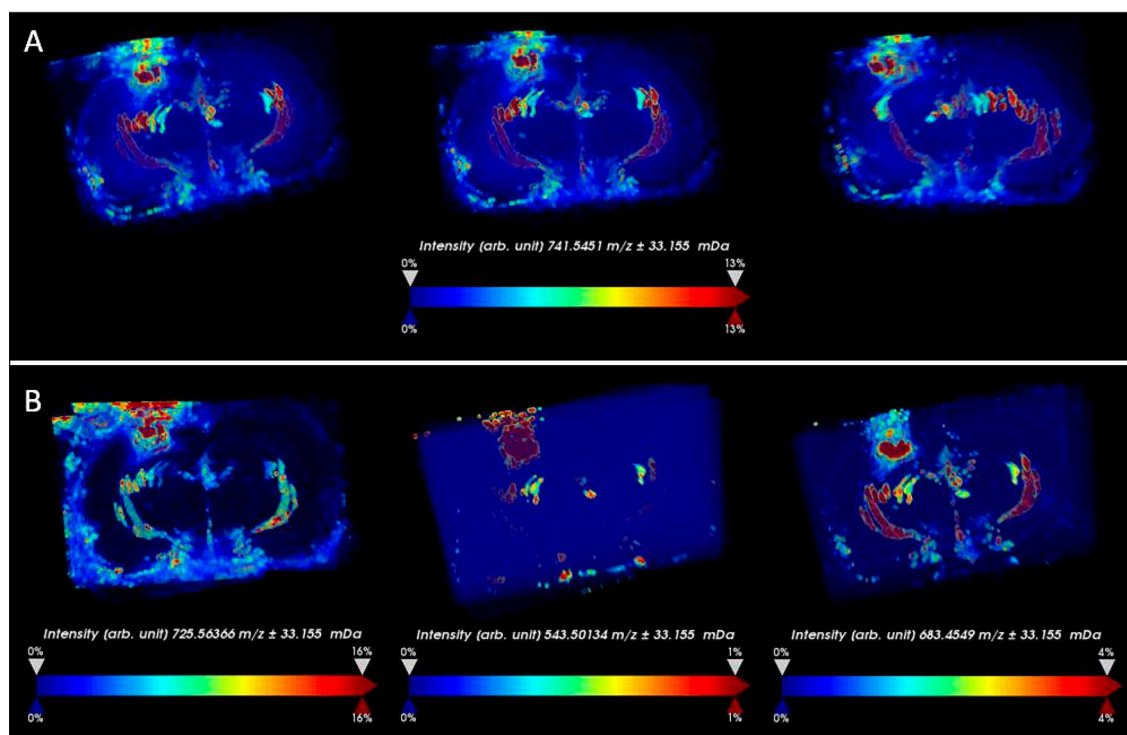


Figure 5. (A) 3D representation of m/z 741.545 in three different view panels. (B) 3D representation of m/z 725.564, 543.501, and 683.455.

close to each other in the PCA grid, they nonetheless showed a complete separation, as demonstrated in Figure 3b.

A scatterplot of the loadings of the first two PCs is plotted in Figure 4. The variables (m/z intervals) corresponding to the heaviest loadings after the 99% error quantile was defined are labeled (Figure 4a), and examples of their ion images are projected in 3D, as shown in Figure 4b. A total of 159 m/z intervals were noted and are shown in Table S-1. Loadings with high contribution to the first component show intense distribution in the contralateral-cortex regions but are absent in the other two lesion groups and in the ventricles, as exemplified by PE(38:1)/PC(35:1) (m/z 774.536) and m/z 869.463. Plots of the normalized intensities of these m/z intervals are shown in the box-plot representation (Figure 4c). On the other hand, loadings with highly positive correlations with the second component, such as PC(38:7) (m/z 804.542) and PC(38:4) (m/z 832.536), show a very intense distribution in the lesion but not in the contralateral cortex or the ventricles (Figure 4c). It should be noted that some of these signals are not lesion-specific but can also be observed in the hippocampus, as in the case of PC(38:7) (m/z 804.542, Figure 4b).

Lesion- and Ventricular-System-Specific Signal after TBI. Data from the spatial segmentation suggest a trend in the lipid distribution along the lesion site and the ventricular system upon induction of TBI. Visualization of lesion-elevated m/z ratios was then performed in the brain 3 days post-TBI (Figure 5). Using SciLS Lab MVS software, processing of the data was performed in order to retrieve all m/z values that colocalized with the site of injury. A total of 30 m/z values were identified with a threshold of 0.3 (Table S-2). Further classification of the data allowed us to obtain high expression values that colocalized in both the ventricles and the lesion found in the cortical tissue. For instance, m/z 741.545 localized in the injury area as well as in the ventricular system of the brain (Figure 5a). As tissue slices progressed further toward the cerebellum in a coronal view, the sizes of the left and right ventricles increased along with a concomitant expansion and distribution of the expression of this m/z in the ventricles. Similarly, m/z 683.454 and 725.564 showed the same localization along the ventricles (Figure 5b). In contrast, m/z 543.501 showed a similar response to those of the previously mentioned molecules at the cortical-injury site, whereas its expression in the ventricles was restricted to the frontal part of the brain, which has a very small ventricular size (Figure 5b).

Lesion-Specific and Ventricle-Specific Signal Post-TBI. In order to identify the m/z that showed increased expression in the cortex-lesion area without any expression in the ventricles, receiver-operating-characteristic (ROC) analysis was performed between the two regions. This analysis allowed us to discern the discriminative values that differentiate the two areas. Indeed, a total of 10 m/z intervals with high AUC values were identified as being responsible for discriminating between the lesion area and the ventricles, after the application of a threshold value of 0.95 for the lesion-discriminative values and a threshold value of 0.12 for the ventricle-discriminative values (Table S-3). Four of these m/z intervals are represented in Figure 6, which shows the clear distribution of lesion-specific and ventricle-specific m/z values within the rat brain. Both m/z 723.508 and PC(42:9) (m/z 856.598) show clear distributions within the cortical tissue of the brain, with elevated expression at the injury site (Figure 6a). Interestingly, the signals can also be observed in the same site as the injury in sections unaffected

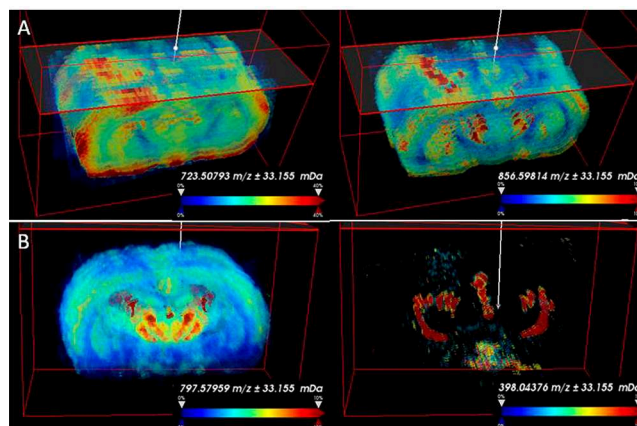


Figure 6. (A) 3D representation of m/z 723.508 and 856.598 viewed in clippings mode with the dissecting plane perpendicular to the coronal axis. (B) 3D representation of m/z 797.580 and 398.044.

by cortical impact; for example, m/z 856.598 appears as a continuous streak in the injury site when the 3D image is clipped horizontally along the z axis, whereas it appears cylindrical in the spatial-segmentation cluster corresponding to the lesion in Figure 2. At the same time, these two molecules show no expression within the ventricular system of the brain. In contrast, one PC (m/z 797.580) and m/z 398.044 show clear increased distribution within the ventricular system (Figure 6b). Along with the increased expression in the ventricles, baseline expression can be found in the cortical tissue for m/z 797.580 but not in the injury, and m/z 398.044 shows unique expression in the ventricle system alone. Similar profiles of expression and localization were obtained for the other two replicates analyzed, as shown in the box-plot representation showing the intensity variations of the lipid markers in the different areas of the rat brains (Supplementary Figure 2).

In the present study, we performed 2D MALDI lipid imaging on rat-brain serial tissue sections and then superposed all images to generate a 3D reconstruction of the injured part of the brain, showing altered lipid distributions after cortical-impact injury. This 3D reconstruction definitely enables us to get a global picture of the molecular changes in the brain postinjury at a larger extension. For example, the distribution of the ventricular system is not uniform throughout the brain from the rostral part to the caudal part. In fact, the lateral ventricle starts with a circular node shape in the rostral part of the brain near the olfactory bulbs and evolves in size as it moves further into the brain, reaching a large-sized cavity toward the caudal part. The expression of m/z related to this system cannot be understood with as much clarity in a 2D manner as with 3D MSI because of the mentioned size evolution. A similar explanation can be stated for the hippocampus, as its progression in size from the rostral part to the caudal part of the brain is nonuniform.

We believe that the 3D reconstruction helps with spatial and theoretical understanding of the injured brain along with the possible involvement of other organs. Unsupervised spatial segmentation revealed clusters that matched the histological observation of the brain. For example, the white matter, mainly the corpus callosum, was grouped together and distinct from the gray-matter cluster, which was mainly composed of the cortex. In addition, the spatial-segmentation data also allowed us to isolate the site of the injury from the remaining parts of

the brain, thus showing that the lipid contents of the injured cortical tissue differs from those of its surroundings. This difference becomes more evident when the injured region in the ipsilateral cortex is compared with an uninjured region of the contralateral cortex.

More importantly, the segmentation data allowed us to distinguish two distinct regions within the injury site. Tentative assignments of lipids specific to each region show that they belong to different lipid classes, suggesting perhaps a graded response to injury. Whether this finding has significant implications with regard to the induction of injury and progression of the ensuing secondary damage and inflammatory processes warrants further investigation. Previous reports on other CNS injuries, such as those induced in the spinal cord, have demonstrated the presence of different immune cells (resident and circulating) at specific locations in the injury site.³⁶

Our results also reveal the presence of signals in the lesion colocalizing all throughout the ventricles. The ventricular system plays a crucial role in the mobilization and transfer of molecules within the brain itself and toward surrounding organs, such as the spinal cord. Indeed, the ventricular system is responsible for the production of the CSF, which circulates in a unidirectional way from the rostral to the caudal parts of the brain and then into the spinal subarachnoid space.³⁷ Thus, tracking injury-implicated molecules along the ventricular system could provide insight into the systemic progression of TBI and how it affects other regions of the brain and the CNS.

In this study, images were taken with a high-resolution mass spectrometer with a high mass accuracy (lower than 5 ppm), which provided a big advantage over the typical time-of-flight (TOF) analyzers linked to MALDI sources.³⁸ This is clearly visualized in our data (Supplementary Figure 3), where a mass difference of 0.07 (m/z 725.564 and 725.497) revealed molecules with different distributions. Both molecules were expressed within the injury site, and m/z 725.564 was also localized in the ventricles but not in the white matter, whereas m/z 725.497 was localized in the white matter, mainly the corpus callosum, but not in the ventricular system.

CONCLUSION

In conclusion, we have demonstrated the capability of using high-resolution MALDI-LTQ-Orbitrap-XL in 3D lipid mass-spectrometry imaging of traumatic brain injury. Our findings suggest a unique lipid profile in the area of injury, with some resemblance to the ventricular system in the brain post injury. We have shown injury-specific lipid distribution in a 3D manner throughout the injury in the right hemisphere of the brain.

ASSOCIATED CONTENT

Supporting Information

The Supporting Information is available free of charge on the ACS Publications website at DOI: 10.1021/acs.analchem.8b02682.

PCA loadings corresponding to the heaviest loadings after defining the 99% error quantile, colocalization of m/z with the area of injury, lesion- and ventricle-discriminative m/z intervals obtained by ROC analysis, MS/MS of selected m/z ion intervals, 3D representation of the spatial-segmentation result, box-plot representa-

tion of ion intensities of m/z peaks, and 3D distribution of m/z 725.497 and 725.564 at 3 days post injury (PDF)

AUTHOR INFORMATION

Corresponding Authors

*Tel.: +33 (0)3 20 43 41 94. Fax: +33 (0)3 20 43 40 54. E-mail: isabelle.fournier@univ-lille.fr (I.F.).

*Tel.: +33 (0)3 20 43 41 94. Fax: +33 (0)3 20 43 40 54. E-mail: michel.salzet@univ-lille.fr (M.S.).

ORCID

Firas Kobeissy: 0000-0002-5008-6944

Michel Salzet: 0000-0003-4318-0817

Isabelle Fournier: 0000-0003-1096-5044

Author Contributions

The manuscript was written through contributions of all authors. All authors have given approval to the final version of the manuscript.

Notes

The authors declare no competing financial interest.

ACKNOWLEDGMENTS

This research was supported by grants from Ministère de l'Enseignement Supérieur, de la Recherche et de l'Innovation (MESRI), Institut National de la Santé et de la Recherche Médicale (Inserm), and Université de Lille. K.M. received a scholarship from the Association of Scientific Orientation and Specialization (ASOS).

REFERENCES

- (1) McAllister, T. W. *Dialogues Clin. Neurosci.* **2011**, *13* (3), 287–300.
- (2) Opara, J. A.; Malecka, E.; Szczygiel, J. *J. Med. Life* **2014**, *7* (2), 124–127.
- (3) Li, M.; Zhao, Z.; Yu, G.; Zhang, J. *Gen. Med.: Open Access* **2016**, *4* (5), 1–14.
- (4) Mckee, A. C.; Daneshvar, D. H. *Handbook Clin. Neurol.* **2015**, *127*, 45–66.
- (5) Weder, N.; Zhang, H.; Jensen, K.; Yang, B. Z.; Simen, A.; Jackowski, A.; Lipschitz, D.; Douglas-Palumberi, H.; Ge, M.; Perepletchikova, F.; et al. *J. Am. Acad. Child Adolesc. Psychiatry* **2014**, *53* (4), 417–424.e5.
- (6) Kidwell, C. S. *JAMA* **2004**, *292* (15), 1823.
- (7) Hulkower, M. B.; Poliak, D. B.; Rosenbaum, S. B.; Zimmerman, M. E.; Lipton, M. L. *Am. J. Neuroradiol.* **2013**, *34*, 2064–2074.
- (8) Shenton, M. E.; Hamoda, H. M.; Schneiderman, J. S.; Bouix, S.; Pasternak, O.; Rathi, Y.; Vu, M.-A.; Purohit, M. P.; Helmer, K.; Koerte, I.; et al. *Brain Imaging Behav.* **2012**, *6* (2), 137–192.
- (9) Pelinka, L. E.; Kroepfl, A.; Leixnering, M.; Buchinger, W.; Raabe, A.; Redl, H. *J. Neurotrauma* **2004**, *21* (11), 1553–1561.
- (10) Berger, R. P.; Beers, S. R.; Richichi, R.; Wiesman, D.; Adelson, P. D. *J. Neurotrauma* **2007**, *24* (12), 1793–1801.
- (11) Blanc, L.; Lenaerts, A.; Dartois, V.; Prideaux, B. *Anal. Chem.* **2018**, *90* (10), 6275–6282.
- (12) Aichler, M.; Walch, A. *Lab. Invest.* **2015**, *95* (4), 422–431.
- (13) Zemski Berry, K. A.; Hankin, J. A.; Barkley, R. M.; Spraggins, J. M.; Caprioli, R. M.; Murphy, R. C. *Chem. Rev.* **2011**, *111* (10), 6491–6512.
- (14) Mériaux, C.; Franck, J.; Park, D. B.; Quanicco, J.; Kim, Y. H.; Chung, C. K.; Park, Y. M.; Steinbusch, H.; Salzet, M.; Fournier, I. *Hippocampus* **2014**, *24* (6), 628–642.
- (15) Le Rhun, E.; Duhamel, M.; Wisztorski, M.; Gimeno, J.-P.; Zairi, F.; Escande, F.; Reyns, N.; Kobeissy, F.; Maurage, C.-A.; Salzet, M.; et al. *Biochim. Biophys. Acta, Proteins Proteomics* **2017**, *1865* (7), 875–890.

- (16) Quanico, J.; Franck, J.; Wisztorski, M.; Salzet, M.; Fournier, I. *Methods Mol. Biol.* **2017**, *1598*, 21–43.
- (17) Thiele, H.; Heldmann, S.; Trede, D.; Strehlow, J.; Wirtz, S.; Dreher, W.; Berger, J.; Oetjen, J.; Kobarg, J. H.; Fischer, B.; et al. *Biochim. Biophys. Acta, Proteins Proteomics* **2014**, *1844* (1), 117–137.
- (18) Crecelius, A. C.; Cornett, D. S.; Caprioli, R. M.; Williams, B.; Dawant, B. M.; Bodenheimer, B. J. *Am. Soc. Mass Spectrom.* **2005**, *16* (7), 1093–1099.
- (19) Lotz, J. M.; Hoffmann, F.; Lotz, J.; Heldmann, S.; Trede, D.; Oetjen, J.; Becker, M.; Ernst, G.; Maas, P.; Alexandrov, T.; et al. *Biochim. Biophys. Acta, Proteins Proteomics* **2017**, *1865* (7), 946–956.
- (20) Adibhatla, R. M.; Hatcher, J. F. *Future Lipidol.* **2007**, *2* (4), 403–422.
- (21) Harrison, J.; Rowe, R.; Lifshitz, J. *Neural Regener. Res.* **2016**, *11* (1), 77.
- (22) Adibhatla, R. M.; Hatcher, J. F.; Dempsey, R. J. *AAPS J.* **2006**, *8* (2), E314–E321.
- (23) Sheth, S. A.; Iavarone, A. T.; Liebeskind, D. S.; Won, S. J.; Swanson, R. A. *PLoS One* **2015**, *10* (6), No. e0129735.
- (24) Novgorodov, S. A.; Riley, C. L.; Yu, J.; Borg, K. T.; Hannun, Y. A.; Proia, R. L.; Kindy, M. S.; Gudz, T. I. *J. Biol. Chem.* **2014**, *289* (19), 13142–13154.
- (25) Abdullah, L.; Evans, J. E.; Ferguson, S.; Mouzon, B.; Montague, H.; Reed, J.; Crynen, G.; Emmerich, T.; Crocker, M.; Pelot, R.; et al. *FASEB J.* **2014**, *28* (12), 5311–5321.
- (26) Woodcock, J. *IUBMB Life* **2006**, *58* (8), 462–466.
- (27) Guo, S.; Zhou, D.; Zhang, M.; Li, T.; Liu, Y.; Xu, Y.; Chen, T.; Li, Z. *Sci. Rep.* **2017**, *7* (1), 5054.
- (28) Roux, A.; Muller, L.; Jackson, S. N.; Post, J.; Baldwin, K.; Hoffer, B.; Balaban, C. D.; Barbacci, D.; Schultz, J. A.; Gouty, S.; et al. *J. Neurosci. Methods* **2016**, *272*, 19.
- (29) Barbacci, D. C.; Roux, A.; Muller, L.; Jackson, S. N.; Post, J.; Baldwin, K.; Hoffer, B.; Balaban, C. D.; Schultz, J. A.; Gouty, S.; et al. *ACS Chem. Neurosci.* **2017**, *8* (10), 2266–2274.
- (30) Osier, N. D.; Dixon, C. E. *Front. Neurol.* **2016**, *7*, 134.
- (31) Franck, J.; Quanico, J.; Wisztorski, M.; Day, R.; Salzet, M.; Fournier, I. *Anal. Chem.* **2013**, *85* (17), 8127–8134.
- (32) Alexandrov, T.; Kobarg, J. H. *Bioinformatics* **2011**, *27* (13), i230–i238.
- (33) McDonnell, L. A.; van Remoortere, A.; van Zeijl, R. J. M.; Deelder, A. M. *J. Proteome Res.* **2008**, *7* (8), 3619–3627.
- (34) Rauser, S.; Marquardt, C.; Balluff, B.; Deininger, S.-O.; Albers, C.; Belau, E.; Hartmer, R.; Suckau, D.; Specht, K.; Ebert, M. P.; et al. *J. Proteome Res.* **2010**, *9* (4), 1854–1863.
- (35) Paxinos, G.; Watson, C. *The Rat Brain in Stereotaxic Coordinates*; Academic Press, 1998.
- (36) Wang, X.; Cao, K.; Sun, X.; Chen, Y.; Duan, Z.; Sun, L.; Guo, L.; Bai, P.; Sun, D.; Fan, J.; et al. *Glia* **2015**, *63* (4), 635–651.
- (37) Stratchko, L.; Filatova, I.; Agarwal, A.; Kanekar, S. *Ultrasound, CT MRI* **2016**, *37* (2), 72–83.
- (38) Moreno-Gordaliza, E.; Esteban-Fernández, D.; Lázaro, A.; Humanes, B.; Aboulmagd, S.; Tejedor, A.; Linscheid, M. W.; Gómez-Gómez, M. M. *Talanta* **2017**, *164*, 16–26.

3D MALDI MSI Reveals Lipid Changes Associated with Traumatic Brain Injury

Khalil Mallah^{1,2}, Jusal Quanico¹, Dennis Trede³, Firas Kobeissy⁴, Kazem Zibara², Michel Salzet^{1,*}, and Isabelle Fournier^{1,*}

¹ Université de Lille, INSERM, U1192 - Laboratoire Protéomique, Réponse Inflammatoire et Spectrométrie de Masse (PRISM), F-59000 Lille, France

² ER045, PRASE, Laboratory of Stem Cells, Department of Biology, Faculty of Sciences-I, Lebanese University, Beirut, Lebanon

³ SCiLS, Bremen, Germany

⁴ Department of Biochemistry and Molecular Genetics, Faculty of Medicine, American University of Beirut, Beirut, Lebanon

Table of Contents

Supplementary Table S-1	2
Supplementary Table S-2	3
Supplementary Table S-3	4
Supplementary Table S-4 and MS/MS Spectra	5
Supplementary Figure 1	8
Supplementary Figure 2	9
Supplementary Figure 3	13

Supplementary Tables

Table S-1. PCA Loadings Corresponding to the Heaviest Loadings after Defining the 99% Error Quantile.

Centroid [m/z] \pm [0.03315]									
300.995	579.542	682.460	723.508	749.503	774.602	794.596	813.495	838.694	869.463
307.029	599.503	683.455	724.503	751.525	775.531	798.541	814.523	840.418	870.458
459.250	600.497	694.529	725.497	752.520	776.591	799.536	815.517	841.446	870.557
466.346	605.537	695.458	725.564	753.515	778.614	800.564	818.601	842.440	871.452
478.316	621.485	695.524	726.558	753.581	780.537	801.558	820.458	844.529	871.551
487.268	622.480	697.480	727.520	754.576	781.565	802.487	824.436	845.524	872.546
504.344	627.520	698.475	728.515	755.537	782.560	802.553	825.431	848.541	873.574
506.366	628.548	709.516	731.499	756.565	783.554	803.481	826.426	851.625	874.503
543.501	645.490	710.477	739.456	757.560	784.582	804.542	828.581	852.487	875.497
546.353	649.503	711.439	740.484	768.601	785.444	808.588	830.504	852.653	896.485
551.492	650.531	711.505	741.479	769.496	785.577	809.450	830.570	853.481	897.480
552.520	656.300	712.500	741.545	769.562	786.472	809.582	832.593	853.647	912.467
558.952	657.328	713.462	742.540	770.557	790.617	810.610	833.588	856.598	913.462
570.524	658.322	714.456	745.491	772.513	791.578	811.472	835.676	857.593	914.456
577.520	666.446	715.451	746.485	773.541	792.573	811.605	836.671	860.610	935.444
578.515	667.440	721.485	747.480	774.536	794.463	812.600	837.666	868.468	

Table S-2. Colocalization m/z with the area of injury

Centroid [m/z]	Maximum correlation in interval	Centroid [m/z]	Maximum correlation in interval
682.460	0.535	795.590	0.369
683.455	0.486	807.626	0.365
741.545	0.480	779.609	0.361
825.630	0.465	838.694	0.350
826.625	0.454	626.591	0.345
809.649	0.454	796.585	0.335
823.641	0.431	542.507	0.334
853.647	0.424	562.334	0.333
725.564	0.415	764.489	0.325
742.540	0.414	818.601	0.311
750.531	0.411	854.675	0.304
726.558	0.398	832.593	0.300
794.596	0.384	833.588	0.299
778.614	0.378	827.653	0.294
837.666	0.372	543.501	0.293

Table S-3. Lesion- and ventricle-discriminative m/z intervals obtained by ROC analysis.

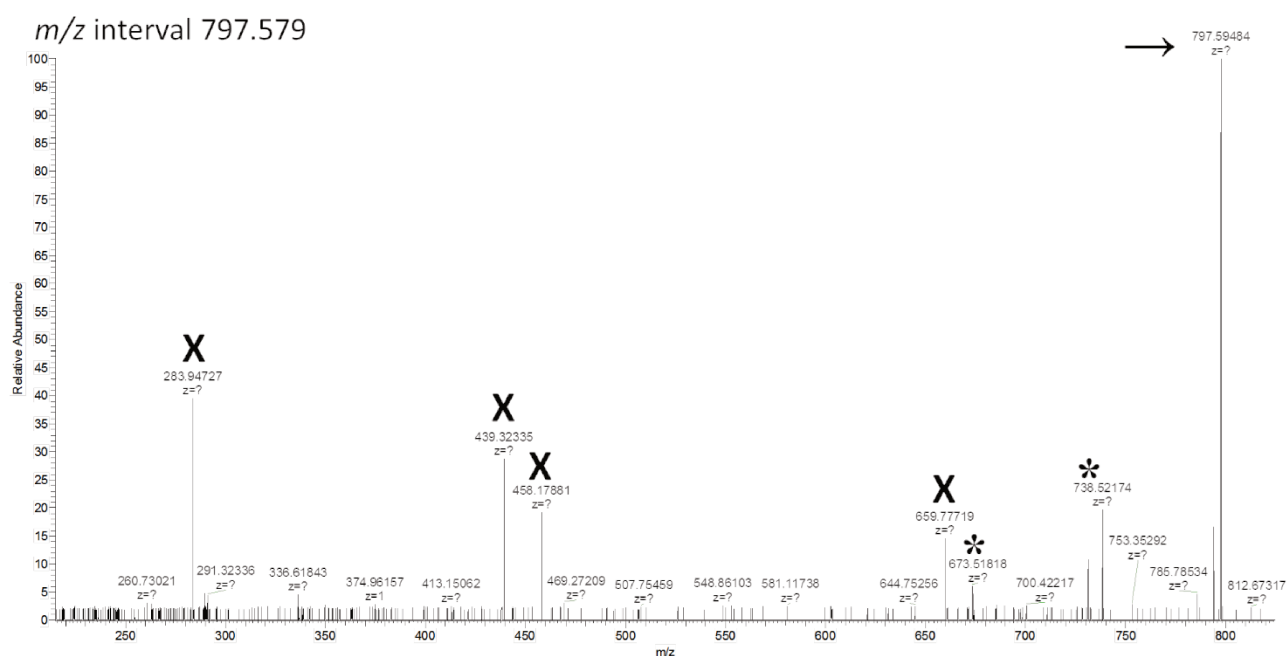
Lesion-discriminative		Ventricle-discriminative	
Centroid [m/z]	AUC _{max} *	Centroid [m/z]	AUC _{max} *
551.492	0.955	398.043	0.118
697.480	0.975	614.920	0.081
698.475	0.966	738.528	0.100
723.508	0.951	790.915	0.118
755.537	0.958	797.580	0.074
756.565	0.983	808.156	0.070
757.560	0.978	809.151	0.107
784.582	0.973	825.630	0.072
785.577	0.968	826.625	0.087
856.598	0.960	982.891	0.109

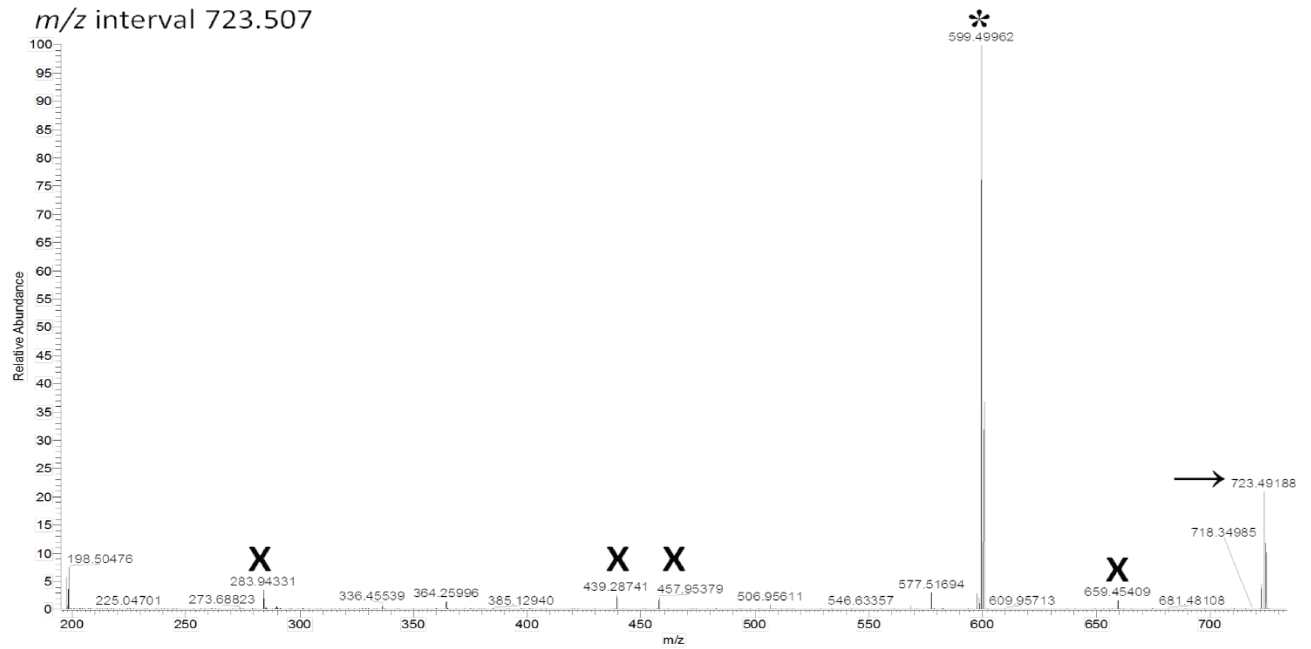
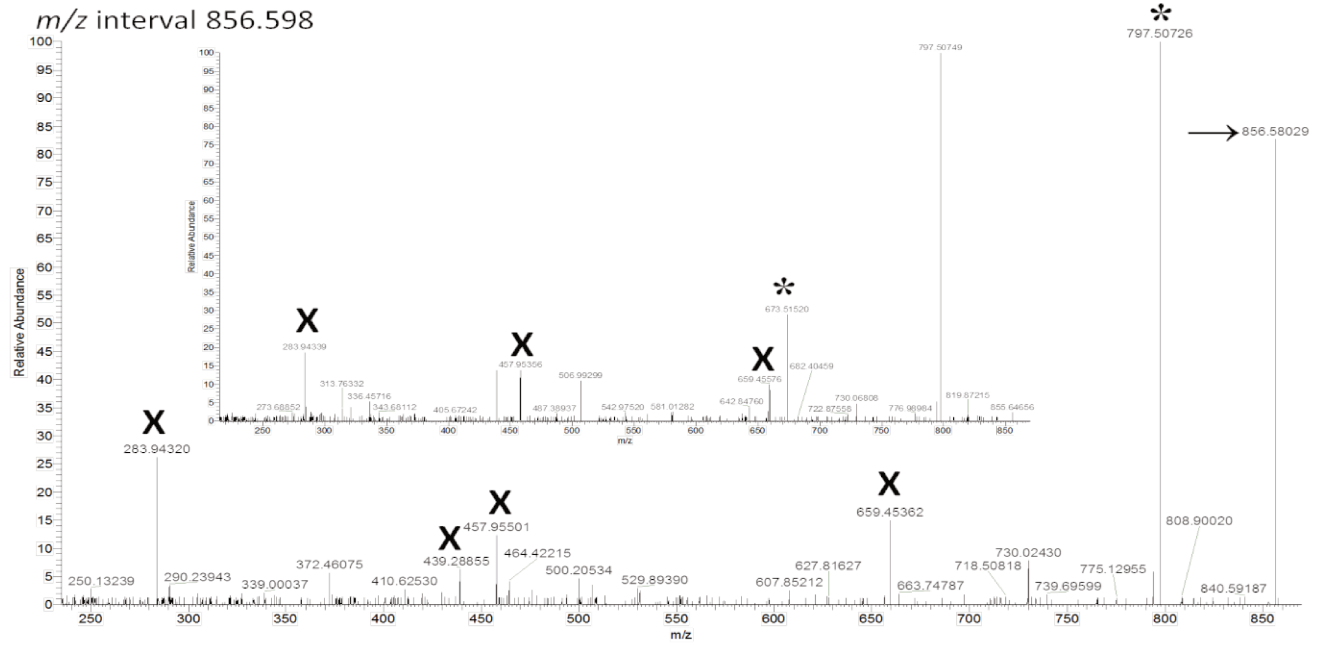
*Maximum area under the curve in the interval

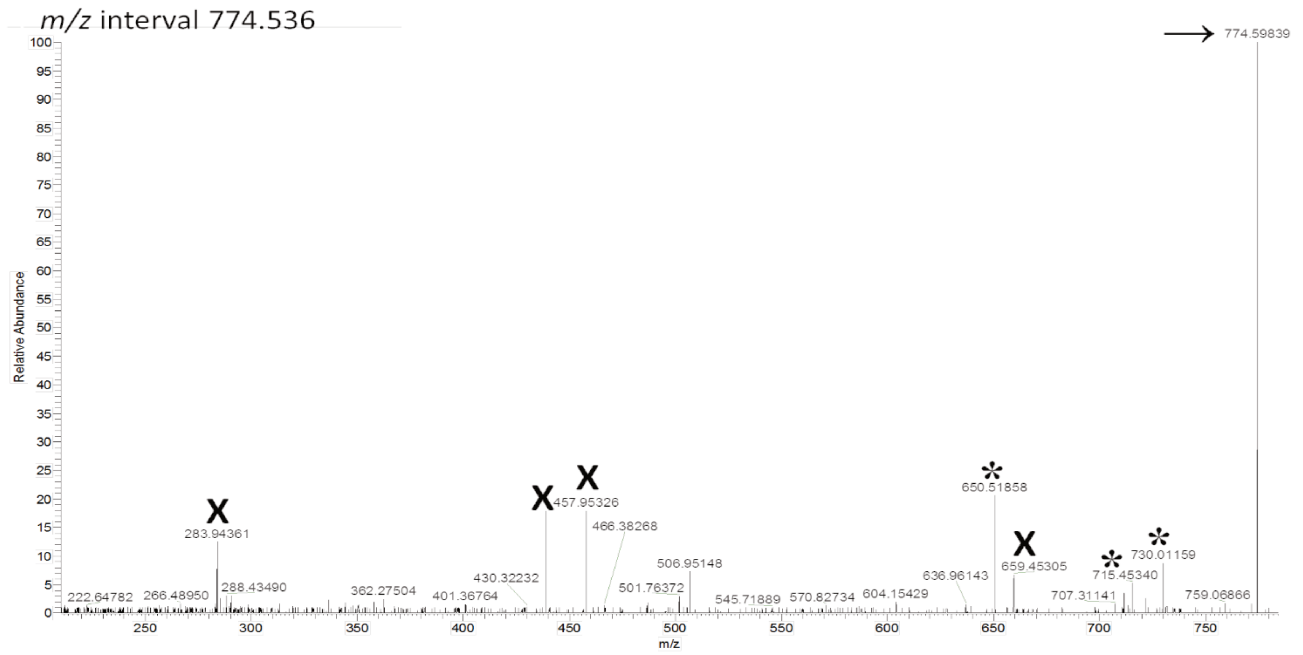
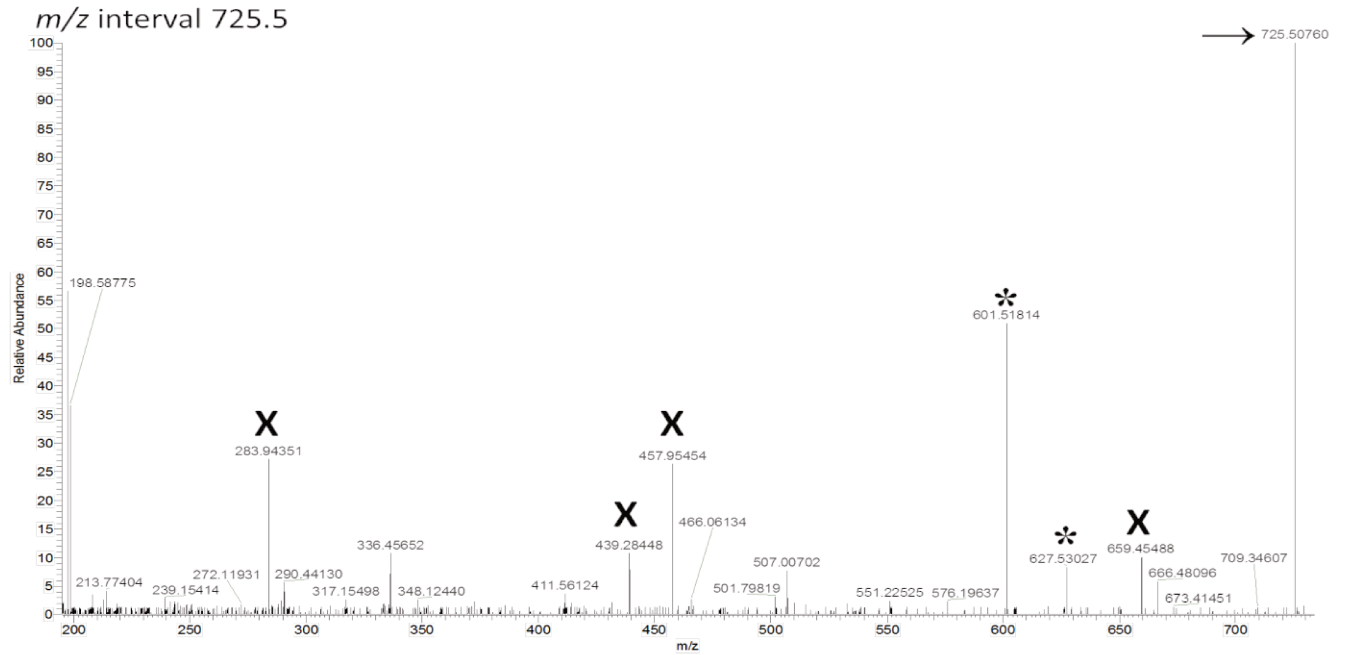
Table S-4: MS/MS of selected m/z ion intervals

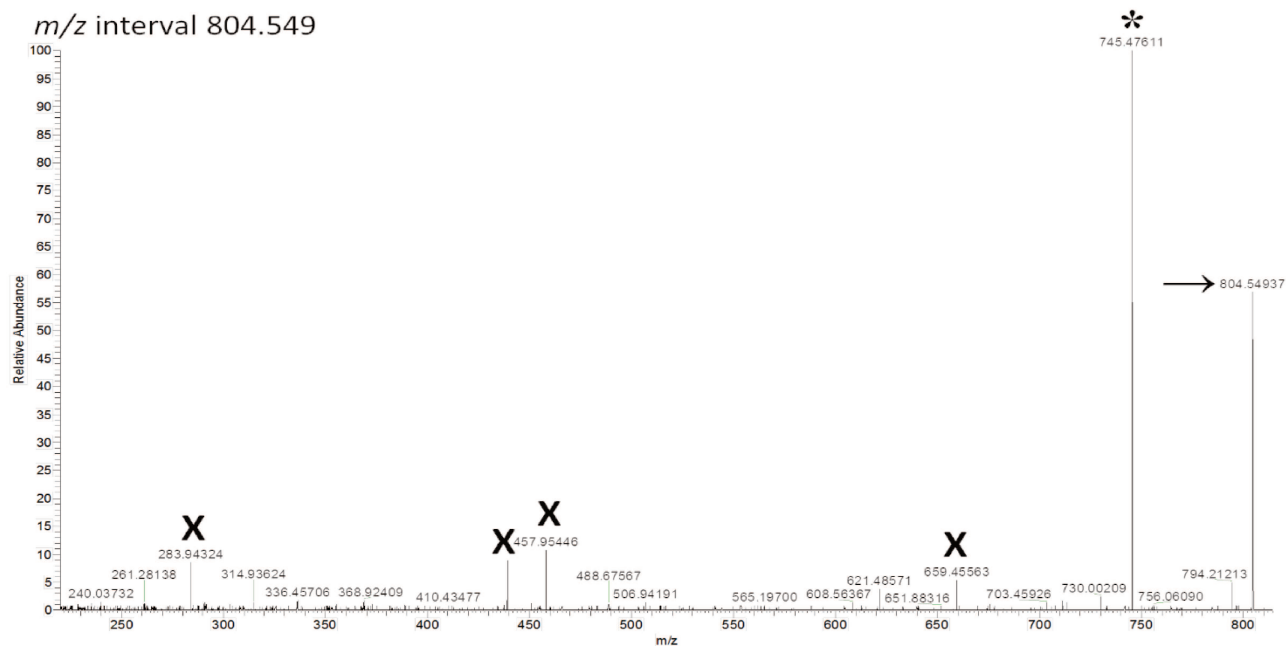
m/z interval	m/z exact mass	Fragment ion	Fragment ion	Fragment ion	Lipid Class attribution
797.579	797.587	738.513 (Neutral loss= trimethyl amine)	673.514 (Neutral loss= cyclophosphate)		PC
856.598	856.58	797.507 (Neutral loss= trimethyl amine)	673.515 (Neutral loss=cyclophosphate)		PC (42:9)
723.507	723.491	599.499 (Neutral loss=cyclophosphate)			PA (36:2)
725.5	725.507	627.530 (Neutral loss= phosphoric acid)	601.518 (Neutral loss= cyclophosphate)		PA (38:4)
774.536	774.598	730.011 (Neutral loss= ethylamine)	715.453 (Neutral loss= trimethyl amine)	650.518 (Neutral loss= cyclophosphate)	PE (38:1)/PC (35:1)
804.542	804.549	745.476 (Neutral loss= trimethyl amine)			PC (38:7)

MS/MS spectra used to annotate the m/z ions are found below. The parent ion is designated by an arrow (→) and the corresponding fragment ions shown in the table above are designated by asterisks (*). Peaks assigned with a cross (X) are background noise and are common to all spectra.

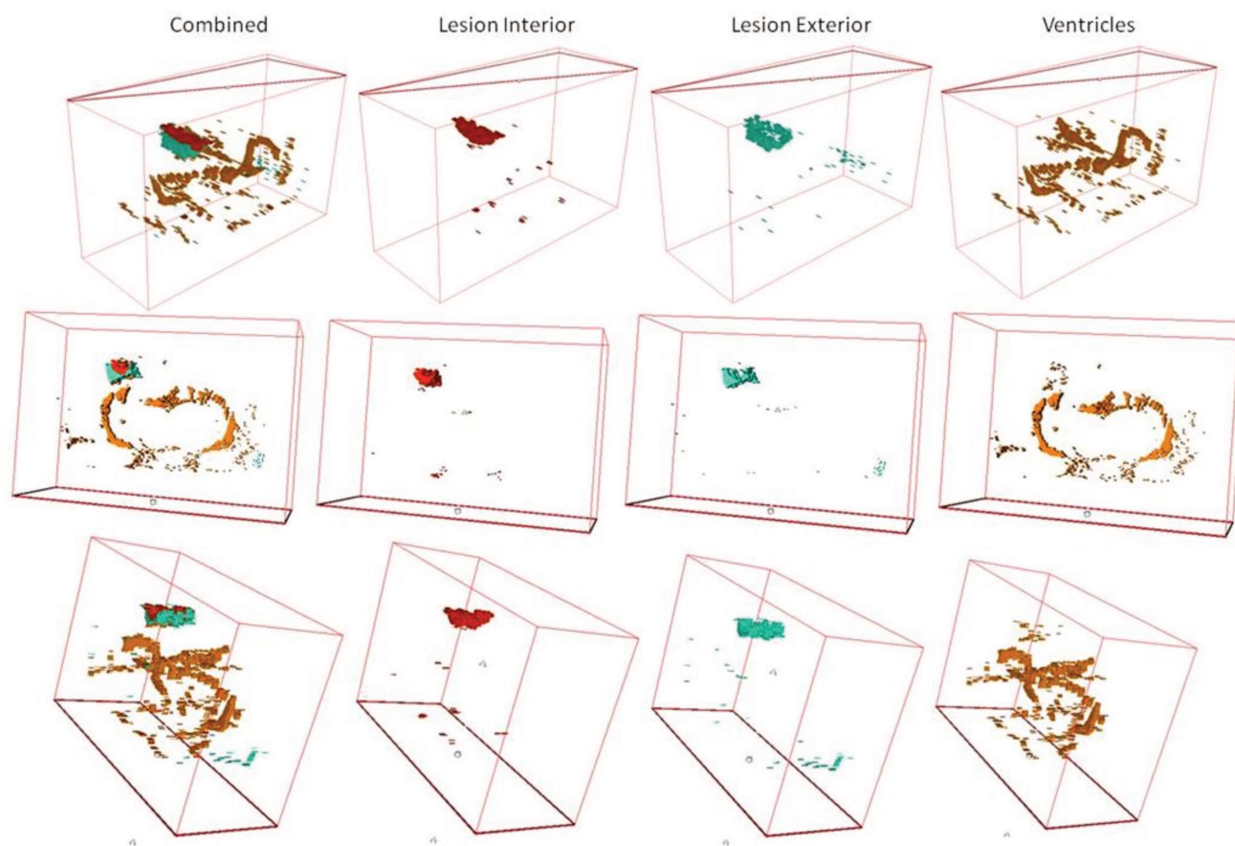








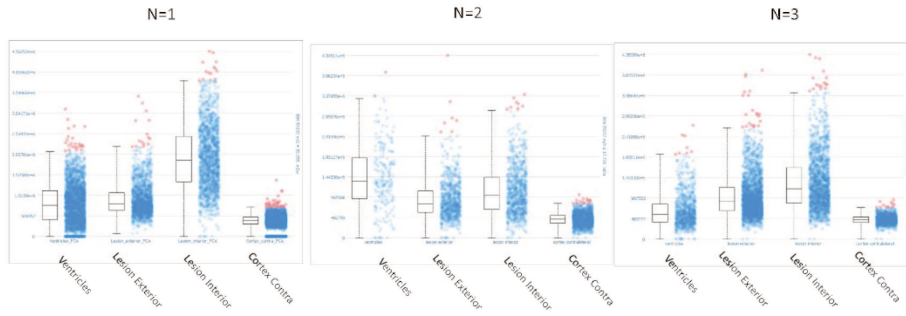
Supplementary Figure 1: 3D representation of the spatial segmentation result after superposing all consecutive MS imaged tissues for clusters corresponding to lesion interior, lesion exterior, and ventricular system alone and combined.



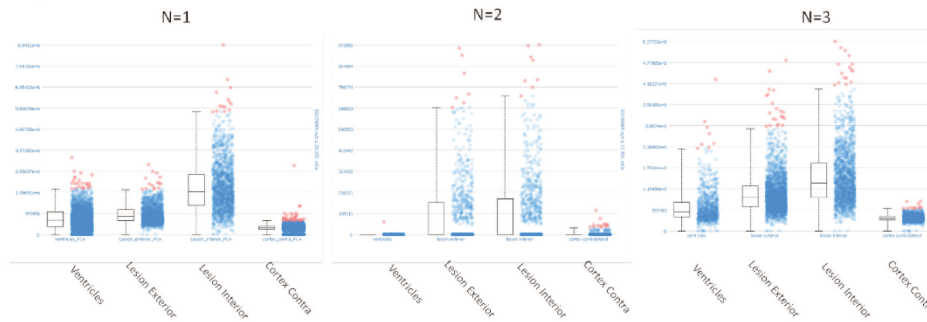
Supplementary Figure 2: Box plot representation of ion intensity of m/z peaks selected in the figures 5, 6, and 7 of the manuscript for all three replicates (number of replicates=3).

A) Box plot intensity representation of m/z 804.542, 832.58, 774.53, and 869.46 corresponding to all three replicates.

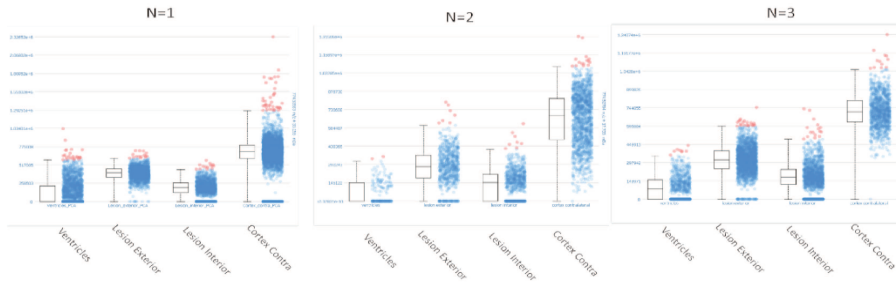
m/z 804.542



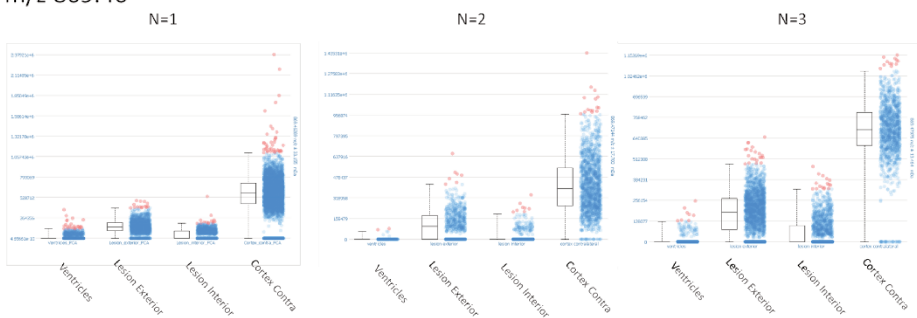
m/z 832.58



m/z 774.53

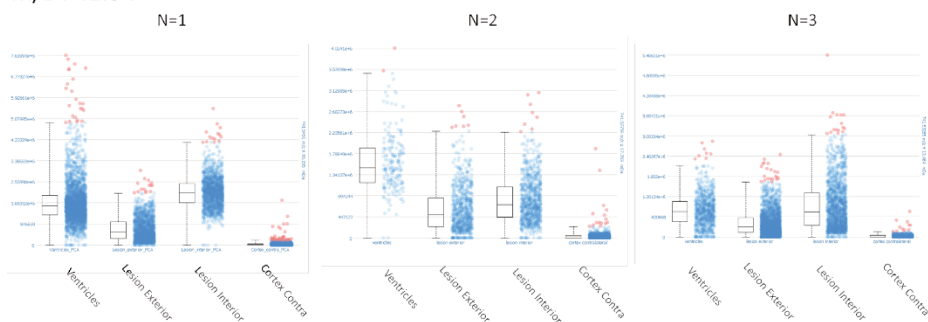


m/z 869.46

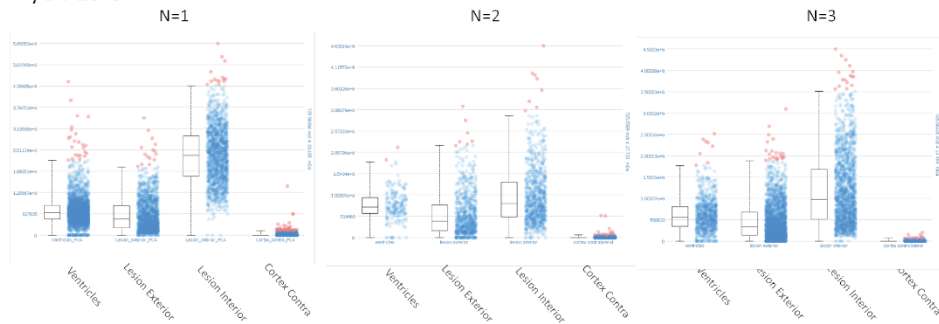


B) Box plot intensity representation of m/z 741.54, 725.54, 543.50, and 683.45 corresponding to all three replicates.

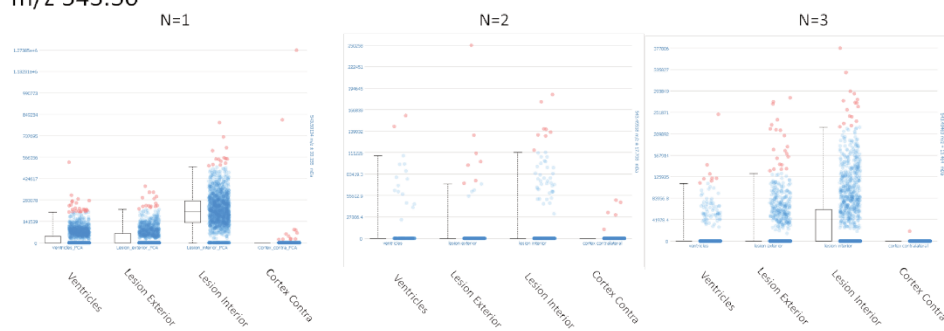
m/z 741.54



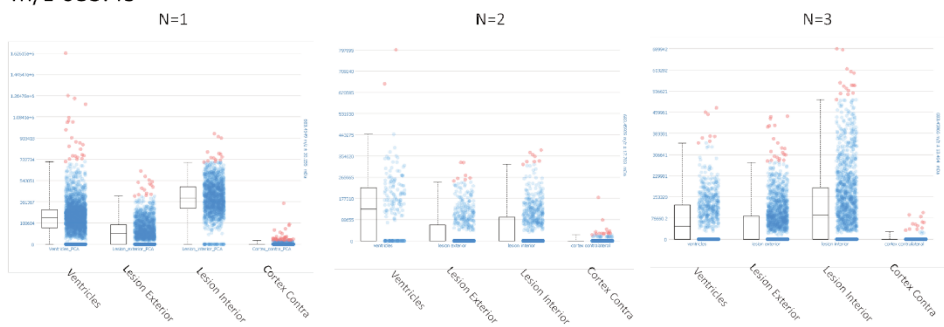
m/z 725.54



m/z 543.50

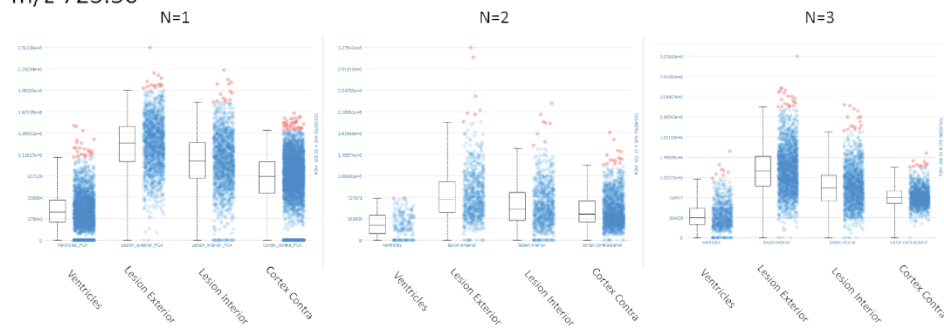


m/z 683.45

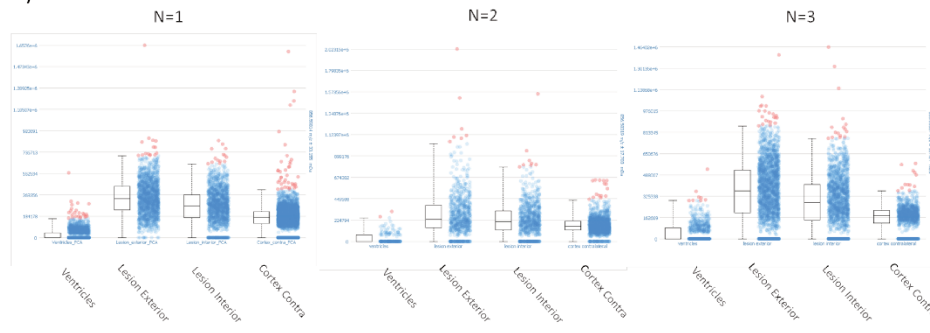


C) Box plot intensity representation of m/z 723.50, 856.59, 797.57, and 398.04 corresponding to all three replicates.

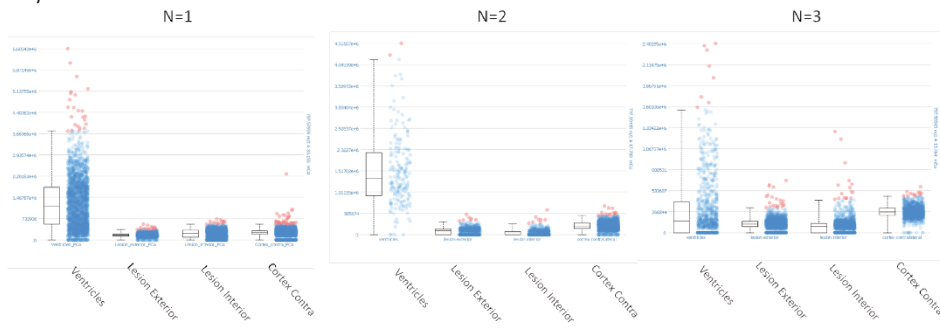
m/z 723.50



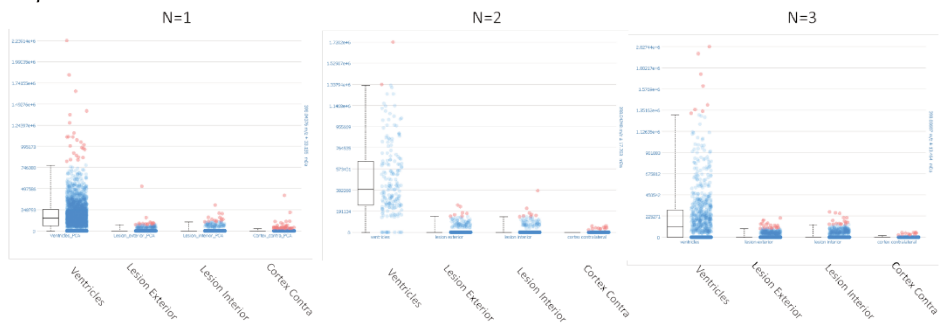
m/z 856.59



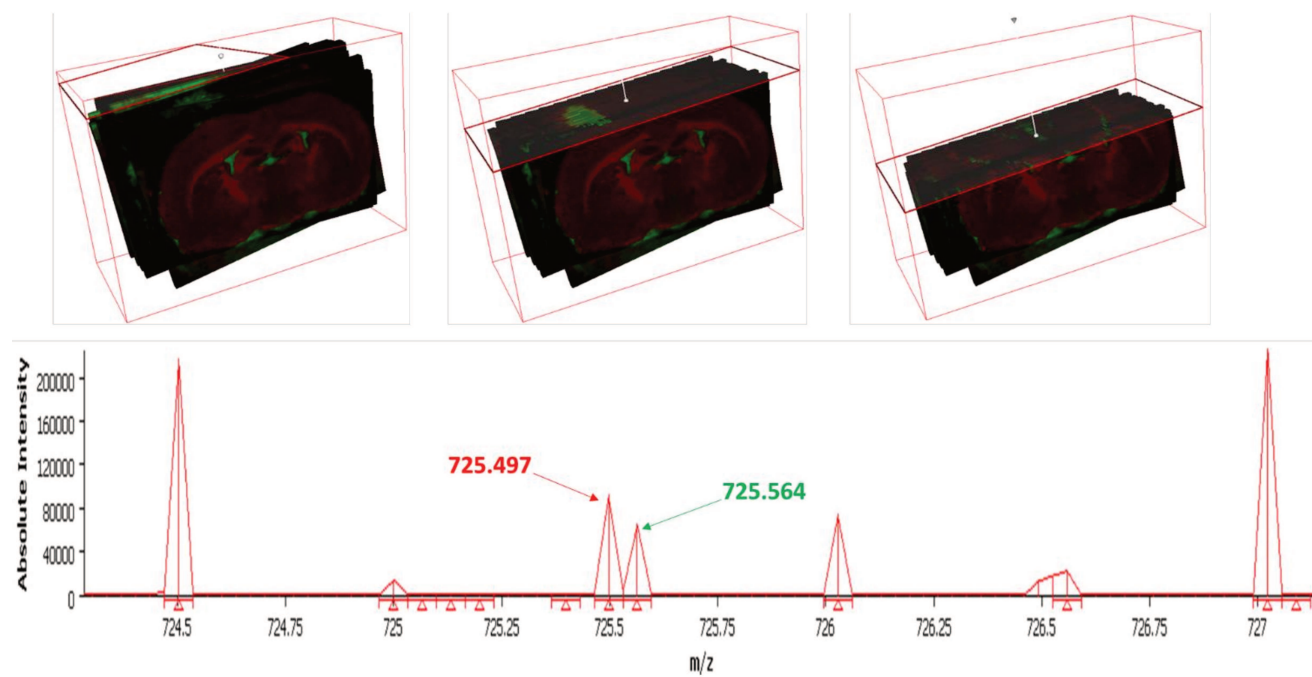
m/z 797.57



m/z 398.04



Supplementary Figure 3: 3D distribution of m/z 725.497 (red) and 725.564 (green) at 3 days post injury.



Conclusion – Chapter 1

We have provided in this paper, an applicable technological workflow to perform 3D MS imaging of tissue/organs using high resolution MALDI-LTQ-XL orbitrap. The use of this instrument showed further advantage of 3D MSI, as it proved the specificity factor when compared to other 3D conventional techniques and other mass spectrometry analyzers (such as the Time-of-Flight), as we were able to differentiate between 2 molecules with a difference of 0.07 Da in size. This workflow shows that by converting large data sets generated by the MALDI-LTQ-XL orbitrap into an imzML neutral vendor format, and then processing the data in SCiLS (GmbH) software, we can obtain a volume filled reconstructed image of the injured rat brain. We also showed the advantage of performing several statistical analysis studies such as ROC analysis and co-localization results in depicting m/z ions corresponding to lipid species that are co-expressed in the ventricular system of the brain and the injured cortical tissue in same manner, or other lipid species which are expressed in each of the mentioned regions solely. Our data clearly showed the expression of lipid species throughout the ventricular system as it evolves from a small circular node the frontal part of the brain to a wide cavity in the rear part near the cerebellum, thus showing again the strength of applying such technique on tissue samples such as TBI. The expression of m/z within such size-evolving organs is much more clearly understood and visualized in 3D manner when compared to a 2D approach. The spatial segmentation, depicted two lesion specific clusters, which by visualizing the complete 3D reconstruction, showed no expression in any other regions of the brain.

After determining such lesion related molecules, and in an aim to obtain a deeper comprehension of the lipid involvement within the cortical tissue, I then carried out a lipid MALDI-MSI analysis of TBI with time course and correlated with proteins involved in the injury which will be acquired in a micro-proteomic approach. These two main points are addressed in Chapter 2.

Chapter 2: Spatially and Temporally Resolved Omics Approach applied to Traumatic Brain Injury

Introduction

In any disease or injury, such as TBI, the analysis and identification of biochemical markers is important in diagnosing dysfunction in the related organ or group of organs. These biochemical markers, “Biomarkers”, can help in explaining the cellular and physiological changes occurring post injury, resulting in a more accurate assessment and case diagnosis, in addition to their possible targeting in a therapeutic approach based on their function. In TBI, many protein biomarkers and other lipid ones have been realized. In fact, there are three main sources to identify TBI-related biomarkers: Brain Tissue, Blood (serum/plasma), and Cerebrospinal Fluid (CSF) (Wang et al. 2005). In CSF, biomarkers such as “Total Tau Protein” and “Gamma-Enolase” as potential fluid biomarkers in mild TBI (Zetterberg et al. 2013), along with Ubiquitin C-terminal hydrolase-L1 (UCH-L1) and Spectrin Breakdown Products (SBDP) have been shown to have highly elevated levels post injury (Kobeissy et al. 2006). Also, glial fibrillary acidic protein (GFAP), an intermediate filament only found in astrocytes, and its breakdown products have emerged as a strong candidate protein biomarker released into the bio-fluids of the body after injury (Yang & Wang 2015).

Along with protein biomarkers, several research groups have focused on identifying lipid biomarkers for TBI. One perfect example is the work done by Roux et. al, where the expression level of abundant lipid families, such as ceramides were tracked using MALDI MSI with respect to days post TBI (Roux et al. 2016). The ceramide expression levels increased as early as 1 day post impact while that of sphingomyelin didn't increase until the third day after trauma. Nielsen and co-workers identified bis(monoacylglycero)phosphate (BMP) species as biomarkers for macrophage/microglia cells performing phagocytosis and N-acyl-phosphatidylethanolamine as a biomarker of dead neurons in a mice cerebral ischemia injury model (Nielsen et al. 2016). This is one of the few studies which linked such identified biomarkers with the cells found in the injured brain, either neuronal cells, or immune system ones.

Although many biomarkers have been characterized for TBI, this form of injury remains a major burden on society with no effective treatment. Several factors can contribute to this slow

progression in treatment for TBI, including lack of a complete understanding of the different protein and lipid factors implicated in the early phases post injury. The link between such species of biomolecules (proteins and lipids as an example) is yet to be studied. In addition, not many studies have tried to link these identified biomarkers with the surrounding systems of the body, mainly the immune system. To add, most of the proteomic studies have been performed on liquid samples (as in the case of plasma/serum related studies) or on large-sized tissue samples, which in turn may lead to inaccurate identification or even loss of detection of several proteins. Such proteins could have low non-abundant expression within the injured tissue. Thus, by studying a large tissue sample, the detection of such low expressed proteins can be more difficult as they may be masked by the higher expression of other abundant proteins.

In this context, I decided to perform a fundamental spatially and temporally resolved study on an open-head TBI model while focusing on the proteomic and lipid changes within the injured microenvironment of the brain tissue. A rat animal model was subjected to TBI, and the animals were kept for 1 day, 3 days, 7 days, and 10 days in order to mimic the acute and sub-acute phases of the injury which last up to 10 days post impact. Using several Omics approaches, including MALDI MSI and LC-MS/MS, we desired to track and possibly identify new biomarkers corresponding to either lipids or proteins. 2-dimensional MALDI-MSI was performed using the same high resolution MALDI-LTQ-XL-Orbitrap as before on injured rat brain at previously mentioned time points, as well as non-injured sham. The injured microenvironment in the tissue sections directly consecutive to the imaged ones, were subjected to a microproteomic approach. Finally, the MALDI imaged data, along with the microproteomic data, were all linked together with involved cells present in the microenvironment of injury in order to have a complete understanding of the involved processes in time manner and location. These results are present in Article 2.

Article 2: Systemic Biology Study of Mild-TBI Unveils the Role of Long Chain Acylcarnitines

Authors: Khalil Mallah, Jusai Quanico, Antonella Raffo-Romero, Soulaymane Aboulouard, Firas Kobeissy, Kazem Zibara, Michel Salzet, and Isabelle Fournier.

Article Status: Submitted to Neuron Journal (Cell Press).

Summary: Experimental manipulations, along with sample preparation and data analysis was performed by Mr. Mallah. He also wrote the paper, along with his co-authors, and participated in the revision. In detail, my contributions include:

- Performing the experimental TBI procedure and collection of tissue.
- MALDI-MSI experimentation and sample preparation including cryosectioning the tissue, matrix deposition and image acquisition on the MALDI-LTQ-XL Orbitrap instrument.
- Lipid extraction and MS/MS analysis for designated m/z identification.
- Performing on-tissue digestion and peptide collection for the micro-proteomics experiments.
- Protein extraction from cell lines along with preparation and digestion for the LC-MS/MS analysis.
- Participated in performing the systems biology proteomic pathway analysis, and ClueGO data analysis. .
- Data interrogation post LC-MS/MS analysis using Maxquant software, followed by statistical analysis using Perseus Software (Heatmaps, Scatter Plots, etc.).
- Data processing on Scils software, including spatial segmentation analysis, ROC analysis, coloc analysis, and principal component analysis.
- In terms of writing the manuscript, Mr. Mallah wrote the initial drafts which were then built upon in the subsequent writing of the final manuscript.

Systemic Biology Study of Mild-TBI Unveils the Role of Long Chain Acylcarnitines

**Khalil Mallah^{1,2}, Jusal Quanico¹, Antonella Raffo-Romero¹, Soulaymane Aboulouard¹,
Firas Kobeissy³, Kazem Zibara², Michel Salzet^{1*}, Isabelle Fournier^{1,4*}**

¹Université de Lille, INSERM, U1192 - Laboratoire Protéomique, Réponse Inflammatoire et Spectrométrie de Masse (PRISM), F-59000 Lille, France

²ER045, PRASE, Laboratory of Stem Cells, Department of Biology, Faculty of Sciences-I, Lebanese University, Beirut, Lebanon

³Department of Biochemistry and Molecular Genetics, Faculty of Medicine, American University of Beirut, Beirut, Lebanon

⁴Lead contact

SUMMARY

Traumatic brain injury (TBI) is a major cause of death worldwide and the leading cause of seizure disorders. In a therapeutic approach, protein biomarker hunting has led to the identification of protein markers such as glial fibrillary acidic protein (GFAP) but in relatively large size tissue samples or liquid samples as serum/plasma. In our work, we performed spatiotemporal systemic biology approach post-TBI using spatially-resolved proteomics within cortical area coupled to lipidomics generated by Mass Spectrometry Imaging (MSI) to deeply understand the processes involved in the microenvironment of the injury. This enabled to establish the molecular spatiotemporal map of TBI markers in time course and highlighted the role of the acylcarnitines. Finally, through microglia production of acylcarnitines in substantia nigra 3 days after lesion and overexpression of leader proteins such as GPR158, HGMB1, Synaptotagmin and Glutamate Decarboxylase proteins, we can correlate mild-TBI with Parkinson's disease.

*Correspondance: **Prof. Isabelle Fournier** (isabelle.fournier@univ-lille.fr), **Prof. Michel Salzet** (michel.salzet@univ-lille.fr), Laboratoire Réponse Inflammatoire et Spectrométrie de Masse (PRISM), Inserm U1192 - Université de Lille, Faculté des Sciences, Campus Cité Scientifique, Bât SN3, 1er étage, F-59655 Villeneuve d'Ascq Cedex. Phone: +33 (0)3 20 43 41 94; Fax: +33 (0)3 20 43 40 54

KEYWORDS

Traumatic brain injury; MALDI Mass Spectrometry Imaging; Spatially-Resolved Microproteomics; Spatiotemporal study; long-chain acylcarnitines; macrophages; astrocyte; Substantia nigra.

INTRODUCTION

Traumatic brain injury (TBI) is a leading cause of mortality and morbidity worldwide. TBI is characterized by the transfer of a force from an external object to the head leading to neuropathology damage and dysfunction (Mckee & Daneshvar 2015). This external force may be a blow or jolt to the head and results in an altered mental state. Due to the lack of awareness, TBI has long been known as a “silent epidemic” contributing massively to the increase in number of worldwide death and disability. In the USA, according to the center of disease control and prevention, and based on data between the years of 2002-2006, approximately 1.7 million people sustain a TBI annually (Faul et al. 2010). Of the 1.7 million cases, 1.4 million are treated and released from the emergency room, 275,000 are hospitalized, and 52,000 die. In addition, approximately 69 million people are estimated to sustain a TBI each year worldwide (Dewan et al. 2018), with majority of the cases being either of mild severity (81%) or moderate severity (11%). Dewan et al. concluded that low and middle income countries witness nearly 3 times more TBI cases when compared to high income countries. Using animal models, several therapeutic strategies have been proposed and studied in TBI, mainly: neuroprotection, neurovascular regeneration, and neurorestoration (Galgano et al. 2017). In the neurorestoration approach, cell-based therapy, mainly neural stem cell (NSC) /neural progenitor cells (NPC) treatment, have been studied in both endogenous and exogenous transplantation methods. One example of exogenous transplantation was the work done by Blaya et al, NPC transplantation led to neuroprotection,

along with enhancement of hippocampal neurogenesis, and improvement of functional outcomes in a fluid percussion TBI model (Blaya et al. 2015). Although several efforts over decades have been put to develop treatment strategies, TBI still lacks an effective therapy. This may be due to a deficiency in the full understanding of molecular mechanisms occurring within the microenvironment of the injury considering the different biomolecule partners including lipids, proteins, and metabolites along with their potential interactions. Such integrative biology study is missing and would clearly benefit to find new therapeutic targets.

The biological processes occurring post injury have been shown to follow two main phases. The so-called primary phase is due to direct mechanical insult to the brain resulting in shearing or stretching of the brain tissue. The secondary phase is characterized by diffuse axonal injury and inflammation (Das et al. 2012). It has been suggested that TBI is implicated in several other neurodegenerative diseases such as Parkinson's disease (PD)(Gardner et al. 2018) and Alzheimer's disease (AD) (Johnson et al. 2010)(Roberts et al. 1994). In fact, Acosta et. al showed that the expression of α -synuclein-positive dopaminergic neurons in the Substantia nigra pars compacta was elevated in the ipsilateral hemisphere of a rat TBI model at 60 days post injury, when compared to the contralateral hemisphere of the same injured condition from one side, and either hemispheres of sham non-injured rat on the other hand (Acosta et al. 2015). The aggregation and accumulation of truncated forms of α -synuclein in the Substantia nigra, along with the continuous loss of dopaminergic neurons is a hallmark of Parkinson's disease (Xu & Pu 2016). In addition, the expression α -synuclein was shown to be regulated by microglia in the Substantia nigra and not astrocytes at 30 days post controlled cortical impact injury in a mouse model (Impellizzeri et al. 2016). Microglia and astrocytes are important mediators of inflammation and cellular response in TBI (Karve et al. 2016).

Lipid metabolism dysfunction is believed to be involved in several neurological disorders such as schizophrenia and neurodegenerative diseases such as Parkinson's and Alzheimer's diseases (Wenk 2005) and CNS injury such as TBI. Thus, studying the lipid change in the nervous system in such cases is of major importance, as this system contains the second highest concentration of lipids in the body (Adibhatla et al. 2006). One of the most advanced and sensitive method for monitoring lipid changes within biological samples is Matrix Assisted Laser Desorption/Ionization-mass spectrometry imaging (MALDI-MSI). MALDI-MSI allows to track and visualize the spatial distribution of a broad panel of lipids within a sample in a single

experiment (Zemski Berry et al. 2011). Several studies have been realized for tracking lipid changes post injury to the brain. Using a controlled cortical impact (CCI) rat model, Sparvero et al. monitored the spatial distribution of cardiolipins within the brain after acute brain injury by performing MALDI-MSI (Sparvero et al. 2016). They showed that the expression level of several cardiolipin species, including CL(72:6) and CL(74:7), decreased in the injured impacted side of the brain when compared to the contralateral non-injured side, and this decrease was also witnessed in the underlying hippocampal and thalamic regions. In similar decreasing expression pattern, several phosphatidylinositol family members, especially PI(38:5) and PI(38:4) were identified. In a rat ischemic/reperfusion injury model, Hankin et al. showed an increase in ceramide (d18:1/18:0) when compared to sham non-injured condition (Hankin et al. 2011). Finally, Roux et al. conducted a temporal study on the CCI model to visualize the differences in lipid expression up to 7 days post impact while conducting MALDI MSI in the abundant lipid mass range from 630 – 950 Da (Roux et al. 2016). In the grey matter post injury, the most significant changes with respect to time were visualized in the lipid classes of ceramide, diacylglycerol, and cholesteryl ester. Ceramides showed the highest expression at 1 day post injury and then this expression decreases gradually to reach lowest levels at 7 days post injury. Diacylglycerol had minimum expression at 1 day, reached maximum at 3 days, and then decreased again at 7 days post injury. Thus the study of such lipid change post impact, along with the molecular mechanisms is of great impact in understanding the processes that occur post injury.

In the present study, we performed a spatiotemporal MALDI MSI analysis on a rat CCI model. The experiments were conducted by considering the acute and sub-acute phases post injury (1 day, 3 days, 7 days, and 10 days) and taking into account different segments within the injured brain (rostral, lesion, and caudal) which correspond to different areas of the brain. Contrary to previously performed MSI studies on TBI, we used a high spectral resolution mass spectrometer instrument while not only focusing on the abundant m/z range (600-900 Da), but also on the lower mass range (<600 Da). In addition, we focused on studying lipid changes in lesion containing tissue segments, along with other segments that contain no direct mechanical damage in an approach to identify other affected parts of the brain rather than only focusing on the impacted cortical tissue. We considered monitoring the proteomic changes within the injured microenvironment (1 mm² surface area) of the cortex by spatially-resolved microproteomics (Quanico et al. 2013), in an aim to have a more accurate characterization of such changes when compared to previously performed studies.

Finally, in a systemic biology view, spatially-resolved microproteomics and lipidomics data were linked to obtain a better understanding of the TBI and possibly identify new biomarkers for TBI.

RESULTS

Spatially-resolved microproteomics analysis reveals time point-specific proteomic phases

The complete workflow of our study design is represented in **Figure S1**. With respect to time, the injured cortical tissue was subjected to on-spot tryptic digestion followed by liquid microjunction extraction within a total surface area of 1 mm² as seen in the zoom picture of the optical scan of a lesion segment at 3 days post injury (**Figure S2A**). The extracted peptides were subjected to shotgun analysis followed by label free quantification. 1950 proteins were identified across all samples, and 306 proteins showed significant difference in expression based on LFQ values after subjecting the data to multiple ANOVA tests with a p-value = 0.01. Principal component analysis (PCA) was applied on the 306 quantified proteins comparing all injured time points and the non-injured sham, in order to describe the variance across all samples of different conditions. The first component explains 63.2% of the variance of samples, while the second component explains 12.8%, thus yielding 76% of the variance observed. Plot of the first two PCs shows that for each time point, all three replicates clustered together with no interference from the other conditions (**Figure S2B**). Time points 3 and 7 days cluster separately from the rest of the time points and are positively correlated to the first component. Hierarchical clustering performed on the 306 proteins shows 5 main clusters (**Figure 1A**), from which we can deduce 4 main phases of protein processes that progress throughout the first 10 days of TBI. Phase 1 is characterized by the proteins which are upregulated in the sham condition and at 10 days post injury, thus showing a possible restore of function at this time point. This phase is divided into two parts: phase 1a corresponding to cluster 1 and phase 1b corresponding to cluster 2 in **Figure 1A**. Phase 1a corresponds to a group of proteins that are elevated at sham and surprisingly at 1 day post injury. This expression decreases at 3 and 7 days post injury and then re-elevates again at 10 days. This cluster includes all proteins which are found in normal cell functions. Detected proteins such as: Atp1a2, Brsk1, Napa, Ppp1r9a and Slca3 are all implicated in neurotransmitter transport as seen in the ClueGo analysis (**Figure S3A**). Several proteins involved in normal cellular respiration were also up-regulated at the mentioned time points including: Sco2, Aldh5a1, Cox4i1, and Dlat. Phase 1b

(cluster 2) shows elevation in expression of 22 proteins at sham condition. This expression decreases at directly after injury i.e. 1 and 3 days, and then restores its upregulated expression at 7 and 10 days. Several proteins in this cluster such as Slc27a1, Acsf2, and Acsbg1 are associated with lipid processes within the cells such as lipid transport and energy production. Phase 2 is represented by cluster 4 in **Figure 2A**, and mainly is characterized by the set of proteins that are upregulated just after injury (1 day post injury) and continue their overexpression throughout 3 and 7 days post impact, were after that, the expression decreases again at 10 days to similar conditions as the sham. Phase 2 is mainly characterized by blood related processes including platelet activation and aggregation (**Figure S3B**), resulting in a platelet plug formation due to the increase in expression of the several fibrinogen proteins including: F2, Fga, Fgb, Fgg, and Hrg. In this phase also, many proteins involved in acute inflammation are overexpressed including complement protein C3, Mug1, and Serpina1. Phase 3 ,corresponding to cluster 5, in the first 10 days is also injury related, but is not present until 3 days post injury and only stays elevated until 7 days post injury were the expression levels of these proteins return to the sham levels at 10 days post injury. In this phase, several proteins involved in apoptotic execution phase are detected, including: Gsn, Lmb1, and Vim. In addition, as Hspb1, Pak2, Psme1, and Psme2 involved in MAPK6/MAPK4 signaling pathway are increased. Finally, and within the same phase several DNA related proteins, especially ones involved in translation have increased expression (**Figure S3C**). These mainly include elongation factor proteins such as Eef1d and Eef2 along with a major amount of ribosomal proteins including: Fau, Rpl10a, Rpl13, Rpl15, Rpl18, Rpl4, Rpl6, Rplp0, Rps13, Rps3, and Rps8. Phase 4 within the first 10 days corresponds to cluster 3 which contains a small group of proteins including GFAP and Heat shock-related protein (Hspa2), and FABP7 that have increased expression at 3, 7, and 10 days post impact. These proteins are mainly injury related but are not expressed until 3 days after impact and remain with high expression even after 10 days of impact. The proteins found in this cluster are mainly implicated in the initiation of regeneration, astrocytosis, and re-myelination. A representative scheme summing up all described phases is found in **Figure 1B**.

MSI followed by spatial segmentation reveals lipid lesion-specific expression

Tissue segments from rostral, lesion, and caudal positions of non-injured rat brain (sham) and open head injured rat brain at 1 day, 3 days, 7 days, and 10 days post injury were subjected to

lipid MALDI-MSI using MALDI-LTQ-Orbitrap-XL. The CCI instrument allows the injury of the same position, and thus allowing all rat samples to be reproducible with regard to injury position within the brain. All rat replicates received an injury in the same position on the right parietal cortex using an impactor tip of 2 mm surface area. As a result, we were able to image lipids on the same rat atlas position (Bregma -3.60 mm) in all brains (injured and sham) corresponding to our chosen lesion segment. In addition, position (bregma -1.80 mm) and position (bregma -5.60 mm) were chosen for the rostral and caudal segments, respectively. Due to the impactor tip size, the selected rostral and caudal tissue segments had little or no tissue loss when compared to the lesion segment. After MALDI-MSI, unsupervised spatial segmentation was performed using Manhattan distance calculation method to visualize regions sharing similar lipid distribution within the same tissue, and in comparison with the remaining time points and tissue positions. **Figure 2A** shows an example representative results for one replicate; other segmentation results can be found in the supplementary data. By dissecting further the cluster tree, a cluster emerged corresponding to the injured cortical tissue (cluster 6742-yellow) can be observed (**Figure 2B**). This injury-unique cluster is localized in the microscopically observed injured area and had little to no presence in all three segments (rostral, lesion, and caudal) of the sham brain as seen in the optical images (**Figure 2C**). In addition, cluster 4396 (light blue) also shows distinct localization within the injury site. However, it is present not only in the cortical tissue, but also in cavities formed after injury. Inter-comparison between the time points shows a wider spread of this injury-related cluster at 3 days post injury, as the cluster can now be also observed in the rostral and caudal segments. Co-registration of optical images of the MALDI imaged brain segments with the spatial segmentation results of the lesion tissue from at all time points shows the precise co-localization of the histologically altered injury site and the obtained injury-related clusters (**Figure 2C**).

To further validate our obtained results, the same unsupervised spatial segmentation approach was applied on only lesion segments from all three replicates in one batch of analysis (**Figure S4A**). Injured cortical tissue at all time points and in all three replicates grouped together in the same cluster (cluster 8087 – green) with very little or no distribution in the sham. To visualize the different and similar profiles corresponding to the area of injury when compared to the uninjured cortical tissue, PCA was applied on manually drawn cortical regions between all conditions of all lesion segments in all three replicates (**Figure S4B**). The data corresponding to the 3 selected cortical tissue regions from sham clearly separate from the remaining clusters

corresponding to the injured cortical tissue (**Figure S4C**). Although this result shows a clear difference in lipid content between sham and injured tissue, no clear separation was observed between different time points post injury. The PCA corresponding to all injured tissues at different time points tend to mix thus yielding an unclear observation for the lipid profile regarding injury at different time points.

MALDI MSI shows altered lipid expression between injury and non-injury

PCA analysis allowed a separation between injured cortical tissue and non-injured sham, but did not separate between the selected time points with respect to the presence or not of certain lipids, and the variation in expression level between different time points post injury. For this reason, receiver operating characteristic (ROC) analysis was performed by comparing the same selected regions that were previously used in the PCA analysis (**Figure S4B**) in order to depict unique signals corresponding to both injured tissue and non-injured tissue (sham). In addition, we aimed to monitor the expression variation of the injury related signal in time course along all the replicates of our lesion segments. With a threshold of 0.75, ROC analysis reveals 67 m/z peaks specific to sham condition when analyzed against all four injury time points (**Table S1**). Of these 67 ion intervals, two examples m/z 769.57 and 798.53 ± 24.967 mDa corresponding to PA(39:0) and PS(37:4) show elevated expression within the sham non-injured cortical tissue and a lower level of expression for the injured cortical tissue at all selected time points (**Figure S5**). The box scatter plot clearly demonstrates this decrease in expression in injured tissue for all replicates of the study.

We then performed the same ROC analysis as before, but now comparing lesion segments from 1D, 3D, 7D, and 10D all combined versus the non-injured sham tissue, in order to obtain lesion-specific signatures and visualize their variation in time. With a threshold of 0.75, the ROC analysis yielded 82 peaks allowing to distinguish injured tissue from non-injured one (**Table S2**). In the most abundant mass range of lipids, which is between 600-900 m/z, molecules such as 666.48 and 780.56 ± 24.967 mDa assigned as PS and PC(36:5) respectively had elevated levels within the injury area when compared to sham (**Figure 3**). These 2 m/z values show a slight increase of expression intensity at 1 day post injury. The expression continues to increase until reaching a maximum expression at 3D post injury and followed by a decrease at 7 and 10 days post injury but still higher than 1D.

Meanwhile, in the lower mass range, $m/z < 600$, we identified several injury specific m/z including: 400.35, 459.25, 475.22, 487.28, 518.32, 534.30, 544.34, 546.36, and 562.34 ± 24.967 mDa. M/Z 400.35 came to our attention as this lipid showed not only an increase and localized expression within the cortical tissue but in the corpus callosum of both hemispheres as well, with a higher intensity in that of the injured hemisphere. This lipid had no expression on the no-injured cortical tissue of the opposite hemisphere within the same brain. A slight increase within the injured tissue is seen at 1D post injury, but the maximum expression intensity is visualized at 3D post injury (**Figure 4**). However, in all injury time points, the m/z 400.35 (green) is outlining the injured tissue along with slight diffusion into the interior, unlike m/z 518.32 (red), assigned as Lysophosphatidylcholine (16:0), which shows clear involvement and direct localization within the center of the lesion and not on the injury border. At 7D and 10D post injury, and although the expression of m/z 518.32 stays localized within the injury, the intensity expression of m/z 400.32 is no longer localized much within the cortical tissue, rather its expression stays focused in the underlying corpus callosum, but is still increased when compared to the sham. Neither m/z 400.35 nor m/z 518.32 were found to be expressed within the non-injured sham tissue.

Injury-related Lipid Biomarker at m/z 400 is Palmitoylcarnitine

m/z 400.35 became of high interest since it has never been described or discussed in the context of traumatic brain injury. In addition, our results suggest that the expression level of this lipid is relevantly high and only detected post injury with highest expression at 3D post injury. We therefore decided to focus our study on understanding the localization of m/z 400.35 along with its identification and possible function post injury. To confirm the identity of m/z 400.35, we performed MS^n analysis using MALDI-LTQ-XL on lipid extracts from the injury site at 3 days post injury. We identified this molecule and assigned it as Palmitoylcarnitine (C23H46NO4) (**Figure S6A**). To further validate the identity of our palmitoylcarnitine molecule, we subjected a commercial pure palmitoylcarnitine standard (AVANTI Polar Lipids) to MS^n in the same manner on MALDI-LTQ-Orbitrap-XL (**Figure S6B**). In addition, we searched in literature for the MS^2 fragmentation pattern of m/z 400.35 and the peaks found by Hulme et al. (Hulme et al. 2017) and those obtained from the MS^2 of our standard lipid were the same MS fragments for m/z 400.34 as in our lipid extract at 3 days post injury. The MS^2 spectrum of m/z 400.34 yielded one strong intensity peak at m/z 341.268 and one small intensity peak at m/z 239.236. When compared to the

molecular structure of palmitoylcarnitine, the peak at 341.268 corresponded to the palmitoylcarnitine with the neutral loss of the N-trimethylamine group (a loss of 59). The second observed signal at m/z 239.236 corresponded to the loss of the glycerol backbone after subjecting the sample to MS3.

In order to obtain a clearer localization of palmitoylcarnitine within the other brain areas, and other possible lipids with same spatial distribution, we performed co-localization analysis with the m/z 400.346 using the sum of spectra from the injured areas for each time point alone. At a threshold of 0.3, 15 peaks were found co-localizing with m/z 400.35 including: 525.39, 518.27, 426.36, 398.32, and 372.31 (**Table S3**). Surprisingly, by preliminary annotation using Metlin online database and later on by MS2, we assigned the peaks at m/z 372, 398, and 426 as tetradecanoylcarnitine, O-palmitoylcarnitine, and oleoylcarnitine respectively which all belong to the same family of lipids as palmitoylcarnitine, the acylcarnitines (**Figure S7**). The difference between palmitoylcarnitine and o-palmitoylcarnitine is the presence of a double bond in the carbon side chain of the latter. Meanwhile the difference of palmitoylcarnitine with tetradecanoylcarnitine and oleoylcarnitine is the number of carbons in the side chain, as palmitoylcarnitine is 16:0, O-palmitoylcarnitine is 16:1, tetradecanoylcarnitine is 14:0, and oleoylcarnitine is 18:1. All four acylcarnitine members had the same distribution as palmitoylcarnitine regarding both time point and distribution within the tissue structures (**Figure S8**).

Expression of Palmitoylcarnitine in the Substantia nigra three days post injury

To further confirm the presence of our detected palmitoylcarnitine (16:0) in other possible affected regions within the remaining parts of the brain, other than the injured cortical tissue, we plotted the ion images of m/z 400 in the rostral and caudal segments of the different time points that we previously described in our paper. Surprisingly, in the caudal segment at 3D post injury and partially within the midbrain area, palmitoylcarnitine intensity was highly elevated in the Substantia nigra of the injured hemisphere (**Figure 5A**). The intensity of expression is equivalent to that present within the injured cortical tissue and not found in the remaining areas of the brain within the same tissue. At the same time, no other Substantia nigra at the caudal segments corresponding to different time points, neither did the sham show any expression of palmitoylcarnitine. The same spatially-resolved microproteomics approach applied to the injured

cortical tissue was now applied on tissue segments containing Substantia nigra of both ipsilateral (hemisphere of injury) and contralateral hemispheres (hemisphere opposite to injury) at 3 days post injury. The shotgun proteomics yielded the identification of 1513 proteins in which 55 were statistically significant between the ipsilateral Substantia nigra and the contralateral based on the LFQ expression with a p-value = 0.05. The generated heat map showed that 41 proteins are upregulated within the ipsilateral Substantia nigra when compared to the contralateral side (see Supplemental Spreadsheet 1). Interestingly, among these different proteins some, including synaptotagmins, High-Mobility Group Protein 1 (HMGB-1), Glutamate Decarboxylase (GAD), and GPR158, have been previously reported to be involved in Parkinson (**Figure 5B**). **This was further shown** using Anova statistical analysis for the LFQ value of the mentioned proteins and all showed increased significant expression within the ipsilateral substantia nigra when compared to the contralateral substantia nigra.

Localization of palmitoylcarnitine with resident microglia of lesion margins

Due to the blood brain barrier breach occurring post injury, circulating macrophages can infiltrate into the injured area of the brain. In addition, resident microglia have been shown to be attracted to the injured cortical tissue and surround the injured tissue. As previously stated, the palmitoylcarnitine expression surrounds the injured tissue in a possible role to isolate this area from the remaining intact non-injured tissue. In order to confirm the localization and correlate it with the resident microglia or infiltrating microglia/macrophages, immunofluorescence staining experiments were performed. For this, we double stained lesion segment at 3 days post injury with CX3C chemokine receptor 1 (CX3CR1) and beta-galactoside-binding S-type lectin galectin-3 (Mac-2) which are expressed on both resident microglia and bone marrow-derived macrophages/microglia. However, it is the intensity ratio difference of expression between these two markers which allows to differentiation between them. In fact, cells expressing high intensity of CX3CR1 when compared to Mac-2 (CX3CR1⁺⁺⁺/Mac-2^{+/-}) corresponds to resident microglia. On the other hand, the more intense signal of Mac-2 when compared to CX3CR1 correspond to bone marrow-derived macrophages/microglia, thus infiltrating cells into the injured environment (Wang et al. 2015). Staining of the tissue at 3D post injury reveals more intense CX3CR1 on the surrounding of the injury thus resident microglia a possible role to sequester and isolate the damaged tissue while the core of the injury shows a more intense signal of Mac-2 thus resembling

the infiltrating macrophages (**Figure 6**). By performing MALDI imaging on consecutive tissue of the one subjected to IF, palmitoylcarnitine clearly co-localizes with the resident microglia of the brain in the same expression pattern, thus forming a barrier around the injured tissue.

Palmitoylcarnitine induces inflammatory action in macrophages and neurogenesis in astrocytes

In order to understand the biological effect of palmitoylcarnitine on different cells present in injured environment, the lipid was used to stimulate macrophage and astrocyte cell lines. Post stimulation, a shotgun bottom-up proteomics approach was performed on the protein extracts from the mentioned cell lines, along with label-free quantification (LFQ). These were then compared with protein extracts from their corresponding non-stimulated controls. Proteomic results were subjected to principal component analysis and (PCA) and results show that the proteomic profile upon palmitoylcarnitine stimulation of all three cell lines differs from the corresponding control non-stimulated condition (**Figure S9**).

Shotgun bottom-up proteomics analysis of astrocytes yielded 1744 protein identifications across all samples, 74 of which showed significant difference in LFQ expression between palmitoylcarnitine-stimulated astrocytes and control (**Figure S10**). 28 proteins were upregulated in the control when compared to the palmitoylcarnitine-stimulated astrocytes including TFRC, CDK2, SKP1, and HSP90AA1, proteins which are implicated in cell homeostasis, meiosis, cell cycle, DNA repair and DNA replication. In addition these same proteins are involved in signaling mechanisms mainly NF- κ B signaling along with other proteins such as BST2 and PABPC1. Finally, upregulated control proteins such as ICAM1, CDK2, and PSMA5 all have function in immunity related proteins. In contrast, 46 proteins were found to be upregulated upon the stimulation with palmitoylcarnitine when compared to the control. Such upregulated proteins include SPARC, CTNNA1, VIM, and LOX proteins which are implicated in axonogenesis and regeneration. At the same time, these same proteins, along with others such as PLEC, CAPG, PTPNS, and SERPINE1 are all involved in cellular processes like invasion, cell adhesion, migration, and spreading. At the mitochondrial level, proteins involved in fatty acid oxidation and lipid metabolism such as PC, ALDH6A1, ACAA1, and ATP5B were all overexpressed after palmitoylcarnitine stimulation. Thus, stimulation of astrocytes by palmitoylcarnitine leads to

altered lipid metabolism, along with increase in the aggressiveness of such cells by performing actions such as cellular invasion and spreading but also trigger the neurogenesis.

A similar approach of palmitoylcarnitine stimulation was applied on WT macrophage cell line. Proteomic analysis yielded a total of 1099 proteins identified across all samples of which 789 were statistically significant between the stimulated and control conditions. Surprisingly, only 19 proteins were upregulated in control condition when compared to stimulated one, while 764 proteins were significantly upregulated after palmitoylcarnitine stimulation (**Figure 7**). In the control condition, proteins involved in synaptogenesis, PLC and phospholipase D signaling such as TXN, CFL1, and MARCKS were identified. However, upon stimulation, major inflammation reactions and inflammatory signaling pathways were overexpressed. Examples of proteins such as LGALS3, PLAA, ASCL1, and RAF1 which are implicated in inflammation were all over expressed. These proteins, along with others such as STAT5B, TMED7, CCDC22, MSN, VAV1, and RPL27A are precisely implicated in NF- κ B signaling, a signaling pathway known for involvement in inflammation (Liu et al. 2017). In addition, a large amount of proteins involved in processes such as immune response and phagocytosis were overexpressed. These include: STAT3, HMGB2, GLS, CD48, GAPDH, PARP1, FBL, PDIA3, and FTH1. Along with the previously mentioned processes observed post palmitoylcarnitine stimulation, others such as ROS generation, cell damage, neuronal death, and injuries were all enhanced by overexpression of several proteins including: RAF1, PLA2G4A, HSPA9, RHOA, PRKCD, and ANXA1. Taken altogether, stimulation of macrophages with palmitoylcarnitine led to an increase in pro-inflammatory response and enhancement of the phagocytic role of these cells. This stimulation led to an activation of such cells towards a full inflammatory phenotype with the ability to induce damage and clear cellular debris, thus possibly explaining one mode of activation of macrophages post-injury as a pro-inflammatory stimulator.

DISCUSSION

In the present study, we performed a spatiotemporal analysis on an open head rat TBI model using MALDI-MSI and spatially-resolved microproteomics. Our microproteomic results collected from within the injured microenvironment allowed us to characterize 4 phases of biological processes occurring within the first 10 days post impact. While phase 1 (a and b) were both characterized by conventional proteomic pathways that occur in uninjured conditions, phases

2, 3, and 4 explained better the injury related processes in time course. Phase 1 (a and b) showed the proteins that loss their expression after impact, but eventually regain the same expression at 10 days after impact. However, phase 2 characterizes the proteins that are elevated from 1 day after impact until 7 days. This phase is mainly characterized by acute inflammation and infiltration of blood-related proteins, which was expected as our injury CCI model induces breach within the blood-brain barrier, thus blood from the circulatory system can enter the injured environment. Surprisingly, phase 3, which corresponds to the proteins elevated at 3 and 7 days post impact, showed dual effect with regard to survival and death of cells within the injured tissue. While the dying cells are undergoing apoptotic execution, the surviving cells are initiating cellular repair at the DNA level by upregulating many ribosomal proteins involved in the translation process. Thus, the initiation of repair at the DNA level occurs as early as 3 days after impact. Taken together, compared to spinal cord injury, in which the inflammatory process when activated fully becomes chronic without any repair (Cizkova et al. 2014; Devaux et al. 2016) the whole of the proteomic data establishes 4 phases which at the end reveal high brain plasticity in mild-TBI. This leads the central question of the lipid role in this physiological mechanism, as it is well known that they act as central players in the regeneration process (Knobloch et al. 2012). To reply to this question, a lipidomic approach coupled to MALDI MSI has been performed and reveals the presence of the long chain acylcarnitine.

Long chain acylcarnitines (LC ACs, including palmitoylcarnitine and oleoylcarnitine) seem to be injury-related lipid biomarkers. In fact, during β -oxidation, these molecules are intermediate compounds in the shuttle of free fatty acids into the inner mitochondrial membrane. Thus, any mitochondrial damage or dysfunction can lead to the accumulation of these acylcarnitines. These LC ACs have been studied by several groups and in different fields of research. Using MALDI-MSI, palmitoylcarnitine was detected with high abundance at the loci of Salmonella typhimurium infection and mesenteric lymph node (MLN) disruption (Hulme et al. 2017). By culturing MLN cells (which include B and T cells, along with macrophages and dendrites) ex-vivo, stimulation with palmitoylcarnitine induced the apoptosis of one subset of T-cells (CD4+CD25+) via the caspase-3/7 pathway. Also palmitoylcarnitine co-localizes with disrupted immune cells, suggesting its possible mode of apoptotic action within the MLN. In MDA-MB-231 breast cancer cell lines, MALDI-MSI revealed the localization of acylcarnitines, mainly palmitoylcarnitine and stearoylcarnitine at m/z 400.3 and 428.3 respectively, along with lysophosphatidylcholine (LPC)

and other lipid species. The two acylcarnitine species were mainly located in the hypoxic regions of the tumor (Chughtai et al. 2013). Our study also revealed the presence of acylcarnitines and LPCs along the injured tissue. In addition, LC ACs are believed to have a pivotal role in the development of atherosclerosis. Treatment of apoE^{-/-} mice with methyl- γ -butyrobetaine (methyl-GBB) phosphate, an inhibitor of L-carnitine biosynthesis and transport, decreased the expression level of short chain (C2 to C4) acylcarnitine by 17 fold, and the expression level of medium chain (C6 to C12) and long chain (C14 to C18) acylcarnitine by 7 fold in aortic tissue. This treatment led to a significant attenuation of atherosclerotic lesions in the whole aorta thus suggesting a possible role of acylcarnitines in the development of atherosclerosis (Vilskersts et al. 2015). Methyl-GBB treatment also decreased the level of infiltration of macrophages and monocytes, thus explaining a possible mode of action for acylcarnitines by activating immune cells in the case of atherosclerosis.

LC ACs and even the medium chain acylcarnitines (MC AC) were proposed to have a pro-inflammatory effect on immune cells. Treatment of bone marrow-derived macrophages with lauroyl carnitine induced an “M1” pro-inflammatory phenotype in these cells (Sampey et al. 2012). In addition, treatment of RAW 264.7 cells, a murine monocytic cell, by acylcarnitine with a 14-carbon side chain led to an increase in COX-2 expression, an important toll-like receptor (TLR) target gene product, along with the increase in reactive oxygen species (ROS) production (Jennifer M Rutkowsky et al. 2014). This same treatment also induced the phosphorylation of JNK and ERK via MyD88 signaling pathway. Deeper into our proteomic data of macrophages stimulated with palmitoylcarnitine, several proteins that can stimulate or are involved in the MyD88 pathway are detected. One detected protein, high mobility group box 1 protein (HMGB1), has been shown to activate macrophages by acting as a ligand for TLR 2 and 4, resulting in the activation of the MyD88 signaling pathway (Peng et al. 2017). Another protein upregulated upon palmitoylcarnitine treatment, tyrosine protein kinase (SYK), plays a critical role as a regulator of MyD88 post-translational modifications, precisely by phosphorylating MyD88 (Gurung et al. 2017). In addition, signal transducer and activator of transcription 3 (STAT3), was also elevated post stimulation with palmitoylcarnitine. In the hypothalamus of mice, and in the state of infection and inflammation, MyD88 was shown to play an important role in the activation of STAT3 (Yamawaki et al. 2010). Thus, the increased expression of this protein post stimulation with palmitoylcarnitine may be an indication of the involvement of MyD88 inflammation in this process. Two major proteins of

importance, which were also increased post stimulation with palmitoylcarnitine are Galectin-3 and Heat shock Protein (HSPD1). HSPD1, also known as 60-KDa heat shock protein (HSP60), mediates neurodegeneration via the TLR4-MyD88 pathway in the cerebral cortex of a mouse model (Rosenberger et al. 2015). Finally, Galectin-3 has been shown to induce the proliferation and survival of cancer cells by signaling through TLR4 pathway, such as in the case of lung adenocarcinoma by activating the TLR4/MyD88/p-p65 pathway expression (Zhou et al. 2018). In a recent study of traumatic brain injury, galectin-3 has been shown to be largely expressed in microglia and detected in cerebrospinal fluid. Galectin-3 is known to bind to TLR-4, and administration of a neutralizing antibody against galectin-3 decreases the expression of IL-1 β , IL-6, TNF α and NOS2 and promotes neuroprotection in the cortical and hippocampal cell populations after head injury (Yip et al. 2017). Galectin-3 is constitutively expressed in the subventricular zone (SVZ) and the rostral migratory stream (RMS) (Comte et al. 2011). Gal-3 does not affect neurogenesis, but, instead, regulates neuronal migration. Gal-3-null mice exhibit aberrant SVZ astrocyte morphology and reduced SVZ neuroblast migration. Explants treated with Gal-3-blocking antibody also show decreased neuronal migration, whereas expression of recombinant Gal-3 increases migration distances.

By comparing with our micoproteomic data, we were able to detect the presence of Galectin-3 and HSPD1 in cluster 5 of the heatmap in **Figure 2**, i.e., with elevated expression at 3 and 7 days post injury. Galectin-3 has been previously described in the context of TBI (Nishikawa & Suzuki 2018). Our work suggests a possible further explanation for the activation mechanism of Galectin-3 post-injury. The expression time point at 3 days post injury in the spatially-resolved microproteomic data is in coherence with the maximum expression of several acylcarnitine members at 3 days post injury. Galectin-3 is a chimeric galectin that possesses both a C-terminal carbohydrate-recognition domain (CRD), and an N-terminal aggregating domain that can interact with non-carbohydrate ligand partners. It has been suggested to act as a pathogen pattern recognition receptor that can detect pathogen-associated molecular patterns (PAMPs) and endogenous ligands from tissue injury, and has been reported to bind to LPS via both C' and N' terminals (J. M. Rutkowski et al. 2014). Saturated medium and long-chain fatty acids have been reported to mimic the pro-inflammatory effect of the Lipid A moiety of LPS, by activating NF-KB via TLR mechanisms. As such, acylcarnitines containing these long chain fatty acids could likewise act in a similar manner, by serving as ligands for galectin-3 binding. This needs to be

further confirmed by PRR reporter gene assays. Both can act as alarmins in this process. The upregulation of Galectin-3 and enhanced presence of LC ACs within the lesion site at specific time points lead us to the proposal of the cycle of events that occur within the 10-day timeframe after injury.

Interestingly, we also demonstrate that 3 days after lesion, acylcarnitines are present in Substantia nigra. Spatially-resolved microproteomic experiments performed at this level established the over-expression of several main proteins including the glutamate decarboxylase, synaptotagmin 11, Hmgb1, palmitoyl-protein thioesterase 1 and GPR158. Most of these proteins have been linked to Parkinson's disease. Synaptotagmin proteins are involved in neurodegeneration (Glavan et al. 2009). High mobility group box-1 (HMGB1) is expressed in neuron, microglia and astrocytes and act as a neurite outgrowth promoting factor and participates in neuronal cell migration. HMGB1 has been reported to induce neuroinflammation, and interact with α -synuclein, in addition to participating in pathogenesis of Parkinson's disease (Ko et al. 2012). Glutamate decarboxylase enzyme is one key enzyme involved in Parkinson's (Lloyd and Hornykiewicz 1973). Gpr158 is abundant in neurons of the CA3 region of the hippocampus, the brain's memory center. Recently it has been shown that Gpr158 mediates osteocalcin's regulation of cognition (Khrimian et al. 2017). Its over-expression in Substantia nigra 3 days after TBI can also be link to depression. Recently GPR158 has been shown to be involve in depression following chronic stress. GPR158 affects key signaling pathways involved in mood regulation in the region of the brain called prefrontal cortex (Sutton et al. 2018).

These results lead us to hypothesize a link between acylcarnitine produced by microglia in Substantia nigra and the initiation of changes associated to Parkinson disease 3 days after injury. As we found all these proteins which are over expressed are directly link to the disease and chronicle stress. It is also known that boxers are developing Parkinson after chronicle TBI. Acylcarnitine expression in Substantia nigra, produced by microglia can be an inducer of the early stage of the disease. Chronicle stress will produce much more of such lipids in this region leading to a local inflammatory environment in which GPR158, synaptotagmin, GAD, HMGB1 will be over-expressed and will be the precursors of the disease. The last question is related to correlation between the location of the head shock and acycarnitine production in the Substantia nigra. We hypothesize that Extracellular Vesicles (EVs) containing acylcarnitines produced by microglia at the lesion site, will impact microglia cells in Substantia nigra or inflammation propagation from

the injury site to the other brain regions or neurite production from these region sites to Substantia nigra. Inflammation is restricted to the lesion site and inflammation linked lipids do not go to the Substantia nigra post TBI as we already published (Mallah et al. 2018). EVs containing carnitine transporter OCTN2 have been recently demonstrated (Console et al. 2018) and even immune cells are known to produce EVs containing acylcarnitines (Colombo et al. 2014). There are growing evidence indicating the role of EVs are implicated in Parkinson (Russo et al. 2012). We can thus speculate as we present in **Figure 8**, that EVs from lesion site can target microglia in Substantia nigra leading a local inflammatory environment stimulating expression of proteins involved in stress. Multiple shocks will provoke a chronicle stress which start the Parkinson disease process at the end.

In conclusion, the spatiotemporal study of mild-TIB conducted by integrative biology combining data from spatially-resolved proteomics and lipid imaging by means of MALDI-MSI together with cross-validation by immunofluorescence enables to better depict molecular mechanisms occurring post-TBI. These integrative data lead to unveil the central role of acylcarnitines lipid family in the inflammation and associated molecular mechanisms giving a more detailed view of the different phases occurring at the lesion. Very interestingly, such study gives also new insights on how TBI can affect at longer spatial distance other area of the brain such as Substantia nigra giving molecular support to clinical observation relating repetitive TBI events and emergence of Parkinson disease.

ACKNOWLEDGEMENT

This research was supported by by funding from Ministère de l'Enseignement Supérieur, de la Recherche et de l'Innovation (MESRI), Institut National de la Santé et de la Recherche Médicale (Inserm) and Université de Lille. KM received a scholarship from the Association of Scientific Orientation and Specialization (ASOS).

AUTHOR CONTRIBUTIONS

Conceptualization, F.K., K.Z., I.F. and M.S.; Methodology, I.F. and M.S.; Software, J.Q. and K.M.; Validation, A.R-R., I.F., J.Q., K. M. and M.S.; Formal Analysis, J.Q. and K.M.; Investigation, A.R-R., J.Q., K.M. and S.A. ; Resources, F.K., K.Z., I.F. and M.S.; Data curation, I.F., J.Q., K.M. and M.S. ; Writing – Original Draft, I.F., J.Q., K.M. and M.S. ; Writing - Review

& Editing, F.K., I.F., J.Q., K.M., K.Z., and M.S. ; Supervision, I.F. and M.S.; Project Administration, I.F. and M.S.; Funding Acquisition, I.F., K.Z. and M.S.

DECLARATION OF INTERESTS

The authors declare no competing interests.

REFERENCES

Acosta, S.A. et al., 2015. Alpha-Synuclein as a Pathological Link Between Chronic Traumatic Brain Injury and Parkinson's Disease. *Journal of Cellular Physiology*, 230(5), pp.1024–1032.

Adibhatla, R., Hatcher, J. & Dempsey, R., 2006. Lipids and Lipidomics in Brain Injury and Diseases. *The AAPS Journal*, 8(2), p.E314.

Alexandrov, T. & Kobarg, J.H., 2011. Efficient spatial segmentation of large imaging mass spectrometry datasets with spatially aware clustering. *Bioinformatics*, 27(13), pp.i230–i238.

Blaya, M.O. et al., 2015. Neural progenitor cell transplantation promotes neuroprotection, enhances hippocampal neurogenesis, and improves cognitive outcomes after traumatic brain injury. *Experimental Neurology*, 264, pp.67–81.

Bonnet, A. et al., 2009. Pathway results from the chicken data set using GOTM, Pathway Studio and Ingenuity softwares. *BMC Proceedings*, 3(Suppl 4), p.S11.

Chughtai, K. et al., 2013. Mass spectrometry images acylcarnitines, phosphatidylcholines, and sphingomyelin in MDA-MB-231 breast tumor models. *Journal of Lipid Research*, 54(2), pp.333–344.

Cizkova, D. et al., 2014. Alterations of protein composition along the rostral-caudal axis after spinal cord injury: proteomic, in vitro and in vivo analyses. *Frontiers in Cellular Neuroscience*, 8.

Colombo, M., Raposo, G. & Théry, C., 2014. Biogenesis, Secretion, and Intercellular Interactions of Exosomes and Other Extracellular Vesicles. *Annual Review of Cell and Developmental Biology*, 30(1), pp.255–289.

Comte, I. et al., 2011. Galectin-3 maintains cell motility from the subventricular zone to the

olfactory bulb. *Journal of Cell Science*, 124(14), pp.2438–2447.

Console, L. et al., 2018. Characterization of Exosomal SLC22A5 (OCTN2) carnitine transporter. *Scientific Reports*, 8(1), p.3758.

Cox, J. & Mann, M., 2008. MaxQuant enables high peptide identification rates, individualized p.p.b.-range mass accuracies and proteome-wide protein quantification. *Nature Biotechnology*, 26(12), pp.1367–1372.

Das, M., Mohapatra, S. & Mohapatra, S.S., 2012. New perspectives on central and peripheral immune responses to acute traumatic brain injury. *Journal of Neuroinflammation*, (c), pp.1–12.

Devaux, S. et al., 2016. Proteomic analysis of the spatio-temporal based molecular kinetics of acute spinal cord injury identifies a time- and segment-specific window for effective tissue repair. *Molecular & Cellular Proteomics*, (October), p.mcp.M115.057794.

Dewan, M.C. et al., 2018. Estimating the global incidence of traumatic brain injury. *Journal of Neurosurgery*, pp.1–18.

Faul, M. et al., 2010. Traumatic Brain Injury in the United States: Emergency Department Visits, Hospitalizations and Deaths, 2002-2006. , (Atlanta, Georgia: Centers for Disease Control and Prevention, National Center for Injury Prevention and Control).

Franck, J. et al., 2013. Quantification-Based Mass Spectrometry Imaging of Proteins by Parafilm Assisted Microdissection. *Analytical Chemistry*, 85(17), pp.8127–8134.

Galgano, M. et al., 2017. Traumatic Brain Injury. *Cell Transplantation*, 26(7), pp.1118–1130.

Gardner, R.C. et al., 2018. Mild TBI and risk of Parkinson disease. *Neurology*, 90(20), pp.e1771–e1779.

Glavan, G., Schliebs, R. & ZìEivin, M., 2009. Synaptotagmins in Neurodegeneration. *The Anatomical Record: Advances in Integrative Anatomy and Evolutionary Biology*, 292(12), pp.1849–1862.

Gurung, P. et al., 2017. Tyrosine Kinase SYK Licenses MyD88 Adaptor Protein to Instigate IL-1 α -Mediated Inflammatory Disease. *Immunity*, 46(4), pp.635–648.

Hankin, J.A. et al., 2011. MALDI Mass Spectrometric Imaging of Lipids in Rat Brain Injury Models. *Journal of The American Society for Mass Spectrometry*, 22(6), pp.1014–1021.

Hulme, H.E. et al., 2017. Mass spectrometry imaging identifies palmitoylcarnitine as an immunological mediator during *Salmonella Typhimurium* infection. *Scientific Reports*, 7(1), p.2786.

Impellizzeri, D. et al., 2016. Traumatic Brain Injury Leads to Development of Parkinson's Disease Related Pathology in Mice. *Frontiers in Neuroscience*, 10, p.458.

Johnson, V.E., Stewart, W. & Smith, D.H., 2010. Traumatic brain injury and amyloid- β pathology: a link to Alzheimer's disease? *Nature Reviews Neuroscience*, 11(5), pp.361–370.

Karve, I.P., Taylor, J.M. & Crack, P.J., 2016. The contribution of astrocytes and microglia to traumatic brain injury. *British Journal of Pharmacology*, 173(4), pp.692–702.

Khrimian, L. et al., 2017. Gpr158 mediates osteocalcin's regulation of cognition. *The Journal of Experimental Medicine*, 214(10), pp.2859–2873.

Knobloch, M. et al., 2012. Metabolic control of adult neural stem cell activity by Fasn-dependent lipogenesis. *Nature*, 493(7431), pp.226–230.

Ko, E.A., Min, H.J. & Shin, J.-S., 2012. Interaction of High Mobility Group Box-1 (HMGB1) with α -synuclein and its aggregation (172.28). *The Journal of Immunology*, 188(1 Supplement).

Liu, T. et al., 2017. NF- κ B signaling in inflammation. *Signal transduction and targeted therapy*, 2, p.17023.

LLOYD, K.G. & HORNYKIEWICZ, O., 1973. L-Glutamic Acid Decarboxylase in Parkinson's Disease: Effect of L-Dopa Therapy. *Nature*, 243(5409), pp.521–523.

Mallah, K. et al., 2018. Lipid Changes Associated with Traumatic Brain Injury Revealed by 3D MALDI-MSI. *Analytical Chemistry*, 90(17), pp.10568–10576.

Mckee, A.C. & Daneshvar, D.H., 2015. The neuropathology of traumatic brain injury. In *Handbook of clinical neurology*. pp. 45–66.

Nishikawa, H. & Suzuki, H., 2018. Possible Role of Inflammation and Galectin-3 in Brain Injury after Subarachnoid Hemorrhage. *Brain Sciences*, 8(2), p.30.

Peng, H.-H. et al., 2017. Mineral particles stimulate innate immunity through neutrophil extracellular traps containing HMGB1. *Scientific Reports*, 7(1), p.16628.

Pyatnitskiy, M. et al., 2014. Clustering gene expression regulators: New approach to disease subtyping N. H. Bishopric, ed. PLoS ONE, 9(1), p.e84955.

Quanico, J. et al., 2013. Development of liquid microjunction extraction strategy for improving protein identification from tissue sections. *Journal of Proteomics*, 79, pp.200–218.

Roberts, G.W. et al., 1994. Beta amyloid protein deposition in the brain after severe head injury: implications for the pathogenesis of Alzheimer's disease. *Journal of neurology, neurosurgery, and psychiatry*, 57(4), pp.419–25.

Rosenberger, K. et al., 2015. Intrathecal heat shock protein 60 mediates neurodegeneration and demyelination in the CNS through a TLR4- and MyD88-dependent pathway. *Molecular Neurodegeneration*, 10(1), p.5.

Roux, A. et al., 2016. Mass spectrometry imaging of rat brain lipid profile changes over time following traumatic brain injury. *Journal of Neuroscience Methods*, 272, pp.19–32.

Russo, I., Bubacco, L. & Greggio, E., 2012. Exosomes-associated neurodegeneration and progression of Parkinson's disease. *American journal of neurodegenerative disease*, 1(3), pp.217–25.

Rutkowski, J.M. et al., 2014. Acylcarnitines activate proinflammatory signaling pathways. *American Journal of Physiology-Endocrinology and Metabolism*, 306(12), pp.E1378–E1387.

Rutkowski, J.M. et al., 2014. Acylcarnitines activate proinflammatory signaling pathways. *AJP: Endocrinology and Metabolism*, 306(12), pp.E1378–E1387.

Sampey, B.P. et al., 2012. Metabolomic Profiling Reveals Mitochondrial-Derived Lipid Biomarkers That Drive Obesity-Associated Inflammation M. B. Aguila, ed. PLoS ONE, 7(6), p.e38812.

Sparvero, L.J. et al., 2016. Imaging mass spectrometry reveals loss of polyunsaturated cardiolipins in the cortical contusion, hippocampus, and thalamus after traumatic brain injury. *Journal of Neurochemistry*, 139(4), pp.659–675.

Sutton, L.P. et al., 2018. Orphan receptor GPR158 controls stress-induced depression. *eLife*, 7.

Vilskersts, R. et al., 2015. Methyl- γ -butyrobetaine decreases levels of acylcarnitines and attenuates the development of atherosclerosis. *Vascular Pharmacology*, 72, pp.101–107.

Wang, X. et al., 2015. Macrophages in spinal cord injury: Phenotypic and functional change from exposure to myelin debris. *Glia*, 63(4), pp.635–651.

Wenk, M.R., 2005. Erratum: The emerging field of lipidomics. *Nature Reviews Drug Discovery*, 4(7), pp.594–610.

Wiśniewski, J.R. et al., 2009. Universal sample preparation method for proteome analysis. *Nature Methods*, 6(5), pp.359–362.

Xu, L. & Pu, J., 2016. Alpha-Synuclein in Parkinson's Disease: From Pathogenetic Dysfunction to Potential Clinical Application. *Parkinson's Disease*, 2016, pp.1–10.

Yamawaki, Y. et al., 2010. MyD88 plays a key role in LPS-induced Stat3 activation in the hypothalamus. *American Journal of Physiology-Regulatory, Integrative and Comparative Physiology*, 298(2), pp.R403–R410.

Yip, P.K. et al., 2017. Galectin-3 released in response to traumatic brain injury acts as an alarmin orchestrating brain immune response and promoting neurodegeneration. *Scientific reports*, 7, p.41689.

Yuryev, A., Kotelnikova, E. & Daraselia, N., 2009. Ariadne's ChemEffect and Pathway Studio knowledge base. *Expert Opinion on Drug Discovery*, 4(12), pp.1307–1318.

Zemski Berry, K.A. et al., 2011. MALDI Imaging of Lipid Biochemistry in Tissues by Mass Spectrometry. *Chemical Reviews*, 111(10), pp.6491–6512.

Zhou, W. et al., 2018. Galectin-3 activates TLR4/NF- κ B signaling to promote lung adenocarcinoma cell proliferation through activating lncRNA-NEAT1 expression. *BMC Cancer*, 18(1), p.580.

STAR METHODS

KEY RESOURCES TABLE

CONTACT FOR REAGENT AND RESOURCE SHARING

Further information and requests for resources and reagents should be directed to and will be fulfilled by the Lead Contact, Isabelle Fournier (isabelle.fournier@univ-lille.fr).

EXPERIMENTAL MODEL AND SUBJECT DETAILS

Rat TBI Model:

Experiments were conducted on adult male Sprague–Dawley rats (225–250g, 7-8 weeks old) in accordance with the National Institute of Health Guidelines for Animal Research (Guide for the Care and Use of Laboratory Animals) and approved by the Institutional Animal Care and Use Committee (IACUC) at the American University of Beirut (AUB). The rats were maintained and housed under pathogen-free conditions. They were also provided with constant temperature and humidity control at the AUB Animal Care Facility (ACF). All surgical procedures were conducted under deep anesthesia.

Cell Lines

NR8383 were cultured in Ham's F12 K medium supplemented with 15% FBS, 100 U/ml penicillin and 100 µg/ml Streptomycin, at 37 °C in a humidified atmosphere (5% CO₂). DITNC1 cell line was grown in DMEM medium supplemented with 10% FBS, 2% L-glutamate, 100 U/ml penicillin, 100 µg/ml Streptomycin and 1% sodium pyruvate, at 37 °C in a humidified atmosphere (5% CO₂). ND7/23 cell line was grown in DMEM medium supplemented with 10% FBS, 1% L-glutamate, 100 U/ml penicillin and 100 µg/ml Streptomycin, at 37 °C in a humidified atmosphere (5% CO₂).

METHOD DETAILS

Experimental Controlled Cortical Impact (CCI), Study Design, Brain Harvesting and Tissue Preparation

Injury induced to the rats was performed as previously described (Mallah et al. 2018). Post injury, the rats heads were sutured and maintained until selected time points for the study, including: 1 day, 3 days, 7days, and 10 days. The sham (non-injured) rats received the exact same procedure except with no craniotomy nor impact to the underlying tissue. At the corresponding time point, rats (n=3 per condition) were anesthetized using 5% isoflurane and sacrificed by decapitation. The complete brain was then collected and snap-frozen on isopentane which was previously cooled on dry-ice. The frozen brains were then stored at -80 °C until the experiments were carried out. At the time of experimentation, the samples were transferred from -80 °C to -20 °C and kept for 2 hours, prevent possible cracking within the tissue samples. Cryostat (Leica Microsystems, Nanterre, France) was used to cut the brain samples in coronal view with a thickness of 20 µm per tissue section. The sections were then thaw-mounted on Polylysine-coated slides. Three segments

per brain were selected for imaging and designated as Rostral, Lesion, and Caudal. With Rostral and Caudal corresponding to tissue slices with no injured cortical tissue, the rostral part is close to the frontal part of the brain near the olfactory bulbs, whereas the caudal segment is in the rear part more close to the cerebellum. Due to the advantage of the reproducibility of injury in the same coordinates between all samples and conditions, the same atlas positions were selected in all the brains for all three segments rostral, lesion, and caudal.

MALDI MSI Data Acquisition

15 min before use, selected tissue sections were placed under vacuum in a desiccator to ensure complete drying. DHB matrix was prepared at a concentration of 20 mg/ml in 70:30 (v:v) ratio of MeOH/0.1%TFA in H₂O. Using a nebulizer which was constructed in-house (Franck et al. 2013), the matrix was manually sprayed on the tissue sections for 12 min, with air pressure=1 bar and flow rate= 300 μ l/hr. Images were acquired using a MALDI-LTQ-Orbitrap-XL (Thermo Fisher Scientific, Bremen, Germany) operated by Xcalibur software version 2.0.7 (Thermo Fisher Scientific) in same manner as previously described (Mallah et al. 2018).

MALDI MSI Data Processing

All images were converted to vendor-neutral *.imzML format using the plug-in available in ImageQuest software version 1.1.0 build S4 (Thermo Fisher Scientific). SCiLS lab MVS software, version 2018b Premium 3D release 6.01.10194 (Bruker Daltonics, Bremen, Germany) was then used to process the uploaded vendor-neutral files. With this version of SCiLS Lab, the baseline removal option is not available, and the peaks are automatically imported. Normalization was performed based on the total ion count (TIC) method and m/z intervals were automatically set at \pm 24.967 mDa. All spectra were subjected to the Move-Peaks-to-Local-Max feature with the reference sample dataset chosen arbitrarily, and the resulting peak list was used in all the subsequent analyses. Using the bisecting k-means algorithm with Manhattan distance metric, spatial segmentation was performed. (Alexandrov & Kobarg 2011). Remaining data analysis, parameters, and data processing including co-localization experiments with injured area and ROC analysis between sham and injured tissue, and vice versa, were performed in same manner as previously (Mallah et al. 2018)

MS/MS Lipids Identification

Four consecutive 20- μ m tissue sections containing the injured cortical area were obtained using a cryostat and collected in an eppendorf tube. Lipid extraction using the Folch method and MSn experiments on MALDI-LTQ-Orbitrap-XL were performed as previously described (Mallah et al. 2018). Palmitoylcarnitine and oleoylcarnitine standards were prepared at a concentration of 50 μ g/ μ L in 50:50 (v:v) of CHCl_3 :MeOH.

Fluorescent Immunohistochemistry (FIHC) Experiments

Immunofluorescence experiments were performed on brain slices directly consecutive to the lesion area of 3D post injury, only 20 μ m away. These staining aimed to differentiate between resident microglia and bone marrow derived macrophages by staining for Mac-2 and CX3CR1. First, a saturation phase was applied for 1 hour by using blocking buffer constituted of: 1% bovine serum albumin, 1% ovalbumin, 1% normal donkey serum, 0.2% of triton 100X, and 0.1 M glycine all dissolved in PBS 1X. After saturation, primary polyclonal antibodies rabbit Anti-CX3CR1 (1:40 Santa Cruz biotechnology, CliniSciences, Nanterre, France) and mouse Anti Mac-2 (1:40, US Biological lab science, bought from Euromedex, Souffelweyersheim, France) were diluted in the same blocking buffer and added to the same tissue section in order to perform the double staining. In addition, these were not added to the negative control where only the blocking buffer was applied. The primary antibodies were then kept incubated at 4°C overnight. The following day, the sections were washed 3 times with PBS 1x. Secondary antibodies Alexa Fluoro donkey anti-rabbit and Alexa Fluoro donkey anti-mouse (Life Technologies, ThermoFisher Scientific, Courtaboeuf, France) were then added and incubated for 1 hour at 37°C. The secondary antibodies were both prepared in same buffer as previously mentioned blocking buffer but with no 0.1M glycine, nor 0.2% triton 100X. After, several 10 min washes using PBS 1X were performed and Hoechst solution (1:10000) was added. After, Soudan black 0.3% was added for 10 min in order to decrease background signal. The slide was then washed 1 more time with PBS 1X and Dako fluorescent mounting medium was added before adding cover slip. All images were then captured using confocal microscopy.

Spatially-Resolved Microproteomics Shotgun Tissue Analysis

- a) **On-tissue LysC tryptic digestion:** The injured cortical tissue within lesion segments of all injured time points (1D, 3D, 7D, and 10D) and a corresponding area from the sham tissue, which were all chosen directly consecutive to the MALDI-MSI imaged segments were subjected to on-tissue tryptic digestion. Briefly, tissue these tissue segments were dried in the vacuum desiccator for 15 min prior to experimentation. The, several washes were performed in a delipidation approach as follows: 30 seconds in 70% ethanol, 30 seconds in 100% ethanol, and 2 x 30 seconds in chloroform. The tissue was subjected to drying in the desiccator between all steps. Post washing steps, LysC trypsin at 40 µg/ml resuspended in Tris-HCl (50 mM, pH 8.0) was spotted on the injured cortical tissue using a piezoelectric microspotter Chemical Inkjet Printer (CHIP-1000, Shimadzu, CO, Kyoto, Japan). The digested area was controlled by assigning a 4x4 grid of microspots to obtain a final digested area of 1 mm². Each spot was 200 µm in diameter and contains a droplet volume of 150 pL/cycle. The digestion was carried out for 2 hours, and 25 cycles of 0.1%TFA were spotted post digestion.
- b) **Liquid Microjunction Microextraction:** Using the TriVersa Nanomate platform (Advion Biosciences Inc., Ithaca, NY, USA) with the installed option of Liquid Extraction Surface Analysis (LESA), the digested peptides within the injured cortical tissue were collected. Briefly, three prepared solvents were used in the extraction process: a) 0.1% TFA, b) ACN/0.1% TFA (8:2 v/v ratio), and MeOH/0.1% TFA (7:3 v/v ratio). After, the tissue is scanned and digested cortical tissue is designated as the target of extraction. An automatically controlled tip deposits a volume of each solvent onto the digested area and performs several aspiration-deposition actions, before finally aspirating all the volume and depositing in small tubes. Two extraction cycles per mentioned solvent type are performed to ensure the maximum collection of peptides as possible. The content of the tubes is then dried using speedvac, and the tubes are stored in -80°C until subjected to LC-MS/MS.

Shotgun Proteomics Analysis after Stimulation with Palmitoyl-carnitine

- I) **Cell line stimulation with Palmitoylcarnitine:** Using a 6-well plate, approximately 1.8 million cells were plated in a 6 wells plate (300 000 cells/well) for macrophages and 2.7 million cells for astrocytes (450 000 cells/ well). The following day, cells were then starved overnight at 37 °C in their corresponding medium (F12 for NR8383 and DMEM for

astrocytes) with lower concentration of serum (2% FBS, 1% penicillin-streptomycin and sodium pyruvate). Finally the cells were then stimulated by adding palmitoyl-L-carnitine (0.1 μ M) to the medium in the absence of serum, thus 0% FBS in medium for all cells. After stimulation for 24 hours, cell were collected and centrifuged at 150 RCF/5 min for the macrophages, and at 1000 RPM/5 min for the astrocytes. The controls of the experiments underwent the same experimental procedure except no stimulation with palmitoyl-L-carnitine.

- II) Protein Extraction:** Protein extraction was performed using sodium dodecyl sulfate buffer (SDS). Precisely, 50 μ l of extraction buffer (4% SDS, Tris 0.1M, pH 7.8) was added to each tube containing the previously stimulated cells, or their corresponding controls. Samples were then heated for 15 min at 95 °C and sonicated for another 15 min. After, a centrifugation step was performed at 16,000 g for 10 min at 20 °C. Post centrifugation, the supernatant containing the extracted proteins were collected. Using Bradford quantification method, all samples were quantified and stored at -80 °C until further experimentation
- III) FASP protocol:** For protein identification, we performed a shotgun bottom-up proteomic approach. All sample concentrations were normalized to obtain a final concentration of 1.5 μ g/ μ l per sample. With a normalized concentration, 30 μ l volume each sample was prepared to obtain a final protein concentration of 45 μ g for digestion. An equal volume, 30 μ l, or reduction solution (Dithiothreitol- DTT 0.1 M) was added to each of the samples and followed by incubation for 40 min at 56 °C. Samples were then transferred and experimentation carried out using filter-aided sample preparation (FASP) method (Wiśniewski et al. 2009). Briefly, this method uses a filter with a nominal molecular weight limit of 30,000 KDa. (Amincon Ultra-0.5 30K, Millipore). After transferring the samples into the FASP filters, an alkylation step was performed in the dark by adding Iodoacetamide (IAA) solution (0.05 M) for 20 min at room temperature. The samples were then digested overnight at an incubation temperature of 37°C by adding LysC/trypsin at a concentration of 40 μ g/ml prepared in 50 mM Tris-HCL solution at pH 8. The following day, the digested proteins in the filter were eluted with 50 μ l of saline solution (NaCl 0.5 M) and the digestion reaction was stopped by adding an acidic solution (10 μ l of TFA 5%) to each of the filters. Desalting of the samples, along with their enrichment, was performed with ZipTip C-18 (Millipore) just before processing using LC-MS/MS.

LC MS & MS/MS Data Acquisition for Shotgun Proteomics

MS analysis was performed by a nanoAcquity UPLC system (Waters) coupled with a Q-Exactive Orbitrap mass spectrometer (Thermo Scientific) containing a nano-electrospray ionization source. The analysis was carried out in reverse phase, and all samples were loaded into a pre-concentration column (nanoAcquity Symmetry C18, 5 μm , 180 μm x 20 mm). The peptides were separated using an analytical column (nanoAcquity BEH C18, 1.7 μm , 75 μm x 250 mm) by applying a linear gradient of acetonitrile in 0.1% formic acid (5% -35%, for 2 hours) at a flow rate of 300 nL/min. Within the Orbitrap mass analyzer, the MS analysis was performed with a resolution of 70,000 FWHM, a m/z mass range between 300-1600, an AGC of 3×10^6 ions and a maximum injection time of 120 ms. The MS/MS was performed in a data dependent acquisition mode defined to analyze the 10 most intense ions within the primary MS analysis (Top 10). With regard to the MS/MS fragmentation parameters, the resolution was set at 17,500 FWHM, a m/z range between 200-2000, an AGC of 5×10^4 ions, and a maximum injection time of 60 ms. The isolation window was set at 4.0 m/z.

QUANTIFICATION AND STATISTICAL ANALYSIS

Data Processing

All raw data were analyzed by MaxQuant software version 1.5.8.3 (Cox & Mann 2008). Proteins were identified by comparing all raw spectra with a proteome reference database of *Rattus norvegicus* (Uniprot, release 20180712, 8027 entries for the palmitoylcarnitine stimulated protein identifications, and release 20180302, 8022 entries for the on-tissue spatially-resolved microproteomics identifications). The parameters chosen for the identification include: digestion enzyme used was trypsin LysC and maximum number allowed of missed cleavages was two. The oxidation of methionine and N-terminal protein acetylation was chosen as variable modifications. As for fixed modifications, carbamidomethylation of cysteine was set for the identification of proteins in the palmitoylcarnitine stimulation case, and this modification was removed for the micro-proteomics approach. Proteins were identified based on a minimum of 2 peptides per protein, in which 1 was unique. As for initial mass tolerance, 6 ppm was selected for MS mode, and 20 ppm was set for fragmentation data with regard to MS/MS tolerance. The false discovery rate (FDR) was specified to 1% for both protein and peptide. The label-free quantification (LFQ)

was performed by keeping the default parameters of MaxQuant. After data treatment using MaxQuant, statistical analysis was done using Perseus software (version 1.6.0.7). Each cell line was processed alone in its own Perseus file. The beginning matrix was filtered by removing the potential contaminants, reverse and only identified by site. Then, the LFQ intensity was logarithmized ($\log_2[x]$). The principal component analysis (PCA) was then applied using the default parameters of the software. Regarding the spatially-resolved microproteomics analysis, the samples were annotated based on the corresponding time point (sham, 1 day, 3 days, 7 days, and 10 days) resulting in 5 different groups with each group containing 3 replicates ($n=3$). The statistical analysis carried out for the spatially-resolved microproteomics data was multiple sample anova test with a p -value=0.01. For each cell line file (macrophages and astrocytes), the samples were categorically annotated into two groups: stimulated by palmitoylcarnitine or control with each group containing 3 replicates ($n=3$). Statistical analysis was performed using Student's T-test with a p -value of 0.05 for the cell line experiments. Normalization was achieved by using the Z-score. The hierarchical clustering and profile plot of only the statistically significant proteins were all performed and visualized by Perseus using default parameters.

Sub-network Enrichment Pathway Analyses

Using Elseviers's Pathway Studio (version 9.0/ Ariadne Genomics/Elsevier), all relationships between the differentially expressed proteins between all conditions were depicted based on the Ariadne ResNet database (Yuryev et al. 2009; Bonnet et al. 2009). For proteins identified in the spatially-resolved microproteomics analysis and the ones identified in the shotgun analysis post stimulation of cell lines with palmitoylcarnitine, Sub-network Enrichment Analysis (SNEA) algorithm was used to detect the statistically significant altered biological pathways in which the identified proteins are involved. This algorithm uses Fisher's statistical test to detect any nonrandom associations between two categorical variables organized by a specific relationship. Also, this algorithm starts by creating a central "seed" from all the relevant identities in the database, and builds connections with associated entities based on their relationship with the seed. SNEA compares the sub-network distribution to the background distribution using one-sided Mann-Whitney U-Test, and calculates a p -value thus representing a statistical significance between different distributions. In all analysis that we performed, the GenBank ID was used to form experimental groups based on the different conditions present for analysis. The pathway

networks were reconstructed based on biological processes and molecular functions for each single protein, along with its associated targets (Pyatnitskiy et al. 2014).

DATA AND SOFTWARE AVAILABILITY

Spatially-resolved microproteomics, astrocytes and macrophages proteomic datasets including MaxQuant files and annotated MS/MS datasets, as well as the MALDI imaging datasets, were uploaded to ProteomeXchange Consortium via the PRIDE database, and was assigned the dataset identifier PXD011262.

SUPPLEMENTAL ITEM TITLES

Supplemental Spreadsheet 1. Related to Figure 5. List of proteins identified to be upregulated by spatially-resolved Shotgun proteomics in the Substantia nigra 3 days post-injury.

KEY RESOURCES TABLE

REAGENT or RESOURCE	SOURCE	IDENTIFIER
Antibodies		
Rabbit Anti-CX3CR1	Santa Cruz Biotechnology	Cat#sc-30030; RRID: AB_2245540
Mouse Anti-Mac2	US Biological Lab Science	Cat# 215294
Alexa Fluoro 488 Donkey Anti-rabbit	Thermo Fisher Scientific	Cat# A21206; RRID:AB_2535792
Alexa Fluoro 555 Donkey Anti-mouse	Thermo Fisher Scientific	Cat# A31570; RRID: AB_2536180
Biological Samples		
Injury and Sham rat brains	Animal Care Facility-(AUB)	https://website.aub.edu.lb/fm/medicalresearch/AnimalCareFac/Pages/Home.aspx
Chemicals and Products		
Methanol (MeOH)	Biosolve	Cat#136847; CAS:67-56-1
HPLC water	Biosolve	Cat#232106; CAS:7732-18-5
Formic acid (FA)	Biosolve	Cat#069141; CAS:64-18-6
Acetonitrile (ACN)	Biosolve	Cat#012078; CAS:75-05-8
Chloroform (CHCl ₃)	Biosolve	Cat#034806; CAS:67-66-3
Trifluoroacetic acid (TFA)	Biosolve	Cat#202306; CAS:76-05-1
2,5 dihydroxybenzoic acid (DHB)	Sigma-Aldrich	Cat#85707; CAS:490-79-9
ProteoMass MALDI Calibration kit	Sigma-Aldrich	Cat#MSCAL4

DL-dithiothreitol (DTT)	Sigma-Aldrich	Cat#43819-5G; CAS:3483-12-3
Iodoacetamide (IAA)	Sigma-Aldrich	Cat#I1149-25G; CAS:144-48-9
Thiourea (CH4N2S)	Fluka	Cat#88810; CAS:62-56-6
LysC/Trypsin	Promega	Cat#V5073
Palmitoyl-L-carnitine chloride	Santa Cruz	Cat#sc-205789; CAS:18877-64-0
Palmitoyl-L-carnitine Standard	Avanti Polar Lipids	Cat#870851; CAS:1935-18-8
Oleoyl-L-Carnitine Standard	Avanti Polar Lipids	Cat#870852; CAS:13962-05-5
OCT embedding Matrix	CellPath	Cat#KMA-0100-00A
Polylysine Coated Slides	Thermo Fisher Scientific	Cat#J2800AMNZ
Penicillin-Streptomycin	Thermo Fisher Scientific	Cat#15140122
Dulbecco's Modified Eagle's Medium (DMEM)	Thermo Fisher Scientific	Cat#31053028
Ham's F12K	Thermo Fisher Scientific	Cat#21765029
Fetal Bovine Serum (FBS)	Thermo Fisher Scientific	Cat#16140071
Phosphate Buffer Saline (PBS)	Thermo Fisher Scientific	Cat#14190094
L-Glutamine	Thermo Fisher Scientific	Cat#25030024
Deposited Data		
Raw Data (Microproteomics, Proteomics cell line experiments and MS images)	ProteomeXchange via PRIDE database	PXD011262
Experimental Models: Cell Lines		
NR8383 rat alveolar macrophage cell line	ATCC	Cat#CRL-2192; RRID:CVCL_4396
Rat brain DI TNC1 cell line (Astrocytes)	Sigma Aldrich	Cat#98102214; RRID: CVCL-0247
Experimental Models: Organisms/Strains		
Rat: Adult male Sprague-Dawley (225-250g, 7-8 weeks old)	Animal Care Facility- (AUB)	https://website.aub.edu.lb/fm/medicalresearch/AnimalCareFac/Pages/Home.aspx
Software and Algorithms		
ImageQuest v1.1.0 build 54	Thermo Fisher Scientific	http://www.thermofisher.com/order/catalog/product/10137985
SCiLS lab v2018b MVS Premium 3D	SCiLS GmbH	https://scils.de/
MaxQuant software version 1.5.8.3	Max Planck Institute of Biochemistry	http://www.biochem.mpg.de/5111795/maxquant
Perseus software version 1.6.0.7	Max Planck Institute of Biochemistry	http://www.biochem.mpg.de/5111810/perseus
Elsevier's Pathway Studio v9.0	Elsevier	https://www.elsevier.com/solutions/pathway-studio-biological-research

Zen Lite Microscopy Software	Zeiss	https://www.zeiss.fr/microscopie/produits/microscope-software/zen-lite/zen-2-lite-download.html
Other		
Lipid Identification Database	Metlin	https://metlin.scripps.edu

MAIN FIGURE TITLES AND LEGENDS

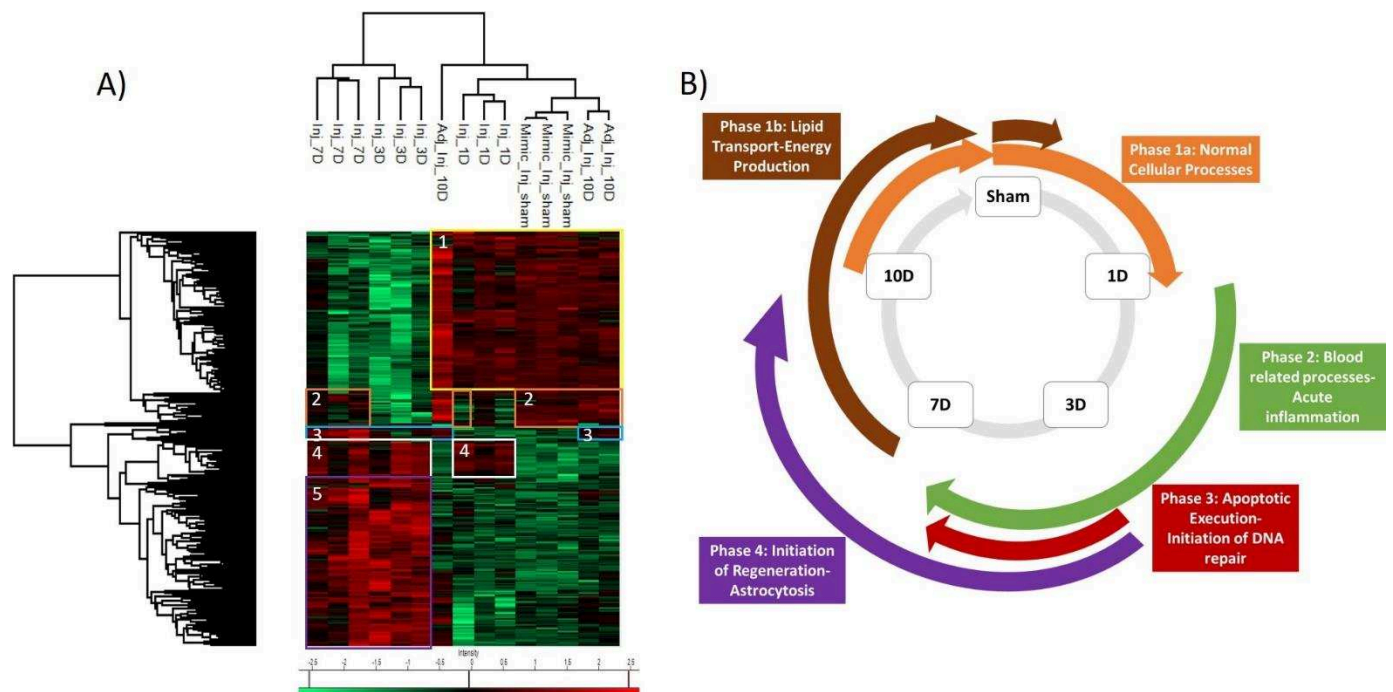


Figure 1: Spatially-resolved microproteomics analysis reveals time point-specific proteomic phases.

A) Heat map based on the hierarchical clustering analysis of the LFQ value corresponding to the detected proteins within the 1 mm² microenvironment of the following conditions: sham, 1 day, 3 days, 7 days, and 10 days post injury. Distinct clusters are highlighted and assigned numbers from 1 to 5. B) Representative scheme of all 4 phases concluded from the spatially-resolved microproteomic data. See also figure S2 (A,B) and figure S3 (A,B,C).

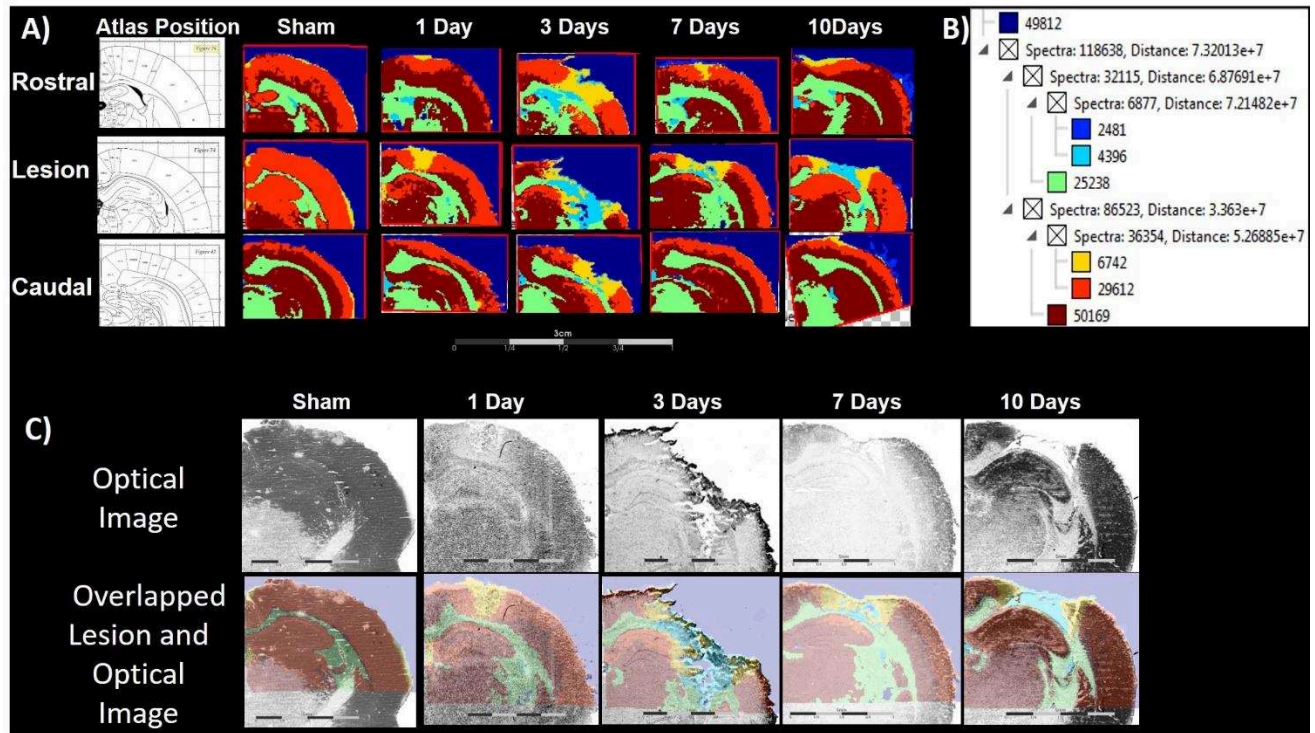


Figure 2: MSI followed by Spatial Segmentation Reveals Lipid Lesion-specific Expression. A) Rat Atlas images selected for the rostral, lesion and caudal segments of the study. Spatially segmented cluster images after processing lipid MALDI MSI data of rostral, lesion, and caudal segments from sham brain and 1 day, 3 day, 7 day, and 10 day injured brains. B) Cluster tree corresponding to the imaged sections based on Manhattan distance calculation method. C) Optical scans of the lesion segment used in figure 3A for all conditions, along with the co-registered optical and spatially segmented images. See also figure S4 (A,B,C).

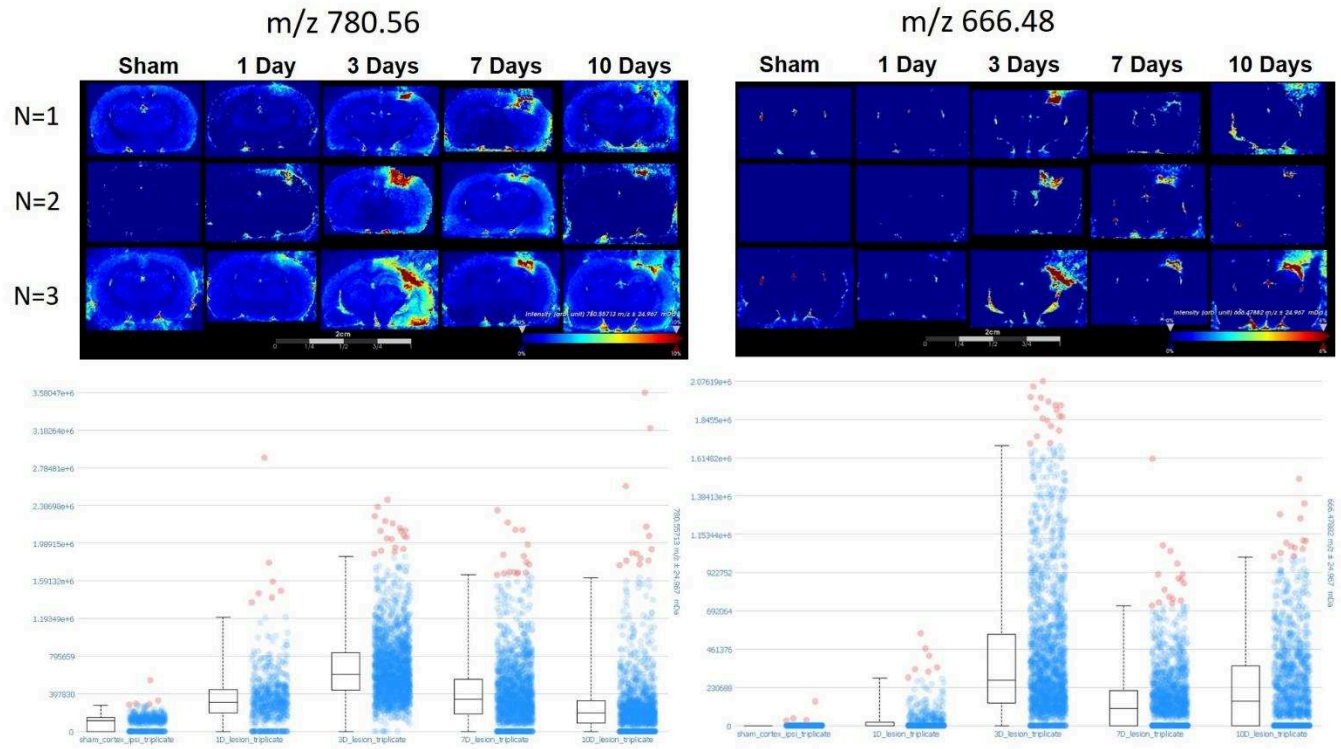


Figure 3: MALDI MSI shows altered lipid expression between injury and non-injury. Plotted Ion images of m/z 780.56 and 666.48 along with their corresponding intensity box plot expression for all three replicates in all conditions: sham, 1 day, 3 days, 7 days, and 10 days. See also figure S5 and tables S1 and S2.

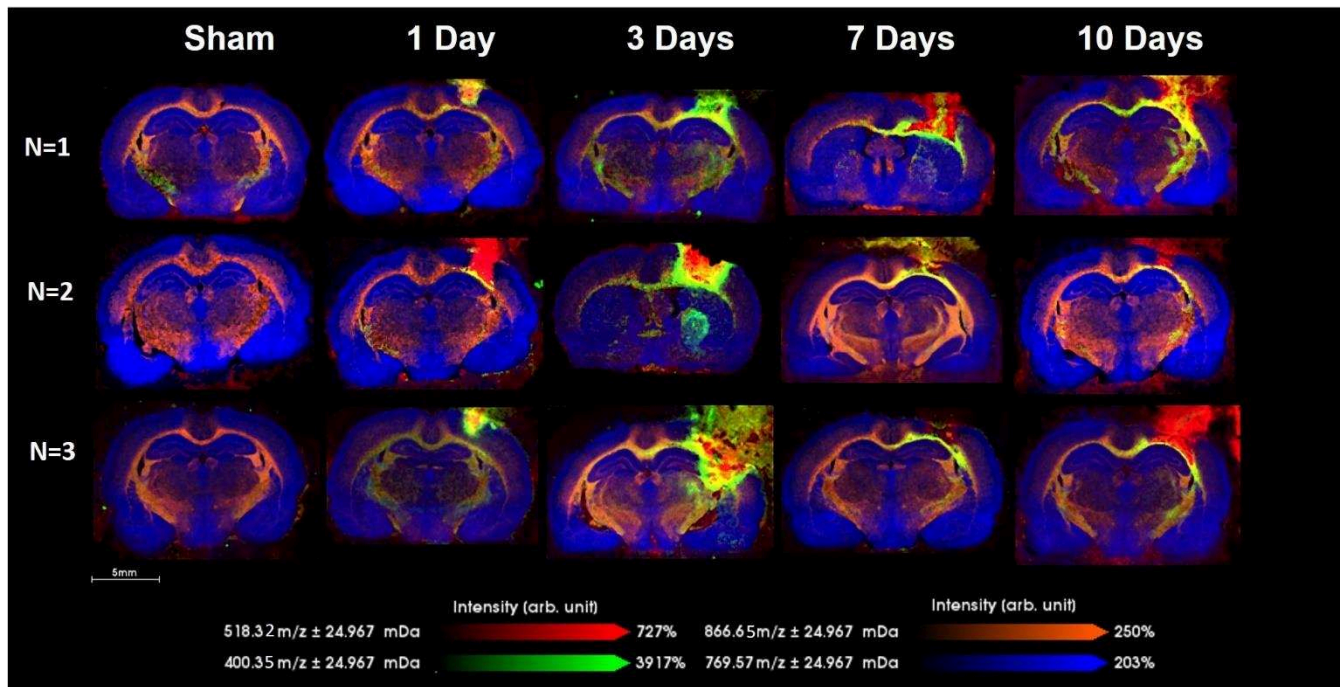


Figure 4: m/z 400 corresponds to Palmitoylcarnitine and is expressed surrounding the injured cortical tissue. Co-plotted Ion images of m/z 400.35, 518.32, 866.65, and 769.57 for all three replicates in all conditions: sham, 1 day, 3 days, 7 days, and 10 days. See also figure S6 (A and B), S7, S8, and table S3.

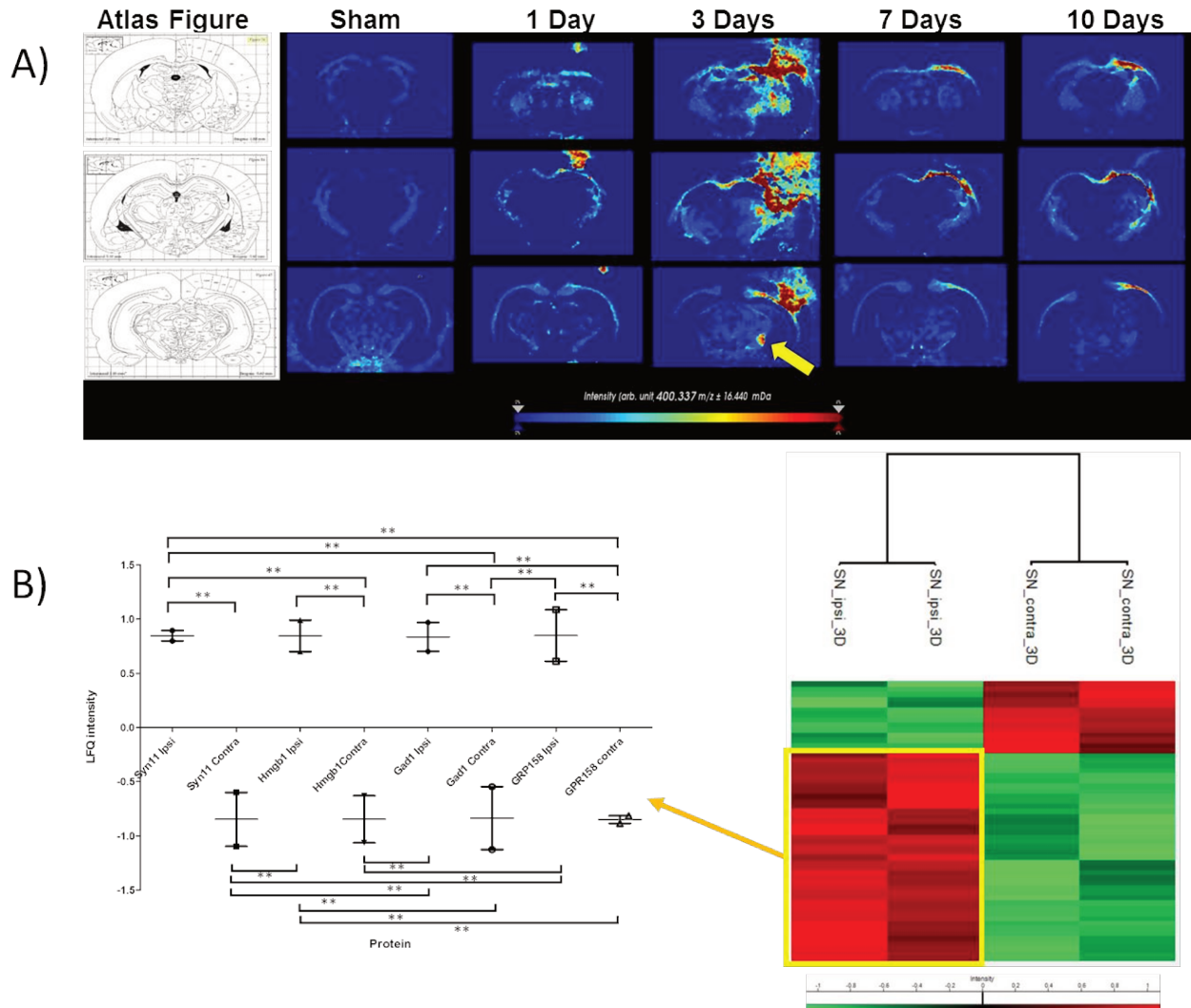


Figure 5: Expression of Palmitoylcarnitine in the Substantia nigra three days post injury. A) Plotted Ion images of m/z 400.35 rostral, lesion, and caudal segments in all conditions: sham, 1 day, 3 days, 7 days, and 10 days. B) Heat map based on the hierarchical clustering analysis of the LFQ value corresponding to the detected proteins in the spatially-resolved microproteomic experiments performed on the Substantia nigra in both ipsilateral and contralateral hemispheres at 3 days post impact. Distinct clusters are highlighted. Expression level of 4 different proteins upregulated in SN ipsi (Syn11, HMGB1, Gad1, and GPR158), when compared to the contralateral substantia nigra, along with the significant values with a threshold of < 0.05 (**).

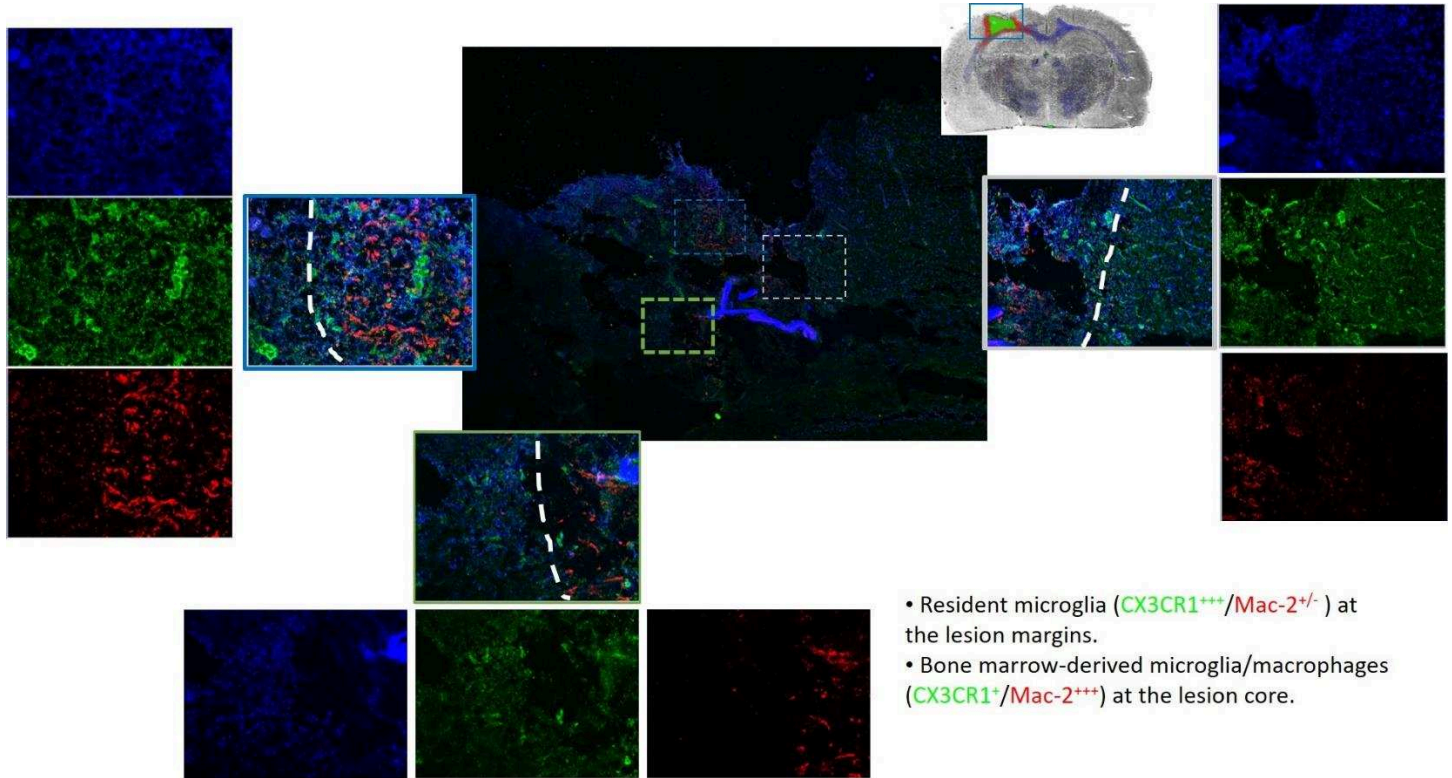


Figure 6: Localization of palmitoylcarnitine with resident microglia of lesion margin. Confocal immunofluorescence images of lesion segment at 3 days post injury along with the zoom images of the lesion borders stained with two markers: CX3CR1 (green) and Mac-2 (red).

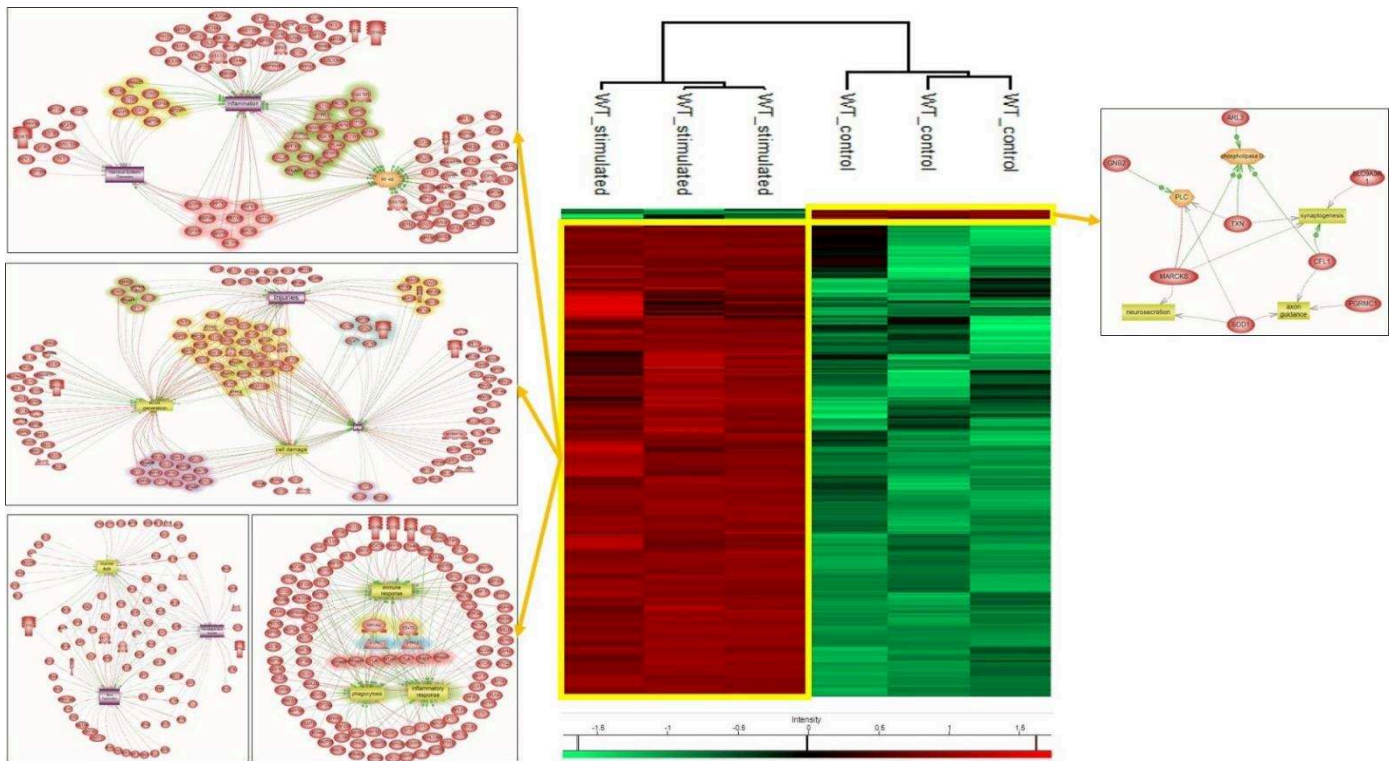


Figure 7: Palmitoylcarnitine induces inflammatory action in macrophages and astrocytes. Heat map based on the hierarchical clustering analysis of the LFQ value corresponding to the detected proteins extracted from macrophages stimulated with palmitoylcarnitine or not. Distinct clusters are highlighted. The system biology analysis for network identification for each of the highlighted clusters issued from heat map of proteins is also shown. See also Figure S9 (A, B) and Figure S10.

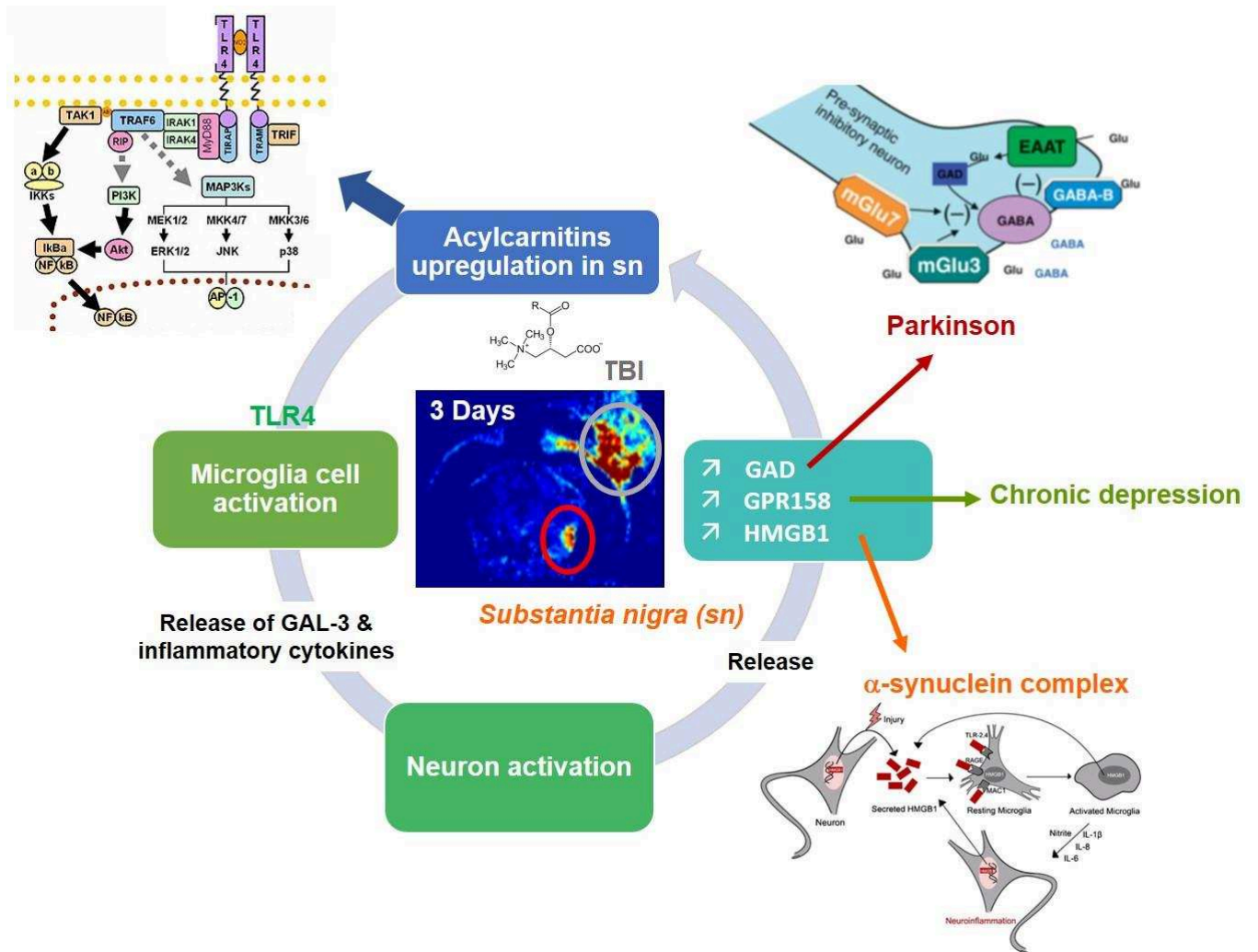


Figure 8: Schematic representation of molecular mechanisms associated with acylcarnitines expression in Substantia nigra 3 days post-TBI. Acylcarnitines were found to be associated with microglia and are specifically found by MALD MSI, 3 days post-TBI, in the Substantia nigra. Spatially-Resolved Proteomics reveals the expression of proteins known to be involved in Parkinson. Acylcarnitines are known to activate microglial through TLR4/MyD88 pathway leading to inflammatory cytokines and alarmins (Galectin-3). GAL-3 is a pro-inflammatory protein known to promote neuron inflammation leading to the expression of proteins which were recently shown to be involved in Parkinson disease (GPR158, HMGB1, GAD). This putative physiological pathway could make a link between chronic TBI and Parkinson's disease.

Supplementary Figures:

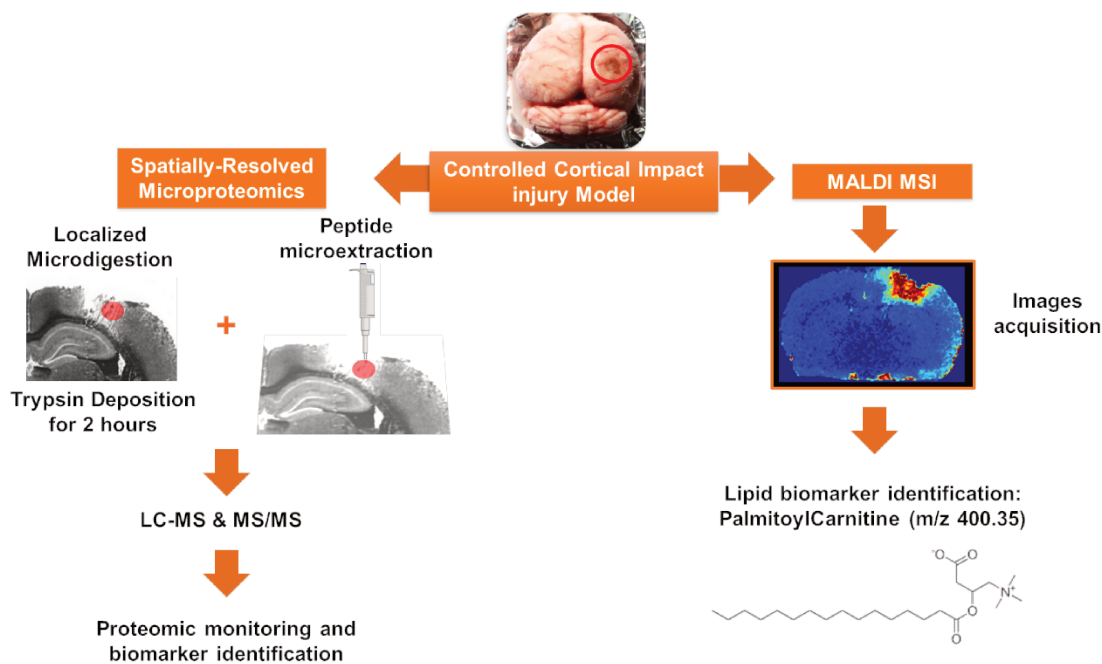


Figure S1: Workflow. The experimental design was carried out to perform both microproteomic analysis and lipid MALDI MSI. At desired time points, the injured brain was obtained and cryosectioned. For each slide that was subjected to lipid MALDI MSI to find lipid biomarker candidates, a second consecutive slide was used for the spatially resolved microproteomics approach. After the proteins were digested and peptides extracted within the injured microenvironment, samples were subjected to LC-MS and MS/MS analysis followed by identification and statistical variation analysis.

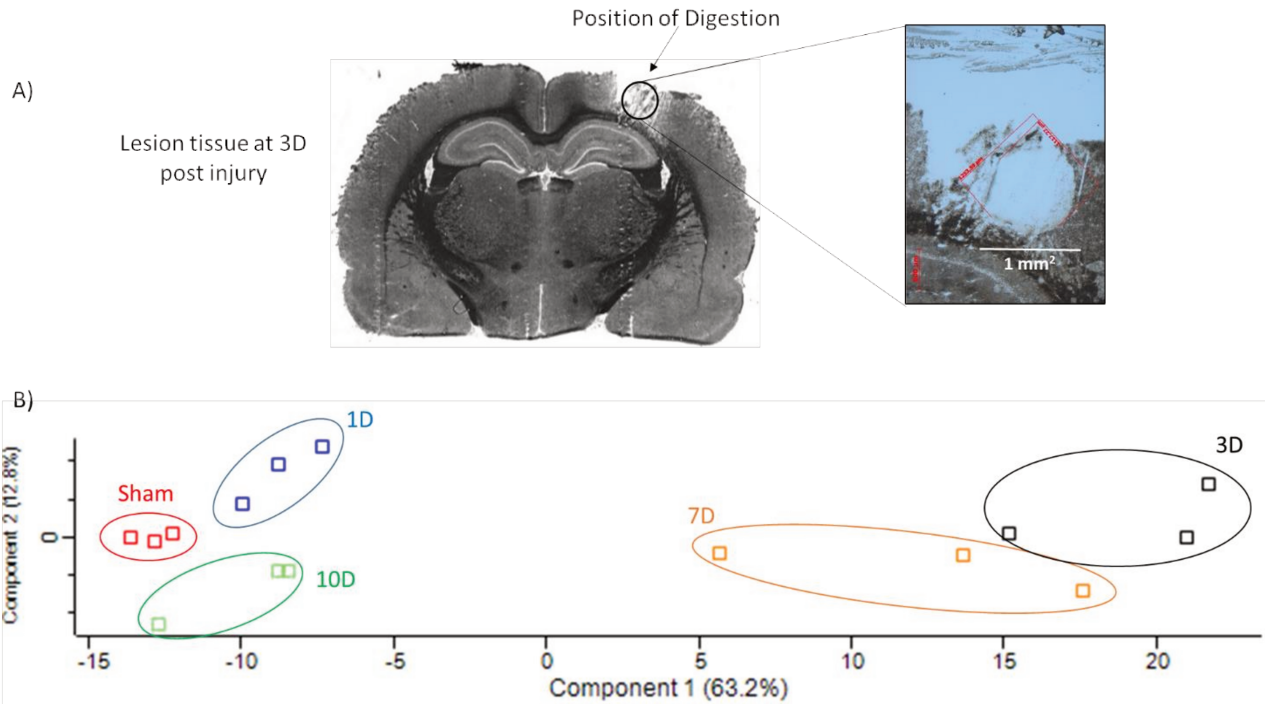


Figure S2: Related to Figure 1. A) Optical image of lesion segment at 3 days post injury along with a zoom image of the area of tryptic digestion and peptide extraction. B) Principal component analysis showing the first two components (1 and 2) of the microproteomic analysis for all three replicates of each of the following: sham, 1D, 3D, 7D, and 10D post injury.

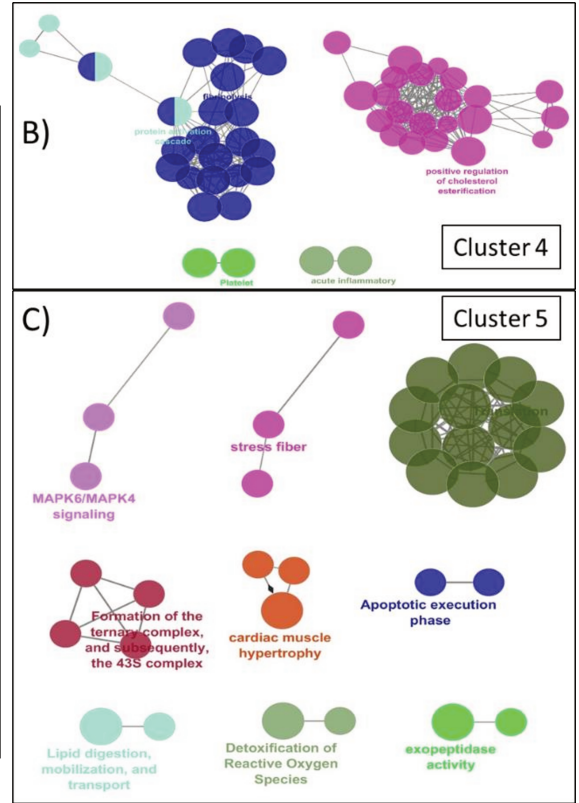
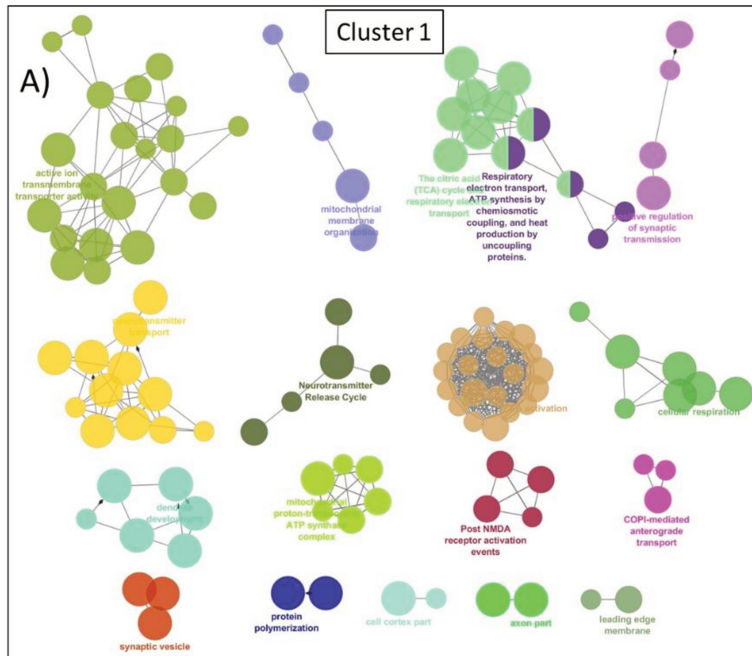


Figure S3: Related to Figure 1. A) ClueGo terms involved in proteins over-expressed in cluster 1. B) ClueGo terms involved in proteins over-expressed in cluster 4. C) ClueGo terms involved in proteins over-expressed in cluster 5.

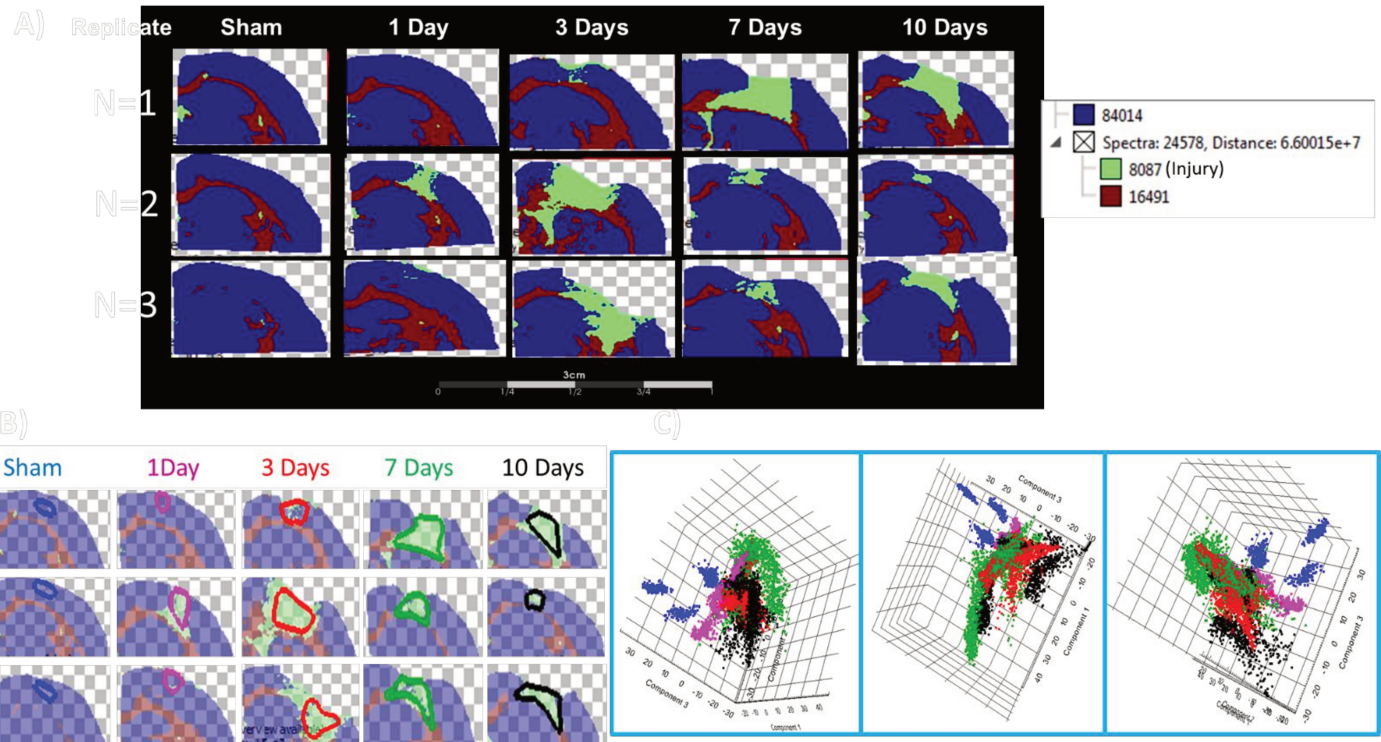


Figure S4: Related to Figure 2: A) Spatially segmented cluster images after processing lipid MALDI MSI data of lesion segments for all three replicates of sham brain and 1 day, 3 day, 7 day, and 10 day injured brains. In addition, the cluster tree corresponding to the imaged sections based on Manhattan distance calculation method is also shown. B) Transparent image of the spatial segmentation shown in figure S3A, with the highlighted selected regions that were further processed in principle component analysis. C) Principle component analysis of the regions selected in S3B.

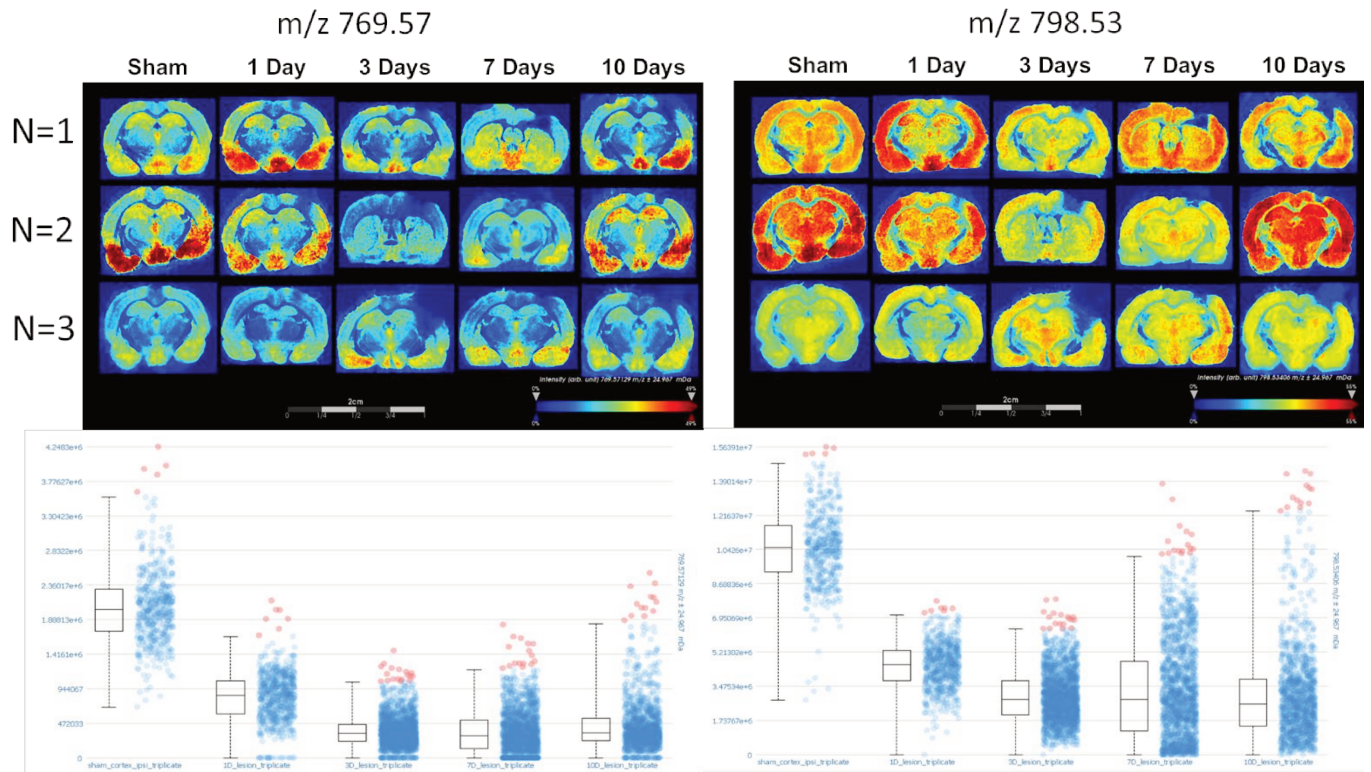


Figure S5: Related to Figure 2 and table S1. Plotted Ion images of m/z 769.57 and 798.53 along with their corresponding intensity box plot expression for all three replicates in all conditions: sham, 1 day, 3 days, 7 days, and 10 days.

Palmitoylcarnitine:
 Theoretical Mass: 400.342
 ($C_{23}H_{46}NO_4$)
 Observed Mass: 400.341

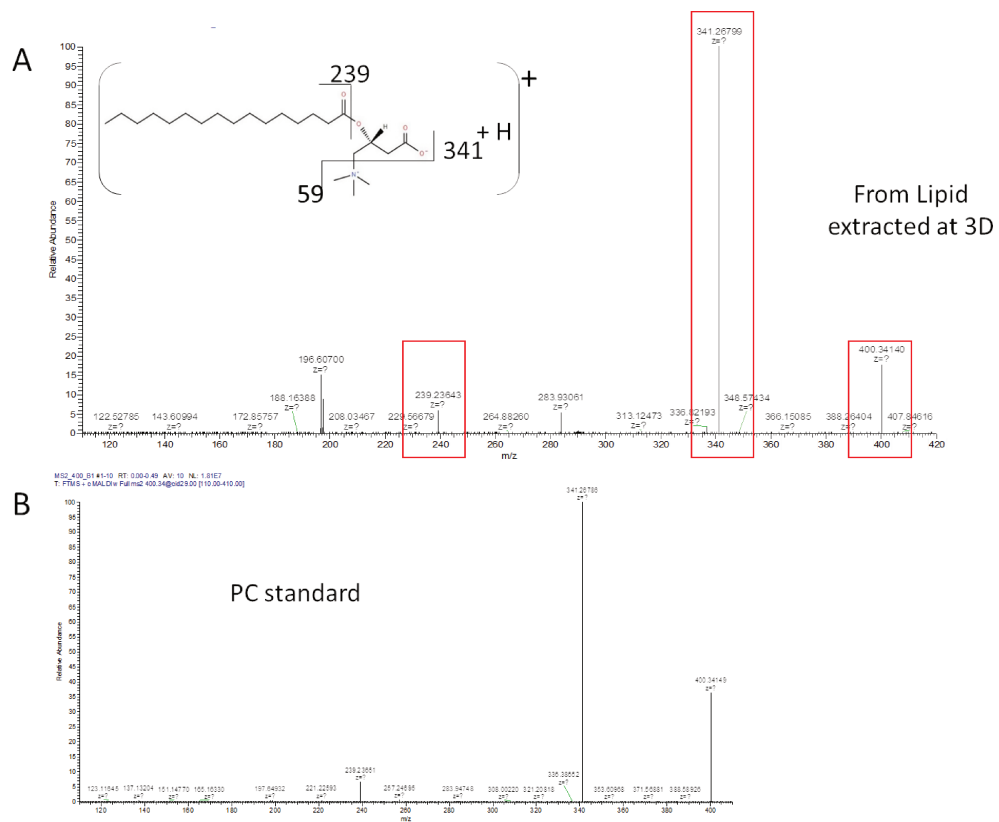


Figure S6: Related to Figure 4. A) MS/MS spectra showing the fragmentation pattern of m/z 400.35 from lipid extract at 3 days post injury. B) MS/MS spectra showing the fragmentation pattern of m/z 400.35 lipid standard.

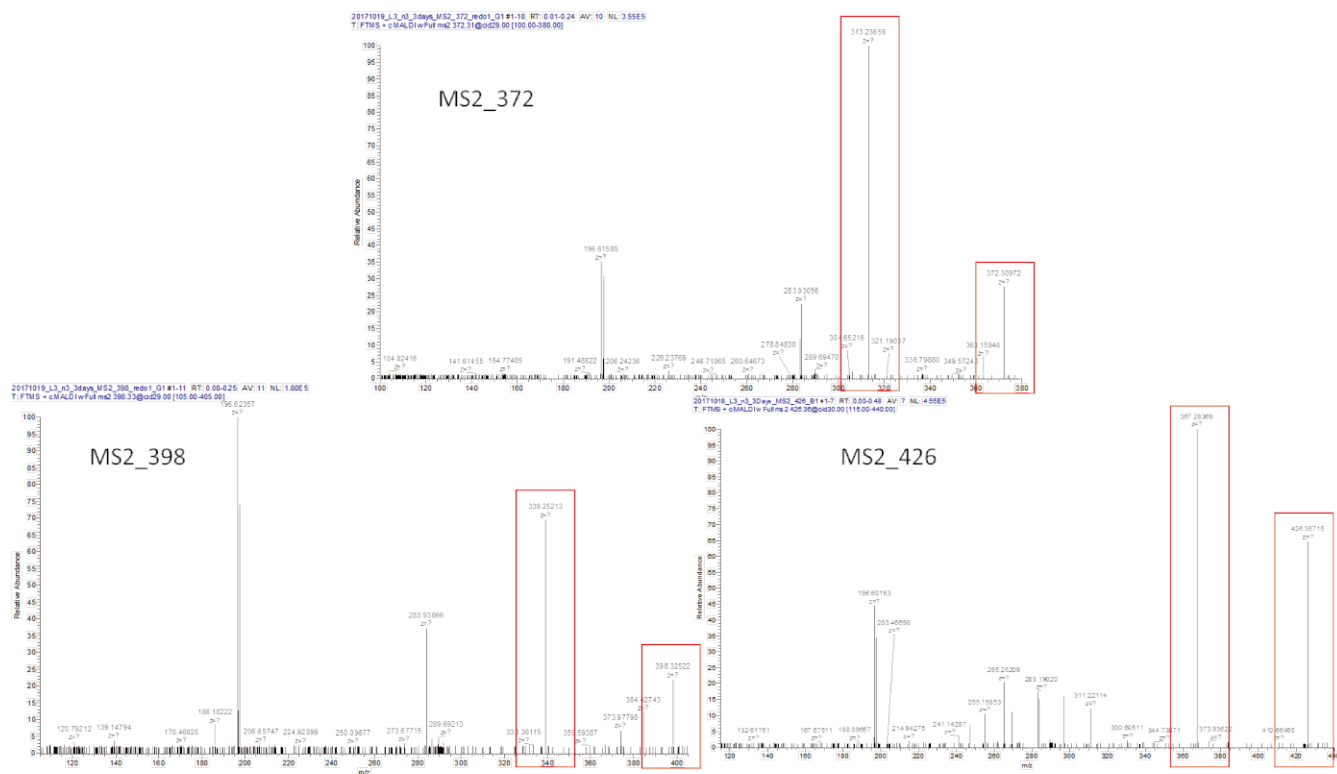


Figure S7: Related to Figure 4 and table S3. MS/MS spectra showing the fragmentation pattern of m/z 372.31, 398.32, and 426.36 from lipid extract at 3 days post injury.

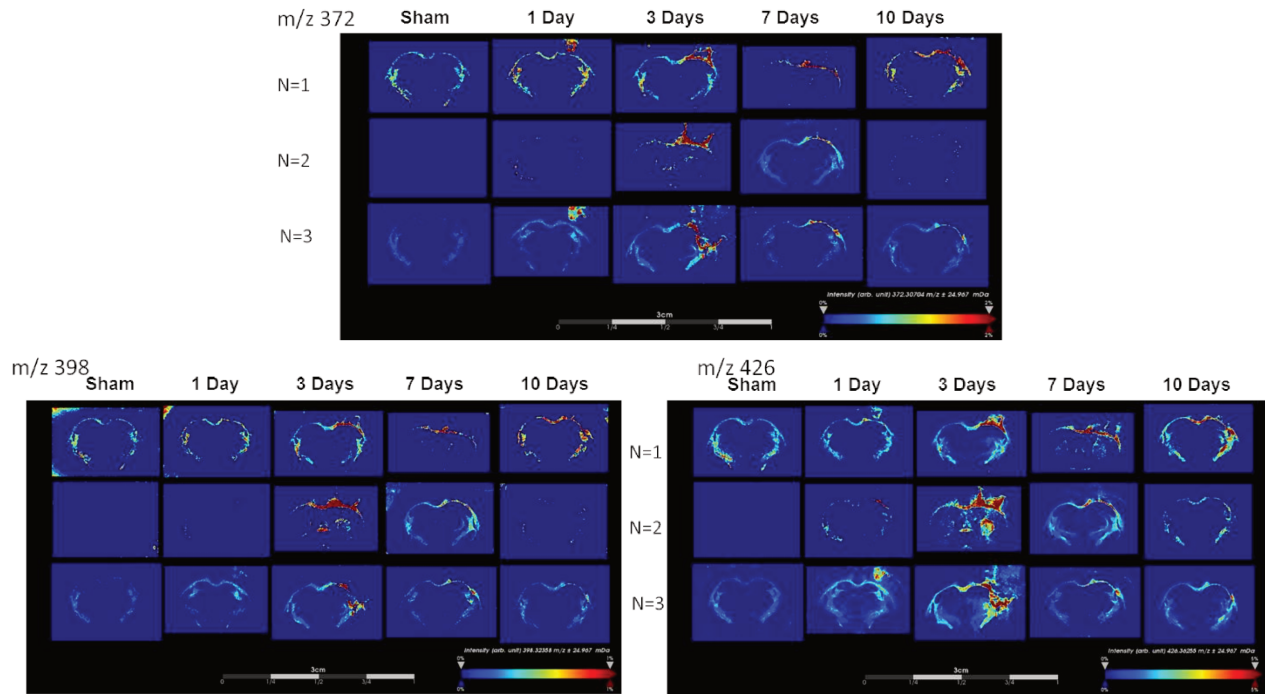
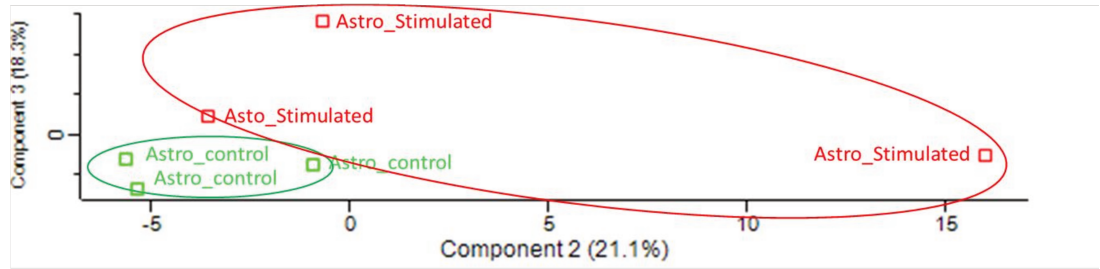


Figure S8: Related to Figure 4 and table 3. Plotted Ion images of m/z 372.31, 398.32, and 426.36 for all three replicates in all conditions: sham, 1 day, 3 days, 7 days, and 10 days.

A)



B)

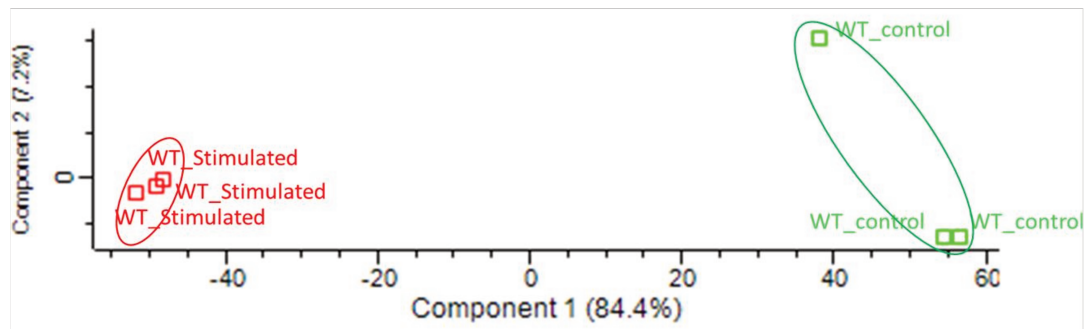


Figure S9: Related to Figure 7. Principle Component analysis of identified proteins between the palmitoylcarnitine stimulated condition or not in A) astrocytes and B) Macrophages.

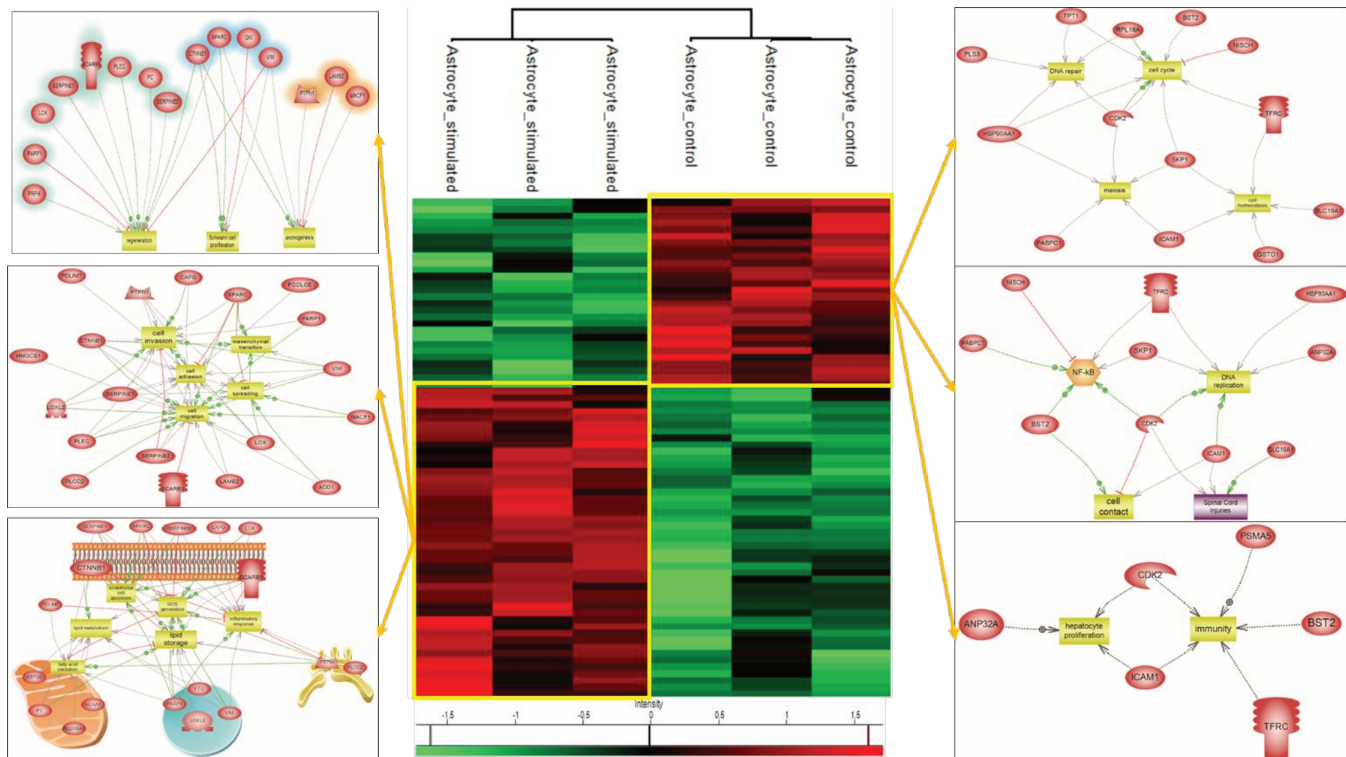


Figure S10: Related to Figure 7. Heat map based on the hierarchical clustering analysis of the LFQ value corresponding to the detected proteins extracted from macrophages stimulated with palmitoylcarnitine or not. Distinct clusters are highlighted. The system biology analysis for network identification for each of the highlighted clusters issued from heat map of proteins is also shown.

Supplementary Tables:

Centroid [m/z] ± 24.967 [mDa]		
393.93	773.54	844.52
423.99	774.54	845.47
614.92	775.54	845.52
615.97	785.45	846.55
617.99	786.47	848.57
710.50	797.59	849.57
711.50	798.53	852.49
713.44	800.56	853.46
714.47	801.53	868.47
738.51	802.48	869.47
739.46	814.51	870.47
740.48	820.53	870.54
741.48	821.53	871.54
753.59	824.45	872.56

754.59	825.42	873.56
767.50	826.57	874.51
767.55	827.57	875.51
769.57	830.52	896.48
770.52	831.52	912.46
770.57	840.43	913.46
771.57	841.45	914.46
772.52	844.47	934.43
		963.47

Table S1: Related to Figure 3. ROC analysis of Sham versus of all injured area in lesion segments. List of all 67 m/z values that discriminate the sham region from the injury region after applying threshold=0.75.

Centroid [m/z] \pm 24.967 [mDa]		
313.03	535.30	744.00
331.04	544.34	752.97
350.98	546.36	757.96
353.03	547.37	758.98
374.00	551.03	759.98
375.00	560.32	760.98
389.98	562.34	768.60
390.98	563.34	780.56
391.98	564.98	780.96
400.35	565.98	781.56
412.95	566.98	792.19
427.39	568.01	808.17
428.38	581.96	808.60
449.36	582.96	809.17
450.36	583.96	809.59
459.25	584.96	835.66
475.22	641.34	851.64
487.28	666.48	919.00
496.35	682.46	928.97
497.35	703.58	933.98
518.32	725.55	934.98
519.32	726.55	935.98
522.36	736.99	949.94
524.39	741.53	950.96
525.39	741.98	951.96
527.01	742.53	952.96
534.30	743.01	956.96

		972.93
--	--	--------

Table S2: Related to Figure 3. ROC analysis of all injured area in lesion segments versus sham. List of all 82 m/z values that discriminate the sham region from the injury region after applying threshold=0.75.

Centroid [m/z] \pm 24.967 [Da]
339.30
344.29
370.28
372.31
398.32
400.35
401.34
426.36
428.38
429.38
438.30
518.27
522.36
524.39
525.39

Table S3: Related to figure 4. m/z ion co-localized with m/z 400. List of 15 m/z ions that were found to be co-localized with m/z 400 at a threshold=0.3.

Conclusion – Chapter 2

Combining lipid MALDI-MSI and microproteomics in a spatio-temporal study of TBI allowed to obtain a global comprehension of several biological processes involving both proteomic and lipid species. Our study yielded the identification of a new family of lipid biomarkers associated with TBI, the long chain acylcarnitines, with main focus on palmitoylcarnitine. This family of lipids falls in the lower mass range < 600 m/z and thanks to our high resolution MALDI-LTQ-Orbitrap-XL, we were able to identify and distinguish them from other mass with close mass range and higher expression intensity which could have masked their expression. One example, is the free fatty acids which are usually liberated after impact and come from several sources, such as cell membranes after shearing. Surprisingly, owing the fact to the spatio-temporal approach that we used in our study, palmitoylcarnitine not only showed expression within the injured cortical tissue, but also had elevated levels within the caudal region of the brain, especially the substantia nigra of the ipsilateral hemisphere at 3D post impact. After identifying such palmitoylcarnitine as a lipid marker involved in the injury, we aimed to understand the impact of this lipid on the cells which accumulate within the cortical environment.

Previous work has shown that both astrocytes and macrophages are two of the major responders to the injury site post impact. We then stimulated both cell types with palmitoylcarnitine and showed that astrocytes upregulate several proteins implicated in neurogenesis and astrogliosis, thus possibly explaining one mode of action for astrocytes and its effect on its surrounding post impact. Also, macrophages over-expressed a large amount of proteins mainly involved in pro-inflammatory actions, and thus we can claim that palmitoylcarnitine can be considered as a major stimulator of inflammation in macrophages post impact. This was further confirmed by further processing the data, that the palmitoylcarnitine stimulation increased several proteins such as Galectin-3 which are mainly involved in pro-inflammatory pathways all mainly passing through TLR4-Myd-88 pathway. This family of molecules also expression linked to the resident microglia of the brain and not infiltrating macrophages, thus hinting to its possible source, the resident microglia. We started to model the possible interaction between acylcarnitine and galectin-3 for TLR4 interaction based on crystallization data obtained on human galectin-3 (Flores-Ibarra et al. 2018) (**Figure 24**). These results point out a possible interaction between the protein and the lipid which can lead to autocrine and paracrine loops between microglia and neurons based on the two molecules integrating

together in order to stimulate TLR4 activation. Further experiments are needed to explore deeper this hypothesis.

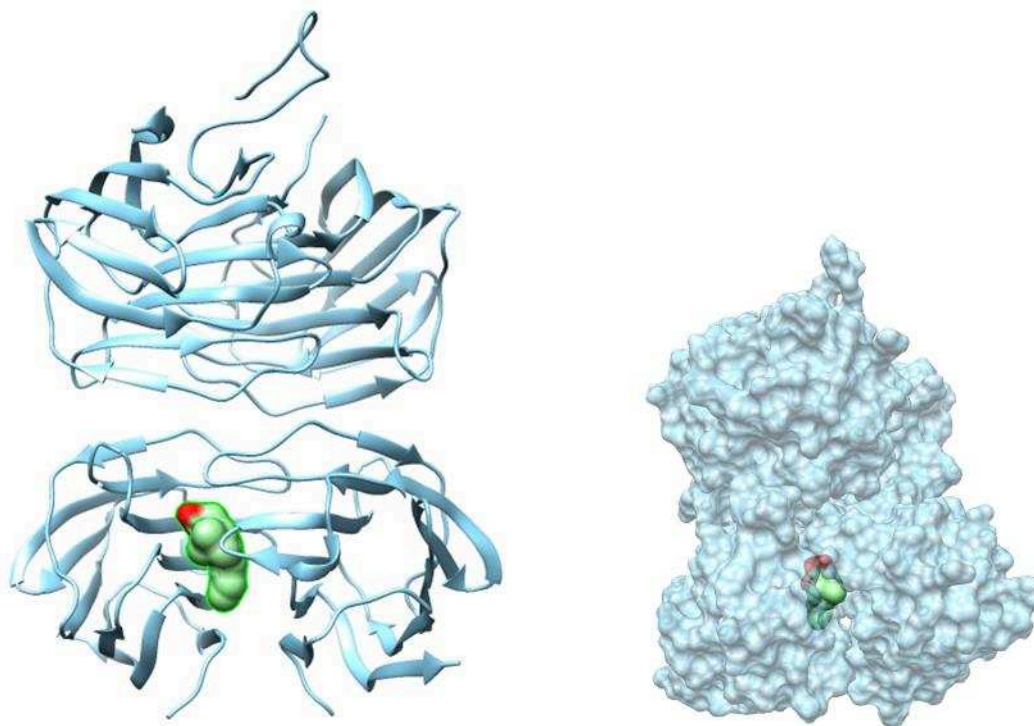


Figure 24: 3D Model representation of interaction between human galectin-3 and acylcarnitine (octanoylcarnitine) obtained by surface docking analysis.

Nevertheless, microproteomics data performed on the Substantia nigra of both ipsilateral and contralateral hemispheres and the same position of palmitoylcarnitine overexpression, demonstrated a possible link between TBI and Parkinson's disease as early as 3 days post injury. We demonstrated that proteins such as synaptotagmin and Glutamate Decarboxylase known to be implicated in Parkinson's disease, have elevated levels of expression in the ipsilateral Substantia nigra at 3 days after impact. The other markers we found (GPR158, HGMB1) are clearly highly interesting for the correlation between mild-TBI and Parkinson's disease. We started to perform a model for HMGB1 and α synuclein in order to better understand how the HMGB1 can affect the synaptic transmission (**Figure 25**). Docking generated by ClusPro 2.0 confirmed that the two proteins have a close intimacy as α -synuclein is shown to roll up the HMGB1. By that way, the α synuclein cannot play its biological function i.e. synaptic transmission. Moreover, HMGB1 has been recently indicated to be involved in the autophagic degradation of α -synuclein (Wang et al.

2016). Taken together, we can hypothesize that TBI can increase HMGB1 level in Substantia nigra that could promote with other factors Parkinson's disease.

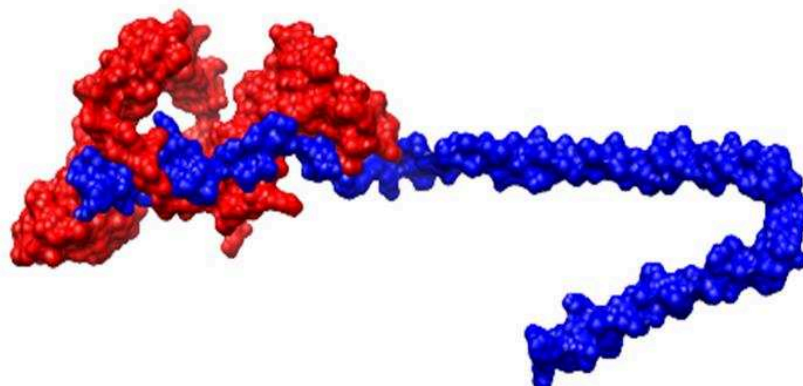


Figure 25: Docking generate by ClusPro 2.0 HmGB1-Synuclein_ITasser corresponding to α -synuclein (blue) and HMGB1 (Red).

For GPR158, it has recently been demonstrated to affect key signaling pathways involved in mood regulation in prefrontal cortex by regulating glutamatergic neurons through AMPA receptor modulation (Sutton et al. 2018). Similarly to what we hypothesized with HMGB1, GPR158 can be another key player in the link between open head TBI, repetitive closed head TBI and Parkinson's Disease. These results need more investigation using HMGB1 $-/-$ and GPR158 $-/-$ mice in order to confirm these first set of proteomic data. However as we quantified using LFQ proteomic data, comparisons between ipsilateral and contralateral hemispheres confirmed the increase of these proteins after TBI. We also pointed out that brain presents a high plasticity factor. In fact, in 10 days, a complete remission is observed after TBI. Nevertheless, we cannot exclude that repetitive TBI will affect this plasticity. This is shown in our current study in progress where we use a close-head injury model (**Figure 26**). We performed a series of 1 and 3 hits to the skull and observed the proteomic pattern 2 days and 1 week after. As it is shown in the heatmap, the proteomic profile of 3 hits is similar in pattern between 2 days and 7 days post impact, which is not the case when comparing to 1 hit to the skull. These data are in line with what we previously demonstrated but need to go further deep into the data to conclude.

Chapter 3: Proteomic Analysis of RhoA Inhibitor Effect on Rat Model of SCI.

Introduction

A Spatio-temporal proteomic approach performed on rat SCI after balloon compression has been recently performed in the laboratory. We combined a global proteomic analysis with a 3D molecular mass spectrometry imaging study, to analyze in time course, the infiltration of immune cells and cytokine microarray quantification (Devaux et al. 2016; Cizkova et al. 2014a). The whole spectrum of the data has allowed us to depict a complete scheme along the spinal cord axis of the cellular and molecular sequel of events occurring in time course of the inflammatory process and abortive regeneration. Specific markers for each spinal cord segment at different time points (3, 7, and 10 days) contributing to the biochemical-pathophysiological processes were observed. Surprisingly, segments below the lesion site (caudal segments) host a robust inflammatory process accompanied by local synthesis of neuroprotective and regenerative molecules. We demonstrated that the caudal segment adjacent to the lesion site possesses, at least temporarily, all the intrinsic components/features that may allow axonal regeneration. Such a caudal-to-rostral altered regenerative potential is likely hampered by inhibitory signals such as glycans that are abundantly detected or even secreted at the lesion site. Among the identified proteins from rostral and lesion segments, some are related to chemokines, cytokines or neurogenesis factors. In contrast, proteins from caudal segments are more related to neurocan, aggrecan, brevican and also to RhoA pathway and immunoglobulins (Devaux et al. 2016). The conditioned media (CM) from each spinal segment were used in-vitro, for culturing microglial BV2 cell lines and DRGs explants, showing a lesion site-dependent impact on microglia activation and DRGs neurite outgrowth. In addition, while naive BV2 cells exhibited insignificant staining for CX3CR1 receptor, the level of CX3CR1 was strongly enhanced in some BV2 cells after their stimulation by CM collected from SCI. The molecular data may perhaps correlate with different polarization of activated microglia and macrophages along the rostro-caudal axis following acute injury. This was partially confirmed in-vivo by mapping CX3CR1 receptor distribution, revealing higher expression in the rostral segment, with potential neuroprotective action (Cizkova et al. 2014a). We also established that when considering different time points after SCI, cytokine production between rostral and caudal segments appear different by means of qualitative and quantitative properties. At three days post injury, cytokines involved in attracting T regulator

lymphocytes have been detected in rostral but not in caudal segments which is line with the immunocytochemical detection of these cells only in rostral segment. These cells expressing CCL20 were found with a certain delay, at 7 days in caudal segments. Taken together, the obtained data clearly establishes a discrepancy in nature of cells and cytokines produced between rostral and caudal segments (Devaux et al. 2016). These data suggest that regionalization in terms of inflammatory and neurotrophic responses may occur between rostral and caudal segments in acute SCI.

Based on the previously obtained data, and in a therapeutic approach, we aimed to target RhoA protein using both in-vivo and in-vitro. We also aimed to further investigate the presence and expression patterns of IgG in SCI. These results are further discussed in Article 3.

Article: This research was originally published in Molecular & Cellular Proteomics.

Article 3: RhoA inhibitor treatment at acute phase of spinal cord injury may induce neurite outgrowth and synaptogenesis.

Authors: Stephanie Devaux*, Dasa Cizkova*, Khalil Mallah*, Melodie Anne Karnoub, Zahra Laouby, Firas Kobeissy, Juraj Blasko, Serge Nataf, Laurent Pays, Céline Mériaux, Isabelle Fournier, Michel Salzet. (*= equal contribution).

Article Status: Published in Molecular and Cellular Proteomics. 2017 Aug; 16(8):1394-1415
DOI: 10.1074/mcp.M116.064881. © the American Society for Biochemistry and Molecular Biology.

Summary: Part of experimental manipulations, along with sample preparation and data analysis was performed by Mr. Mallah. He also contributed to the writing of the paper. In detail, my contributions include:

- 1) Performing the data interrogation and statistical analysis of the proteomic data, including the LFQ value and heatmaps of the selected proteins in the different conditions.
- 2) Performing the in-vitro experiments including neurite outgrowth measurement upon stimulation with different conditioned medium from different segments of SCI, and with or without RhoA inhibitor.
- 3) Participated in performing all sub-network enrichment pathway analysis including the protein pathway maps and sub-cellular localization of the involved processes for the selected proteins, in addition to all venn analysis within the manuscript.
- 4) With regard to the manuscript, Mr. Mallah participated in writing and reviewing the final version of the paper.



RhoA Inhibitor Treatment At Acute Phase of Spinal Cord Injury May Induce Neurite Outgrowth and Synaptogenesis*[§]

Stephanie Devaux^{‡§}, Dasa Cizkova^{‡¶§§}, Khalil Mallah^{‡§§},
Melodie Anne Karnoub[‡], Zahra Laoubi[‡], Firas Kobeissy^{||}, Juraj Blasko^{**},
Serge Nataf^{‡‡}, Laurent Pays^{‡‡},  Céline Mériaux[‡],  Isabelle Fournier[‡],
and  Michel Salzet^{¶¶}

The therapeutic use of RhoA inhibitors (RhoAi) has been experimentally tested in spinal cord injury (SCI). In order to decipher the underlying molecular mechanisms involved in such a process, an *in vitro* neuroproteomic-systems biology platform was developed in which the pan-proteomic profile of the dorsal root ganglia (DRG) cell line ND7/23 DRG was assessed in a large array of culture conditions using RhoAi and/or conditioned media obtained from SCI *ex vivo* derived spinal cord slices. A fine mapping of the spatio-temporal molecular events of the RhoAi treatment in SCI was performed. The data obtained allow a better understanding of regeneration/degeneration induced above and below the lesion site. Results notably showed a time-dependent alteration of the transcription factors profile along with the synthesis of growth cone-related factors (receptors, ligands, and signaling pathways) in RhoAi treated DRG cells. Furthermore, we assessed in a rat SCI model the *in vivo* impact of RhoAi treatment administered *in situ* via alginate scaffold that was combined with FK506 delivery. The improved recovery of locomotion was detected only at the early postinjury time points, whereas after overall survival a dramatic increase of synaptic contacts on outgrowing neurites in affected segments was observed. We validate these re-

sults by *in vivo* proteomic studies along the spinal cord segments from tissue and secreted media analyses, confirming the increase of the synaptogenesis expression factors under RhoAi treatment. Taken together, we demonstrate that RhoAi treatment seems to be useful to stimulate neurite outgrowth in both *in vitro* as well *in vivo* environments. However, for *in vivo* experiments there is a need for sustained delivery regiment to facilitate axon regeneration and promote synaptic reconnections with appropriate target neurons also at chronic phase, which in turn may lead to higher assumption for functional improvement. *Molecular & Cellular Proteomics* 16: 10.1074/mcp.M116.064881, 1394–1415, 2017.

Among the inhibitory factors that prevent axonal regrowth in spinal cord injury (SCI)¹, RhoA, an intracellular GTPase, is considered as a key target for the design of proregenerative strategies. Previous experiments have shown that lysophosphatidic acid, via activation of the RhoA pathway, induced neurite retraction and neuronal soma rounding (1). Conversely, the use of C3 transferase to inactivate Rho in primary neuronal culture confirmed the role of Rho in neurite outgrowth inhibition (2–4). Thus, blockers of the post-receptor components of RhoA are now used to improve long-distance axon regeneration and sprouting (5). Furthermore, there is evidence that RhoA-ROCK signaling mediates the inhibitory effects of chondroitin sulfate proteoglycans (CSPG) in neurons; whereas, the sustained delivery of Rho inhibitor and BDNF promotes axonal growth in CSPG region after SCI. Along this line, novel inhibitors *i.e.* cholesterol and sphingomyelin as novel myelin-associated inhibitors have also demonstrated to operate via RhoA-dependent mechanism(s) (6–8). On this basis, the RhoA pathway in neurons is considered to mediate the intracellular signaling of several major extracellular cues that inhibit neuroregeneration in SCI. Accord-

From the [‡]Univ. Lille, Inserm, U-1192 - Laboratoire Protéomique, Réponse Inflammatoire et Spectrométrie de Masse-PRISM, F-59000 Lille, France; [§]Institute of Neuroimmunology, Slovak Academy of Sciences, Dúbravská cesta 9, 845 10 Bratislava, Slovakia; [¶]Department of Anatomy, Histology and Physiology, University of Veterinary Medicine and Pharmacy in Košice, Komenského 73, 041 81 Košice, Slovakia; ^{||}Department of Biochemistry and Molecular Genetics, Faculty of Medicine, American University of Beirut; ^{**}Institute of Neurobiology, Slovak Academy of Sciences, Soltesovej 4–6 Kosice, Slovakia; ^{‡‡}Univ Lyon, CarMeN laboratory, Inserm U1060, INRA U1397, Université Claude Bernard Lyon 1, INSA Lyon, Charles Merieux Medical School, Fr-69600, Oullins, France

Received October 20, 2016, and in revised form, June 28, 2017

Published, MCP Papers in Press, June 28, 2017, DOI 10.1074/mcp.M116.064881

Author contributions: D.C. and M.S. designed research; S.D., D.C., K.M., M.K., Z.L., J.B., C.M., I.F., and M.S. performed research; S.D., D.C., K.M., M.K., Z.L., F.K., J.B., S.N., L.P., C.M., I.F., and M.S. analyzed data; S.D., D.C., and M.S. wrote the paper.

¹ The abbreviations used are: SCI, spinal cord injury; DRG, dorsal root ganglia; CSPG, chondroitin sulfate proteoglycan; RhoGDI α , rho GDP dissociation inhibitor alpha; FASP, filter aided sample preparation; PSM, peptide spectrum matches.

ingly, the RhoA inhibitor Cethrin is currently under phase I/IIa clinical trials for the treatment of SCI (9).

One of the mechanism by which RhoA signaling inhibits neurite growth involves the p75 neurotrophin receptor. Indeed, several studies, using for some of them the p75 neurotrophin receptor- (p75^{NTR}) -null mutant mice (7) showed that RhoA binds to p75^{NTR} and forms part of the membrane raft receptor complex responsible for growth inhibition signaling (10–12). However, a pan-proteomic approach that would identify the whole range of effects exerted by RhoA inhibition on neurons is still missing. In this context, we have recently demonstrated, based on spatial and temporal proteomic studies, that major differences between the rostral and caudal segments adjacent to the lesion could be demonstrated at day 3 post-SCI, in terms of injury mechanisms, inflammatory regulation and regeneration processes (13). In the rostral or lesion segments, multiple proteins belonging to the chemokines/cytokines family or exerting neurotrophic functions were identified. In contrast, multiple proteins identified in caudal segments appeared to relate with injury and necrosis events. Our data suggest that in acute SCI regionalization in terms of inflammatory and neurotrophic responses may occur because of alterations in protein dynamics between rostral and caudal segments (13). In addition, the proteomic profile in caudal segments was characterized by the neuronal expression of IgG2a neuronal and by a signature of axonal regrowth inhibition associating CSPG and proteins of the MEMO1-RHOA-DIAPH1 signaling pathway (14). The MEMO1-RHOA-DIAPH1 signaling pathway plays an important role in ERBB2-dependent stabilization of microtubules at the cell cortex and inhibits neurite outgrowth. Interestingly, a comparative proteomic approach performed by Liu *et al.* (2015) (15) at the caudal segment level has shown that the eukaryotic translation initiation factor 5A1 (eIF5A1) and Rho GDP dissociation inhibitor alpha (RhoGDI α), a member of Rho GDI family, played a major role in determining the extent of spontaneous functional recovery (15). *In vitro*, eIF5A1 overexpression in primary neurons increased cell survival and elongated neurite length whereas eIF5A1 knockdown reversed these effects (15). Moreover, eIF5A1 and RhoGDI α were involved in the same pathway as, both *in vivo* and *in vitro*, RhoGDI α up-regulation or down-regulation rescued the neuroregeneration impact of eIF5A1 down- or upregulation respectively (15).

In this context, the present study was designed to: (1) optimize SCI neurotherapy with RhoA inhibitors (RhoAi) and (2) gain further molecular insights on the mechanism(s) by which RhoAi may exert its neuroregenerative effects in SCI. For this purpose, we developed an *in vitro* neuroproteomic-systems biology platform in which the pan-proteomic profile of the dorsal root ganglia (DRG) cell line ND7/23 DRG was assessed in a large array of culture conditions using RhoAi and/or conditioned media obtained from SCI *ex vivo* derived spinal cord slices. In addition, pan-proteomic analyses and identification of functional biochemical pathways were cou-

pled to the assessment of a large array of transcription factors.

This innovative analytical platform allowed a fine mapping of the spatio-temporal molecular events supporting the neuroregenerative impact of RhoAi in SCI. We then validate our finding by *in vivo* proteomic study at the level of the tissue segments and conditioned media. Our findings highlight the large molecular effects of RhoAi and provide an integrated mapping of such effects on the secretome, regulome and intra-cellular proteome of injured neurons.

Finally, our work points to the possible therapeutic potential of RhoAi administered in alginate scaffolds and delivered in a time- and segment-specific fashion. In particular, we show that RhoAi is able to promote neurite outgrowth and synaptic reconnection, but is not sufficient to induce and maintain a real beneficial outcome evaluated by BBB score. Thus our work open the door for new treatment scenario where a RhoA is a key player.

MATERIALS AND METHODS

Reagents—DMEM media, Phosphate buffer saline (PBS), fetal calf serum (FCS) were purchased from Invitrogen Life Technologies (Milan, Italy). All chemicals were of the highest purity obtainable. Water, formic acid (FA), trifluoroacetic acid (TFA), acetonitrile (ACN) were purchased from Biosolve B.V. (Valkenswaard, the Netherlands). Sodium dodecyl sulfate (SDS), DL-dithiothreitol (DTT), and iodoacetamide (IAA) were purchased from SIGMA (Saint-Quentin Fallavier, France). Trypsin/Lys-C Mix and Trypsin Mass Spec Grade was purchased from Promega (Charbonnières, France). RhoA inhibitor was purchased from Cytoskeleton, Inc (Denver, CO). FK506 was purchased from Invivogen (Toulouse, France).

Experimental Design and Statistical Rational—All the experiments were performed with biological replicates. For protein extraction was performed from SCI tissues from control rats ($n = 3$) and rats 12 h after SCI treated with RhoAi + FK506 ($n = 3$) or not treated ($n = 3$). For the collection of the conditioned media, control rats (no balloon inflation, $n = 6$), rats 12 h post-injury ($n = 6$) and rats 3 days post-injury ($n = 6$) were sacrificed. For the behavioral experiments, 5 rats received saline and 5 rats received RhoAi + FK506. Statistical analysis: For the proteomic statistical analysis of conditioned media, as a criterion of significance, we applied an ANOVA significance threshold of $p < 0.05$, and heat maps were generated. Normalization was achieved using a Z-score with a matrix access by rows. Obtained data from tissue analyses and behavioral testing were reported as mean \pm S.E. Mean values among different experimental groups were statistically compared by one-way ANOVA and Tukey's post hoc tests using Graph pad PRISM software. Values of $p < 0.05$ were considered statistically significant ($*p$ value of < 0.05 , $**p$ value of < 0.01 , $***p < 0.001$).

Intraspinal Delivery of RhoAi—Seven days after SCI, animals ($n = 10$) were anesthetized with 1.5–2% isoflurane and partial laminectomy at Th6–12 level was performed. Using a 50- μ l Hamilton syringe (30G needle, Cole Parmer, Anjou, Quebec) connected to Ultra-MicroPump III with Micro4 Controller, 4-Channel (World Precious Instruments, Inc., Sarasota, FL) and stereotactic device, 2 intraspinal injections per animal were applied bilaterally to the lesion site and to the rostral and caudal segments (6 injections total). In most cases the lesion cavity was apparent through the dorsal site of spinal cord. Bilateral delivery of (1) saline ($n = 5$), (2) RhoAi, 0.1 μ g/ μ l ($n = 5$) (2 injections of 2 μ l of alginate containing RhoAi per injection on left and right sides with delivery rate of 0.5 μ l/min, was performed at lesion

cavity and 1 μ l of pure RhoAi per injection at rostral and caudal segments. The volume of 1 μ l was used in the case of intraspinal injections, whereas 2 μ l injections for administration to the cavity site. Each delivery was positioned 1 mm from the spinal cord midline and injected at the depth of 1.8–2 mm from the pial surface of the spinal cord. The distance between injections was 1 mm, avoiding vessels. Intraspinal injections were followed by procedure published in our study (16). After injecting the dose of saline or RhoAi, the needle was maintained in the tissue for an additional 30 s. No antibiotic treatment was performed. Rats treated with RhoAi received daily intraperitoneal (i.p.) injection of FK506 0.5 mg/kg/animal/3 \times during the first week, followed by dose of 0.25 mg/kg/animal/3 \times during the second week, whereas rats with vehicles received i.p. saline. A separate group of SCI rats ($n = 6$) injected with RhoAi with respective saline controls ($n = 6$) that survived 12 h was performed for proteomic analyses.

Collection of Conditioned Media (CM) from Control and Lesioned Spinal Cord Segments—Experimental SCI rats at 3 days ($n = 3$) and at 12 h with ($n = 3$) or without RhoAi treatment ($n = 3$) and respective controls ($n = 3/3D$; $n = 3/12h$) were sacrificed by isoflurane anesthesia followed by decapitation. The spinal cord was pressure expressed by injecting sterile saline (10 ml) throughout the vertebrate canal, along the caudo-rostral axis. Each spinal cord was macroscopically observed to check that lesion was well centered at the Th8-Th9 level on the longitudinal axis. Entire spinal cord was divided into transversally sectioned slides (~1.0 cm thick each) obtained from the lesion site (Th7-Th11) and from the segments rostral (C1-Th6) and caudal (Th12-L6) to the site of injury. Slides were then chopped into 0.5 cm thick sections (2 sections per segment) and deposited into a 12-well culture plate containing 1 ml DMEM without FCS. After 24 h incubation in a humidified atmosphere with 5% CO₂ at 37 °C, 1 ml of SCI-derived conditioned media (SCI-CM) were collected (rostral (R1), lesion (L), caudal (C1) segments) and centrifuged 30 min at 15,000 rpm at 4 °C. Samples were stored at –80 °C.

Protein Extraction from SCI Tissues—1 mm thick sections from rostral, lesioned and caudal segments from 12 h post-SCI rats ($n = 3$) were ground in 1.5 ml tubes. Two hundred microliters of extraction buffer (CHAPS 3.5%, Tris 0.1 M, Dithiothreitol (DTT) 50 mM, pH 10.0) were added in each tube. Samples were mixed for 5 min and sonicated for 20 min. Cell debris were removed by centrifugation (15 min, 15000 $\times g$). 30 μ l of supernatant were used for FASP analysis using Amicon 30 kDa (Millipore) and LysC/trypsin enzymatic mix (30 μ g/ml in 0.05 M NH₄HCO₃) (17). After overnight incubation at 37 °C, the digests were collected by centrifugation. The filters were rinsed with 50 μ l of NaCl 0.5 M. Digestion was quenched by adding TFA 5% to the digests. The peptides were desalted with a Millipore ZipTip device before LC-MS/MS analysis.

Protein Digestion of SCI-CM—One hundred fifty microliters of SCI-CM and control CM were denatured with 6 M urea in 40 mM HEPES, pH 8.0 by sonication on ice. The proteins were reduced with 50 μ l DTT 10 mM for 40 min at 56 °C and alkylated with iodoacetamide 55 mM for 40 min in the dark. The alkylation reaction was quenched with thiourea 100 mM. The proteins were digested overnight at 37 °C with 30 μ g/ml LysC/Trypsin mixture. The digestion was stopped with 10 μ l TFA 17.5%. The peptides were desalted with a Millipore ZipTip device before LC MS/MS analysis.

In Vitro Neurite Outgrowth With SCI-CM—ND7/23 cell line (Sigma mouse neuroblastoma X rat neuron hybrid) was used to visualize *in vitro* the neurite outgrowth in presence of R1 and C1 conditioned media 3 days post injury in combination or not with RhoAi. ND7/23 cells were plated at a density of 18,000 cells/per well in 96-wells plate. The cells were starved overnight with DMEM medium supplemented with 2% Fetal bovine serum (FBS) + 1% antibiotics + 1% L-glutamine. Afterward, cells were stimulated with 1/3 R1 or C1 CM and 2/3 DMEM + 1% L-1% L-Glutamine + 1% penicillin-streptomycin

(serum free medium) (14). The cells were treated or not with 1 μ g/ml RhoAi in combination with 1/3 of CM with 2/3 DMEM supplemented medium 24 h after C1 or R1 stimulation in order to reproduce the injured environment. The optimum split ratio 1/3 (CM, RhoAi): 2/3 culture DMEM was set to perform sustained culture conditions for cells, according to our previous studies (14). Live images of cells not stimulated with RhoAi were captured 48 h after R1 or C1 CM stimulation and the images of ND7/23 cells stimulated with CM and RhoAi were captured 24 h after RhoAi stimulation (corresponding to 48 h after CM stimulation) with a camera mounted on a phase-contrast microscope (Nikon Eclipse TS100). Measurements were performed by using ImageJ software to determine the neurite length and statistical significance evaluated with One-Way ANOVA followed by Tukey Kramer Test (GraphPadInStat 3.0).

Total Protein Extracts and Conditioned Media (CM) Collection—ND7/23 cells were plated in 6-well plates until confluent. The cells were starved overnight with DMEM supplemented with 2% FBS, 1% L-Glutamine and 1% penicillin-streptomycin. Cells were first stimulated with 1/3 of R1 or lesion or C1 CM 3 days post injury and 2/3 DMEM + 1% L-Glu + 1% antibiotics, or left untreated. After 24 h of CM stimulation, 1 μ g/ml of RhoAi is added to the media. 24 h after RhoAi stimulation, the cell supernatants were collected, centrifuged (1000 rpm, 5 min) and immediately frozen at –80 °C, and the cells were collected and then lysed with RIPA buffer for total protein extraction (150 mM NaCl, 50 mM Tris, 5 mM EGTA, 2 mM EDTA, 100 mM NaF, 10 mM sodium pyrophosphate, 1% Nonidet P-40, 1 mM PMSF, 1 \times protease inhibitors). Cell debris was removed by centrifugation (20000 $\times g$, 10 min, 4 °C). For the time course experiment after RhoAi, the cells were starved overnight. Cells were stimulated with RhoAi for 30 min (T30), 1 h (T1) and 4 h (T4) followed by the same protocol for total proteins extraction. The supernatants were collected and the protein concentrations were measured using the Bio-Rad Protein Assay. Experiments were performed in triplicates but not for T0, T30 min, T1 h, T4 h experiment with only one replicate.

Filter-aided Sample Preparation (FASP)—The total protein extract (0.1 mg) was used for FASP analysis as described previously (17). We performed FASP using Microcon devices YM-10 (Millipore) before adding trypsin for protein digestion (40 μ g/ml in 0.05 M NH₄HCO₃). The samples were incubated overnight at 37 °C. The digests were collected by centrifugation, and the filter device was rinsed with 50 μ l of NaCl 0.5 M. Next, 5% TFA was added to the digests, and the peptides were desalted with a Millipore ZipTip device before LC-MS/MS analysis.

Protein Digestion of Condition Medium—One hundred microliters of the CM were collected for each condition. Secretome digestion was performed as previously described (18). In brief, the cell supernatants were denatured with 2 M urea in 10 mM HEPES, pH 8.0 by sonication on ice. The proteins were reduced with 10 mM DTT for 40 min followed by alkylation with 55 mM iodoacetamide for 40 min in the dark. The iodoacetamide was quenched with 100 mM thiourea. The proteins were digested with 20 μ g/ml LysC/Trypsin mixture overnight at 37 °C. The digestion was stopped with 0.5% TFA. The peptides were desalted with a Millipore ZipTip device in a final volume of 20 μ l of 80% ACN elution solution. The solution was then dried using the SpeedVac. Dried samples were solubilized in water/0.1% formic acid before LC MS/MS analysis.

LC MS/MS Analysis—Samples were separated by online reversed-phase chromatography using a Thermo Scientific Proxeon Easy-nLC1000 system equipped with a Proxeon trap column (100 μ m ID \times 2 cm, Thermo Scientific) and a C18 packed-tip column (Acclaim PepMap, 75 μ m ID \times 15 cm, Thermo Scientific). Peptides were separated using an increasing amount of acetonitrile (5–35% over 120 min) at a flow rate of 300 nL/min. The LC eluent was electrosprayed directly from the analytical column and a voltage of 1.7 kV was

applied via the liquid junction of the nanospray source. The chromatography system was coupled to a Thermo Scientific Q-exactive mass spectrometer programmed to acquire in a data-dependent mode Top 10 most intense ion method. The survey scans were done at a resolving power of 70,000 FWHM (m/z 400), in positive mode and using an AGC target of $3e6$. Default charge state was set at 2, unassigned and +1 charge states were rejected and dynamic exclusion was enabled for 25 s. The scan range was set to 300–1600 m/z . For ddMS², the scan range was between 200–2000 m/z , 1 microscan was acquired at 17,500 FWHM and an isolation window of 4.0 m/z was used.

MS Data Analysis of T0, T30 min, T1 h and T4 h Protein Extract After RhoAi Treatment—Tandem mass spectra were processed with Thermo Scientific Proteome Discoverer software version 1.4. Spectra were searched against UniprotKB/Swiss-Prot (version January 2016) filtered with *Rattus norvegicus* (31093 sequences) taxonomy using the SEQUEST HT algorithm (version 1.4.1.14). The search was performed choosing trypsin as the enzyme with one missed cleavage allowed. Precursor mass tolerance was 10 ppm, and fragment mass tolerance was 0.1 Da. N-terminal acetylation; and cysteine carbamidomethylation; methionine oxidation were set as variable modifications and cysteine carbamidomethylation as fixed modification. Peptide validation was performed with the Percolator algorithm by filtering based on a q -value below 0.01, which corresponds to a false discovery rate (FDR) of 1%. Proteins were identified with a minimum of 2 peptides with at least one unique peptide per protein. The data sets used for analysis and the annotated MS/MS spectra were deposited at the ProteomeXchange Consortium (<http://proteomecentral.proteomexchange.org>) via the PRIDE partner repository with the data set identifier PXD004639 (for review: Username: reviewer60033@ebi.ac.uk Password: 7008Fxxe).

MS Data Analysis of Protein Extract and Secretome After SCI-CM With or Without RhoAi Treatment—All the MS data were processed with MaxQuant (version 1.5.6.5) (19) using the Andromeda (20) search engine. Secretome and protein extract from ND7/23 cell line were processed in two different files. Proteins were identified by searching MS and MS/MS data against Decoy version of the complete proteome for *Rattus norvegicus* of the UniProt database (21) (Release June 2014, 33,675 entries) combined with 262 commonly detected contaminants. Trypsin specificity was used for the digestion mode with N-terminal acetylation and methionine oxidation selected as the variable. Carbamidomethylation of cysteines was set as a fixed modification, with up to two missed cleavages. For MS spectra, an initial mass accuracy of 6 ppm was selected, with a minimum of 2 peptides and at least 1 unique peptide per protein, and the MS/MS tolerance was set to 20 ppm for HCD data. For identification, the FDR at the peptide spectrum matches (PSMs) and protein level was set to 0.01. Relative, label-free quantification of proteins was performed using the MaxLFQ algorithm (22) integrated into MaxQuant with the default parameters. The data sets, the Perseus result files used for analysis and the annotated MS/MS spectra were deposited at the ProteomeXchange Consortium (23) (<http://proteomecentral.proteomexchange.org>) via the PRIDE partner repository (24) with the data set identifier PXD004639 (for review: Username: reviewer60033@ebi.ac.uk Password: 7008Fxxe) for cellular extracts and secretomes. Analysis of the proteins identified was performed using Perseus software (<http://www.perseus-framework.org/>) (version 1.5.6.0). The file containing the information from identification was used with hits to the reverse database, and proteins only identified with modified peptides and potential contaminants were removed. Then, the LFQ intensity was logarithmized ($\log_2[x]$). Categorical annotation of rows was used to defined different groups after grouping replicates (1) Replicate (DMEM, R1, L, C1, R1 RhoAi, L RhoAi, C1 RhoAi), (2) Rho versus NT (DMEM, DMEM RhoAi, Rho (R1, L and

C1 + RhoAi) and NT (R1, L and C1 without RhoAi). Multiple-samples tests were performed using ANOVA test with a FDR of 5% and preserving grouping in randomization. Normalization was achieved using a Z-score with a matrix access by rows.

For the statistical analysis, only proteins presenting as significant by the ANOVA test were used for statistical analysis. Hierarchical clustering depending protein extract or secretome were first performed using the Euclidean parameter for distance calculation and average option for linkage in row and column trees using a maximum of 300 clusters. For visualization of the variation of proteins expression depending to the condition, the profile plot tool was used with a reference profile and an automatic selection of the 10 or 15 correlated profiles. To quantify fold changes of proteins across samples, we used MaxLFQ. To visualize these fold changes in the context of individual protein abundances in the proteome, we projected them onto the summed peptide intensities normalized by the number of theoretically observable peptides. Specifically, to compare relative protein abundances between and within samples, protein lengths normalized to \log_2 protein intensities (termed “iBAQ” value in MaxQuant) were added to the MaxLFQ differences. Functional annotation and characterization of identified proteins were obtained using PANTHER software (version 9.0, <http://www.pantherdb.org>) and STRING (version 9.1, <http://string-db.org>).

Subnetwork Enrichment Pathway Analyses and Statistical Testing—The Elsevier’s Pathway Studio version 9.0 (Ariadne Genomics/Elsevier) was used to deduce relationships among differentially expressed proteomics protein candidates using the Ariadne ResNet database (25, 26). “Subnetwork Enrichment Analysis” (SNEA) algorithm was selected to extract statistically significant altered biological and functional pathways pertaining to each identified set of protein hits (C1, R1, L after RhoA inhibitor treatment sets). SNEA utilizes Fisher’s statistical test used to determine if there are nonrandomized associations between two categorical variables organized by specific relationship. SNEA starts by creating a central “seed” from all relevant entities in the database, and retrieving associated entities based on their relationship with the “seed” (*i.e.* binding partners, expression targets, protein modification targets, regulation). The algorithm compares the sub-network distribution to the background distribution using one-sided Mann-Whitney U-Test, and calculates a p value indicating the statistical significance of difference between two distributions. In our analysis, “GenBank” ID and gene symbols from each set were imported to the software to form an experimental data set. For the reconstruction of networks of pathways, biological processes and molecular function were evaluated for each single protein hit and its associated targets (networks and pathways) (27, 28). Integrated Venn diagram analysis was performed using “the InteractiVenn”; a web-based tool for the analysis of complex data sets.

Behavioral Testing—Animals were evaluated using Basso, Beattie, and Bresnahan (BBB) open-field test to assess motor function after SCI at day 0, 7, 14, 21, 28, 35, 42 and 49 days post injury. Each rat was tested for 5 min by two blinded examiners. BBB test measures locomotor outcome (hind limb activity, body position, trunk stability, tail position and walking paw placement) of rats utilizing the rating scale ranges from 0 (no observable hind limbs movements) to a maximum of 21 (plantar stepping, coordination and trunk stability like control rats).

Immunohistochemistry—After survival period, animals were deeply anesthetized by intraperitoneal thiopental injection (50 mg/kg) and perfused transcardially with 500 ml saline, followed by 500 ml of 4% paraformaldehyde (PFA) in 0.1 M phosphate buffer (PB). Spinal cords were removed, postfixed in 4% PFA at 4 °C overnight, embedded in gelatin-egg albumin protein matrix (10% ovalbumin, 0.75% gelatin) polymerized by glutaraldehyde (albumin from chicken egg white, grade II, Sigma-Aldrich) subsequently fixed in 4% PFA, and cryopro-

tected with 30% sucrose in 0.1 M PB at 4 °C. Cryostat sagittal spinal cord sections (40 μm) were cut from rostral, central or caudal blocks (each 0.5 cm thick) and collected in 24-well plates with 0.1 M PBS containing 0.1% sodium aside. For immunohistochemistry, free floating sections (40 μm) were immersed in PBS (0.1 M; pH 7.4) containing 10% normal goat serum (NGS), 0.2% Triton X-100 for 2 h at room temperature to block nonspecific protein activity. This was followed by overnight incubation at 4 °C with primary antibodies: rabbit anti-growth associated protein-GAP-43 (GAP-43; 1:500, Merck-Millipore), and mouse anti-synaptophysin (SYN; 1:500, Merck-Millipore) for 24 h. Afterward sections were washed in 0.1 M PBS and incubated with secondary fluorescent antibodies goat anti-mouse, goat anti-rabbit conjugated with Texas Red (Alexa Flour 594) and fluorescein isothiocyanate (FITC) (Alexa Flour 488) at room temperature for 2 h. For general nuclear staining 4–6-diaminidino-2-phenylindol (DAPI) (1:200) was added to the final secondary antibody solutions. Finally, sections were mounted and cover slipped with Vectashield mounting medium (Vector Laboratories).

Quantification Analysis—Immunohistochemically stained sections were analyzed using confocal microscope (Leica DM1500) and quantification was performed by ImageJ software. Five sections per animal were analyzed for each staining in rostral, lesion and caudal segments. For synaptophysin quantification analysis, images were first transformed into monochromatic 8-bit images and then threshold was adjusted to optimal value. Synaptophysin positivity was evaluated as a percentage of black pixels in overall image (value 0–255, where 0 = white pixels, 255 = black pixels). For axonal regrowth evaluation, GAP-43 positive fibers were measured manually in micrometers. Total length of axon fibers was averaged for each image.

RESULTS

We previously performed a spatio-temporal study of the SCI from 3 days to 10 days after lesion. Our data suggest that in acute SCI regionalization in terms of inflammatory and neurotrophic responses may occur because of alterations in protein dynamics between rostral and caudal segments (13). In addition, the proteomic profile in caudal segments was characterized by the neuronal expression of IgG2a and by a signature of axonal regrowth inhibition associating CSPG and proteins of the MEMO1-RHOA-DIAPH1 signaling pathway (14). The MEMO1-RHOA-DIAPH1 signaling pathway plays an important role in ERBB2-dependent stabilization of microtubules at the cell cortex and inhibits neurite outgrowth. In this context, we established an *in vitro* proteomic system biology platform in order to better understand the impact of RhoAi on DRG neurons in time course, followed by *in vivo* SCI experiments to further compare and validate the similarities and differences of treatment approaches.

In Vitro Neuroproteomic-systems Biology Platform Targeting RhoA Signaling—

Impact of RhoAi Treatment on Neurite Outgrowth—*In vitro*, RhoAi was added to ND7/23 DRGs cell line cultivated with spinal cord conditioned media (CM-SCI) collected from lesion (L), rostral (R1) and caudal (C1) segments (Fig. 1). Time course analysis showed that ND7/23 cells in presence of R1 or C1 conditioned media initiated neurite outgrowth at 24 h after cultivation and the results were statistically significant at 48h (Figs. 1A, 1B). Afterward, the ND7/23 cells were treated with 1 μg/ml of RhoAi in combination with 1/3 of CM and 2/3

DMEM supplemented medium 24 h after C1 or R1 stimulation to reproduce the injured environment. In this context, neurite outgrowth appeared at 48 h with longer extensions when compared with non-RhoAi treatment (Figs. 1A, 1B). These results established the ability to block the MEMO1-RHOA-DIAPH1 signaling pathway and stimulate neurogenesis using such RhoAi.

Impact of RhoAi Treatment on ND7/23 DRGs Proteome—In order to identify proteins involved with RhoAi the proteomic approach was then performed with ND7/23 DRGs cell lines incubated with CM-SCI collected from L, R1, and C1 segments in presence or absence of RhoA inhibitor, using identical scenario as in experiments for neurite outgrowth evaluation (Fig. 1C). Secretomes collected in each condition have been processed by shotgun analyses. Proteins with an abundance that was significantly different among the samples were determined according to the MaxQuant and Perseus software. As a criterion of significance, we applied an ANOVA significance threshold of $p < 0.05$, and heat maps were generated (Fig. 1C, supplemental Data S1). Heat maps were performed and hierarchical clustering indicated two main branches *i.e.* one for Control branch (CTB)(DMEM conditions with or without RhoAi) and the second one is related to Conditioned medium branch (CMB) (L, R1, or C1 conditions with or without RhoAi). This branch is then sub-divided into two sub-branches: lesion on one side and R1 or C1 on the other side (Fig. 1Ca). From these data, clear clusters could be retrieved between the two branches. By contrast, in the CMB, only one main cluster allowed to differentiate all media in presence or absence of Rhoi (a yellow boxed area). A zoom of this cluster is presented in Fig. 1Cb and the iBAQ quantitative values in Table I. Main proteins found in this cluster that could be sorted according to their over-expressed intensities are in the following order: immunoglobulins (IgG chains light and heavy), AKT proteins (AKT1, AKT2, and AKT3), BMP1, syntaxin 12, serpin 3, GMP ganglioside activator, meosin, hemopexin, protein VSP26b, 14-3-3 protein theta, and protein disulfide isomerase. The important finding is that the iBAQ value showed that most of these proteins are under-expressed under DMEM conditions whereas, in presence of CMB alone or with RhoAi, they are over expressed, with some exemptions (Table I). Immunoglobulins were overexpressed particularly in the samples associated with lesion, treated with CM from Lesion segment alone and with RhoAi and in CM from C1 alone. For AKT proteins family, real differences could be registered between AKT3, AKT1, and AKT2 in relation to CM from rostral and lesion segments. With RhoAi, the level of AKT3 was diminished when compared with untreated cells. For AKT1 and AKT2 proteins, RhoAi increased their level in R1 and diminished these in lesion and C1. Serpina3c, Snx12, Gm2a, meosin, Timm44, Cthrc1, Stx6, vsp26b, Ith1, Aqp4, aggrecan core protein, BMP1 were over-expressed in C1 in presence of RhoAi compared with R1 or lesion with or without treatment. In R1, with RhoA inhibitor, only AK1 and AKT2 were

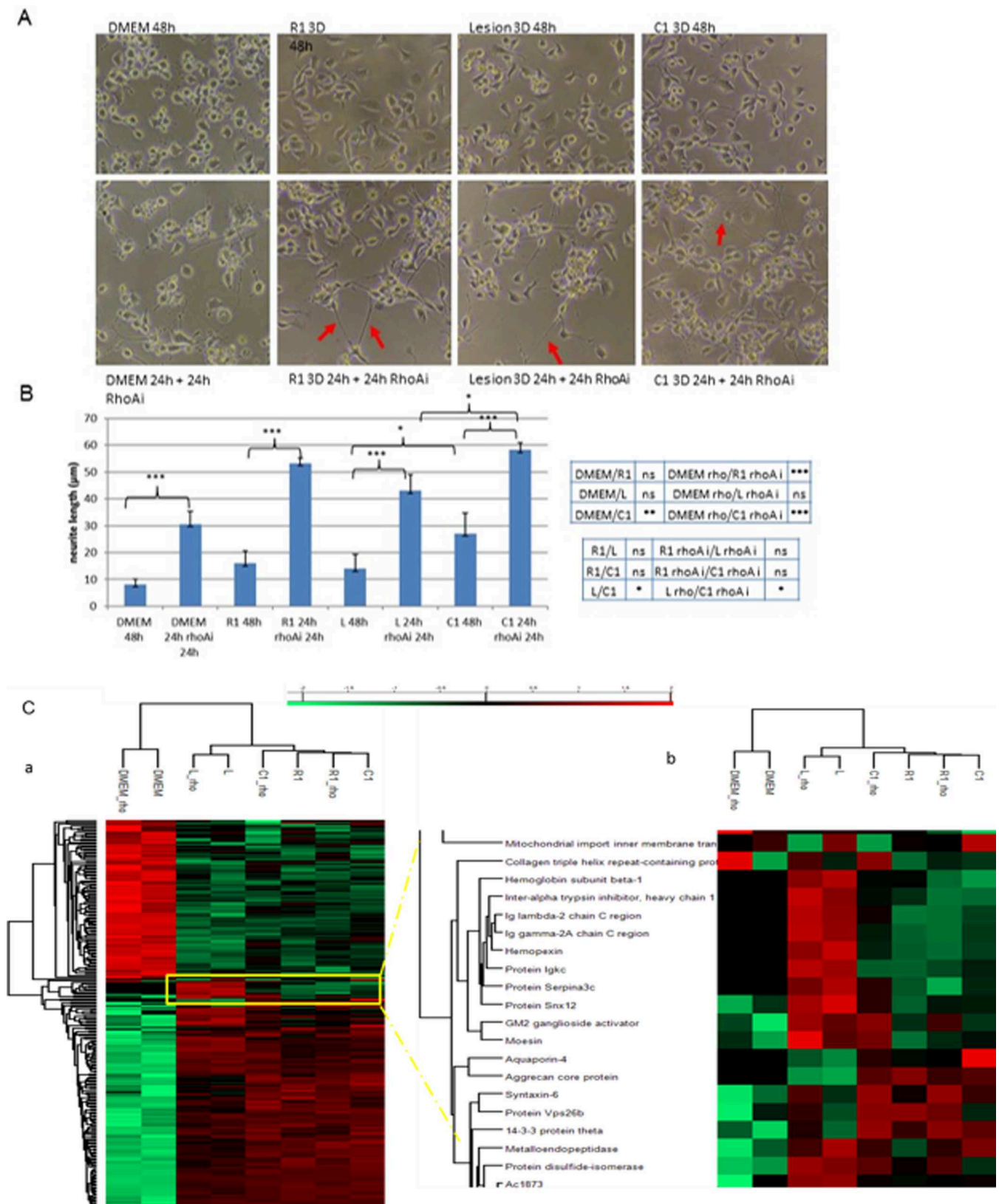


FIG. 1. The effect of the downstream Rho kinase inhibition on the neurite outgrowth *in vitro*. Representative Fields showing the ND7/23 DRGs cell line cultivated in presence of R1, L or C1 CM with or without RhoAi stimulation during after 24 h with CM and for a total stimulation of 48 h (A–B). The cultured cells in presence of R1, L or C1 CM at 3 days after SCI start to produce neurite outgrowth, with statistical

TABLE I

*i*BAQ value of the selected cluster reflecting the more divergent quantitative value of between treatment and conditioned medium from R1, lesion or C1 at 3 days after SCI

	DMEM	DMEM_rho	R1	R1_rho	L	L_rho	C1	C1_rho
Ig kappa chain C region, B allele	18.6	NaN	25.3	25.2	26.9	27.4	25.6	25.5
Ig lambda-2 chain C region	17.9	16.4	22.2	21.8	23.3	23.8	22.0	22.0
Ig gamma-1 chain C region	NaN	NaN	22.0	20.4	24.4	22.8	22.7	20.9
Ig gamma-2A chain C region	18.6	17.4	25.1	25.1	27.0	27.2	26.0	25.4
Ig gamma-2B chain C region	15.5	20.2	25.1	24.7	26.7	27.3	26.0	26.1
Ig gamma-2C chain C region	19.0	NaN	19.6	19.3	21.8	21.4	22.0	19.9
Hemopexin	17.5	17.6	24.9	24.9	26.5	26.3	25.2	25.2
Akt3	19.3	18.7	20.2	18.4	19.2	20.1	20.4	19.8
Akt1;Akt2	15	17.7	19.6	20.2	20.3	19.1	16.7	NaN
Serpina3c	NaN	NaN	21.9	21.0	24.1	23.3	22.4	22.6
Snx12	22.6	22.4	22.9	23.0	22.4	23.2	23.3	23.7
Gm2a	21.9	22.9	23.0	23.8	23.9	24.4	24.7	24.6
Moesin	26.5	26.6	25.8	26.4	26.2	26.9	26.9	27.2
Timm44	19.3	19.6	18.1	16.9	18.5	17.9	18.7	18.2
Cthrc1	22.9	24.5	22.9	24.0	23.7	23.8	24.2	24.6
Hemoglobin subunit beta-1	21.1	21.3	25.3	25.0	28.4	28.4	25.1	26.6
Itih1	16.9	17.7	19.2	19.0	22.3	21.4	19.9	19.4
Aqp4	NaN	NaN	24.4	24.7	23.8	23.8	25.5	25.3
Aggrecan core protein	17.4	NaN	20.3	20.1	19.2	17.8	20.9	19.9
Stx6	20.5	21.3	21.2	20.7	20.4	21.9	21.3	22.1
Vps26b	20.8	21.2	22.5	21.4	20.7	21.0	21.4	21.5
14-3-3 protein theta	27.1	27.5	27.8	27.8	27	27.6	27.9	28.2
Metalloendopeptidase, BMP1	19.3	18.9	19.4	19.8	21.1	19.5	19.8	20.4
Protein disulfide-isomerase	23.9	23.5	24.2	24.6	24.2	25.1	24.5	24.6

NaN: NonAssigned Number.

overexpressed, by contrast Timm44, STX6, Cthrc1, AKT3, STX6 were under-expressed. In lesion, most of proteins present in this cluster were under-expressed or had the same level with RhoAi treatment except of Gm2a, hemopexin, Protein disulfide-isomerase, Stx6 that are over-expressed.

Proteomic Analyses of RhoAi Effect on ND7/23 DRGs Cell Line—Global analysis was then performed by regrouping all conditioned medium treatment with RhoAi samples compared with nontreated (NT) samples with RhoA and compared with control *i.e.* DRG cells cultivated with only DMEM with or without RhoAi. We have identified 3133 proteins (Fig. 2A) that clustered (Fig. 2B). In this context, two branches separated the secreted factors. The first branch separates the factors detected in control (culture medium with DMEM) from the ones cultivated with SCI CM. The second branches separated the ones treated with or without RhoAi (Fig. 2B). Of the 5 differentiated clusters that were identified (See yellow boxes), 2 contained over-expressed proteins (clusters 1,2) and 3 under-expressed proteins (clusters 3,4,5) (Fig. 2B). These clusters have been regrouped (Table II) and functional pathways

extracted from Subnetwork Enrichment Analysis (SEA) was generated (Fig. 2C). Although 16 secreted proteins from ND7/23 DRGs cell line were overexpressed after RhoAi treatment, 23 were under-expressed (Table II, supplemental Data S2). Among the 16 overexpressed proteins, some were already known to be implicated in neurites outgrowth or neurogenesis *e.g.* Pde6d (29), Ltbp4 (30), Clip2 (31), Enah (32), Vps26b (33), Sema7a (34), BDNF/NT3 (35), UNC5C (36), Ephrin A5 and Ephrin B receptor (34), VEGF (37). Pathway analyses reflected that nucleic proteins involved in cell cycle regulation, transcription activation, and cell survival were under-expressed in cells treated with RhoAi. On the other hand, proteins involved in stem cell proliferation, neuronal migration, axon guidance, neurotransmission, synaptic transmission, and nerve development were over-expressed (Fig. 2C). These results confirm that despite the presence of an inflammatory medium containing neurites outgrowth inhibitors, RhoAi still positively impacts the functional behavior of DRG cells and stimulates the neurite outgrowth process. On this basis, a time course proteomic study was undertaken in order to

significance at 48 h (A). Arrows indicate the neurite outgrowth (A). Control was done in DMEM media without serum, to be in the same media than CM after SCI. Enhanced outgrowth referred to dense network of elongated processes interconnecting cells was documented in treatment group. Quantification of neurite outgrowth by ImageJ demonstrates the effect of RhoAi on neurite outgrowth (B) (One Way ANOVA followed by Tukey-Kramer test **p* < 0.05, ***p* < 0.01, ****p* < 0.001, ns = nonsignificant). C, Heat map of proteins from the secretome after different stimulation of ND7/23 DRG cell line. Control (DMEM) or lesion (L), rostral (R1) or caudal (C1) conditioned media from spinal cord 3 days after injury were used to stimulate the cells with or without stimulation of RhoA inhibitor 24 h after CM stimulation (a). Zoom of the cluster showing a difference between SCI-CM media stimulation with lesion CM and proteins name expressed in this cluster (b).

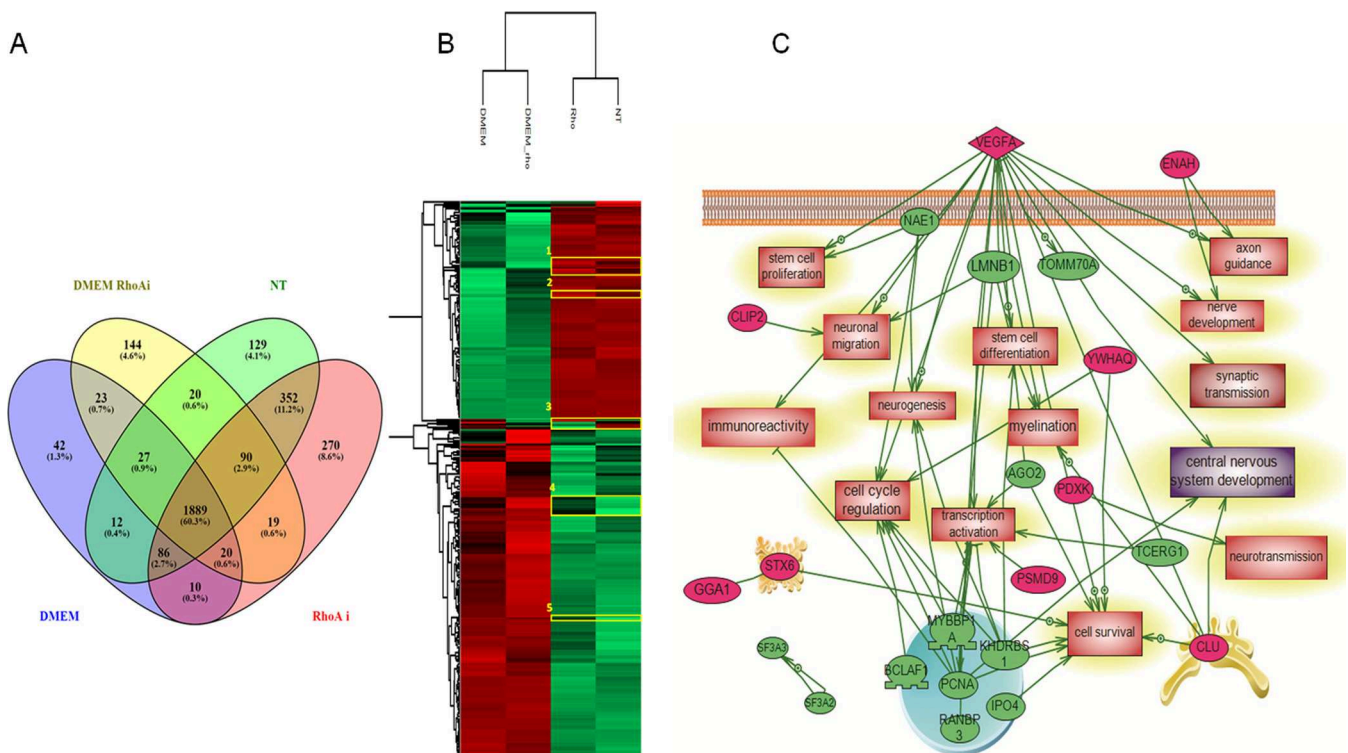


FIG. 2. A, Venn diagram of identified secreted proteins from ND7/23 DRG cell line with DMEM (control) or with pool of SCI secreted factors (Lesion, Rostral, Caudal) after RhoAi treatment or not (NT). B, Heat map of proteins from the secretome after treatment with RhoA inhibitor (Rho) or not (Not treated, NT) of ND7/23 DRG cell line with DMEM (control) or with SCI secreted factors (Lesion, Rostral, Caudal). C, System biology analysis for network identification in the proteins over and under expressed in the 5 selected clusters issued from heat map of proteins with different secretion profiles of ND7/23 DRG cell line incubated with DMEM (control) or with pool of SCI secreted factors (Lesion, Rostral, Caudal) after RhoA inhibitor treatment.

further identify the molecular and functional targets of RhoAi in DRG cells in presence of C1, R1, or lesion secreted factors.

Cellular Proteomic Investigation of RhoAi Treatment of ND7/23 DRG Cell Line Cultivated With Conditioned Media from Spinal Cord Injury Segments—The proteomic analyses performed 24 h after treatment, allowed to identify 4030 proteins from which 179 modulated proteins were found between nontreated and treated cells (supplemental Data S2, supplemental Data S3A). From these 179 proteins, numerous factors were identified that could regulate the intrinsic growth capacity, including certain transcription factors (TF), such as cAMP-responsive element binding protein (CREB), signal transducer and activator of transcription 3 (STAT3), nuclear factor of activated T cell (NFAT), c-Jun activating transcription factor 3 (AFT3) and Krüppel-like factors (KLFs), and intracellular signaling proteins, such as PI3 kinase, Akt, phosphatase and tensin homolog (PTEN), suppressor of cytokine signaling 3 (SOCS3), B-RAF, dual leucine zipper kinase (DLK), and insulin/insulin-like growth factor-1 (IGF-1) signaling have been detected (38, 39). The Ibaq value confirmed the over-expression of Tp53, Stat2, Stat3, Proteins of the Smad family (smad1, smad2, smad3, smad4, and smad5), Smarcc1 (Baf155), and Smarcc2 (Baf170), Akt3, rpap3, b-raf, and

PTEN (Table III). The string protein analysis confirms that all these proteins can be gathered in the same network (supplemental Data S3B). Nevertheless, one most intriguing is the presence of PTEN. Subnetwork global Analysis was generated between RhoAi treated DRG cells incubated with conditioned medium of R1, Lesion or C1 (Fig. 3). 24 h after treatment, complete disparities are observed between the 3 conditioned media after treatment. Only C1 medium clearly showed over-expressed proteins involved in neurite outgrowth, neuronal migration, and neurogenesis (Fig. 3A). Whereas with R1 medium, proteins detected are involved in neurite outgrowth, neuronal cell death, inflammation and cell proliferation and differentiation (Fig. 3B). The proteomic profile of DRG cells stimulated with lesion medium showed a unique enrichment in molecules involved in apoptosis and necrosis, inflammation, T cell response and, as well as neutrophils chemotaxis (Fig. 3C). Subnetwork Enrichment Analysis (supplemental Data S3) confirmed the presence of specific complementary proteins involved in dendrite morphogenesis such as CAMK1, SIPA1L1 and L1CAM (supplemental Data S3Ca). Proteins involved in cell death and proteins degradation such as TSC1, WDFY3 and OGT were found to be specific to lesion treatment (supplemental Data S3Cb). Proteins involved in neurite outgrowth and neuronal migration such as

TABLE II

*i*BAQ values of the selected cluster reflecting the modulated expressed proteins in conditioned media treated or not with RhoA inhibitor. NT regroups all nontreated cells and RhoAi are all treated cells with RhoA inhibitor

Gene name	Protein name	DMEM	DMEM RhoAi	NT	RhoAi
Ctlb	Clathrin light chain B	22.9108	20.9079	24.6101	24.5589
Psmid9	26S proteasome non-ATPase regulatory subunit 9	22.0575	22.5024	23.731	23.3539
Ltbp4	Protein Ltbp4	20.7261	21.3022	21.4152	21.2313
Vegfa	Vascular endothelial growth factor A	22.2847	21.7441	22.6636	22.6461
Ctsz	Cathepsin Z	22.2676	22.4209	23.5532	23.7262
Pde6d	Phosphodiesterase 6D, cGMP-specific, rod, delta	22.9597	22.3894	23.2059	23.9704
Stx6	Syntaxin-6	20.5775	21.3753	21.159	21.6134
Clip2	CAP-Gly domain-containing linker protein 2	18.8133	19.9872	20.7688	20.9273
Ywhaq	14-3-3 protein theta	27.1402	27.5267	27.636	27.8027
Gga1	Golgi associated, gamma adaptin ear containing, ARF binding protein 1	21.1791	21.474	21.5419	21.8458
Gm2a	GM2 ganglioside activator	21.9105	22.9234	23.9187	24.059
Clu	Clusterin	21.5919	21.6096	24.059	24.173
Fkbp2	Peptidyl-prolyl cis-trans isomerase	24.2425	25.0884	25.3438	25.2155
Pdxk	Pyridoxal kinase	21.3779	23.0917	23.8266	24.1404
Enah	Protein Enah	21.4766	22.2339	21.0658	22.1981
Vps26b	Protein Vps26b	20.8545	21.2238	21.3013	21.4243
Phax	Phosphorylated adapter RNA export protein	20.6057	21.5545	20.0058	19.9327
C1orf123	UPF0587 protein C1orf123 homolog	19.8283	21.1305	23.2625	22.6816
Ddt	D-dopachrome decarboxylase	16.4287	NaN	23.5922	22.1647
Minpp1	Multiple inositol polyphosphate phosphatase 1	20.7669	21.2727	20.8248	20.6688
Sar1b	GTP-binding protein SAR1b	21.694	21.3152	22.3763	21.0747
Timm44	Mitochondrial import inner membrane translocase subunit TIM44	19.3845	19.6954	18.3148	17.6879
Mvd	Diphosphomevalonate decarboxylase	21.7602	22.097	21.6105	20.9859
Ranbp3	Protein Ranbp3	21.6703	21.842	20.7514	20.5318
Ipo4	Importin 4	21.2689	22.5999	20.5059	21.1659
Gtpbp4	Nucleolar GTP-binding protein 1	20.5677	21.7242	19.3613	19.1347
Fnta	Farnesyltransferase, CAAX box, alpha	20.1966	21.4274	19.902	19.6791
Cul2	Protein Cul2	22.5187	22.6432	21.8199	21.1874
Nae1	NEDD8-activating enzyme E1 regulatory subunit	21.1429	22.6173	21.6993	21.0846
Eif1a	Eukaryotic translation initiation factor 1A	24.6291	24.4566	23.3243	23.0823
Aimp2	Aminoacyl tRNA synthase complex-interacting multifunctional protein 2	24.6959	24.8529	24.2577	24.0347
Cstf2	Protein Cstf2	19.0881	19.8525	17.8731	18.7524
Mybbp1a	Myb-binding protein 1A	20.4748	20.2285	20.4614	19.8938
Psmid1	26S proteasome non-ATPase regulatory subunit 1	24.2726	24.1721	23.5677	23.3707
Sf3a2	Splicing factor 3A subunit 2	24.508	24.8563	22.9886	22.9425
Tomm70a	Mitochondrial import receptor subunit TOM70	21.4271	22.0365	20.8489	19.3298
Pcna	Proliferating cell nuclear antigen	25.5532	26.1335	24.8067	25.222
Arpc3	Actin-related protein 2/3 complex subunit 3	24.4744	24.7873	24.3182	24.6005
Ago2	Protein argonaute-2	19.1549	20.7609	18.8243	18.982
Lmnb1	Lamin-B1	25.0612	25.1812	24.723	24.7027
Rps16	40S ribosomal protein S16	27.2324	27.7085	26.8235	26.6169
Khdrbs1	KH domain-containing, RNA-binding, signal transduction-associated protein 1	25.7151	25.6983	25.0325	25.056
Bclaf1	BCL2-associated transcription factor 1, isoform CRA_a	24.1191	24.2525	22.9701	23.1659
Rps19l1	Protein Rps19l1	27.747	27.8637	26.4202	26.8181
Snrpd3	Protein Snrpd3	25.7155	26.0016	25.3816	26.0275
Slc39a10	Protein Slc39a10	20.4879	21.6648	19.3242	19.6973
Tcerg1	Protein Tcerg1	22.7216	22.8235	22.1174	22.4468
Sf3a3	Protein Sf3a3	24.4827	24.3498	23.7063	23.5636

NaN: NonAssigned Number.

FARP1, srGAP2, RAB6B, MAP3K4, and STK25 are specific to C1 treatment (supplemental Data S3Cc).

Proteomic Investigation of the Time Course of RhoAi Treatment on ND7/23 DRGs Cells Line—To investigate the time

course of molecular events induced by RhoA inhibitor on ND27/23 DRG cell line, we performed a kinetic proteomic study on cell extracts obtained at 30 min, 1h or 4 h post-treatment (supplemental Data S4). 2389 proteins were overall

TABLE III

*i*BAQ values of transcription factors present in protein extract between treated and not treated cells in presence of not the SCI-CM

	DMEM	DMEM RhoAi	NT	RhoAi
Tp53	23.5	23.6	23.6	25.2
Stat3	18.6	19.4	21.8	21.9
Stat2	17.8	19.0	21.0	21.1
Smad5;Smad1	17.7	19.2	17.8	18.9
Smad2;Smad3	20.3	23.2	21.0	24.0
Smad4	17.2	19.8	20.3	17.6
Smarcc1	21.8	23.0	22.0	22.8
Smarcc2	19.6	22.5	17.6	21.0
Akt3	14.9	19	16.8	22.1
Rpap3	20.6	21.7	20.5	21.0
B-raf	0.0	0.0	20.6	20.8
Pten	18.4	15.7	19.5	20.9

identified (supplemental Data S4A and S5) Global networks were generated from specific proteins identified in each conditions (supplemental Data S4). Compared with T0 where it can be observed that proteins are integrated in 4 overexpressed clusters (mRNA degradation, mitotic spindle checkpoint, ER to Golgi transport and vesicular trafficking) (data not shown), at 30 min after treatment, several specific cellular events occurred including chromatin condensation, cellular stress response, anchorage independent growth and malignant transformation (supplemental Data S4Ba). At 1 h, all intracellular signaling converged to NFkB (supplemental Data S4Bb) and at 4 h, secretory pathways, cell invasion and mitochondrial respiration were the major pathways activated by RhoA inhibitor treatment in DRG cells (supplemental Data S4Bc) Specific enrichments were performed from the comparisons of each time points after treatment. From T0 to T1 h, most induced proteins were involved in nucleocytoplasmic transport (Fig. 4), from T0 to T4 h, a majority of the differentially expressed proteins were implicated in ER-associated protein catabolism (Fig. 4), from T0 to T30 min and to T4 h, two clusters of proteins were detected, namely nonselective vesicle building and cell spreading (data not shown). From T1 h to T4 h, chaperones proteins are identified (Fig. 4). Finally, transition from T0, T30 min, and T1 h to T4 h involved several clusters linked to oxidative stress, cell proliferation, differentiation and migration (data not shown) and in particular some TF are observed at specific time points after treatment (Table IV). In particular, BAF155 and BAF170 were present from time T0 to T24 h, whereas Smad2 was detected from T0 to T1h, and then at T24 h. AKT3 protein only showed at 1h with no detection before and after this time point. All the other TFs were detected only after 24 h of treatment (Table IV).

Investigate RhoA inhibitor in Vivo—According to the time course experiments results (Fig. 4) and the fact that at 24 h exposure to RhoA inhibitor all transcription processes in DRG cells are impacted, we decided to investigate the treatment 12 h after SCI. Proteomic studies were realized from tissues in

the 3 segments at both side of the lesion and also in secretome (Fig. 5).

Tissue extracted proteins collected in each condition have been processed by shotgun analyses. Heat maps of proteins with an ANOVA significance threshold of $p < 0.05$, were generated (Fig. 5A, supplemental Data S6). Heat maps were performed and hierarchical clustering indicated two main branches *i.e.* one for SCI and the second one is related to treated animal with RhoA Inhibitor and control (without lesion). This branch is then subdivided between RhoA inhibitor treatment in function of the considered segment (Rostral, Lesion and Caudal) on one side and control in the other side (Fig. 5A). From these data, clear clusters could be retrieved between the two branches. Clusters 1 and 2 are specifically found in Rostral and Caudal segments after SCI. Cluster 1 integrates many subexpressed proteins in SCI segments (Fig. 5A, supplemental Data S6). By contrast, cluster 2 constitutes the one of overexpressed proteins in SCI. Such proteins are in control and treated animals sub-expressed in caudal and lesion segments. A slight overexpression is registered in rostral segments (control and treated animals). No inflammatory proteins were detected in cluster 2 whereas proteins involved in neurites outgrowth are present (*e.g.* CD166, advinin, neuritin, Neurocan, L1Cam, Vcan, Limbic system-associated membrane protein, neuronal growth regulator 1 precursor, C1qBp, SLIT-ROBO Rho GTPase-activating protein 2, Roundabout homolog 1, Ciliary neurotrophic factor) (Table V). In RhoA inhibitor treatment, these neurite outgrowth factors expression is less important in both tissue (Table V) but also in secretome (Table VI). However, proteins involved in synaptogenesis, their level of expression is increased after RhoA inhibitor treatment. The LFQ of synapsins, synthaxins, GAP43, Synaptojanin-1 is higher in lesions segment in treated animals compared with the only injured ones (Tables V and VI).

Interestingly, it must be noticed that Rock1 and RhoA are overexpressed in SCI and inhibited in RhoA inhibitory treated samples, confirming the efficiency of the treatment. Immune components are only detected in cluster 4. These are overexpressed in lesion after SCI, sub expressed in control and modulated in RhoA inhibitor treated animals (Fig. 5A, supplemental Data S6, Table V). Among the identified inflammatory proteins like complement proteins family (C3, C4a, C9), C-reactive protein, Alpha-1-macroglobulin, Alpha-2-macroglobulin, Plasminogen Plasmin heavy chain A Activation peptide are detected in segments after SCI with a higher ratio in Lesion compared with rostral and caudal segments (Table V, supplemental Data S6) which is in line with the data obtained in collected secretome (Fig. 5B, Table VI, supplemental Data S7). RhoA inhibitor treatment increased the level of IgG2b and IgG2c in lesion and caudal segments. In summary, RhoA inhibitor did not diminished the level of the antibodies in segments but their sub classes. The proportion of IgG2 (a,b,c) compared with IgG1 is higher in treated animals. Moreover, concerning the global impact of the RhoA inhibitor treatment

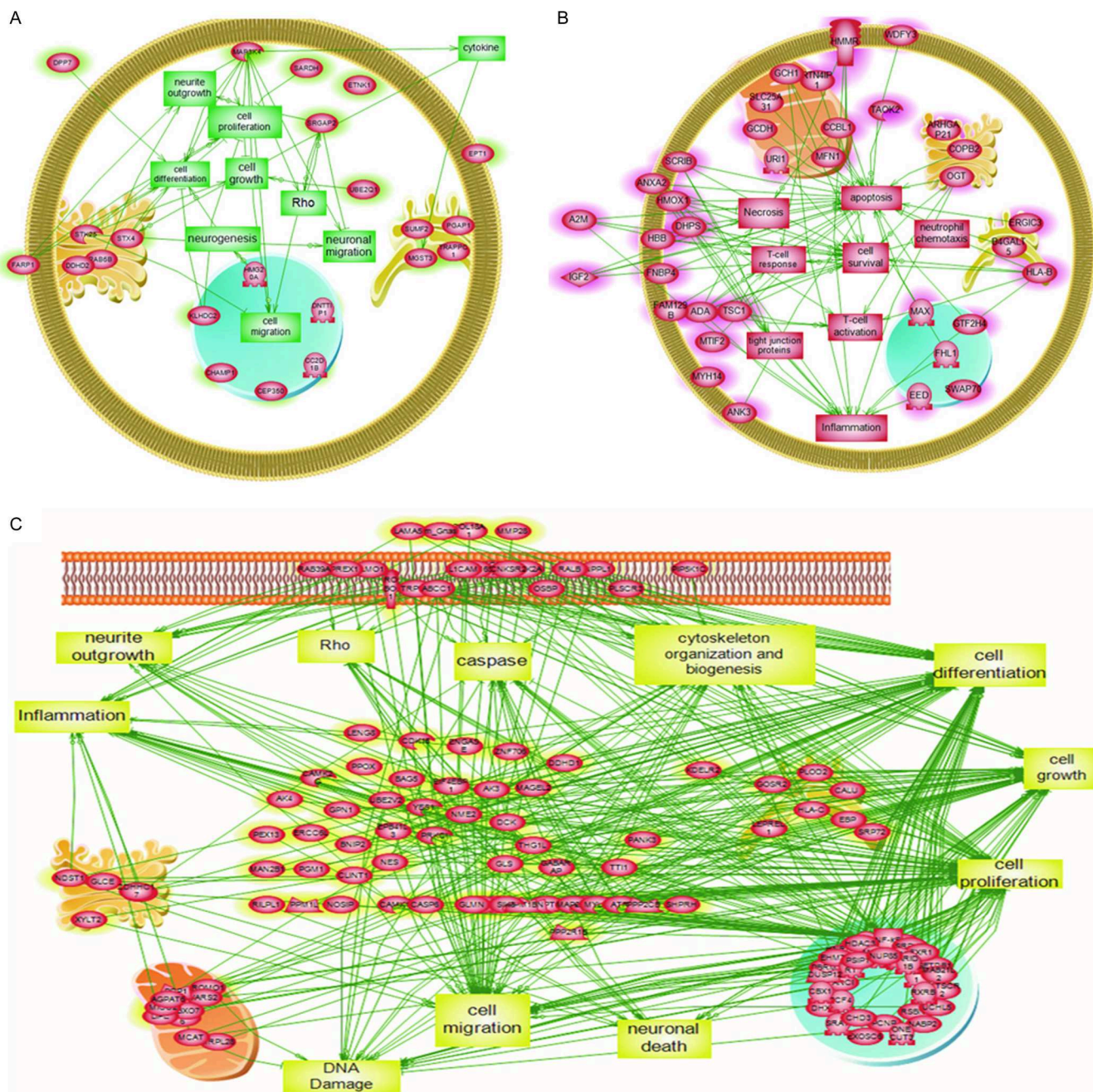


FIG. 3. System biology analysis for network identification in the proteins overexpressed in extract of treated ND7/23 DRG cell line incubated with of SCI secreted factors (A) Caudal, (B) Rostral, (C) Lesion.

12 h after SCI on the proteome pattern in both sides of lesion segment (Tables V and VI). It is clearly that the treatment turned the proteome of the lesion and the caudal segments close to the one found in control, except for the rostral which is more divergent (Fig. 5A). Moreover, what was the most surprising is the low level of proteins involved in inflammation in tissue and in secretome (Tables V and VI). More proteins which are involved in neurite outgrowth, neurogenesis and synaptogenesis are identified in SCI compared with ones identified with RhoA inhibitor treatment (Tables V

and VI). It seems that factors produced by the cells in tissue promote neurogenesis itself and RhoA will modify such process.

To confirm the proteomic data outlining the role of the RhoAi treatment at early stage of the lesion, we decided to design *in vivo* experiments consisting in the local intraspinal delivery of RhoAi and by an intraperitoneal injection of an immunosuppressant, calcineurin inhibitor (FK506) to diminish inflammation (14). Here were administered RhoAi in an alginate scaffold (with no growth factors) which biocompatibility

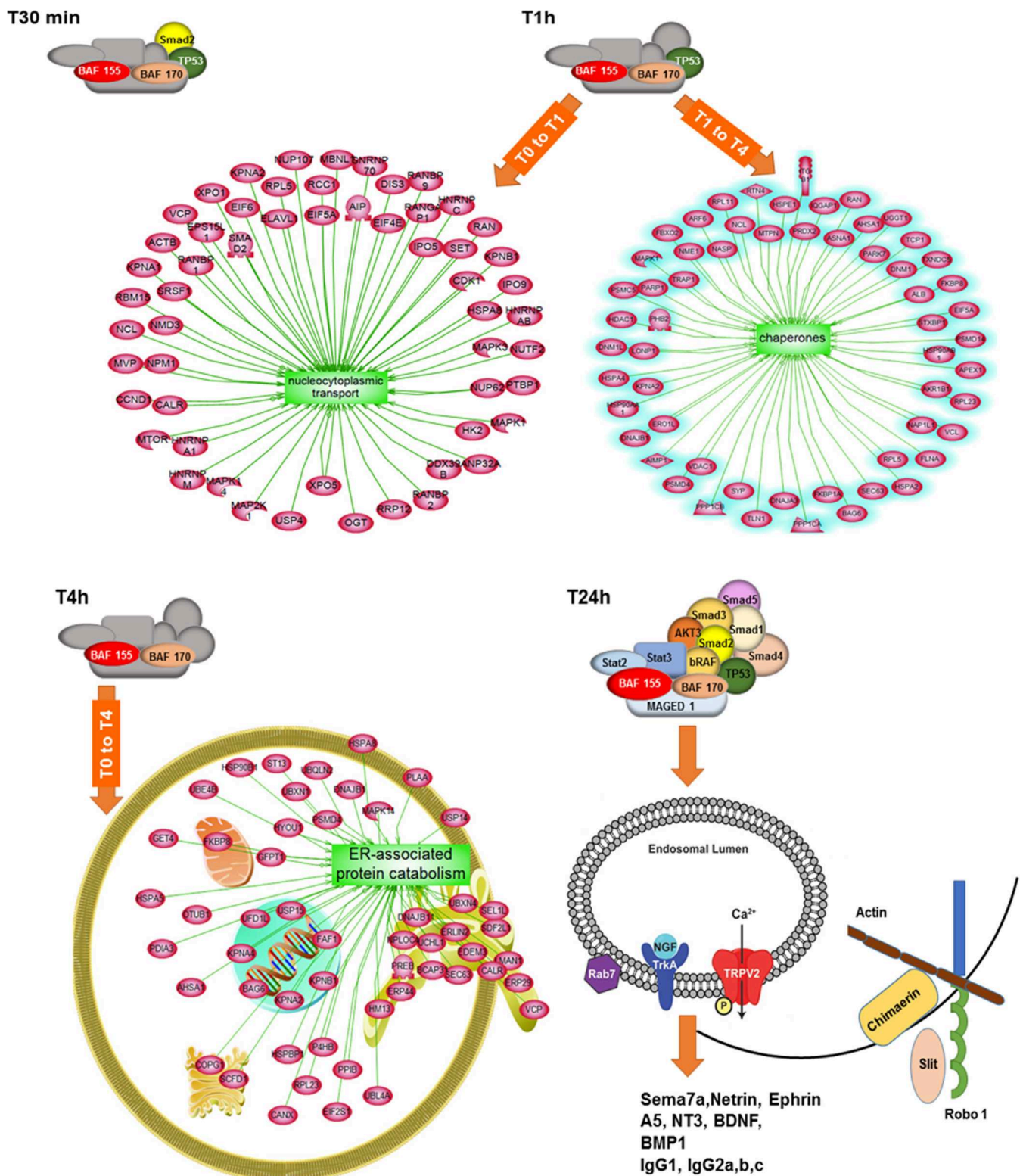


FIG. 4. Enrichment subnetwork associated to specific over-regulated proteins in time course of RhoA inhibitor treatment with emphases of transcription factors identified *i.e.* ND7/23 DRG cells line treated with or not RhoA inhibitor and proteins were extracted at different time (T30 min, T1 h, T4 h, T24 h) before analyzed by subnetwork enrichment analysis.

TABLE IV
LFQ values of transcription factors identified in DRG cell extracted in time course after RhoA inhibitor treatment

	T0	30min_RhoAi	1h_RhoAi	4h_RhoAi	24h_RhoAi
TP53	NaN	NaN	NaN	NaN	25.0195
stat1	NaN	NaN	NaN	NaN	23.0283
stat2	NaN	NaN	NaN	NaN	24.2915
smad1, smad5, smad9	NaN	NaN	NaN	NaN	19.3541
smad2	26.367	26.2884	25.7629	NaN	26.1066
BAF155	27.6803	27.7077	27.634	27.3488	27.7905
BAF170	25.9233	25.7679	26.8157	26.6822	26.5469
AKT3	NaN	NaN	22.8568	NaN	NaN

NaN: NonAssigned Number.

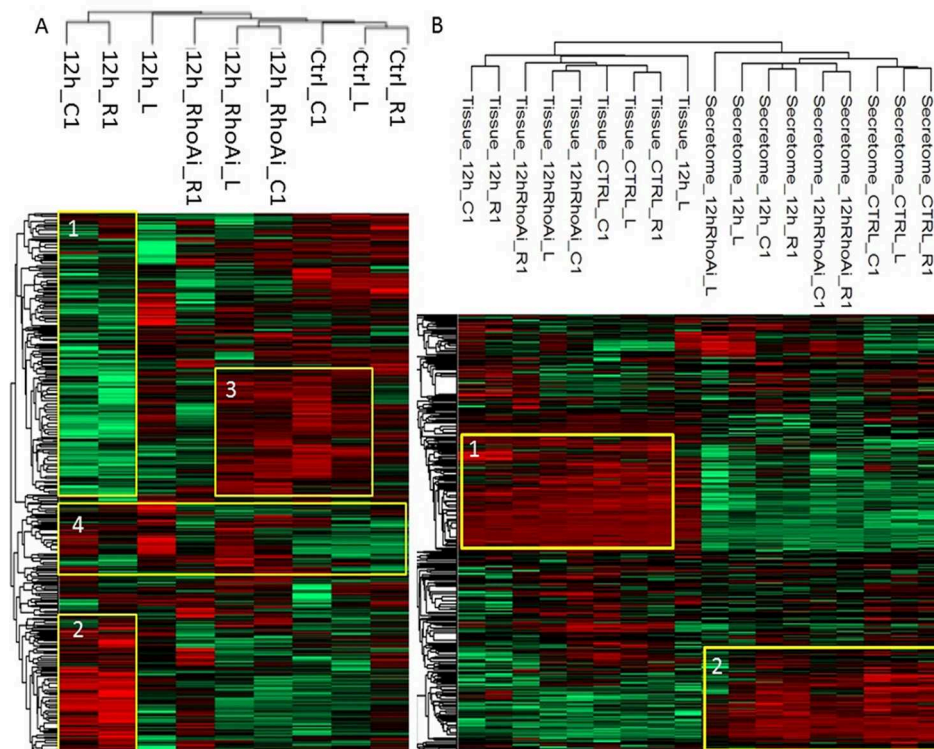


FIG. 5. **A**, Heat map of proteins from the extracted tissues segments (rostral, lesion, caudal) after 12h SCI, control or SCI + RhoA inhibitor treatment. **B**, Heat map of proteins from the secreted factors from segments (rostral, lesion, caudal) after 12h SCI, control or SCI + RhoA inhibitor treatment.

and its intrinsic beneficial impact on neurite outgrowth was previously showed (16).

Behavioral assessment by BBB open field scale showed that 7 days after treatment with RhoAi and FK506, the score significantly increased to score 5.0 when compared with SCI group (Fig. 6J). Nevertheless, the locomotor function remained unchanged during the entire survival and reached a plateau. In contrary, SCI group showed slow gradual improvement from beginning reaching score 5.0 with certain time delay at 30 days when compared with treated group, but still slightly improving with score around 6 at final 49 days. These data clearly demonstrated that compared with SCI without treatment, the beneficial effect of RhoAi was seen only at early time points of the treatment but not during later survival, even

in combination with alginate and anti-inflammatory compound. On the other hand the immunohistochemical analyses of spinal cord tissue showed that RhoAi + FK506 treated group exhibited significantly higher density of synaptophysin (SYN)+vesicles at lesion site (Figs. 6A) in comparison to SCI group (Figs. 6A, 6C) but no apparent differences between rostral and caudal segments were detected (Figs. 6E). Similarly, quantification of GAP-43 immunoreactivity outlining re-growth axons within damaged dorsal and lateral white matter tracts did not show significant differences between SCI and SCI RhoAi + FK506 treated groups (Fig. 6I). Dense network of GAP-43 immunoreactive axons of different thickness oriented in various directions were present in both rostral and caudal segments as well as at the lesion epicenter in both experi-

TABLE V

LFQ values of extracted proteins from Rostral, Lesion and Caudal spinal cord tissue segments after SCi treated or not with RhoAi inhibitor. Ctrl are control (non injured spinal cord), R: Rostral, L: Lesion, C: caudal

	CTRL_R:	CTRL_L:	CTRL_C:	12h_R1:	12h_L:	12h_C1:	12hRhoAi:	12hRhoAi:	12hRhoAi_C:
Immune response									
C1qbp	28.7281	28.9566	28.492	30.3982	28.5262	30.5145	29.2501	29.1898	28.682
Complement C3	29.886	29.6559	29.9432	31.0477	34.1094	32.3526	31.1368	33.1222	31.7935
Complement C4	24.1624	25.5162	25.4897	26.4889	30.5689	28.4565	25.685	29.19	27.2686
Complement C1q subcomponent subunit B	0	0	0	0	0	0	26.0273	0	0
Complement C1q subcomponent subunit C	0	24.3657	0	0	0	0	0	0	0
Complement component C8 beta chain	0	0	0	0	27.0921	0	0	25.5121	24.1331
Complement component C9	20.6843	21.907	21.584	23.2098	29.1238	26.3681	27.3374	27.7471	25.9411
Complement component receptor 1-like protein	25.9538	25.7398	25.7819	26.1517	26.6249	25.6688	25.9764	26.0176	26.0884
Plasma protease C1 inhibitor	21.9091	21.6787	0	24.0432	25.6243	23.9382	22.9491	24.5487	24.0977
Complement component C6	0	0	0	26.6044	0	0	0	0	0
Complement factor I	0	21.8155	0	21.9156	24.2797	23.1515	0	23.6044	22.6531
CD59 glycoprotein	29.3553	28.7384	28.5483	30.045	0	29.8041	29.431	28.3659	28.5551
Calreticulin	30.3539	30.4037	30.1042	31.5178	30.0788	31.0377	30.1996	30.5428	30.2458
C-reactive protein	26.9635	27.0947	26.4773	27.9756	31.1635	30.0916	28.2168	29.7884	28.6591
Granulin	0	0	0	0	0	0	24.682	0	0
Cathepsin D	29.7399	29.7065	29.9347	29.7652	29.9342	29.177	29.6499	29.8039	29.734
Cathepsin B	26.4879	26.2006	26.1943	26.7471	27.1834	27.2444	26.627	26.6212	26.3421
Metalloproteinase inhibitor 1	24.4787	0	0	0	23.7008	24.4859	0	23.6957	0
Coronin-1B	27.8259	27.9756	27.7563	27.5874	27.5131	27.5089	27.5923	27.9777	27.9927
Macrophages									
Macrophage migration inhibitory factor	29.1689	28.7423	29.053	31.0293	29.9068	30.4098	29.0155	29.2374	28.5224
CD44 antigen	28.3697	27.4084	26.6637	29.0996	28.3202	28.2835	28.8144	27.7426	27.4679
40S ribosomal protein S19	26.2744	26.1574	26.4055	26.099	26.2149	26.444	26.6833	26.1101	26.369
Monocyte differentiation antigen CD14	0	0	0	24.3638	0	24.4814	0	24.5376	23.7652
Galectin-3	27.4	26.8846	26.9943	27.267	26.6923	27.0701	28.1228	27.082	27.637
Lymphocytes									
OX-2 membrane glycoprotein CD200	27.1098	26.8565	27.3148	27.9532	27.721	26.8187	27.1825	26.8036	27.2357
Interleukin-6	0	0	0	0	0	0	0	24.5464	0
Galectin-9	0	0	0	0	0	0	0	24.8124	0
Galectin-1	28.0673	28.1859	27.8461	29.5435	28.2439	29.1543	28.9204	28.6793	28.2582
Axone guidance and neuroprojection									
Neuronal cell adhesion molecule	28.3747	28.2927	27.7871	29.35	27.4188	29.064	28.4497	27.7616	28.2066
Neural cell adhesion molecule 1	32.4232	32.194	30.2964	32.9503	31.7339	32.5599	32.5278	31.6936	32.1682
Contactin-1	32.2173	31.9221	31.8193	31.9986	31.6651	31.7923	32.2479	31.626	31.857
Contactin-2	28.9387	28.8157	28.8216	28.8182	28.7005	29.1454	28.9924	28.6006	28.7917
Contactin-6	23.2088	0	0	0	0	0	0	0	0
Ciliary neurotrophic factor	25.9902	25.5696	0	25.8031	26.6816	25.2438	26.3952	25.8348	0
Ciliary neurotrophic factor receptor subunit alpha	26.2012	25.6966	24.6474	26.0656	0	26.1004	26.176	25.0767	25.3544
Microtubule-associated protein tau	26.573	27.1903	26.4541	28.1576	24.4961	27.5894	26.7015	26.0034	25.9388
Serine/threonine-protein kinase PAK 1	28.8507	28.6902	28.3637	29.0165	28.8644	28.8778	28.6802	28.4948	28.3956
Serine/threonine-protein kinase PAK 2	28.9398	28.9734	28.773	28.6315	29.173	28.6132	29.0577	28.8708	28.7119
Serine/threonine-protein kinase PAK 3	26.4831	26.3709	25.8599	26.0144	25.602	26.4497	26.1559	25.7755	25.9308
Ras-related C3 botulinum toxin substrate 1	30.5455	30.4461	30.394	29.8527	29.6301	30.1777	30.0043	30.1716	30.4824
Stathmin	27.2512	27.2802	27.0872	28.2757	27.1847	28.1408	27.4795	26.6755	26.615
Dynactin subunit 1	29.2738	29.54	29.961	29.2582	29.8643	29.5239	29.1975	29.9102	29.9308
Dynactin subunit 2	29.7365	29.3865	28.9563	31.4829	28.5675	30.1708	30.012	28.8102	28.9053
Neurofilament light polypeptide	34.2938	34.1048	34.1248	35.5144	33.9815	34.9206	34.5556	34.2306	33.8022
Neurofascin	31.6569	31.5308	31.6061	31.6377	31.2274	31.7652	31.4217	31.2587	31.326
Neurotrimin	27.8574	27.7146	27.3797	28.9268	27.3013	28.87	28.0115	27.4806	27.5792
Synaptogenesis									
Amphiphysin	29.4976	29.241	28.7458	29.5412	28.4997	29.5075	29.6889	29.3147	28.9834
Neuromodulin (Gap43)	26.0049	26.2203	25.0803	27.8744	27.3324	28.5281	26.9088	26.9559	25.7284
Septin-2	30.7857	30.7968	30.7657	30.703	30.5815	30.3587	30.6164	30.5811	30.8189
Septin-7	31.2706	31.0765	31.1749	30.9634	30.9051	30.9054	30.8971	30.8622	31.1669
Septin-11	30.5869	30.3154	30.3478	30.4453	30.2735	30.2949	30.2648	30.2315	30.3821
Neuronal-specific septin-3	26.0469	26.1993	26.6058	26.5943	26.8693	26.1907	26.0773	26.1151	26.2937
Synaptosomal-associated protein 25	29.803	29.4783	29.7242	30.3553	29.8905	29.8291	30.2962	29.6259	29.3015
Clathrin coat assembly protein AP180	30.5941	30.1753	30.1606	30.0674	29.0666	29.8655	29.7581	29.7103	29.9472
Syntaxin-1A	26.0896	25.0462	25.5124	26.6115	25.8905	26.8451	26.1068	24.8309	24.7728
Syntaxin-1B	31.73	31.4813	31.7764	32.6772	31.5843	32.5454	31.8193	31.3674	31.4307

TABLE V—continued

	CTRL_R:	CTRL_L:	CTRL_C:	12h_R1:	12h_L:	12h_C1:	12hRhoAi:	12hRhoAi:	12hRhoAi_C:	
Syntaxin-4	26.2012	26.2102	25.9347	27.1188	0	26.4108	26.6618	25.714	25.6763	
Syntaxin-6	0	0	0	24.6624	0	24.8498	25.3597	23.9229	24.6809	
Syntaxin-7	25.8101	25.4393	25.34	26.2645	25.5659	26.0658	26.516	25.3204	25.2442	
Syntaxin-12	27.1608	26.8334	26.3655	28.1826	27.9286	27.7641	27.8767	27.3567	26.9969	
Transitional endoplasmic reticulum ATPase	32.37	32.3843	32.3696	32.4276	32.5097	32.4979	32.5959	32.3411	32.4893	
Synapsin-1	31.5567	31.6679	31.823	31.0818	30.3824	30.7278	30.8602	31.1259	31.3804	
Synapsin-2	31.0072	31.0899	31.3307	30.0422	30.2673	30.26	30.3979	30.7083	30.9847	
Synapsin-3	25.7542	25.908	26.0802	24.9825	0	25.3337	25.6177	25.2498	26.0414	
Synaptojanin-1	30.7919	30.7568	30.7616	30.3893	30.6522	30.4433	30.1267	30.3779	30.433	35_37
Neurochondrin	30.5182	30.6686	30.7907	30.1339	29.8085	30.722	30.303	30.4256	30.5542	
Pyridoxal phosphate phosphatase	27.9193	28.1961	28.1013	27.8666	28.3912	28.1327	27.3449	27.7145	28.0545	32_35
Neurite inhibitor										
Reticulon-3 NSPL2	31.1689	30.8046	30.9321	30.9646	31.4276	30.5861	31.1854	30.5309	30.9663	29_32
Reticulon-4 NOGO	30.6277	30.4752	29.8974	30.0109	29.6917	29.3222	31.3016	30.4981	30.463	
Reticulon-1 NSP	29.2289	28.8309	28.3363	28.4483	28.4548	27.7247	29.516	28.8732	28.2107	26–29
Neurocan core protein;150 kDa adult core glycoprotein	27.6527	27.7243	27.8845	27.8121	25.7571	28.4479	27.8713	28.2034	27.9606	
Transforming protein RhoA	30.1643	30.1233	29.8269	30.9399	30.204	31.2588	30.7987	29.6035	29.9969	23–26
Motoneuron degeneration										
Superoxide dismutase [Cu-Zn]	29.5928	29.4838	28.7923	30.4429	29.6148	30.8709	29.1448	29.1306	28.2098	20–23
Superoxide dismutase [Mn], mitochondrial	30.7542	30.8809	30.5194	30.6183	30.1651	30.2116	30.5079	30.6009	30.3795	
Vesicle-associated membrane protein-associated protein	28.3033	27.8166	27.2693	27.8553	27.9969	28.3629	29.5427	27.8769	28.2573	0
Vesicle-associated membrane protein-associated protein	28.4227	28.7318	28.0221	28.5148	28.8434	28.5188	29.6487	28.632	28.6503	

mental groups (Fig. 6f). Furthermore, the sections taken from control-naive rats revealed no GAP-43 immunoreactivity, nor in the gray or white matter regions (data not shown), confirming that GAP-43 positivity strictly correlates with axonal outgrowth after SCI (Fig. 6Ha, b). These data show that single intraspinal delivery of RhoAi in combination with FK506 promote neurite outgrowth and synaptogenesis in distinct segments, but without the ultimate clinical improvement of locomotion.

DISCUSSION

We previously demonstrated the benefic impact on neurite outgrowth *in vivo* after delivery of functionalized alginate scaffold loaded with Epidermal Growth factor (EGF) and basic Fibroblast Growth Factor (bFGF) (16). Significant enhancement of spinal cord tissue sparing and an increased number of choline acetyltransferase motoneurons and sensory fibers were registered. We also document the enhancement of axonal outgrowth in corticospinal tracts and an increased density of blood vessels in central lesion. However, although a switch of microglia functional behavior was observed, this therapeutic strategy did not appear to impact astrocytes functions (16). In our recently published spatio-temporal study of acute SCI (13), we demonstrated that in terms of inflammatory and neurotrophic responses, the rostral segments could be clearly distinguished from caudal ones, which indicated a regionalization effect. Among the factors detected in caudal segments, CSPG, neuronal IgG2a were identified along with the MEMO1-RHOA-DIAPH1 signaling pathway (14) which is known to inhibit neurite outgrowth.

In vitro and *in vivo* studies confirmed the effect of the RhoA inhibitor on synaptogenesis and modulation of neurogenesis. In fact, DRG cell line incubated with conditioned media obtained from 24 h conditioned medium of rostral, lesion and caudal segments 3 days after SCI, as we previously published (14), showed a slight increase of neurites outgrowth whereas in presence of RhoA inhibitor, this outgrowth is significant. The proteomic analyses of the secreted factors of the DRG cells under RhoA inhibitor treatment in presence of the different collected conditioned medium clearly showed difference between segments. Immunoglobulins are overexpressed particularly in the samples associated with lesion, and from caudal segment. AKT proteins family expressed real differences between rostral and lesion segments. Level of AKT3 diminished whereas the ones of AKT1 and AKT2 proteins, RhoAi increased their level in rostral and diminished in lesion and caudal segments. Serpina3c, Snx12, Gm2a, meosin, Timm44, Cthrc1, Stx6, vsp26b, Itih1, Aqp4, aggrecan core protein, BMP1 are over-expressed in caudal in presence of RhoAi compared with rostral segment or lesion. In rostral segment, with RhoA inhibitor, only AK1 and AKT2 are overexpressed, by contrast Timm44, STX6, Cthrc1, AKT3, STX6 are under-expressed. In lesion, most of proteins present in this cluster were under-expressed or had the same level with RhoAi treatment except of Gm2a, hemopexin, Protein disulfide-isomerase, Stx6 that are over-expressed. Global proteomic analyses, confirmed that among the 16 over-expressed proteins under RhoAi treatments, some were already known to be implicated in neurites outgrowth or neurogenesis e.g. Pde6d (29), Ltbp4 (30), Clip2 (31), Enah (32), Vps26b (33), Sema7a

TABLE VI

LFQ values of proteins in conditioned medium from Rostral, Lesion and Caudal spinal cord after SCi treated or not with RhoAi inhibitor. Ctrl are control (noninjured spinal cord), R: Rostral, L: Lesion, C: caudal

	CTRL_R:	CTRL_L:	CTRL_C:	12h_R1:	12h_L:	12h_C1:	12hRhoAi_R:	12hRhoAi_L:	12hRhoAi_C
Immune response									
C1qbp	24.738	26.3726	25.4189	24.998	26.9301	25.9556	26.1525	26.3788	25.8713
Complement C3	30.1649	30.2469	30.4003	32.4697	33.64	31.612	33.4385	34.7228	33.4798
Complement C4	25.4776	25.8759	26.1018	28.9522	30.6004	27.9489	29.893	31.8007	30.1023
Complement C5	25.9602	25.7853	23.9819	23.2276	25.3591	24.2936	23.6097	26.4624	24.4067
Complement C1q subcomponent subunit A	0	23.325	23.1357	24.2908	25.3708	24.7565	25.3859	26.1327	24.9915
Complement C1q subcomponent subunit B	25.2074	24.6629	25.0491	24.8465	25.914	25.4211	25.3622	26.8024	25.6331
Complement C1q subcomponent subunit C	23.4591	23.0113	23.2329	24.0514	25.0646	24.2719	25.2219	26.943	25.3557
Complement component C1q receptor	0	0	0	0	24.5259	0	0	0	0
Complement factor D	0	0	0	24.5028	27.4706	24.7466	26.0636	27.7602	25.6997
Complement component C8 beta chain	0	0	24.1013	24.8709	26.8099	25.5902	25.695	27.912	26.2396
Complement component C9	23.9076	24.2238	23.2094	26.7085	29.5338	26.3446	28.03	30.3084	28.5837
Complement component receptor 1-like protein	0	0	0	0	0	0	0	0	0
Complement C1s subcomponent	0	0	0	0	24.2484	0	0	0	0
Plasma protease C1 inhibitor	24.3359	24.1063	24.2612	27.1953	28.9329	26.5912	27.3051	28.9396	28.2716
Complement component C6	0	0	0	26.4634	26.3165	25.0005	25.4934	27.0124	25.6378
Complement factor I	23.1836	23.4684	24.3513	26.5448	29.4083	24.7069	27.2249	30.242	28.494
CD59 glycoprotein	28.4292	28.4786	28.3672	27.1374	28.138	27.9081	27.6525	26.6107	28.2075
Calreticulin	26.8708	27.3492	27.092	28.9193	29.3654	29.1833	28.5346	29.1985	28.5683
C-reactive protein	0	0	0	26.502	28.0808	25.9519	26.858	28.1045	26.7323
Granulin	25.6662	25.6306	25.533	26.1775	26.2815	26.2632	25.3612	26.2861	25.9562
Cathepsin D	27.1854	27.1477	27.3999	27.8205	27.9832	27.7454	27.9087	27.879	27.6514
Cathepsin B	26.4328	26.6551	26.1484	28.1505	28.3689	27.5517	27.1771	28.3135	27.4103
Metalloproteinase inhibitor 1	22.0379	0	21.8268	28.9081	29.5229	28.0251	25.9409	26.9787	26.7214
Metalloproteinase inhibitor 2	0	0	0	0	22.2404	0	0	0	0
Man0-binding lectin serine protease 1	0	0	0	0	22.5053	26.1173	23.8029	23.3006	22.9136
Coronin-1B	27.9178	27.581	27.9542	27.7296	27.546	27.5622	27.4981	27.1976	27.3889
Macrophages									
Macrophage migration inhibitory factor	28.6312	28.6472	29.1578	30.025	29.8091	29.8451	29.1279	29.0539	29.368
CD44 antigen	28.6619	28.6368	28.9394	28.7988	27.3233	27.7898	27.0054	27.7731	27.2653
40S ribosomal protein S19	26.936	26.5581	26.6926	26.971	26.5204	26.7498	26.7398	26.0823	26.6695
Monocyte differentiation antigen CD14	0	0	0	23.9354	25.0241	24.5459	23.9976	24.7557	24.1249
C-C motif chemokine 7	0	0	0	23.1407	22.0415	22.5686	24.707	24.4162	22.9219
Galectin-3	30.2327	30.1402	30.038	28.8223	28.8036	28.1901	28.625	28.7123	28.0306
Lymphocytes									
OX-2 membrane glycoprotein CD200	25.7871	0	23.9863	24.7009	0	24.314	24.0589	24.3939	0
Interleukin-6	24.2086	25.4681	25.5759	26.3852	26.3842	25.2731	24.483	25.7921	25.3782
Galectin-9	0	0	0	0	0	0	0	25.9002	0
Galectin-1	32.6737	32.5669	32.6506	32.9122	32.5662	32.6704	32.5203	31.9418	32.3181
Axone guidance and neuroprojection									
SLIT-ROBO Rho GTPase-activating protein 2	25.811	25.6238	25.7599	25.3082	25.0385	0	25.3939	25.5015	25.5566
Roundabout homolog 1	0	0	0	0	0	0	24.2002	0	0
Neuronal cell adhesion molecule	30.0049	30.0433	30.1589	29.9667	29.358	29.534	29.3445	28.5453	29.3049
Neural cell adhesion molecule 1	31.8917	31.7802	31.8729	31.4973	30.8715	31.4746	30.9124	30.4901	30.9638
Contactin-1	31.1681	31.1474	31.1927	31.2253	30.5841	31.0327	30.7078	29.9266	30.6822
Contactin-2	27.1585	27.0329	26.9043	27.9345	27.5488	27.9311	27.2592	27.2804	27.6615
Contactin-6	0	0	0	0	0	0	0	0	0
Ciliary neurotrophic factor	24.8506	22.9907	24.8529	25.702	24.2431	23.1797	24.9799	0	23.9798
Ciliary neurotrophic factor receptor subunit alpha	25.5707	25.9662	26.225	26.2736	25.7004	25.3727	25.4933	25.4363	25.8105
Microtubule-associated protein tau	29.8709	29.8023	29.8523	30.1694	30.0955	30.3025	29.0003	29.1989	29.4275
Serine/threonine-protein kinase PAK 1	26.9748	26.9665	27.1239	27.0781	27.6013	27.5802	27.0074	26.7041	26.8892
Serine/threonine-protein kinase PAK 2	28.2927	28.3138	28.3501	28.2557	28.1431	28.3057	28.1116	27.3161	27.8498
Serine/threonine-protein kinase PAK 3	25.1338	25.6572	25.0201	25.5953	25.7014	25.6594	25.0651	24.3002	24.6999
Ras-related C3 botulinum toxin substrate 1	28.0705	27.898	27.8852	27.7834	28.1549	27.8566	27.6868	27.5539	27.683
Stathmin	29.9996	29.7308	29.304	29.5653	29.1745	29.2003	28.6635	27.8664	28.5358
Stathmin-2	26.8569	0	27.3217	26.9841	25.8723	27.0713	0	27.2374	27.1862
Stathmin-3	0	0	0	0	25.0665	0	0	25.2965	23.8687
Dynactin subunit 1	28.0911	28.3327	28.6056	28.9071	28.9773	28.9652	28.4454	28.2142	28.4339
Dynactin subunit 2	28.7806	28.9857	28.9949	29.2243	29.2137	28.8862	28.856	28.0408	28.7832
Neurofilament light polypeptide	34.2667	34.2316	34.4903	34.4496	34.5105	34.7609	34.4873	34.3372	34.4296
Neurofascin	30.9973	30.9744	31.0475	31.0709	30.8239	30.9752	30.5183	30.2627	30.5834
Neurotrimin	28.0367	28.2084	28.2405	27.692	26.4522	27.3746	27.1734	26.5754	27.3955

TABLE VI—continued

	CTRL_R:	CTRL_L:	CTRL_C:	12h_R1:	12h_L:	12h_C1:	12hRhoAi_R:	12hRhoAi_L:	12hRhoAi_C	
Synaptogenesis										
Amphiphysin	30.2217	30.0149	29.9956	29.9535	29.6507	29.9519	29.3595	29.2831	29.5719	
Neuromodulin (Gap43)	28.8527	28.5882	28.2403	28.5208	28.9444	29.3156	27.9061	29.0011	28.1697	
Septin-2	29.028	28.3363	28.5575	29.3037	28.892	29.0671	29.1068	27.862	28.9142	
Septin-7	29.0049	28.8985	28.7175	29.2234	29.0177	28.9794	29.1438	28.5489	28.8042	
Septin-11	29.3508	29.4111	29.2963	29.3621	29.4668	29.2324	28.5523	28.3832	28.8227	
Neuronal-specific septin-3	25.9282	26.3278	26.7128	25.007	25.666	24.9764	25.0325	26.1522	25.8445	
Synaptosomal-associated protein 25	28.4208	28.3124	28.0879	28.5773	28.772	28.6392	27.9596	27.9273	27.9611	
Clathrin coat assembly protein AP180	29.1256	29.1284	29.5914	29.6023	29.4552	29.9059	29.5692	29.2666	29.8548	
Syntaxin-1A	0	0	25.5853	24.2792	0	0	0	0	0	
Syntaxin-1B	29.1377	29.0178	29.4568	29.1801	29.0735	29.4064	28.6937	28.9094	28.8049	
Syntaxin-4	0	0	0	24.4928	0	23.1944	0	0	0	
Syntaxin-6	25.9919	25.8572	25.6012	25.5197	25.2579	25.3073	25.1944	25.5921	25.118	
Syntaxin-7	26.9034	26.7065	26.7391	26.7648	26.7745	26.6727	26.0186	25.8722	25.7425	
Syntaxin-12	27.8446	28.1482	28.1291	28.0619	28.0481	28.0051	27.4685	27.1641	27.5336	
Transitional endoplasmic reticulum ATPase	32.0864	32.077	32.1498	32.0258	32.2272	32.1135	31.8542	31.8688	31.9899	
Synapsin-1	28.0302	28.3761	28.7221	28.6303	28.4171	29.0134	28.3068	27.9067	28.4044	
Synapsin-2	25.725	25.7088	26.2018	27.6418	27.6301	27.4681	27.1919	27.1391	27.7261	
Synapsin-3	0	25.1638	25.838	25.4378	24.7563	25.856	24.4428	24.885	23.6882	
Synaptojanin-1	29.4918	29.7069	29.8756	30.1903	30.4005	30.5397	30.2573	29.8646	30.4292	35_37
Neurochondrin	29.3351	29.4719	29.5332	29.5585	29.2703	29.9478	29.6878	28.5345	29.6794	
Pyridoxal phosphate phosphatase	28.8329	28.7449	29.1759	28.9972	28.7643	29.188	28.5418	28.2626	28.7458	32_35
Neurite inhibitor										
Reticulon-3 NSPL2	25.569	25.9135	27.4908	26.5108	27.3052	27.245	25.4609	25.9404	26.456	29–32
Reticulon-4 NOGO	28.851	28.847	28.1195	29.7588	30.207	29.573	29.1236	29.0453	29.1769	
Reticulon-1 NSP	29.332	29.2308	28.9172	29.6171	30.0765	29.4196	28.6395	28.7221	28.6849	26–29
Neurocan core protein;150 kDa adult core glycoprotein	29.6908	29.7793	29.5196	29.1797	28.2469	28.8289	28.4866	27.6944	28.2507	
Transforming protein RhoA	28.0322	27.9209	28.4694	28.2827	28.1263	28.0672	28.0185	27.9293	28.0899	23–26
Motoneuron degeneration										
Superoxide dismutase [Cu-Zn]	33.3356	33.0349	33.3785	33.2127	33.0219	33.0858	32.5989	32.6046	32.6408	20–23
Superoxide dismutase [Mn]	25.1239	25.2252	25.8339	27.7429	28.0497	27.5506	27.9035	27.6236	27.5134	
Vesicle-associated membrane protein-associated	29.3076	29.0153	29.1555	28.5349	28.6744	28.2749	28.2185	28.1113	28.0187	0
Vesicle-associated membrane protein-associated	29.7099	29.3958	29.9305	29.2614	29.2928	28.9969	28.6397	28.7428	28.848	

(34), BDNF/NT3 (35), UNC5C (36), Ephrin A5 and Ephrin B receptor (34), VEGF (37). *In vivo* experiments, reflected that under RhoAi treatment 12 h after SCI, neurites outgrowth factors are detected in both tissues extracts and secretome (e.g. CD166, advinin, neuritin, Neurocan, L1Cam, Vcan, Limbic system-associated membrane protein, neuronal growth regulator 1 precursor, C1qBp, SLIT-ROBO Rho GTPase-activating protein 2, Roundabout homolog 1, Ciliary neurotrophic factor). Similarly, proteins involved in synaptogenesis like synapsins, synthaxins, GAP43, Synaptojanin-1 are also elevated after RhoAi treatment.

We also showed by our time course proteomic experiments that several transcription factors are produced. Smad proteins family is one of the key players in the regeneration process. Smad1 is known to integrate signals from BMP receptors. Together with Smad4, phosphorylated Smad1 assembles a multi-subunits complex that regulates transcription (40). In the absence of Smad1, conditioned DRG neurons show impairment in axon elongation *in vitro* (40). Moreover, blockade of BMP signaling with the BMP antagonist Noggin inhibits axonal growth in both naive and preconditioned DRG neurons (40). The LFQ results reflected that Smad1, Smad5

and Smad9 appeared at 24 h whereas Smad2 is always present except at 4 Hours (Table IV). The second important player appears to be the tumor suppressor p53. Previous studies have shown that following SCI, transcriptionally active p53 undergoes a series of acetylation events on its C-terminal domain (41, 42). After injury, active gene transcription is necessary to synthesize new proteins needed for axon growth. Acetylated-p53, together with CBP/p300 and PCAF, selectively occupies regulatory regions upstream to the TSS of proneurite and axon-outgrowth genes such as Coronin1b, Rab13, and GAP-43 during an early regenerative response (43). Acetylated-p53 may have a critical role in modulating different transcriptional responses during axonal regeneration (44–46). For STATs proteins, absence of STAT3, peripheral nerve regeneration is impaired in DRG neurons (47, 48). Interestingly, sustained STAT3 expression promotes terminal and collateral sprouting by controlling initiation of axon growth after dorsal columns injury (47, 48). Stat3 is detected in detected only at 1 h. Interestingly is the presence of SWI/SNF complex subunit SMARCC1 (BAF155) and SMARCC2 (BAF170) proteins (49). These two proteins belong to the neural progenitors-specific chromatin remodeling complex

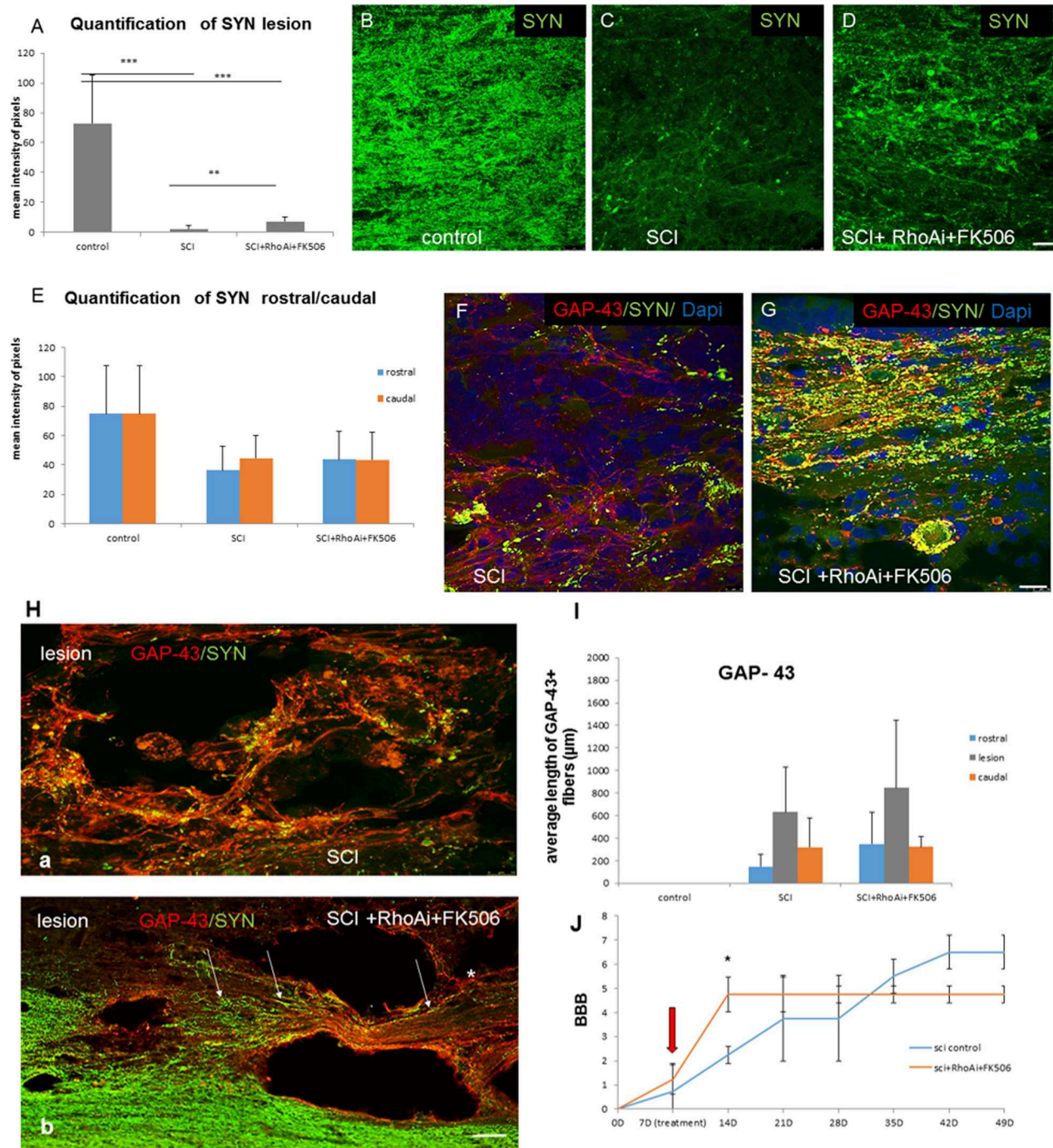


FIG. 6. Quantification of synaptophysin (SYN) positivity at the lesion site (A) and rostral-caudal segments (E) showed significant decrease of SYN after injury, whereas RhoAi + FK506 treatment increased SYN expression significantly at lesion, but not in rostral or caudal segments (E), * $p < 0.05$, ** $p < 0.001$, * $p < 0.0001$, One-way ANOVA. Representative images of synaptophysin immunoreactivity (SYN, green) revealed intensely stained synaptic vesicles - punctate structures within the spinal cord- lesion site in control (B) and treated group (D), note only occasional synaptic vesicles on sections from SCI rats (C). Confocal imaging with double labeling of GAP-43 (red) and SYN (green) antibodies, confirmed enhanced growth of axons with dense synaptic vesicles distribution after RhoAi + FK506 treatment at lesion (G). Note, areas containing GAP-43 positive fibers, but only occasional SYN expression at lesion in SCI group (F). Quantification of GAP-43 positive fibers did not reveal significant differences between SCI and SCI RhoAi + FK506 groups (I), outlining growing axons within damaged dorsal and lateral white matter tracts (Ha, Hb). Note, high number of GAP-43 axons penetrating the lesion site, with dense (arrowheads) or sporadic positive synaptic vesicles (asterisk) (Ha). Scale bar = 25 μm . BBB open field test in SCI rats (blue line) and SCI rats treated with RhoAi + FK506 (red line) at 0, 7, 14, 21, 28, 35, 42 and 49 days post injury, reveals that BBB score in treated rats reached 5 at 14 days and remained unchanged, whereas, rats without treatment reached score 5 at 30 days and further slightly improved (J).**

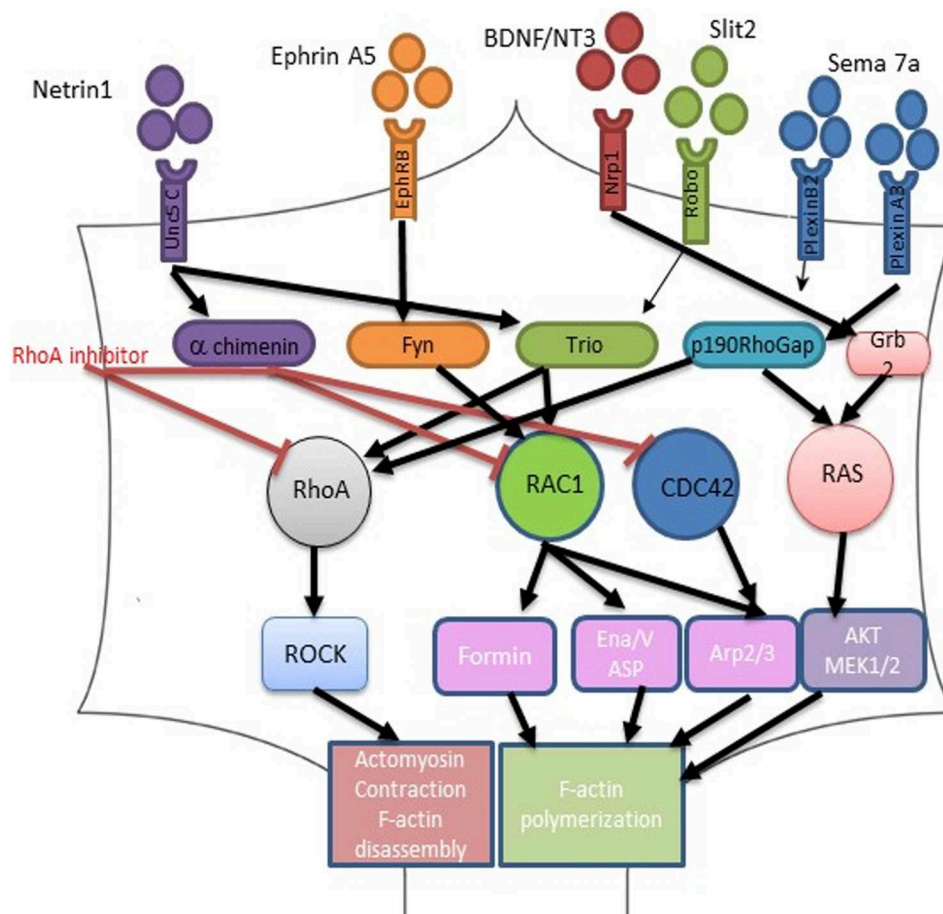


FIG. 7. **Schematic representation of the positive growth cone guidance after RhoA inhibitor treatment.** The scheme integrates the specific proteins identified after proteins cell extraction or from the secretome. Signaling pathways linked to identify proteins are also presented.

(npBAF complex) and the neuron-specific chromatin remodeling complex (nBAF complex). The npBAF complex is essential for the self-renewal/proliferative capacity of the multipotent neural stem cells. The nBAF complex along with CREST plays a role regulating the activity of genes essential for dendrite growth (50). These two proteins are overexpressed after RhoAi treatment. Altogether these data pointed out that the chromatin-remodeling BAF complex (formed by the two subunits BAF155 and BAF170) known to play a role in brain development (51) is a key target of RhoAi treatment in acute SCI. BAF (Brg1/Brm Associated Factors) complex is a multi-subunit chromatin remodeling complex that alters the position of nucleosomes thereby regulating gene expression. Although, specific BAF subunits selectively interact with transcription factors to regulate gene expression programs, the logic underlying the composition of the BAF complex remains largely unknown. Here we showed that this complex can interact with Smad2/3 and TP53 transcription factors at the early stage of the treatment impacting the cellular traffic and increase vesicles production that are secreted at least 24 h after treatment. The transcription factors Smad2 and Smad3

are known to mediate a large set of gene responses induced by TGF- β and recent observations have showed interactions between the two Smads and BAF complex. BAF complex is incorporated into transcriptional complexes that are formed by activated Smads in the nucleus, on target promoters (52). At 24 h, all TF implicated in control of neurites outgrowth factors expression are present. Expression in DRG cell of robo1, nestin, N chimaerin, glomulin, MAGED 1, TRPV2 in presence of R1 conditioned medium or, slit, FARP1, srGAP2, and STK25 in C1 conditioned medium confirms the differential activation of the DRG cells dependently to the medium considered.

In this context, we investigated the impact of a local treatment of RhoAi in conjunction with an intraperitoneal injection of FK506. The main scenario was to combine factors with both anti-inflammatory and neuro-stimulatory potential to scale up the treatment. Because in our previous study, we did not observe beneficial effect of sustained, long term FK506 delivery, we have decided to shorten the delivery regiment up to 14 days (53). Spinal cord sections dissected from different segments revealed numerous synaptophysin labeling at the

lesion site and adjacent segments. Moreover, dense network of GAP-43 immunoreactive axons of different thickness oriented in various directions were present in both rostral and caudal segments as well as at the lesion epicenter. These data confirmed that the treatment has enhanced neurite outgrowth in both segments with dense synaptic contacts at the epicenter of the lesion. The BBB score showed a significant improvement at 7 days after treatment and continued with plateau characteristics, whereas the SCI group revealed delayed and gradual locomotor improvement during entire survival. These data clearly showed different locomotor outcome between both groups, thus revealing beneficial effect of RhoAi + FK 506 delivery at the initial phase of the treatment, but not at longer survival. Thus, treated group launched recovery much earlier than SCI, which regenerate more slowly but at overall survival both groups revealed similar recovery pattern at long term (49 days). This could be caused by low dose of RhoAi delivered *via* single application that was probably not sufficient for long term stimulation and inhibition of RhoA pathways. For example, previous study demonstrating beneficial recovery of injured CNS axons treated with RhoA-inhibiting NSAID ibuprofen delivery was initiated 1 h after the injury until 5 days post-trauma, via daily subcutaneous injections (54). It is also difficult to determine whether concentration of RhoAi (1 $\mu\text{g}/10 \mu\text{l}$) that was set according to published studies, represented an optimal concentration and was biologically attainable to the concentration used *in vitro*. To address this, it would require a complex of comparative and dose response studies processed under *in vitro* and *in vivo* conditions. Second important factor that should be mentioned is the route of RhoAi administration. Oral, intramuscular, subcutaneous, or intravenous drug deliveries which imposes a minimal burden on the animals could be applied on daily basis, but not intraspinal-local delivery which requires surgery. Thus, complex factors have to be taken in account to develop an optimal treatment scenario that could complementary sum the efficacy of RhoAi treatment.

Taken together, we demonstrated here that RhoAi treatment provokes sequential activation events in time course resulting in chromatin remodeling, selective and timely activation of transcription factors leading to the expression of a large array of factors involved in neurite outgrowth. Major factors include receptors (Robo1, Plexin A3, Plexin B2, UNC5C, neuropilin 1), ligands (semaphorin 7A, netrin, Ephrin A5, Slit2, BDNF/NT3) and transcription factor (β catenin, WLS, Phox2a, Pho2b) previously shown to regulate axonal regrowth (Fig. 7). We confirm *in vivo* their presence under RhoAi treatment in tissue and in secreted factors. Regional differences regarding the effects of conditioned medium generated from distinct spinal cord segments indicate that each segment is endowed with a specific ability to secrete axonal regrowth-modifying molecules. Interestingly, in this context, both the R1 and C1 segments harbor a potential to produce such neurites outgrowth factors allowing growth cone formation and activation

as we evidence by *in vitro* and *in vivo* experiments. These segments are the most impacted by the RhoAi treatment at the early stage of the growth cone formation leading enhanced neurite outgrowth and synaptogenesis. Thus, to improve the efficiency of SCI treatment with RhoAi, it appears essential to specifically target the R1 and C1 segments and to operate in a timely fashion to bypass the regeneration plateau observed 7 days after the treatment.

DATA AVAILABILITY

The raw data and annotated MS/MS spectra were deposited at the ProteomeXchange Consortium (<http://proteomecentral.proteomexchange.org>) via the PRIDE partner repository with the data set identifier PXD004639.

* This research was supported by a collaboration between the Fundamental and Applied Biology Mass Spectrometry Laboratory (MS) and grants from Ministère de L'Education Nationale, L'Enseignement Supérieur et de la Recherche, INSERM, Région Nord-Pas de Calais (to SD), SIRIC ONCOLille Grant INCa-DGOS-Inserm 6041aa (IF) and Université de Lille 1 (SD), APVV-15-0613 (DC), VEGA 2/0125/15, Stefanik (MS) APVV SK-FR-2015-0018 (DC).

☒ This article contains supplemental material.

✉ To whom correspondence should be addressed: University Lille, INSERM, U1192 - Laboratoire Protéomique, Réponse Inflammatoire et Spectrométrie de Masse-PRISM, F-59000 Lille, France. Tel.: +33-320-4194; Fax: +33-320-4354; E-mail: Michel.salzet@univ-lille1.fr.

§§ Authors contributed equally to the work.

Author contribution statement: DC, MS have got the funding for the project and have written the paper. SD, DC, KM, MAK, ZL, CM, JB, IF have done the experiments. SN, LP, FK have performed part of the bioinformatics analyses. All authors have reviewed the manuscript.

REFERENCES

1. Tigyi, G., Fischer, D. J., Sebok, A., Yang, C., Dyer, D. L., and Miledi, R. (1996) Lysophosphatidic acid-induced neurite retraction in PC12 cells: control by phosphoinositide-Ca²⁺ signaling and Rho. *J. Neurochem.* **66**, 537–548
2. Jalink, K., van Corven, E. J., Hengeveld, T., Morii, N., Narumiya, S., and Moolenaar, W. H. (1994) Inhibition of lysophosphatidate- and thrombin-induced neurite retraction and neuronal cell rounding by ADP ribosylation of the small GTP-binding protein Rho. *J. Cell Biol.* **126**, 801–810
3. Leeuwen, F. N., Kain, H. E., Kammen, R. A., Michiels, F., Kranenburg, O. W., and Collard, J. G. (1997) The guanine nucleotide exchange factor Tiam1 affects neuronal morphology; opposing roles for the small GTPases Rac and Rho. *J. Cell Biol.* **139**, 797–807
4. Ruchhoeft, M. L., Ohnuma, S., McNeill, L., Holt, C. E., and Harris, W. A. (1999) The neuronal architecture of *Xenopus* retinal ganglion cells is sculpted by rho-family GTPases *in vivo*. *J. Neurosci.* **19**, 8454–8463
5. Schwab, M. E. (2002) Repairing the injured spinal cord. *Science* **295**, 1029–1031
6. Mar, F. M., da Silva, T. F., Morgado, M. M., Rodrigues, L. G., Rodrigues, D., Pereira, M. I., Marques, A., Sousa, V. F., Coentro, J., Sa-Miranda, C., Sousa, M. M., and Brites, P. (2016) Myelin Lipids Inhibit Axon Regeneration Following Spinal Cord Injury: a Novel Perspective for Therapy. *Mol. Neurobiol.* **53**, 1052–1064
7. Yamashita, T., Higuchi, H., and Tohyama, M. (2002) The p75 receptor transduces the signal from myelin-associated glycoprotein to Rho. *J. Cell Biol.* **157**, 565–570
8. Winzeler, A. M., Mandemakers, W. J., Sun, M. Z., Stafford, M., Phillips, C. T., and Barres, B. A. (2011) The lipid sulfatide is a novel myelin-associated inhibitor of CNS axon outgrowth. *J. Neurosci.* **31**, 6481–6492

9. Fehlings, M. G., and Vawda, R. (2011) Cellular treatments for spinal cord injury: the time is right for clinical trials. *Neurotherapeutics* **8**, 704–720
10. Yamashita, T., Tucker, K. L., and Barde, Y. A. (1999) Neurotrophin binding to the p75 receptor modulates Rho activity and axonal outgrowth. *Neuron* **24**, 585–593
11. Yamashita, T., and Tohyama, M. (2003) The p75 receptor acts as a displacement factor that releases Rho from Rho-GDI. *Nat. Neurosci.* **6**, 461–467
12. Gehler, S., Gallo, G., Veien, E., and Letourneau, P. C. (2004) p75 neurotrophin receptor signaling regulates growth cone filopodial dynamics through modulating RhoA activity. *J. Neurosci.* **24**, 4363–4372
13. Cizkova, D., Le Marec-Croq, F., Franck, J., Slovinska, L., Grulova, I., Devaux, S., Lefebvre, C., Fournier, I., and Salzet, M. (2014) Alterations of protein composition along the rostro-caudal axis after spinal cord injury: proteomic, in vitro and in vivo analyses. *Front. Cell Neurosci.* **8**, 105
14. Devaux, S., Cizkova, D., Quanic, J., Franck, J., Nataf, S., Pays, L., Hauberg-Lotte, L., Maass, P., Kobarg, J. H., Kobeissy, F., Meriaux, C., Wisztorski, M., Slovinska, L., Blasko, J., Cigankova, V., Fournier, I., and Salzet, M. (2016) Proteomic analysis of the spatio-temporal based molecular kinetics of acute spinal cord injury identifies a time- and segment-specific window for effective tissue repair. *Mol. Cell. Proteomics*
15. Liu, W., Shang, F. F., Xu, Y., Belegu, V., Xia, L., Zhao, W., Liu, R., Wang, W., Liu, J., Li, C. Y., and Wang, T. H. (2015) eIF5A1/RhoGDIalpha pathway: a novel therapeutic target for treatment of spinal cord injury identified by a proteomics approach. *Sci. Reports* **5**, 16911
16. Grulova, I., Slovinska, L., Blasko, J., Devaux, S., Wisztorski, M., Salzet, M., Fournier, I., Kryukov, O., Cohen, S., and Cizkova, D. (2015) Delivery of Alginate Scaffold Releasing Two Trophic Factors for Spinal Cord Injury Repair. *Sci. Reports* **5**, 13702
17. Wisniewski, J. R., Ostasiewicz, P., and Mann, M. (2011) High recovery FASP applied to the proteomic analysis of microdissected formalin fixed paraffin embedded cancer tissues retrieves known colon cancer markers. *J. Proteome Res.* **10**, 3040–3049
18. Meissner, F., Scheltema, R. A., Mollenkopf, H. J., and Mann, M. (2013) Direct proteomic quantification of the secretome of activated immune cells. *Science* **340**, 475–478
19. Cox, J., and Mann, M. (2008) MaxQuant enables high peptide identification rates, individualized p.p.b.-range mass accuracies and proteome-wide protein quantification. *Nat. Biotechnol.* **26**, 1367–1372
20. Cox, J., Neuhauser, N., Michalski, A., Scheltema, R. A., Olsen, J. V., and Mann, M. (2011) Andromeda: a peptide search engine integrated into the MaxQuant environment. *J. Proteome Res.* **10**, 1794–1805
21. UniProt, C. (2012) Reorganizing the protein space at the Universal Protein Resource (UniProt). *Nucleic Acids Res.* **40**, D71–D75
22. Cox, J., Hein, M. Y., Lubner, C. A., Paron, I., Nagaraj, N., and Mann, M. (2014) Accurate proteome-wide label-free quantification by delayed normalization and maximal peptide ratio extraction, termed MaxLFQ. *Mol. Cell. Proteomics* **13**, 2513–2526
23. Vizcaino, J. A., Deutsch, E. W., Wang, R., Csordas, A., Reisinger, F., Rios, D., Dianes, J. A., Sun, Z., Farrah, T., Bandeira, N., Binz, P. A., Xenarios, I., Eisenacher, M., Mayer, G., Gatto, L., Campos, A., Chalkley, R. J., Kraus, H. J., Albar, J. P., Martinez-Bartolome, S., Apweiler, R., Omenn, G. S., Martens, L., Jones, A. R., and Hermjakob, H. (2014) ProteomeXchange provides globally coordinated proteomics data submission and dissemination. *Nat. Biotechnol.* **32**, 223–226
24. Vizcaino, J. A., Cote, R. G., Csordas, A., Dianes, J. A., Fabregat, A., Foster, J. M., Griss, J., Alpi, E., Birim, M., Contell, J., O'Kelly, G., Schoenegger, A., Ovelleiro, D., Perez-Riverol, Y., Reisinger, F., Rios, D., Wang, R., and Hermjakob, H. (2013) The PRoteomics IDentifications (PRIDE) database and associated tools: status in 2013. *Nucleic Acids Res.* **41**, D1063–D1069
25. Yuryev, A., Kotelnikova, E., and Daraselia, N. (2009) Ariadne's ChemEffect and Pathway Studio knowledge base. *Expert Opin. Drug Discov.* **4**, 1307–1318
26. Bonnet, A., Lagarrigue, S., Liaubet, L., Robert-Granie, C., Sancristobal, M., and Tosser-Klopp, G. (2009) Pathway results from the chicken data set using GOTM, Pathway Studio and Ingenuity softwares. *BMC Proceedings* **3**, S11
27. Pyatnitskiy, M., Mazo, I., Shkrob, M., Schwartz, E., and Kotelnikova, E. (2014) Clustering gene expression regulators: new approach to disease subtyping. *PLoS ONE* **9**, e84955
28. Daraselia, N., Wang, Y., Budoff, A., Lituev, A., Potapova, O., Vansant, G., Monforte, J., Mazo, I., and Ossovskaya, V. S. (2012) Molecular signature and pathway analysis of human primary squamous and adenocarcinoma lung cancers. *Am. J. Cancer Res.* **2**, 93–103
29. Tweedie, D., Rachmany, L., Kim, D. S., Rubovitch, V., Lehmann, E., Zhang, Y., Becker, K. G., Perez, E., Pick, C. G., and Greig, N. H. (2016) Mild traumatic brain injury-induced hippocampal gene expressions: The identification of target cellular processes for drug development. *J. Neurosci. Methods*
30. Dobolyi, A., and Palkovits, M. (2008) Expression of latent transforming growth factor beta binding proteins in the rat brain. *J. Comp. Neurol.* **507**, 1393–1408
31. Ota, H., Hikita, T., Nishioka, T., Matsumoto, M., Ito, J., Asai, N., Enomoto, A., Takahashi, M., Kaibuchi, K., and Sobue, K. (2013) Proteomic analysis of Girdin-interacting proteins in migrating new neurons in the postnatal mouse brain. *Biochem. Biophys. Res. Commun.* **442**, 16–21
32. Doss, M. X., Gaspar, J. A., Winkler, J., Hescheler, J., Schulz, H., and Sachinidis, A. (2012) Specific gene signatures and pathways in mesodermal cells and their derivatives derived from embryonic stem cells. *Stem Cell Rev. Reports* **8**, 43–54
33. Chan, S. F., Huang, X., Mc Kercher, S. R., Zaidi, R., Okamoto, S.-i., Nakaniishi, N., Lipton, S. A. (2015) Transcriptional profiling of MEF2-regulated genes in human neural progenitor cells derived from embryonic stem cells. *Genomics Data* **3**, 24–27
34. Püschel, A. W. (2002) The function of neuropilin/plexin complexes. *Neuropilin: From Nervous System to Vascular and Tumor Biology*, pp. 71–80, Springer
35. Yao, J., Sasaki, Y., Wen, Z., Bassell, G. J., and Zheng, J. Q. (2006) An essential role for β -actin mRNA localization and translation in Ca²⁺-dependent growth cone guidance. *Nat. Neurosci.* **9**, 1265–1273
36. Round, J., and Stein, E. (2007) Netrin signaling leading to directed growth cone steering. *Current Opin. Neurobiol.* **17**, 15–21
37. Foehring, D., Brand-Saberl, B., and Theiss, C. (2012) VEGF-induced growth cone enhancement is diminished by inhibiting tyrosine-residue 1214 of VEGFR-2. *Cells Tissues Organs* **196**, 195–205
38. Fagoe, N. D., van Heest, J., and Verhaagen, J. (2014) Spinal cord injury and the neuron-intrinsic regeneration-associated gene program. *Neuromolecular Med.* **16**, 799–813
39. Byrne, A. B., Walrad, T., Gardner, K. E., Hubbert, A., Reinke, V., and Hammarlund, M. (2014) Insulin/IGF1 signaling inhibits age-dependent axon regeneration. *Neuron* **81**, 561–573
40. Zhong, J., and Zou, H. (2014) BMP signaling in axon regeneration. *Curr. Opin. Neurobiol.* **27**, 127–134
41. Tedeschi, A., Nguyen, T., Steele, S. U., Feil, S., Naumann, U., Feil, R., and Di Giovanni, S. (2009) The tumor suppressor p53 transcriptionally regulates cGKI expression during neuronal maturation and is required for cGMP-dependent growth cone collapse. *J. Neurosci.* **29**, 15155–15160
42. Tedeschi, A., and Di Giovanni, S. (2009) The non-apoptotic role of p53 in neuronal biology: enlightening the dark side of the moon. *EMBO Rep.* **10**, 576–583
43. Floriddia, E. M., Rathore, K. I., Tedeschi, A., Quadrato, G., Wuttke, A., Lueckmann, J. M., Kigerl, K. A., Popovich, P. G., and Di Giovanni, S. (2012) p53 Regulates the neuronal intrinsic and extrinsic responses affecting the recovery of motor function following spinal cord injury. *J. Neurosci.* **32**, 13956–13970
44. Tedeschi, A., Nguyen, T., Puttagunta, R., Gaub, P., and Di Giovanni, S. (2009) A p53-CBP/p300 transcription module is required for GAP-43 expression, axon outgrowth, and regeneration. *Cell Death Differ.* **16**, 543–554
45. Gaub, P., Tedeschi, A., Puttagunta, R., Nguyen, T., Schmandke, A., and Di Giovanni, S. (2010) HDAC inhibition promotes neuronal outgrowth and counteracts growth cone collapse through CBP/p300 and P/CAF-dependent p53 acetylation. *Cell Death Differ.* **17**, 1392–1408
46. Gaub, P., Joshi, Y., Wuttke, A., Naumann, U., Schnichels, S., Heiduschka, P., and Di Giovanni, S. (2011) The histone acetyltransferase p300 promotes intrinsic axonal regeneration. *Brain* **134**, 2134–2148
47. Lang, C., Bradley, P. M., Jacobi, A., Kerschensteiner, M., and Bareyre, F. M. (2013) STAT3 promotes corticospinal remodelling and functional recovery after spinal cord injury. *EMBO Rep.* **14**, 931–937
48. Bareyre, F. M., Garzorz, N., Lang, C., Misgeld, T., Buning, H., and Kerschensteiner, M. (2011) In vivo imaging reveals a phase-specific role of STAT3 during central and peripheral nervous system axon regeneration. *Proc. Natl. Acad. Sci. U.S.A.* **108**, 6282–6287
49. Son, E. Y., and Crabtree, G. R. (2014) The role of BAF (mSWI/SNF) com-

- plexes in mammalian neural development. *American journal of medical genetics. Part C, Sem. Med. Gen.* **166C**, 333–349
50. Staahl, B. T., Tang, J., Wu, W., Sun, A., Gitler, A. D., Yoo, A. S., and Crabtree, G. R. (2013) Kinetic analysis of npBAF to nBAF switching reveals exchange of SS18 with CREST and integration with neural developmental pathways. *J. Neurosci.* **33**, 10348–10361
51. Narayanan, R., Pirouz, M., Kerimoglu, C., Pham, L., Wagener, R. J., Kiszka, K. A., Rosenbusch, J., Seong, R. H., Kessel, M., Fischer, A., Stoykova, A., Staiger, J. F., and Tuoc, T. (2015) Loss of BAF (mSWI/SNF) Complexes Causes Global Transcriptional and Chromatin State Changes in Forebrain Development. *Cell Rep.* **13**, 1842–1854
52. Xi, Q., He, W., Zhang, X. H., Le, H. V., and Massague, J. (2008) Genome-wide impact of the BRG1 SWI/SNF chromatin remodeler on the transforming growth factor beta transcriptional program. *J. Biol. Chem.* **283**, 1146–1155
53. Saganova, K., Orendacova, J., Sulla, I., Jr, Filipcik, P., Cizkova, D., and Vanicky, I. (2009) Effects of long-term FK506 administration on functional and histopathological outcome after spinal cord injury in adult rat. *Cell Mol. Neurobiol.* **29**, 1045–1051
54. Xing, B., Li, H., Wang, H., Mukhopadhyay, D., Fisher, D., Gilpin, C. J., and Li, S. (2011) RhoA-inhibiting NSAIDs promote axonal myelination after spinal cord injury. *Exp. Neurol.* **231**, 247–260

Conclusion – Chapter 3

We assessed in a rat SCI model the in-vivo impact of a sustained RhoA inhibitor treatment administered in situ via a functionalized alginate scaffold. The clinical therapeutic effects were detected only at the early post-injury time points, and then overall survival was accompanied by a dramatic increase of synaptic contacts on outgrowing neurites. Results notably showed a time-dependent alteration of the profile of transcription factors along with the synthesis of growth cone-related factors (receptors, ligands, and signaling pathways) in treated DRG cells. Furthermore, we demonstrated that the inflammatory response process involvement via immunoglobulins occurs by binding to their Fc γ II/III receptors on the DRG cells upon neurite outgrowth initiation. This interaction results in modulating the neurite outgrowth process. Of interest, our data indicate that treatment at late time points led to an inhibition of several factors implicated in neurogenesis reflecting a global inhibition status as observed in-vivo at 2 weeks following SCI. We demonstrate that RhoA inhibitor treatment is useful to initiate the neurogenesis process at acute early time points which necessitates the need for a second treatment intervention at chronic time points to facilitate and enhance synaptic connections and promote neuronal reconnections. The second major point that we have evidenced is the presence of immunoglobulins following SCI at early stages of lesion. IgGs which have been detected even when no injury occurs in spinal cord, followed the time course and the spatial repartition with presence of IgG1 and IgG2 subclasses (a, b, c). IgG1 is clearly mostly abundant at 12h and switches in time course to IgG2a at 24h where it remains predominant during 3, 7 and 10 days after SCI. RhoA inhibitor treatment influenced the IgG switching to IgG2c. We have established that IgGs are found in neurons and astrocytes (neural origin) by co-localization immunofluorescence study with specific anti-IgG, anti-NeuN and anti-GFAP antibodies. While in-vitro studies have revealed the neural origin of IgGs, it is necessary to clarify this in-vivo. Treatment with anti-CD20, did not affect the neural detection of these IgG. We established using primary cultures of astrocytes issued from either cortex or spinal cord 24h after LPS, immunolabelling with anti-IgG (**Figure 27**). Therefore, our work demonstrates that acute inflammation after SCI is a key phenomenon, and any therapeutic tool must be used as early as the inflammation spreading is initiated. These tentative results on immunoglobulin production in CNS offer a new avenue to study immune response in CNS and neuro-inflammatory diseases.

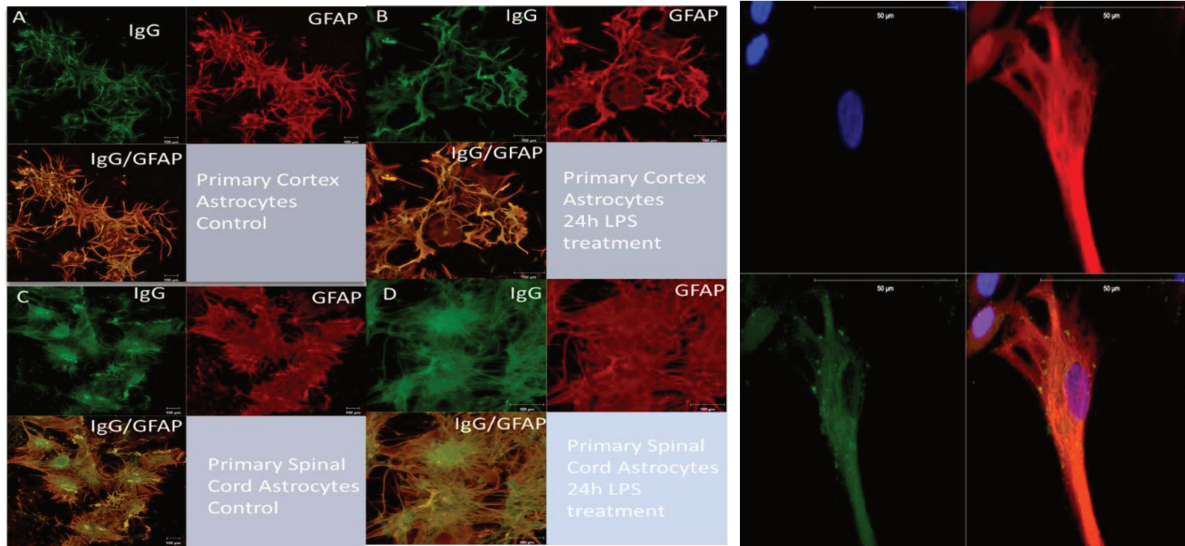


Figure 27: Immunofluorescence performed with anti-IgG coupled to fluorescein and anti-GFAP coupled to Texas Red on primary culture of astrocytes extracted either from Cortex or spinal cord of rat pups (P3) after LPS treatment or not. Inserted pictures correspond to spinal cord astrocytes stimulated by LPS at 63X.

Discussion

In the previous parts, we conducted a spatio-temporal study on TBI, using a CCI rat open head model of injury by studying the lipid and proteomic changes post impact. One essential aim of this study was to compare the biological processes occurring within the injured environment of the brain to that occurring post impact to the spinal cord. Using a spatially-resolved micro-proteomics approach applied to the injured cortical tissue, we were able to characterize 4 main phases of molecular events that take place in the first 10 days after impact to the brain. Phase 1 was mainly characterized by normal cellular processes that are also found in the sham condition, and are restored at 10 days post impact. Phase 2 was expected, as our CCI injury system induces a BBB breach, and thus at 1 day after injury and until around 7 days, several blood related processes and acute inflammation are detected. Phase 3 is mainly involved in the apoptotic execution within the injured microenvironment. Surprisingly, within phase 3 of the first 10 days, initiation of DNA repair occurs at 3 days after impact. At 3 days also, processes involved in initiation of regeneration and astrogliosis are launched (Phase 4), thus showing that the brain starts its compensatory actions of repair, at the level of DNA, as early as 3 days after impact. This is not detected in the case of spinal cord injury, as previous results have shown the involvement of chronic inflammation at the 3 days after SCI with no suggestion of DNA repair (Devaux et al. 2016; Cizkova et al. 2014b). However, it is noteworthy to mention that both injury models show reduced inflammation at 10 days post impact, but initiation of DNA repair is only found in TBI at the early mentioned time point. This shows the plasticity factor of the brain when compared to spinal cord, especially that although inflammation and recruitment of the immune cells is escalating to reach a maximum level at 3 days post impact, the cellular response in adjusting at the DNA level, occurs in parallel to this inflammatory reaction. In addition, our studies assured the overexpression of IgG's in the spinal cord at 3 days after impact. This was not fully confirmed in the case of TBI, however preliminary results have shown possible expression of IgG at 3 days post TBI. It will be important to confirm this finding and search across other time points than 3 days for the expression of IgG in the brain after impact, to possibly link with what we found in the spinal cord.

Also in SCI, RhoA inhibitor was used to study its effect on the injured spinal cord both in-vitro using several DRG cell lines, and in-vivo by administrating this inhibitor locally to the injury

site using scaffold alginate biomaterial. The in-vitro results show a promising effect of RhoA inhibitor by increasing the neurite length and neurogenesis, even in the presence of conditioned medium from lesion, rostral and caudal segments. In addition, the in-vivo experiments also showed positive results as the BBB score of the treated animals showed a significant increase when compared to the non-treated animals, however, only until 7 days after treatment, where a plateau in the BBB score is shown with no more increase. The complexity of SCI pathology requires the development of novel therapeutic strategies that would overcome specific pathological factors in the formation of the inhibitory environment and the suppression of axonal regeneration. One of the major events at the beginning of the SCI is the development of acute inflammatory process characterized by fluid accumulation and the recruitment of immune cells (neutrophils, T-cells, macrophages and monocytes) and microglia. Mammalian microglial cells normally function as sentinel immune cells regulating tissue homeostasis in the adult central nervous system and participate in pathological processes, orchestrating tissue remodeling. Their function appear to be complex as they exhibit both neuroprotective and neurotoxic effects. When the CNS is injured or affected by diseases, the resident ramified microglia morphologically transform into activated microglia” or “reactive microglia” with retracted processes and enlarged cell bodies, accumulate at the affected site and release various bioactive substances. Some are cytotoxic or pro-inflammatory and others may aid survival and regeneration. Thus, it is important to control acute inflammation after SCI through microglial/macrophage cell polarization by promoting conversion of M1 pro-inflammatory to M2 reparative macrophages. For this purpose, we would like to combine RhoA inhibitor treatment, with extracellular vesicles (EVs) secreted from mesenchymal stem cells, in an aim to continue the improvement of the BBB score for the treated subjects for more than 7 days. Among EVs, exosomes from spinal cord microglia share anti-regenerative properties (Murgoci et al. 2018) and intrathecal administration of secretome of mesenchymal stem cells (MSCs) containing EVs improve BBBs core and neurogenesis processes (Cizkova et al. 2018). In addition, our micro-proteomic data in TBI have also shown the involvement of RhoA protein within the injured cortical tissue. As we are also using an open injury model for the brain, it would be worth applying the same approach of local administration of RhoA inhibitor associated with EVs from MSCs to the injury site using scaffold alginate biomaterial. But, we believe that we will not have the same promising results in TBI as in the case of SCI. This is mainly due to the fact that the extent of injury caused by the impact to the cortical tissue does not necessarily have

to be restricted to the mechanically injured area, but could spread to other regions of the brain. This is clearly demonstrated by the lipid MALDI-MSI that we have performed in both 2D and 3D manner. We have shown that a group of molecules, the acylcarnitines have shown to be highly elevated in the injured cortex of the brain. But, they also showed expression within the substantia nigra (SN) of the ipsilateral hemisphere at 3 days post impact. Although the SN was not affected by direct mechanical damage, such injury-related molecules showed expression in the SN only after impact. Taken all-together, this clearly demonstrates that any locally administered therapeutic approach may not be clearly followed with respect to affected areas. This is mainly due to the complexity and plasticity of the brain which results in an unpredictable outcome of any mechanical impact with regard to the location and extent of injury. This is clearly different from the SCI where the extent of damage is mainly restricted to the area of the mechanical force.

3-Dimensional MALDI MSI of TBI allowed to better visualize the extent of the injury in the brain, and showed possible flow of lipid molecules back and forth from the injury site to the cerebrospinal fluid, which is in direct contact with the spinal cord. As previously mentioned, we have characterized a new family of lipid biomarkers, the acylcarnitines, mainly palmitoylcarnitine, that clearly showed elevated expression in the cortical tissue of the brain post impact when compared to non-injured tissue. This family of molecules had highest expression at 3 days post impact and was found to be co-localized with the resident microglia of the brain surrounding the injury core. This expression was not only restricted in the damaged cortical tissue, but also in the underlying corpus callosum and surprisingly as previously mentioned, within the ipsilateral SN. The SN is the main region of the brain affected in the case of Parkinson's disease, as this part of the brain is mainly characterized by the loss of dopaminergic neurons (Alexander 2004). By microproteomics applied on the SN of injured brain at 3D post TBI, several proteins implicated in Parkinson's disease showed elevated expression including synaptotagmins, GAD, GPR158 and HMGB1. Cell lines stimulated with palmitoylcarnitine showed an elevated expression of proteins such as Galectin-3 and HMGB1 also. This stimulation also induced a major repertoire of pro-inflammatory action on wild type macrophages, and a neurogenesis/astrocytosis effect on astrocyte cell lines. Our results have shown a possible link between TBI and Parkinson's disease as early as 3 days after TBI. For the future work, we would like to go deeper in the exact mechanism of action of palmitoylcarnitine on the cells of the substantia nigra. For example, we would like to understand if this lipid molecule is binding to a cellular receptor on the surface of these cells, is it being

phagocytized to the interior part of the cells, or can it integrate itself through the plasma membrane. In addition, we would like to understand if there is a direct link of acylcarnitines to the death of dopaminergic cells or by stimulating other cells such as macrophages, to induce injury to these dopaminergic ones. Finally, as we have applied both a microproteomic and lipid MSI approaches, we would like to study the transcriptomic changes that can occur in a spatio-temporal manner post TBI. By combining all of lipid, proteomic, and transcriptomic data, we could obtain a more comprehensive systemic picture of all the molecular mechanism occurring post impact starting from the gene level, and finishing with the protein and lipid ones. We aim also to develop a new micro-tissue RNA extraction from within the injured cortical tissue with same 1 mm² surface area as in the case of microproteomics. Extracted RNA will be subjected to RNA seq, to monitor the whole transcriptomic changes. Such approach will allow us to directly link our obtained proteomic data to the transcriptomic variations that occur in time manner and different locations of the brain.

In the end, we believe that this study has provided a more fundamental comprehension of the proteomic and lipid changes that occur within the injured micro-environment of TBI for a possible better biomarker characterization and more efficient therapeutic targeting. We also believe that follow-up on the identified acylcarnitine family, and targeting of this group of lipids could have potential in a decrease of the outcomes of TBI, and may help in the regeneration process as we showed that this molecule has a highly pro-inflammatory affect.

References

- Abbott, N.J. et al., 2010. Structure and function of the blood–brain barrier. *Neurobiology of Disease*, 37(1), pp.13–25.
- Ahuja, C.S. et al., 2017. Traumatic spinal cord injury. *Nature Reviews Disease Primers*, 3, p.17018.
- Alali, A.S. et al., 2015. Economic Evaluations in the Diagnosis and Management of Traumatic Brain Injury: A Systematic Review and Analysis of Quality. *Value in Health*, 18(5), pp.721–734.
- Alexander, G.E., 2004. Biology of Parkinson’s disease: pathogenesis and pathophysiology of a multisystem neurodegenerative disorder. *Dialogues in clinical neuroscience*, 6(3), pp.259–80.
- Alexandrov, T. et al., 2013. Analysis and Interpretation of Imaging Mass Spectrometry Data by Clustering Mass-to-Charge Images According to Their Spatial Similarity. *Analytical Chemistry*, 85(23), pp.11189–11195.
- Allen, N.J. & Barres, B.A., 2009. Neuroscience: Glia - more than just brain glue. *Nature*, 457(7230), pp.675–677.
- Altelaar, A.F.M. et al., 2006. Gold-Enhanced Biomolecular Surface Imaging of Cells and Tissue by SIMS and MALDI Mass Spectrometry. *Analytical Chemistry*, 78(3), pp.734–742.
- Ballios, B.G. et al., 2011. Central Nervous System. In *Principles of Regenerative Medicine*. Elsevier, pp. 1023–1046.
- Benzinger, T.L.S. et al., 2009. Special Proceedings on Blast Injury and Roundtable Participants*. *Journal of NEUROTRAUMA*.
- Beynon, S.B. & Walker, F.R., 2012. Microglial activation in the injured and healthy brain: What are we really talking about? Practical and theoretical issues associated with the measurement of changes in microglial morphology. *Neuroscience*, 225, pp.162–171.
- Bianchi, M.E., 2007. DAMPs, PAMPs and alarmins: all we need to know about danger. *Journal of Leukocyte Biology*, 81(1), pp.1–5.
- Biber, K. et al., 2007. Neuronal “On” and “Off” signals control microglia. *Trends in Neurosciences*, 30(11), pp.596–602.
- Blight, A., 2000. Animal Models of Spinal Cord Injury. *Topics in Spinal Cord Injury Rehabilitation*, 6(2), pp.1–13.

- Bodzon-Kulakowska, A. et al., 2015. DESI-MS as a tool for direct lipid analysis in cultured cells. *Cytotechnology*, 67(6), pp.1085–1091.
- Bodzon-Kulakowska, A. & Suder, P., 2016. Imaging mass spectrometry: Instrumentation, applications, and combination with other visualization techniques. *Mass Spectrometry Reviews*, 35(1), pp.147–169.
- Borgens, R. Ben & Liu-Snyder, P., 2012. Understanding secondary injury. *The Quarterly review of biology*, 87(2), pp.89–127.
- Boughton, B.A. et al., 2016. Mass spectrometry imaging for plant biology: a review. *Phytochemistry Reviews*, 15(3), pp.445–488.
- Bradl, M. & Lassmann, H., 2010. Oligodendrocytes: biology and pathology. *Acta Neuropathologica*, 119(1), pp.37–53.
- Brooks, N. et al., 1986. The five year outcome of severe blunt head injury: a relative's view. *Journal of neurology, neurosurgery, and psychiatry*, 49(7), pp.764–70.
- Brown, G.C. & Vilalta, A., 2015. How microglia kill neurons. *Brain Research*, 1628(Pt B), pp.288–297.
- Bruce, J.C., Oatway, M.A. & Weaver, L.C., 2002. Chronic pain after clip-compression injury of the rat spinal cord. *Experimental neurology*, 178(1), pp.33–48.
- Cameron, L.C., 2012. Mass spectrometry imaging: Facts and perspectives from a non-mass spectrometrists point of view. *Methods*, 57(4), pp.417–422.
- Campbell, D.I. et al., 2012. Improved spatial resolution in the imaging of biological tissue using desorption electrospray ionization. *Analytical and Bioanalytical Chemistry*, 404(2), pp.389–398.
- Caprioli, R.M., Farmer, T.B. & Gile, J., 1997. Molecular imaging of biological samples: localization of peptides and proteins using MALDI-TOF MS. *Analytical chemistry*, 69(23), pp.4751–60.
- Carvey, P.M., Hendey, B. & Monahan, A.J., 2009. The blood-brain barrier in neurodegenerative disease: a rhetorical perspective. *Journal of Neurochemistry*, 111(2), pp.291–314.
- Castaing & Slodzian, 1962. Optique corpusculaire—Premiers essais de microanalyse par emission ionique secondaire.e. *Microscopie*, 1, pp.395–399.
- Cekanaviciute, E. & Buckwalter, M.S., 2016. Astrocytes: Integrative Regulators of Neuroinflammation in Stroke and Other Neurological Diseases. *Neurotherapeutics*, 13(4),

pp.685–701.

- Chavarría, A. & Cárdenas, G., 2013. Neuronal influence behind the central nervous system regulation of the immune cells. *Frontiers in Integrative Neuroscience*, 7, p.64.
- Cheriyian, T. et al., 2014. Spinal cord injury models: a review. *Spinal Cord*, 52(8), pp.588–595.
- Chiu, C.-W., Cheng, H. & Hsieh, S.-L., 2017. Contusion Spinal Cord Injury Rat Model. *BIO-PROTOCOL*, 7(12).
- Chung, S. & Shen, W., 2015. Laser capture microdissection: from its principle to applications in research on neurodegeneration. *Neural Regeneration Research*, 10(6), p.897.
- Cizkova, D. et al., 2014a. Alterations of protein composition along the rostro-caudal axis after spinal cord injury: proteomic, in vitro and in vivo analyses. *Frontiers in Cellular Neuroscience*, 8(April), p.105.
- Cizkova, D. et al., 2014b. Alterations of protein composition along the rostro-caudal axis after spinal cord injury: proteomic, in vitro and in vivo analyses. *Frontiers in Cellular Neuroscience*, 8.
- Cizkova, D. et al., 2018. Localized Intrathecal Delivery of Mesenchymal Stromal Cells Conditioned Medium Improves Functional Recovery in a Rat Model of Spinal Cord Injury. *International Journal of Molecular Sciences*, 19(3), p.870.
- Clairmont, A.C. & Matkovic, V., 2005. Acute Spinal Cord Injury and Traumatic Brain Injury. In *The Bone and Mineral Manual*. Elsevier, pp. 75–79.
- Colombo, E. & Farina, C., 2016. Astrocytes: Key Regulators of Neuroinflammation. *Trends in Immunology*, 37(9), pp.608–620.
- Colton, C.A., 2009. Heterogeneity of Microglial Activation in the Innate Immune Response in the Brain. *Journal of Neuroimmune Pharmacology*, 4(4), pp.399–418.
- Cordiglieri, C. & Farina, C., 2010. Astrocytes Exert and Control Immune Responses in the Brain. *Current Immunology Reviews*, 6(3), pp.150–159.
- Crececius, A.C. et al., 2005. Three-dimensional visualization of protein expression in mouse brain structures using imaging mass spectrometry. *Journal of the American Society for Mass Spectrometry*, 16(7), pp.1093–1099.
- Crews, F.T. & Vetreno, R.P., 2016. Mechanisms of neuroimmune gene induction in alcoholism. *Psychopharmacology*, 233(9), pp.1543–1557.
- Das, M., Mohapatra, S. & Mohapatra, S.S., 2012. New perspectives on central and peripheral

- immune responses to acute traumatic brain injury. *Journal of Neuroinflammation*, 9(1), p.742.
- Delcourt, V. et al., 2017. Combined Mass Spectrometry Imaging and Top-down Microproteomics Reveals Evidence of a Hidden Proteome in Ovarian Cancer. *EBioMedicine*, 21, pp.55–64.
- Delcourt, V. et al., 2018. Spatially-Resolved Top-down Proteomics Bridged to MALDI MS Imaging Reveals the Molecular Physiome of Brain Regions. *Molecular & Cellular Proteomics*, 17(2), pp.357–372.
- Devaux, S. et al., 2016. Proteomic Analysis of the Spatio-temporal Based Molecular Kinetics of Acute Spinal Cord Injury Identifies a Time- and Segment-specific Window for Effective Tissue Repair. *Molecular & Cellular Proteomics*, 15(8), pp.2641–2670.
- DeVivo, M. et al., 2011. Costs of Care Following Spinal Cord Injury. *Topics in Spinal Cord Injury Rehabilitation*, 16(4), pp.1–9.
- Dixon, C.E. et al., 1987. A fluid percussion model of experimental brain injury in the rat. *Journal of Neurosurgery*, 67(1), pp.110–119.
- Dolan, E.J. & Tator, C.H., 1979. A new method for testing the force of clips for aneurysms or experimental spinal cord compression. *Journal of Neurosurgery*, 51(2), pp.229–233.
- Donnelly, D.J. et al., 2011. Deficient CX3CR1 Signaling Promotes Recovery after Mouse Spinal Cord Injury by Limiting the Recruitment and Activation of Ly6Clo/iNOS⁺ Macrophages. *Journal of Neuroscience*, 31(27), pp.9910–9922.
- Fenn, J.B. et al., 1989. Electrospray ionization for mass spectrometry of large biomolecules. *Science (New York, N.Y.)*, 246(4926), pp.64–71.
- Ferrante, C.J. & Leibovich, S.J., 2012. Regulation of Macrophage Polarization and Wound Healing. *Advances in Wound Care*, 1(1), pp.10–16.
- Fleminger, S. et al., 2003. The neuropsychiatry of depression after brain injury. *Neuropsychological Rehabilitation*, 13(1–2), pp.65–87.
- Flores-Ibarra, A. et al., 2018. Crystallization of a human galectin-3 variant with two ordered segments in the shortened N-terminal tail. *Scientific Reports*, 8(1), p.9835.
- Fournier, I., Day, R. & Salzet, M., 2003. Direct analysis of neuropeptides by in situ MALDI-TOF mass spectrometry in the rat brain. *Neuro endocrinology letters*, 24(1–2), pp.9–14.
- Franck, J. et al., 2009. MALDI Imaging Mass Spectrometry. *Molecular & Cellular Proteomics*,

- 8(9), pp.2023–2033.
- Franck, J. et al., 2010. MALDI mass spectrometry imaging of proteins exceeding 30,000 daltons. *Medical science monitor : international medical journal of experimental and clinical research*, 16(9), p.BR293-9.
- Franck, J. et al., 2009. On-Tissue N-Terminal Peptide Derivatizations for Enhancing Protein Identification in MALDI Mass Spectrometric Imaging Strategies. *Analytical Chemistry*, 81(20), pp.8305–8317.
- Franck, J. et al., 2013. Quantification-Based Mass Spectrometry Imaging of Proteins by Parafilm Assisted Microdissection. *Analytical Chemistry*, 85(17), pp.8127–8134.
- Gadani, S.P. et al., 2015. Dealing with Danger in the CNS: The Response of the Immune System to Injury. *Neuron*, 87(1), pp.47–62.
- G Marshall, A. et al., 2013. Mass resolution and mass accuracy: how much is enough? *Mass spectrometry (Tokyo, Japan)*, 2(Spec Iss), p.S0009.
- Gamble, L.J. & Anderton, C.R., 2016. Secondary Ion Mass Spectrometry Imaging of Tissues, Cells, and Microbial Systems. *Microscopy today*, 24(2), pp.24–31.
- Gattlen, C. et al., 2016. Spinal Cord T-Cell Infiltration in the Rat Spared Nerve Injury Model: A Time Course Study. *International Journal of Molecular Sciences*, 17(3), p.352.
- Gemperline, E., Chen, B. & Li, L., 2014. Challenges and recent advances in mass spectrometric imaging of neurotransmitters. *Bioanalysis*, 6(4), pp.525–540.
- Graeber, M.B., 2010. Changing Face of Microglia. *Science*, 330(6005), pp.783–788.
- Gutstein, H.B. et al., 2008. Microproteomics: Analysis of protein diversity in small samples. *Mass Spectrometry Reviews*, 27(4), pp.316–330.
- Hankin, J.A., Barkley, R.M. & Murphy, R.C., 2007. Sublimation as a method of matrix application for mass spectrometric imaging. *Journal of the American Society for Mass Spectrometry*, 18(9), pp.1646–1652.
- Hartline, D.K. & Colman, D.R., 2007. Rapid Conduction and the Evolution of Giant Axons and Myelinated Fibers. *Current Biology*, 17(1), pp.R29–R35.
- Haydon, P.G. & Carmignoto, G., 2006. Astrocyte Control of Synaptic Transmission and Neurovascular Coupling. *Physiological Reviews*, 86(3), pp.1009–1031.
- Heyman, H.M. & Dubery, I.A., 2016. The potential of mass spectrometry imaging in plant metabolomics: a review. *Phytochemistry Reviews*, 15(2), pp.297–316.

- Hong, S.-M. et al., 2013. Increased Expression of High-Mobility Group Protein B1 in Chronic Rhinosinusitis. *American Journal of Rhinology & Allergy*, 27(4), pp.278–282.
- Hu, P. et al., 2016. Single Cell Isolation and Analysis. *Frontiers in cell and developmental biology*, 4, p.116.
- Humphreys, I. et al., 2013. The costs of traumatic brain injury: a literature review. *ClinicoEconomics and Outcomes Research*, 5, p.281.
- Jackson, S.N., Wang, H.-Y.J. & Woods, A.S., 2005. Direct Profiling of Lipid Distribution in Brain Tissue Using MALDI-TOFMS. *Analytical Chemistry*, 77(14), pp.4523–4527.
- Kelly, Á. et al., 2001. The Anti-inflammatory Cytokine, Interleukin (IL)-10, Blocks the Inhibitory Effect of IL-1 β on Long Term Potentiation. *Journal of Biological Chemistry*, 276(49), pp.45564–45572.
- Kerschensteiner, M. et al., 1999. Activated human T cells, B cells, and monocytes produce brain-derived neurotrophic factor in vitro and in inflammatory brain lesions: a neuroprotective role of inflammation? *The Journal of experimental medicine*, 189(5), pp.865–70.
- Kirshblum, S.C. et al., 2011. International standards for neurological classification of spinal cord injury (Revised 2011). *The Journal of Spinal Cord Medicine*, 34(6), pp.535–546.
- Kobeissy, F.H. et al., 2006. Novel Differential Neuroproteomics Analysis of Traumatic Brain Injury in Rats. *Molecular & Cellular Proteomics*, 5(10), pp.1887–1898.
- Lemaire, R., Wisztorski, M., et al., 2006. MALDI-MS Direct Tissue Analysis of Proteins: Improving Signal Sensitivity Using Organic Treatments. *Analytical Chemistry*, 78(20), pp.7145–7153.
- Lemaire, R., Tabet, J.C., et al., 2006. Solid Ionic Matrixes for Direct Tissue Analysis and MALDI Imaging. *Analytical Chemistry*, 78(3), pp.809–819.
- LIGHTHALL, J.W., 1988. Controlled Cortical Impact: A New Experimental Brain Injury Model. *Journal of Neurotrauma*, 5(1), pp.1–15.
- Linker, R.A. et al., 2010. Functional role of brain-derived neurotrophic factor in neuroprotective autoimmunity: therapeutic implications in a model of multiple sclerosis. *Brain*, 133(8), pp.2248–2263.
- Maezawa, I. & Jin, L.W., 2010. Rett Syndrome Microglia Damage Dendrites and Synapses by the Elevated Release of Glutamate. *Journal of Neuroscience*, 30(15), pp.5346–5356.
- Majdan, M. et al., 2017. Mortality due to traumatic spinal cord injuries in Europe: a cross-

- sectional and pooled analysis of population-wide data from 22 countries. *Scandinavian Journal of Trauma, Resuscitation and Emergency Medicine*, 25(1), p.64.
- Mann, M. & Kelleher, N.L., 2008. Precision proteomics: The case for high resolution and high mass accuracy. *Proceedings of the National Academy of Sciences*, 105(47), pp.18132–18138.
- Mantovani, A. et al., 2011. Neutrophils in the activation and regulation of innate and adaptive immunity. *Nature Reviews Immunology*, 11(8), pp.519–531.
- Marklund, N., 2016. Rodent Models of Traumatic Brain Injury: Methods and Challenges. In *Methods in molecular biology* (Clifton, N.J.). pp. 29–46.
- Marklund, N. & Hillered, L., 2011. Animal modelling of traumatic brain injury in preclinical drug development: where do we go from here? *British Journal of Pharmacology*, 164(4), pp.1207–1229.
- Martinotti, S., Patrone, M. & Ranzato, E., 2015. Emerging roles for HMGB1 protein in immunity, inflammation, and cancer. *ImmunoTargets and therapy*, 4, pp.101–9.
- Meaney, D.F., Morrison, B. & Dale Bass, C., 2014. The mechanics of traumatic brain injury: a review of what we know and what we need to know for reducing its societal burden. *Journal of biomechanical engineering*, 136(2), p.21008.
- Meriaux, C. et al., 2010. Liquid ionic matrixes for MALDI mass spectrometry imaging of lipids. *Journal of proteomics*, 73(6), pp.1204–18.
- Miller, B.A., Bresnahan, J.C. & Beattie, M.S., 2009. Apoptosis in Nervous System Injury. In *Encyclopedia of Neuroscience*. Elsevier, pp. 523–529.
- Monnier, P.P. et al., 2003. The Rho/ROCK pathway mediates neurite growth-inhibitory activity associated with the chondroitin sulfate proteoglycans of the CNS glial scar. *Molecular and cellular neurosciences*, 22(3), pp.319–30.
- Moreno-Gordaliza, E. et al., 2017. MALDI-LTQ-Orbitrap mass spectrometry imaging for lipidomic analysis in kidney under cisplatin chemotherapy. *Talanta*, 164, pp.16–26.
- Muldoon, L.L. et al., 2013. Immunologic Privilege in the Central Nervous System and the Blood–Brain Barrier. *Journal of Cerebral Blood Flow & Metabolism*, 33(1), pp.13–21.
- Murgoci, A.-N. et al., 2018. Brain-Cortex Microglia-Derived Exosomes: Nanoparticles for Glioma Therapy. *ChemPhysChem*, 19(10), pp.1205–1214.
- Mustafa, D., Kros, J.M. & Luiders, T., 2008. Combining laser capture microdissection and

- proteomics techniques. *Methods in molecular biology* (Clifton, N.J.), 428, pp.159–78.
- Nakae, A. et al., 2011. The Animal Model of Spinal Cord Injury as an Experimental Pain Model. *Journal of Biomedicine and Biotechnology*, 2011, pp.1–11.
- Neniskyte, U., Vilalta, A. & Brown, G.C., 2014. Tumour necrosis factor alpha-induced neuronal loss is mediated by microglial phagocytosis. *FEBS Letters*, 588(17), pp.2952–2956.
- Nielsen, M.M.B. et al., 2016. Mass spectrometry imaging of biomarker lipids for phagocytosis and signalling during focal cerebral ischaemia. *Nature Publishing Group*, (May), pp.1–14.
- Nimmerjahn, A., 2005. Resting Microglial Cells Are Highly Dynamic Surveillants of Brain Parenchyma in Vivo. *Science*, 308(5726), pp.1314–1318.
- Norris, J.L. & Caprioli, R.M., 2013. Analysis of Tissue Specimens by Matrix-Assisted Laser Desorption/Ionization Imaging Mass Spectrometry in Biological and Clinical Research. *Chemical Reviews*, 113(4), pp.2309–2342.
- O’Connell, K.M. & Littleton-Kearney, M.T., 2013. The Role of Free Radicals in Traumatic Brain Injury. *Biological Research For Nursing*, 15(3), pp.253–263.
- de Oliveira, S. et al., 2013. Cxcl8 (IL-8) Mediates Neutrophil Recruitment and Behavior in the Zebrafish Inflammatory Response. *The Journal of Immunology*, 190(8), pp.4349–4359.
- Orendáčová, J. et al., 2001. Cauda equina syndrome. *Progress in Neurobiology*, 64(6), pp.613–637.
- Ostermann, K.M. et al., 2014. MALDI Orbitrap mass spectrometry for fast and simplified analysis of novel street and designer drugs. *Clinica Chimica Acta*, 433, pp.254–258.
- Palmer, A.D. & Alexandrov, T., 2015. Serial 3D Imaging Mass Spectrometry at Its Tipping Point. *Analytical Chemistry*, 87(8), pp.4055–4062.
- Pérez-Cerdá, F., Sánchez-Gómez, M.V. & Matute, C., 2015. Pío del Río Hortega and the discovery of the oligodendrocytes. *Frontiers in Neuroanatomy*, 9.
- Perry, V.H. & Teeling, J., 2013. Microglia and macrophages of the central nervous system: the contribution of microglia priming and systemic inflammation to chronic neurodegeneration. *Seminars in Immunopathology*, 35(5), pp.601–612.
- Pflugradt, R. et al., 2011. A novel and effective separation method for single mitochondria analysis. *Mitochondrion*, 11(2), pp.308–314.
- Popescu C et al., 2015. Actual data on epidemiological evolution and prevention endeavours regarding traumatic brain injury. *Journal of Medicine and Life*, 8(3), pp.272–277.

- Popovich, P.G. et al., 1999. Depletion of Hematogenous Macrophages Promotes Partial Hindlimb Recovery and Neuroanatomical Repair after Experimental Spinal Cord Injury. *Experimental Neurology*, 158(2), pp.351–365.
- Popovich, P.G., Stokes, B.T. & Whitacre, C.C., 1996. Concept of autoimmunity following spinal cord injury: possible roles for T lymphocytes in the traumatized central nervous system. *Journal of neuroscience research*, 45(4), pp.349–63.
- Quanico, J. et al., 2013a. Development of liquid microjunction extraction strategy for improving protein identification from tissue sections. *Journal of Proteomics*, 79, pp.200–218.
- Quanico, J. et al., 2013b. Development of liquid microjunction extraction strategy for improving protein identification from tissue sections. *Journal of Proteomics*, 79, pp.200–218.
- Quanico, J. et al., 2015. Parafilm-assisted microdissection: a sampling method for mass spectrometry-based identification of differentially expressed prostate cancer protein biomarkers. *Chemical Communications*, 51(22), pp.4564–4567.
- van Remoortere, A. et al., 2010. MALDI Imaging and Profiling MS of Higher Mass Proteins from Tissue. *Journal of the American Society for Mass Spectrometry*, 21(11), pp.1922–9.
- Römpp, A. & Spengler, B., 2013. Mass spectrometry imaging with high resolution in mass and space. *Histochemistry and Cell Biology*, 139(6), pp.759–783.
- Roozenbeek, B., Maas, A.I.R. & Menon, D.K., 2013. Changing patterns in the epidemiology of traumatic brain injury. *Nature Reviews Neurology*, 9(4), pp.231–236.
- Rosales, C. et al., 2016. Neutrophils: Their Role in Innate and Adaptive Immunity. *Journal of Immunology Research*, 2016, pp.1–2.
- Roux, A. et al., 2016. Mass spectrometry imaging of rat brain lipid profile changes over time following traumatic brain injury. *Journal of neuroscience methods*, pp.1–14.
- Rudge, J.S. & Silver, J., 1990. Inhibition of neurite outgrowth on astroglial scars in vitro. *The Journal of neuroscience : the official journal of the Society for Neuroscience*, 10(11), pp.3594–603.
- RUSSELL, W.R. & SMITH, A., 1961. Post-Traumatic Amnesia in Closed Head Injury. *Archives of Neurology*, 5(1), pp.4–17.
- Saatman, K.E. et al., 2006. Differential Behavioral and Histopathological Responses to Graded Cortical Impact Injury in Mice. *Journal of Neurotrauma*, 23(8), pp.1241–1253.
- Sawant, K. V. et al., 2016. Chemokine CXCL1 mediated neutrophil recruitment: Role of

- glycosaminoglycan interactions. *Scientific Reports*, 6(1), p.33123.
- Schwartz, S.A., Reyzer, M.L. & Caprioli, R.M., 2003. Direct tissue analysis using matrix-assisted laser desorption/ionization mass spectrometry: practical aspects of sample preparation. *Journal of Mass Spectrometry*, 38(7), pp.699–708.
- Sharif-Alhoseini, M. & Rahimi-Movaghar, V., 2014. Animal Models in Traumatic Spinal Cord Injury. In *Topics in Paraplegia*. InTech.
- Sharma, D. & Kanneganti, T.-D., 2016. The cell biology of inflammasomes: Mechanisms of inflammasome activation and regulation. *The Journal of Cell Biology*, 213(6), pp.617–629.
- Shoichet, M.S. et al., 2008. *Strategies for Regeneration and Repair in the Injured Central Nervous System*, CRC Press/Taylor & Francis.
- Soares, H.D. et al., 1995. Inflammatory leukocytic recruitment and diffuse neuronal degeneration are separate pathological processes resulting from traumatic brain injury. *The Journal of neuroscience : the official journal of the Society for Neuroscience*, 15(12), pp.8223–33.
- Sofroniew, M. V & Vinters, H. V, 2010. Astrocytes: biology and pathology. *Acta Neuropathologica*, 119(1), pp.7–35.
- Sperlágh, B. & Illes, P., 2014. P2X7 receptor: an emerging target in central nervous system diseases. *Trends in Pharmacological Sciences*, 35(10), pp.537–547.
- Sroga, J.M. et al., 2003. Rats and mice exhibit distinct inflammatory reactions after spinal cord injury. *The Journal of Comparative Neurology*, 462(2), pp.223–240.
- SUGIURA, Y., SHIMMA, S. & SETOU, M., 2006. Thin Sectioning Improves the Peak Intensity and Signal-to-Noise Ratio in Direct Tissue Mass Spectrometry. *Journal of the Mass Spectrometry Society of Japan*, 54(2), pp.45–48.
- Sutton, L.P. et al., 2018. Orphan receptor GPR158 controls stress-induced depression. *eLife*, 7.
- Tagliaferri, F. et al., 2006. A systematic review of brain injury epidemiology in Europe. *Acta Neurochirurgica*, 148(3), pp.255–268.
- Takats, Z., 2004. Mass Spectrometry Sampling Under Ambient Conditions with Desorption Electrospray Ionization. *Science*, 306(5695), pp.471–473.
- Takeuchi, O. & Akira, S., 2010. Pattern Recognition Receptors and Inflammation. *Cell*, 140(6), pp.805–820.
- Tambuyzer, B.R., Ponsaerts, P. & Nouwen, E.J., 2009. Microglia: gatekeepers of central nervous system immunology. *Journal of Leukocyte Biology*, 85(3), pp.352–370.

- Tang, D. et al., 2012. PAMPs and DAMPs: signal 0s that spur autophagy and immunity. *Immunological Reviews*, 249(1), pp.158–175.
- Taoka, Y. et al., 1997. Role of neutrophils in spinal cord injury in the rat. *Neuroscience*, 79(4), pp.1177–82.
- TARLOV, I.M., KLINGER, H. & VITALE, S., 1953. Spinal cord compression studies. I. Experimental techniques to produce acute and gradual compression. *A.M.A. archives of neurology and psychiatry*, 70(6), pp.813–9.
- Taylor, C.A. et al., 2017. Traumatic Brain Injury–Related Emergency Department Visits, Hospitalizations, and Deaths — United States, 2007 and 2013. *MMWR. Surveillance Summaries*, 66(9), pp.1–16.
- Teasdale, G. & Jennett, B., 1974. ASSESSMENT OF COMA AND IMPAIRED CONSCIOUSNESS. *The Lancet*, 304(7872), pp.81–84.
- The national SCI statistical center., 2012. Spinal Cord Injury Facts and Figures at a Glance. *The Journal of Spinal Cord Medicine*, 35(1), pp.68–69.
- Thiele, H. et al., 2014. 2D and 3D MALDI-imaging: Conceptual strategies for visualization and data mining. *Biochimica et Biophysica Acta (BBA) - Proteins and Proteomics*, 1844(1), pp.117–137.
- Turner, C.M. et al., 2014. Is the inflammasome a potential therapeutic target in renal disease? *BMC Nephrology*, 15(1), p.21.
- Walsh, J.T. et al., 2015. MHCII-independent CD4+ T cells protect injured CNS neurons via IL-4. *Journal of Clinical Investigation*, 125(2), pp.699–714.
- Walsh, J.T., Watson, N. & Kipnis, J., 2014. T cells in the central nervous system: messengers of destruction or purveyors of protection? *Immunology*, 141(3), pp.340–344.
- Wang, J., 2018. Neutrophils in tissue injury and repair. *Cell and Tissue Research*, 371(3), pp.531–539.
- Wang, K. et al., 2016. Beclin1 and HMGB1 ameliorate the α -synuclein-mediated autophagy inhibition in PC12 cells. *Diagnostic Pathology*, 11(1), p.15.
- Wang, K.K. et al., 2005. Proteomic identification of biomarkers of traumatic brain injury. *Expert Review of Proteomics*, 2(4), pp.603–614.
- Wanner, I.B. et al., 2013. Glial Scar Borders Are Formed by Newly Proliferated, Elongated Astrocytes That Interact to Corral Inflammatory and Fibrotic Cells via STAT3-Dependent

- Mechanisms after Spinal Cord Injury. *Journal of Neuroscience*, 33(31), pp.12870–12886.
- Waters, R.L., Adkins, R.H. & Yakura, J.S., 1991. Definition of complete spinal cord injury. *Spinal Cord*, 29(9), pp.573–581.
- Watson, B.D. et al., 1986. Photochemically induced spinal cord injury in the rat. *Brain research*, 367(1–2), pp.296–300.
- Wisztorski, M. et al., 2010. MALDI Direct Analysis and Imaging of Frozen Versus FFPE Tissues: What Strategy for Which Sample? In *Methods in molecular biology* (Clifton, N.J.). pp. 303–322.
- Wisztorski, M. et al., 2013. Microproteomics by liquid extraction surface analysis: Application to FFPE tissue to study the fimbria region of tubo-ovarian cancer. *PROTEOMICS - Clinical Applications*, 7(3–4), pp.234–240.
- Wood, R.L. & Yurdakul, L.K., 1997. Change in relationship status following traumatic brain injury. *Brain injury*, 11(7), pp.491–501.
- Wu, C. et al., 2012. A protease for “middle-down” proteomics. *Nature Methods*, 9(8), pp.822–824.
- Wu, C. et al., 2013. Mass spectrometry imaging under ambient conditions. *Mass Spectrometry Reviews*, 32(3), pp.218–243.
- Xiong, Y., Mahmood, A. & Chopp, M., 2013. Animal models of traumatic brain injury. *Nature Reviews Neuroscience*, 14(2), pp.128–142.
- Yang, J. & Caprioli, R.M., 2011. Matrix Sublimation/Recrystallization for Imaging Proteins by Mass Spectrometry at High Spatial Resolution. *Analytical Chemistry*, 83(14), pp.5728–5734.
- Yang, Z. & Wang, K.K.W., 2015. Glial fibrillary acidic protein: From intermediate filament assembly and gliosis to neurobiomarker. *Trends in Neurosciences*, 38(6), pp.364–374.
- Yates, J.R., 2004. Mass Spectral Analysis in Proteomics. *Annual Review of Biophysics and Biomolecular Structure*, 33(1), pp.297–316.
- Yin, Y. et al., 2006. Oncomodulin is a macrophage-derived signal for axon regeneration in retinal ganglion cells. *Nature Neuroscience*, 9(6), pp.843–852.
- Zetterberg, H., Smith, D.H. & Blennow, K., 2013. Biomarkers of mild traumatic brain injury in cerebrospinal fluid and blood. *Nature Reviews Neurology*, 9(4), pp.201–210.
- Zhang, Y. et al., 2013. Protein Analysis by Shotgun/Bottom-up Proteomics. *Chemical Reviews*,

113(4), pp.2343–2394.

Zhao, X. et al., 2018. Noninflammatory Changes of Microglia Are Sufficient to Cause Epilepsy.
Cell Reports, 22(8), pp.2080–2093.

ANNEX

**JOHN WILEY AND SONS LICENSE
TERMS AND CONDITIONS**

Oct 17, 2018

This Agreement between INSERM U1192, Universite de Lille -- Khalil Mallah ("You") and John Wiley and Sons ("John Wiley and Sons") consists of your license details and the terms and conditions provided by John Wiley and Sons and Copyright Clearance Center.

License Number	4451380692016
License date	Oct 17, 2018
Licensed Content Publisher	John Wiley and Sons
Licensed Content Publication	Journal of Neurochemistry
Licensed Content Title	The blood-brain barrier in neurodegenerative disease: a rhetorical perspective
Licensed Content Author	Paul M. Carvey, Bill Hendey, Angela J. Monahan
Licensed Content Date	Sep 23, 2009
Licensed Content Volume	111
Licensed Content Issue	2
Licensed Content Pages	24
Type of use	Dissertation/Thesis
Requestor type	University/Academic
Format	Print and electronic
Portion	Figure/table
Number of figures/tables	1
Original Wiley figure/table number(s)	Figure 1
Will you be translating?	No
Title of your thesis / dissertation	In Depth Systemic Biology Analysis of Central Nervous System Injuries
Expected completion date	Oct 2018
Expected size (number of pages)	300
Requestor Location	INSERM U1192, Universite de Lille Cité Scientifique, Bât SN3, 1er étage Villeneuve D'Ascq, 59650 France Attn: Khalil Mallah
Publisher Tax ID	EU826007151
Total	0.00 EUR

TERMS AND CONDITIONS

This copyrighted material is owned by or exclusively licensed to John Wiley & Sons, Inc. or one of its group companies (each a "Wiley Company") or handled on behalf of a society with which a Wiley Company has exclusive publishing rights in relation to a particular work (collectively "WILEY"). By clicking "accept" in connection with completing this licensing transaction, you agree that the following terms and conditions apply to this transaction (along with the billing and payment terms and conditions established by the Copyright Clearance Center Inc., ("CCC's Billing and Payment terms and conditions"), at the time that you opened your RightsLink account (these are available at any time at <http://myaccount.copyright.com>).

Terms and Conditions

- The materials you have requested permission to reproduce or reuse (the "Wiley Materials") are protected by copyright.
- You are hereby granted a personal, non-exclusive, non-sub licensable (on a stand-alone basis), non-transferable, worldwide, limited license to reproduce the Wiley Materials for the purpose specified in the licensing process. This license, **and any CONTENT (PDF or image file) purchased as part of your order**, is for a one-time use only and limited to any maximum distribution number specified in the license. The first instance of republication or reuse granted by this license must be completed within two years of the date of the grant of this license (although copies prepared before the end date may be distributed thereafter). The Wiley Materials shall not be used in any other manner or for any other purpose, beyond what is granted in the license. Permission is granted subject to an appropriate acknowledgement given to the author, title of the material/book/journal and the publisher. You shall also duplicate the copyright notice that appears in the Wiley publication in your use of the Wiley Material. Permission is also granted on the understanding that nowhere in the text is a previously published source acknowledged for all or part of this Wiley Material. Any third party content is expressly excluded from this permission.
- With respect to the Wiley Materials, all rights are reserved. Except as expressly granted by the terms of the license, no part of the Wiley Materials may be copied, modified, adapted (except for minor reformatting required by the new Publication), translated, reproduced, transferred or distributed, in any form or by any means, and no derivative works may be made based on the Wiley Materials without the prior permission of the respective copyright owner. **For STM Signatory Publishers clearing permission under the terms of the [STM Permissions Guidelines](#) only, the terms of the license are extended to include subsequent editions and for editions in other languages, provided such editions are for the work as a whole in situ and does not involve the separate exploitation of the permitted figures or extracts**, You may not alter, remove or suppress in any manner any copyright, trademark or other notices displayed by the

Wiley Materials. You may not license, rent, sell, loan, lease, pledge, offer as security, transfer or assign the Wiley Materials on a stand-alone basis, or any of the rights granted to you hereunder to any other person.

- The Wiley Materials and all of the intellectual property rights therein shall at all times remain the exclusive property of John Wiley & Sons Inc, the Wiley Companies, or their respective licensors, and your interest therein is only that of having possession of and the right to reproduce the Wiley Materials pursuant to Section 2 herein during the continuance of this Agreement. You agree that you own no right, title or interest in or to the Wiley Materials or any of the intellectual property rights therein. You shall have no rights hereunder other than the license as provided for above in Section 2. No right, license or interest to any trademark, trade name, service mark or other branding ("Marks") of WILEY or its licensors is granted hereunder, and you agree that you shall not assert any such right, license or interest with respect thereto
- NEITHER WILEY NOR ITS LICENSORS MAKES ANY WARRANTY OR REPRESENTATION OF ANY KIND TO YOU OR ANY THIRD PARTY, EXPRESS, IMPLIED OR STATUTORY, WITH RESPECT TO THE MATERIALS OR THE ACCURACY OF ANY INFORMATION CONTAINED IN THE MATERIALS, INCLUDING, WITHOUT LIMITATION, ANY IMPLIED WARRANTY OF MERCHANTABILITY, ACCURACY, SATISFACTORY QUALITY, FITNESS FOR A PARTICULAR PURPOSE, USABILITY, INTEGRATION OR NON-INFRINGEMENT AND ALL SUCH WARRANTIES ARE HEREBY EXCLUDED BY WILEY AND ITS LICENSORS AND WAIVED BY YOU.
- WILEY shall have the right to terminate this Agreement immediately upon breach of this Agreement by you.
- You shall indemnify, defend and hold harmless WILEY, its Licensors and their respective directors, officers, agents and employees, from and against any actual or threatened claims, demands, causes of action or proceedings arising from any breach of this Agreement by you.
- IN NO EVENT SHALL WILEY OR ITS LICENSORS BE LIABLE TO YOU OR ANY OTHER PARTY OR ANY OTHER PERSON OR ENTITY FOR ANY SPECIAL, CONSEQUENTIAL, INCIDENTAL, INDIRECT, EXEMPLARY OR PUNITIVE DAMAGES, HOWEVER CAUSED, ARISING OUT OF OR IN CONNECTION WITH THE DOWNLOADING, PROVISIONING, VIEWING OR USE OF THE MATERIALS REGARDLESS OF THE FORM OF ACTION, WHETHER FOR BREACH OF CONTRACT, BREACH OF WARRANTY, TORT, NEGLIGENCE, INFRINGEMENT OR OTHERWISE (INCLUDING, WITHOUT LIMITATION, DAMAGES BASED ON LOSS OF PROFITS, DATA, FILES, USE, BUSINESS OPPORTUNITY OR CLAIMS OF THIRD PARTIES), AND WHETHER OR NOT THE PARTY HAS BEEN ADVISED OF THE POSSIBILITY OF SUCH DAMAGES. THIS LIMITATION SHALL

APPLY NOTWITHSTANDING ANY FAILURE OF ESSENTIAL PURPOSE OF ANY LIMITED REMEDY PROVIDED HEREIN.

- Should any provision of this Agreement be held by a court of competent jurisdiction to be illegal, invalid, or unenforceable, that provision shall be deemed amended to achieve as nearly as possible the same economic effect as the original provision, and the legality, validity and enforceability of the remaining provisions of this Agreement shall not be affected or impaired thereby.
- The failure of either party to enforce any term or condition of this Agreement shall not constitute a waiver of either party's right to enforce each and every term and condition of this Agreement. No breach under this agreement shall be deemed waived or excused by either party unless such waiver or consent is in writing signed by the party granting such waiver or consent. The waiver by or consent of a party to a breach of any provision of this Agreement shall not operate or be construed as a waiver of or consent to any other or subsequent breach by such other party.
- This Agreement may not be assigned (including by operation of law or otherwise) by you without WILEY's prior written consent.
- Any fee required for this permission shall be non-refundable after thirty (30) days from receipt by the CCC.
- These terms and conditions together with CCC's Billing and Payment terms and conditions (which are incorporated herein) form the entire agreement between you and WILEY concerning this licensing transaction and (in the absence of fraud) supersedes all prior agreements and representations of the parties, oral or written. This Agreement may not be amended except in writing signed by both parties. This Agreement shall be binding upon and inure to the benefit of the parties' successors, legal representatives, and authorized assigns.
- In the event of any conflict between your obligations established by these terms and conditions and those established by CCC's Billing and Payment terms and conditions, these terms and conditions shall prevail.
- WILEY expressly reserves all rights not specifically granted in the combination of (i) the license details provided by you and accepted in the course of this licensing transaction, (ii) these terms and conditions and (iii) CCC's Billing and Payment terms and conditions.
- This Agreement will be void if the Type of Use, Format, Circulation, or Requestor Type was misrepresented during the licensing process.
- This Agreement shall be governed by and construed in accordance with the laws of the State of New York, USA, without regards to such state's conflict of law rules. Any legal action, suit or proceeding arising out of or relating to these Terms

and Conditions or the breach thereof shall be instituted in a court of competent jurisdiction in New York County in the State of New York in the United States of America and each party hereby consents and submits to the personal jurisdiction of such court, waives any objection to venue in such court and consents to service of process by registered or certified mail, return receipt requested, at the last known address of such party.

WILEY OPEN ACCESS TERMS AND CONDITIONS

Wiley Publishes Open Access Articles in fully Open Access Journals and in Subscription journals offering Online Open. Although most of the fully Open Access journals publish open access articles under the terms of the Creative Commons Attribution (CC BY) License only, the subscription journals and a few of the Open Access Journals offer a choice of Creative Commons Licenses. The license type is clearly identified on the article.

The Creative Commons Attribution License

The [Creative Commons Attribution License \(CC-BY\)](#) allows users to copy, distribute and transmit an article, adapt the article and make commercial use of the article. The CC-BY license permits commercial and non-

Creative Commons Attribution Non-Commercial License

The [Creative Commons Attribution Non-Commercial \(CC-BY-NC\)License](#) permits use, distribution and reproduction in any medium, provided the original work is properly cited and is not used for commercial purposes.(see below)

Creative Commons Attribution-Non-Commercial-NoDerivs License

The [Creative Commons Attribution Non-Commercial-NoDerivs License](#) (CC-BY-NC-ND) permits use, distribution and reproduction in any medium, provided the original work is properly cited, is not used for commercial purposes and no modifications or adaptations are made. (see below)

Use by commercial "for-profit" organizations

Use of Wiley Open Access articles for commercial, promotional, or marketing purposes requires further explicit permission from Wiley and will be subject to a fee.

Further details can be found on Wiley Online

Library <http://olabout.wiley.com/WileyCDA/Section/id-410895.html>

Other Terms and Conditions:

v1.10 Last updated September 2015

Questions? customercare@copyright.com or +1-855-239-3415 (toll free in the US) or +1-978-646-2777.

**JOHN WILEY AND SONS LICENSE
TERMS AND CONDITIONS**

Oct 17, 2018

This Agreement between INSERM U1192, Universite de Lille -- Khalil Mallah ("You") and John Wiley and Sons ("John Wiley and Sons") consists of your license details and the terms and conditions provided by John Wiley and Sons and Copyright Clearance Center.

License Number	4451391186529
License date	Oct 17, 2018
Licensed Content Publisher	John Wiley and Sons
Licensed Content Publication	Immunology
Licensed Content Title	T cells in the central nervous system: messengers of destruction or purveyors of protection?
Licensed Content Author	James T. Walsh, Nikki Watson, Jonathan Kipnis
Licensed Content Date	Feb 10, 2014
Licensed Content Volume	141
Licensed Content Issue	3
Licensed Content Pages	5
Type of use	Dissertation/Thesis
Requestor type	University/Academic
Format	Print and electronic
Portion	Figure/table
Number of figures/tables	1
Original Wiley figure/table number(s)	Figure 1
Will you be translating?	No
Title of your thesis / dissertation	In Depth Systemic Biology Analysis of Central Nervous System Injuries
Expected completion date	Oct 2018
Expected size (number of pages)	300
Requestor Location	INSERM U1192, Universite de Lille Cité Scientifique, Bât SN3, 1er étage Villeneuve D'Ascq, 59650 France Attn: Khalil Mallah
Publisher Tax ID	EU826007151
Total	0.00 EUR

TERMS AND CONDITIONS

This copyrighted material is owned by or exclusively licensed to John Wiley & Sons, Inc. or one of its group companies (each a "Wiley Company") or handled on behalf of a society with which a Wiley Company has exclusive publishing rights in relation to a particular work (collectively "WILEY"). By clicking "accept" in connection with completing this licensing transaction, you agree that the following terms and conditions apply to this transaction (along with the billing and payment terms and conditions established by the Copyright Clearance Center Inc., ("CCC's Billing and Payment terms and conditions"), at the time that you opened your RightsLink account (these are available at any time at <http://myaccount.copyright.com>).

Terms and Conditions

- The materials you have requested permission to reproduce or reuse (the "Wiley Materials") are protected by copyright.
- You are hereby granted a personal, non-exclusive, non-sub licensable (on a stand-alone basis), non-transferable, worldwide, limited license to reproduce the Wiley Materials for the purpose specified in the licensing process. This license, **and any CONTENT (PDF or image file) purchased as part of your order**, is for a one-time use only and limited to any maximum distribution number specified in the license. The first instance of republication or reuse granted by this license must be completed within two years of the date of the grant of this license (although copies prepared before the end date may be distributed thereafter). The Wiley Materials shall not be used in any other manner or for any other purpose, beyond what is granted in the license. Permission is granted subject to an appropriate acknowledgement given to the author, title of the material/book/journal and the publisher. You shall also duplicate the copyright notice that appears in the Wiley publication in your use of the Wiley Material. Permission is also granted on the understanding that nowhere in the text is a previously published source acknowledged for all or part of this Wiley Material. Any third party content is expressly excluded from this permission.
- With respect to the Wiley Materials, all rights are reserved. Except as expressly granted by the terms of the license, no part of the Wiley Materials may be copied, modified, adapted (except for minor reformatting required by the new Publication), translated, reproduced, transferred or distributed, in any form or by any means, and no derivative works may be made based on the Wiley Materials without the prior permission of the respective copyright owner. **For STM Signatory Publishers clearing permission under the terms of the [STM Permissions Guidelines](#) only, the terms of the license are extended to include subsequent editions and for editions in other languages, provided such editions are for the work as a whole in situ and does not involve the separate exploitation of the permitted figures or extracts**, You may not alter, remove or suppress in any manner any copyright, trademark or other notices displayed by the

Wiley Materials. You may not license, rent, sell, loan, lease, pledge, offer as security, transfer or assign the Wiley Materials on a stand-alone basis, or any of the rights granted to you hereunder to any other person.

- The Wiley Materials and all of the intellectual property rights therein shall at all times remain the exclusive property of John Wiley & Sons Inc, the Wiley Companies, or their respective licensors, and your interest therein is only that of having possession of and the right to reproduce the Wiley Materials pursuant to Section 2 herein during the continuance of this Agreement. You agree that you own no right, title or interest in or to the Wiley Materials or any of the intellectual property rights therein. You shall have no rights hereunder other than the license as provided for above in Section 2. No right, license or interest to any trademark, trade name, service mark or other branding ("Marks") of WILEY or its licensors is granted hereunder, and you agree that you shall not assert any such right, license or interest with respect thereto
- NEITHER WILEY NOR ITS LICENSORS MAKES ANY WARRANTY OR REPRESENTATION OF ANY KIND TO YOU OR ANY THIRD PARTY, EXPRESS, IMPLIED OR STATUTORY, WITH RESPECT TO THE MATERIALS OR THE ACCURACY OF ANY INFORMATION CONTAINED IN THE MATERIALS, INCLUDING, WITHOUT LIMITATION, ANY IMPLIED WARRANTY OF MERCHANTABILITY, ACCURACY, SATISFACTORY QUALITY, FITNESS FOR A PARTICULAR PURPOSE, USABILITY, INTEGRATION OR NON-INFRINGEMENT AND ALL SUCH WARRANTIES ARE HEREBY EXCLUDED BY WILEY AND ITS LICENSORS AND WAIVED BY YOU.
- WILEY shall have the right to terminate this Agreement immediately upon breach of this Agreement by you.
- You shall indemnify, defend and hold harmless WILEY, its Licensors and their respective directors, officers, agents and employees, from and against any actual or threatened claims, demands, causes of action or proceedings arising from any breach of this Agreement by you.
- IN NO EVENT SHALL WILEY OR ITS LICENSORS BE LIABLE TO YOU OR ANY OTHER PARTY OR ANY OTHER PERSON OR ENTITY FOR ANY SPECIAL, CONSEQUENTIAL, INCIDENTAL, INDIRECT, EXEMPLARY OR PUNITIVE DAMAGES, HOWEVER CAUSED, ARISING OUT OF OR IN CONNECTION WITH THE DOWNLOADING, PROVISIONING, VIEWING OR USE OF THE MATERIALS REGARDLESS OF THE FORM OF ACTION, WHETHER FOR BREACH OF CONTRACT, BREACH OF WARRANTY, TORT, NEGLIGENCE, INFRINGEMENT OR OTHERWISE (INCLUDING, WITHOUT LIMITATION, DAMAGES BASED ON LOSS OF PROFITS, DATA, FILES, USE, BUSINESS OPPORTUNITY OR CLAIMS OF THIRD PARTIES), AND WHETHER OR NOT THE PARTY HAS BEEN ADVISED OF THE POSSIBILITY OF SUCH DAMAGES. THIS LIMITATION SHALL

APPLY NOTWITHSTANDING ANY FAILURE OF ESSENTIAL PURPOSE OF ANY LIMITED REMEDY PROVIDED HEREIN.

- Should any provision of this Agreement be held by a court of competent jurisdiction to be illegal, invalid, or unenforceable, that provision shall be deemed amended to achieve as nearly as possible the same economic effect as the original provision, and the legality, validity and enforceability of the remaining provisions of this Agreement shall not be affected or impaired thereby.
- The failure of either party to enforce any term or condition of this Agreement shall not constitute a waiver of either party's right to enforce each and every term and condition of this Agreement. No breach under this agreement shall be deemed waived or excused by either party unless such waiver or consent is in writing signed by the party granting such waiver or consent. The waiver by or consent of a party to a breach of any provision of this Agreement shall not operate or be construed as a waiver of or consent to any other or subsequent breach by such other party.
- This Agreement may not be assigned (including by operation of law or otherwise) by you without WILEY's prior written consent.
- Any fee required for this permission shall be non-refundable after thirty (30) days from receipt by the CCC.
- These terms and conditions together with CCC's Billing and Payment terms and conditions (which are incorporated herein) form the entire agreement between you and WILEY concerning this licensing transaction and (in the absence of fraud) supersedes all prior agreements and representations of the parties, oral or written. This Agreement may not be amended except in writing signed by both parties. This Agreement shall be binding upon and inure to the benefit of the parties' successors, legal representatives, and authorized assigns.
- In the event of any conflict between your obligations established by these terms and conditions and those established by CCC's Billing and Payment terms and conditions, these terms and conditions shall prevail.
- WILEY expressly reserves all rights not specifically granted in the combination of (i) the license details provided by you and accepted in the course of this licensing transaction, (ii) these terms and conditions and (iii) CCC's Billing and Payment terms and conditions.
- This Agreement will be void if the Type of Use, Format, Circulation, or Requestor Type was misrepresented during the licensing process.
- This Agreement shall be governed by and construed in accordance with the laws of the State of New York, USA, without regards to such state's conflict of law rules. Any legal action, suit or proceeding arising out of or relating to these Terms

and Conditions or the breach thereof shall be instituted in a court of competent jurisdiction in New York County in the State of New York in the United States of America and each party hereby consents and submits to the personal jurisdiction of such court, waives any objection to venue in such court and consents to service of process by registered or certified mail, return receipt requested, at the last known address of such party.

WILEY OPEN ACCESS TERMS AND CONDITIONS

Wiley Publishes Open Access Articles in fully Open Access Journals and in Subscription journals offering Online Open. Although most of the fully Open Access journals publish open access articles under the terms of the Creative Commons Attribution (CC BY) License only, the subscription journals and a few of the Open Access Journals offer a choice of Creative Commons Licenses. The license type is clearly identified on the article.

The Creative Commons Attribution License

The [Creative Commons Attribution License \(CC-BY\)](#) allows users to copy, distribute and transmit an article, adapt the article and make commercial use of the article. The CC-BY license permits commercial and non-

Creative Commons Attribution Non-Commercial License

The [Creative Commons Attribution Non-Commercial \(CC-BY-NC\)License](#) permits use, distribution and reproduction in any medium, provided the original work is properly cited and is not used for commercial purposes.(see below)

Creative Commons Attribution-Non-Commercial-NoDerivs License

The [Creative Commons Attribution Non-Commercial-NoDerivs License](#) (CC-BY-NC-ND) permits use, distribution and reproduction in any medium, provided the original work is properly cited, is not used for commercial purposes and no modifications or adaptations are made. (see below)

Use by commercial "for-profit" organizations

Use of Wiley Open Access articles for commercial, promotional, or marketing purposes requires further explicit permission from Wiley and will be subject to a fee.

Further details can be found on Wiley Online

Library <http://olabout.wiley.com/WileyCDA/Section/id-410895.html>

Other Terms and Conditions:

v1.10 Last updated September 2015

Questions? customercare@copyright.com or +1-855-239-3415 (toll free in the US) or +1-978-646-2777.

ELSEVIER LICENSE TERMS AND CONDITIONS

Oct 17, 2018

This Agreement between INSERM U1192, Universite de Lille -- Khalil Mallah ("You") and Elsevier ("Elsevier") consists of your license details and the terms and conditions provided by Elsevier and Copyright Clearance Center.

License Number	4451390174303
License date	Oct 17, 2018
Licensed Content Publisher	Elsevier
Licensed Content Publication	Neuron
Licensed Content Title	Dealing with Danger in the CNS: The Response of the Immune System to Injury
Licensed Content Author	Sachin P. Gadani,James T. Walsh,John R. Lukens,Jonathan Kipnis
Licensed Content Date	Jul 1, 2015
Licensed Content Volume	87
Licensed Content Issue	1
Licensed Content Pages	16
Start Page	47
End Page	62
Type of Use	reuse in a thesis/dissertation
Intended publisher of new work	other
Portion	figures/tables/illustrations
Number of figures/tables/illustrations	1
Format	both print and electronic
Are you the author of this Elsevier article?	No
Will you be translating?	No
Original figure numbers	Figure 1
Title of your thesis/dissertation	In Depth Systemic Biology Analysis of Central Nervous System Injuries
Publisher of new work	Inserm U1192-Universite de Lille
Expected completion date	Oct 2018
Estimated size (number of pages)	300
Requestor Location	INSERM U1192, Universite de Lille Cité Scientifique, Bât SN3, 1er étage

Villeneuve D'Ascq, 59650
France
Attn: Khalil Mallah

Publisher Tax ID GB 494 6272 12

Total 0.00 EUR

[Terms and Conditions](#)

INTRODUCTION

1. The publisher for this copyrighted material is Elsevier. By clicking "accept" in connection with completing this licensing transaction, you agree that the following terms and conditions apply to this transaction (along with the Billing and Payment terms and conditions established by Copyright Clearance Center, Inc. ("CCC"), at the time that you opened your Rightslink account and that are available at any time at <http://myaccount.copyright.com>).

GENERAL TERMS

2. Elsevier hereby grants you permission to reproduce the aforementioned material subject to the terms and conditions indicated.

3. Acknowledgement: If any part of the material to be used (for example, figures) has appeared in our publication with credit or acknowledgement to another source, permission must also be sought from that source. If such permission is not obtained then that material may not be included in your publication/copies. Suitable acknowledgement to the source must be made, either as a footnote or in a reference list at the end of your publication, as follows:

"Reprinted from Publication title, Vol /edition number, Author(s), Title of article / title of chapter, Pages No., Copyright (Year), with permission from Elsevier [OR APPLICABLE SOCIETY COPYRIGHT OWNER]." Also Lancet special credit - "Reprinted from The Lancet, Vol. number, Author(s), Title of article, Pages No., Copyright (Year), with permission from Elsevier."

4. Reproduction of this material is confined to the purpose and/or media for which permission is hereby given.

5. Altering/Modifying Material: Not Permitted. However figures and illustrations may be altered/adapted minimally to serve your work. Any other abbreviations, additions, deletions and/or any other alterations shall be made only with prior written authorization of Elsevier Ltd. (Please contact Elsevier at permissions@elsevier.com). No modifications can be made to any Lancet figures/tables and they must be reproduced in full.

6. If the permission fee for the requested use of our material is waived in this instance, please be advised that your future requests for Elsevier materials may attract a fee.

7. Reservation of Rights: Publisher reserves all rights not specifically granted in the combination of (i) the license details provided by you and accepted in the course of this licensing transaction, (ii) these terms and conditions and (iii) CCC's Billing and Payment terms and conditions.

8. License Contingent Upon Payment: While you may exercise the rights licensed immediately upon issuance of the license at the end of the licensing process for the transaction, provided that you have disclosed complete and accurate details of your proposed use, no license is finally effective unless and until full payment is received from

you (either by publisher or by CCC) as provided in CCC's Billing and Payment terms and conditions. If full payment is not received on a timely basis, then any license preliminarily granted shall be deemed automatically revoked and shall be void as if never granted. Further, in the event that you breach any of these terms and conditions or any of CCC's Billing and Payment terms and conditions, the license is automatically revoked and shall be void as if never granted. Use of materials as described in a revoked license, as well as any use of the materials beyond the scope of an unrevoked license, may constitute copyright infringement and publisher reserves the right to take any and all action to protect its copyright in the materials.

9. Warranties: Publisher makes no representations or warranties with respect to the licensed material.

10. Indemnity: You hereby indemnify and agree to hold harmless publisher and CCC, and their respective officers, directors, employees and agents, from and against any and all claims arising out of your use of the licensed material other than as specifically authorized pursuant to this license.

11. No Transfer of License: This license is personal to you and may not be sublicensed, assigned, or transferred by you to any other person without publisher's written permission.

12. No Amendment Except in Writing: This license may not be amended except in a writing signed by both parties (or, in the case of publisher, by CCC on publisher's behalf).

13. Objection to Contrary Terms: Publisher hereby objects to any terms contained in any purchase order, acknowledgment, check endorsement or other writing prepared by you, which terms are inconsistent with these terms and conditions or CCC's Billing and Payment terms and conditions. These terms and conditions, together with CCC's Billing and Payment terms and conditions (which are incorporated herein), comprise the entire agreement between you and publisher (and CCC) concerning this licensing transaction. In the event of any conflict between your obligations established by these terms and conditions and those established by CCC's Billing and Payment terms and conditions, these terms and conditions shall control.

14. Revocation: Elsevier or Copyright Clearance Center may deny the permissions described in this License at their sole discretion, for any reason or no reason, with a full refund payable to you. Notice of such denial will be made using the contact information provided by you. Failure to receive such notice will not alter or invalidate the denial. In no event will Elsevier or Copyright Clearance Center be responsible or liable for any costs, expenses or damage incurred by you as a result of a denial of your permission request, other than a refund of the amount(s) paid by you to Elsevier and/or Copyright Clearance Center for denied permissions.

LIMITED LICENSE

The following terms and conditions apply only to specific license types:

15. **Translation:** This permission is granted for non-exclusive world **English** rights only unless your license was granted for translation rights. If you licensed translation rights you may only translate this content into the languages you requested. A professional translator must perform all translations and reproduce the content word for word preserving the integrity of the article.

16. **Posting licensed content on any Website:** The following terms and conditions apply as follows: Licensing material from an Elsevier journal: All content posted to the web site must maintain the copyright information line on the bottom of each image; A hyper-text

must be included to the Homepage of the journal from which you are licensing at <http://www.sciencedirect.com/science/journal/xxxxx> or the Elsevier homepage for books at <http://www.elsevier.com>; Central Storage: This license does not include permission for a scanned version of the material to be stored in a central repository such as that provided by Heron/XanEdu.

Licensing material from an Elsevier book: A hyper-text link must be included to the Elsevier homepage at <http://www.elsevier.com> . All content posted to the web site must maintain the copyright information line on the bottom of each image.

Posting licensed content on Electronic reserve: In addition to the above the following clauses are applicable: The web site must be password-protected and made available only to bona fide students registered on a relevant course. This permission is granted for 1 year only. You may obtain a new license for future website posting.

17. For journal authors: the following clauses are applicable in addition to the above:

Preprints:

A preprint is an author's own write-up of research results and analysis, it has not been peer-reviewed, nor has it had any other value added to it by a publisher (such as formatting, copyright, technical enhancement etc.).

Authors can share their preprints anywhere at any time. Preprints should not be added to or enhanced in any way in order to appear more like, or to substitute for, the final versions of articles however authors can update their preprints on arXiv or RePEc with their Accepted Author Manuscript (see below).

If accepted for publication, we encourage authors to link from the preprint to their formal publication via its DOI. Millions of researchers have access to the formal publications on ScienceDirect, and so links will help users to find, access, cite and use the best available version. Please note that Cell Press, The Lancet and some society-owned have different preprint policies. Information on these policies is available on the journal homepage.

Accepted Author Manuscripts: An accepted author manuscript is the manuscript of an article that has been accepted for publication and which typically includes author-incorporated changes suggested during submission, peer review and editor-author communications.

Authors can share their accepted author manuscript:

- immediately
 - via their non-commercial person homepage or blog
 - by updating a preprint in arXiv or RePEc with the accepted manuscript
 - via their research institute or institutional repository for internal institutional uses or as part of an invitation-only research collaboration work-group
 - directly by providing copies to their students or to research collaborators for their personal use
 - for private scholarly sharing as part of an invitation-only work group on commercial sites with which Elsevier has an agreement
- After the embargo period
 - via non-commercial hosting platforms such as their institutional repository

- via commercial sites with which Elsevier has an agreement

In all cases accepted manuscripts should:

- link to the formal publication via its DOI
- bear a CC-BY-NC-ND license - this is easy to do
- if aggregated with other manuscripts, for example in a repository or other site, be shared in alignment with our hosting policy not be added to or enhanced in any way to appear more like, or to substitute for, the published journal article.

Published journal article (JPA): A published journal article (PJA) is the definitive final record of published research that appears or will appear in the journal and embodies all value-adding publishing activities including peer review co-ordination, copy-editing, formatting, (if relevant) pagination and online enrichment.

Policies for sharing publishing journal articles differ for subscription and gold open access articles:

Subscription Articles: If you are an author, please share a link to your article rather than the full-text. Millions of researchers have access to the formal publications on ScienceDirect, and so links will help your users to find, access, cite, and use the best available version.

Theses and dissertations which contain embedded PJAs as part of the formal submission can be posted publicly by the awarding institution with DOI links back to the formal publications on ScienceDirect.

If you are affiliated with a library that subscribes to ScienceDirect you have additional private sharing rights for others' research accessed under that agreement. This includes use for classroom teaching and internal training at the institution (including use in course packs and courseware programs), and inclusion of the article for grant funding purposes.

Gold Open Access Articles: May be shared according to the author-selected end-user license and should contain a [CrossMark logo](#), the end user license, and a DOI link to the formal publication on ScienceDirect.

Please refer to Elsevier's [posting policy](#) for further information.

18. **For book authors** the following clauses are applicable in addition to the above: Authors are permitted to place a brief summary of their work online only. You are not allowed to download and post the published electronic version of your chapter, nor may you scan the printed edition to create an electronic version. **Posting to a repository:** Authors are permitted to post a summary of their chapter only in their institution's repository.

19. **Thesis/Dissertation:** If your license is for use in a thesis/dissertation your thesis may be submitted to your institution in either print or electronic form. Should your thesis be published commercially, please reapply for permission. These requirements include permission for the Library and Archives of Canada to supply single copies, on demand, of the complete thesis and include permission for Proquest/UMI to supply single copies, on demand, of the complete thesis. Should your thesis be published commercially, please reapply for permission. Theses and dissertations which contain embedded PJAs as part of the formal submission can be posted publicly by the awarding institution with DOI links back to the formal publications on ScienceDirect.

Elsevier Open Access Terms and Conditions

You can publish open access with Elsevier in hundreds of open access journals or in nearly 2000 established subscription journals that support open access publishing. Permitted third party re-use of these open access articles is defined by the author's choice of Creative Commons user license. See our [open access license policy](#) for more information.

Terms & Conditions applicable to all Open Access articles published with Elsevier:

Any reuse of the article must not represent the author as endorsing the adaptation of the article nor should the article be modified in such a way as to damage the author's honour or reputation. If any changes have been made, such changes must be clearly indicated. The author(s) must be appropriately credited and we ask that you include the end user license and a DOI link to the formal publication on ScienceDirect.

If any part of the material to be used (for example, figures) has appeared in our publication with credit or acknowledgement to another source it is the responsibility of the user to ensure their reuse complies with the terms and conditions determined by the rights holder.

Additional Terms & Conditions applicable to each Creative Commons user license:

CC BY: The CC-BY license allows users to copy, to create extracts, abstracts and new works from the Article, to alter and revise the Article and to make commercial use of the Article (including reuse and/or resale of the Article by commercial entities), provided the user gives appropriate credit (with a link to the formal publication through the relevant DOI), provides a link to the license, indicates if changes were made and the licensor is not represented as endorsing the use made of the work. The full details of the license are available at <http://creativecommons.org/licenses/by/4.0>.

CC BY NC SA: The CC BY-NC-SA license allows users to copy, to create extracts, abstracts and new works from the Article, to alter and revise the Article, provided this is not done for commercial purposes, and that the user gives appropriate credit (with a link to the formal publication through the relevant DOI), provides a link to the license, indicates if changes were made and the licensor is not represented as endorsing the use made of the work. Further, any new works must be made available on the same conditions. The full details of the license are available at <http://creativecommons.org/licenses/by-nc-sa/4.0>.

CC BY NC ND: The CC BY-NC-ND license allows users to copy and distribute the Article, provided this is not done for commercial purposes and further does not permit distribution of the Article if it is changed or edited in any way, and provided the user gives appropriate credit (with a link to the formal publication through the relevant DOI), provides a link to the license, and that the licensor is not represented as endorsing the use made of the work. The full details of the license are available at <http://creativecommons.org/licenses/by-nc-nd/4.0>. Any commercial reuse of Open Access articles published with a CC BY NC SA or CC BY NC ND license requires permission from Elsevier and will be subject to a fee.

Commercial reuse includes:

- Associating advertising with the full text of the Article
- Charging fees for document delivery or access

- Article aggregation
- Systematic distribution via e-mail lists or share buttons

Posting or linking by commercial companies for use by customers of those companies.

20. Other Conditions:

v1.9

Questions? customercare@copyright.com or +1-855-239-3415 (toll free in the US) or +1-978-646-2777.



Confirmation Number: 11757248

Order Date: 10/17/2018

If you paid by credit card, your order will be finalized and your card will be charged within 24 hours. If you choose to be invoiced, you can change or cancel your order until the invoice is generated.

Payment Information

Khalil Mallah
INSERM U1192, Universite de Lille
k.mallah@outlook.com
+33 763498133
Payment Method: n/a

Order Details

Molecular & cellular proteomics

- **Order detail ID:**71612037
- **Order License Id:**4451410706498
- **ISSN:**1535-9484
- **Publication Type:**e-Journal
- **Volume:**
- **Issue:**
- **Start page:**
- **Publisher:**AMERICAN SOCIETY FOR BIOCHEMISTRY AND MOLECULAR BIOLOGY
- **Author/Editor:**American Society for Biochemistry and Molecular Biology
- **Permission Status:**  **Granted**
- **Permission type:**Republish or display content
- **Type of use:**Thesis/Dissertation
- [Hide details](#)

○	
Requestor type	Academic institution
Format	Print, Electronic
Portion	chart/graph/table/figure
Number of charts/graphs/tables/figures	1
The requesting person/organization	Khalil Mallah, INSERM U1992, Universite de Lille
Title or numeric reference of the portion(s)	Figure 1
Title of the article or chapter the portion is from	MALDI Imaging Mass Spectrometry - STATE OF THE ART TECHNOLOGY IN CLINICAL PROTEOMICS
Editor of portion(s)	N/A
Author of portion(s)	Julien Franck, Karim Arafah, Mohamed Elayed, David Bonnel, Daniele Vergara, Amelie Jacquet, Denis Vinatier, Maxence Wisztorski, Robert Day, Isabelle Fournier, and Michel Salzet
Volume of serial or monograph	N/A
Page range of portion	2024
Publication date of portion	May 18, 2009

Rights for	Main Product, any product related to main product, and other compilations/derivative products
Duration of use	Life of current edition
Creation of copies for the disabled	no
With minor editing privileges	no
For distribution to	Worldwide
In the following language(s)	Original language of publication
With incidental promotional use	no
Lifetime unit quantity of new product	Up to 499
Title	In Depth Systemic Biology Analysis of Central Nervous System Injuries
Institution name	Inserm U1192-Universite de Lille
Expected presentation date	Oct 2018

Note: This item will be invoiced or charged separately through CCC's **RightsLink** service. [More info](#) \$ 0.00

Title: Analysis of Tissue Specimens by Matrix-Assisted Laser Desorption/Ionization Imaging Mass Spectrometry in Biological and Clinical Research

Author: Jeremy L. Norris, Richard M. Caprioli

Publication: Chemical Reviews

Publisher: American Chemical Society

Date: Apr 1, 2013

Copyright © 2013, American Chemical Society

Logged in as:

Khalil Mallah
INSERM U1192,
Universite de Lille

Account #:

[LOGOUT](#)

PERMISSION/LICENSE IS GRANTED FOR YOUR ORDER AT NO CHARGE

This type of permission/license, instead of the standard Terms & Conditions, is sent to you because no fee is being charged for your order. Please note the following:

- Permission is granted for your request in both print and electronic formats, and translations.
- If figures and/or tables were requested, they may be adapted or used in part.
- Please print this page for your records and send a copy of it to your publisher/graduate school.
- Appropriate credit for the requested material should be given as follows: "Reprinted (adapted) with permission from (COMPLETE REFERENCE CITATION). Copyright (YEAR) American Chemical Society." Insert appropriate information in place of the capitalized words.
- One-time permission is granted only for the use specified in your request. No additional uses are granted (such as derivative works or other editions). For any other uses, please submit a new request.

If credit is given to another source for the material you requested, permission must be obtained from that source.

Title: Quantification-Based Mass Spectrometry Imaging of Proteins by Parafilm Assisted Microdissection

Author: Julien Franck, Jusal Quanico, Maxence Wisztorski, et al

Publication: Analytical Chemistry

Publisher: American Chemical Society

Date: Sep 1, 2013

Copyright © 2013, American Chemical Society

Logged in as:
Khalil Mallah
INSERM U1192, Universite de Lille

Account #:

[LOGOUT](#)

PERMISSION/LICENSE IS GRANTED FOR YOUR ORDER AT NO CHARGE

This type of permission/license, instead of the standard Terms & Conditions, is sent to you because no fee is being charged for your order. Please note the following:

- Permission is granted for your request in both print and electronic formats, and translations.
- If figures and/or tables were requested, they may be adapted or used in part.
- Please print this page for your records and send a copy of it to your publisher/graduate school.
- Appropriate credit for the requested material should be given as follows: "Reprinted (adapted) with permission from (COMPLETE REFERENCE CITATION). Copyright (YEAR) American Chemical Society." Insert appropriate information in place of the capitalized words.
- One-time permission is granted only for the use specified in your request. No additional uses are granted (such as derivative works or other editions). For any other uses, please submit a new request.

If credit is given to another source for the material you requested, permission must be obtained from that source.



Title: Lipid Changes Associated with Traumatic Brain Injury Revealed by 3D MALDI-MSI
Author: Khalil Mallah, Jusal Quanico, Dennis Trede, et al
Publication: Analytical Chemistry
Publisher: American Chemical Society
Date: Sep 1, 2018
Copyright © 2018, American Chemical Society

Logged in as:
Khalil Mallah
INSERM U1192, Universite de Lille

Account #:

LOGOUT

PERMISSION/LICENSE IS GRANTED FOR YOUR ORDER AT NO CHARGE

This type of permission/license, instead of the standard Terms & Conditions, is sent to you because no fee is being charged for your order. Please note the following:

- Permission is granted for your request in both print and electronic formats, and translations.
- If figures and/or tables were requested, they may be adapted or used in part.
- Please print this page for your records and send a copy of it to your publisher/graduate school.
- Appropriate credit for the requested material should be given as follows: "Reprinted (adapted) with permission from (COMPLETE REFERENCE CITATION). Copyright (YEAR) American Chemical Society." Insert appropriate information in place of the capitalized words.
- One-time permission is granted only for the use specified in your request. No additional uses are granted (such as derivative works or other editions). For any other uses, please submit a new request.

BACK

CLOSE WINDOW

**SPRINGER NATURE LICENSE
TERMS AND CONDITIONS**

Oct 17, 2018

This Agreement between INSERM U1192, Universite de Lille -- Khalil Mallah ("You") and Springer Nature ("Springer Nature") consists of your license details and the terms and conditions provided by Springer Nature and Copyright Clearance Center.

License Number	4451430364095
License date	Oct 17, 2018
Licensed Content Publisher	Springer Nature
Licensed Content Publication	Nature Reviews Disease Primers
Licensed Content Title	Traumatic spinal cord injury
Licensed Content Author	Christopher S. Ahuja, Jefferson R. Wilson, Satoshi Nori, Mark R. N. Kotter, Claudia Druschel et al.
Licensed Content Date	Apr 27, 2017
Licensed Content Volume	3
Type of Use	Thesis/Dissertation
Requestor type	academic/university or research institute
Format	print and electronic
Portion	figures/tables/illustrations
Number of figures/tables/illustrations	1
High-res required	no
Will you be translating?	no
Circulation/distribution	<501
Author of this Springer Nature content	no
Title	In Depth Systemic Biology Analysis of Central Nervous System Injuries
Institution name	Inserm U1192-Universite de Lille
Expected presentation date	Oct 2018
Portions	Figure 1
Requestor Location	INSERM U1192, Universite de Lille Cit� Scientifique, B�t SN3, 1er �tage Villeneuve D'Ascq, 59650 France Attn: Khalil Mallah

Billing Type Invoice
Billing Address INSERM U1192, Universite de Lille
Cité Scientifique, Bât SN3, 1er étage

Villeneuve D'Ascq, France 59650
Attn: Khalil Mallah
Total 0.00 EUR

Terms and Conditions

Springer Nature Terms and Conditions for RightsLink Permissions
Springer Nature Customer Service Centre GmbH (the Licensor) hereby grants you a non-exclusive, world-wide licence to reproduce the material and for the purpose and requirements specified in the attached copy of your order form, and for no other use, subject to the conditions below:

1. The Licensor warrants that it has, to the best of its knowledge, the rights to license reuse of this material. However, you should ensure that the material you are requesting is original to the Licensor and does not carry the copyright of another entity (as credited in the published version).

If the credit line on any part of the material you have requested indicates that it was reprinted or adapted with permission from another source, then you should also seek permission from that source to reuse the material.

2. Where **print only** permission has been granted for a fee, separate permission must be obtained for any additional electronic re-use.
3. Permission granted **free of charge** for material in print is also usually granted for any electronic version of that work, provided that the material is incidental to your work as a whole and that the electronic version is essentially equivalent to, or substitutes for, the print version.
4. A licence for 'post on a website' is valid for 12 months from the licence date. This licence does not cover use of full text articles on websites.
5. Where '**reuse in a dissertation/thesis**' has been selected the following terms apply: Print rights of the final author's accepted manuscript (for clarity, NOT the published version) for up to 100 copies, electronic rights for use only on a personal website or institutional repository as defined by the Sherpa guideline (www.sherpa.ac.uk/romeo/).
6. Permission granted for books and journals is granted for the lifetime of the first edition and does not apply to second and subsequent editions (except where the first edition permission was granted free of charge or for signatories to the STM Permissions Guidelines <http://www.stm-assoc.org/copyright-legal-affairs/permissions/permissions-guidelines/>), and does not apply for editions in other languages unless additional translation rights have been granted separately in the licence.
7. Rights for additional components such as custom editions and derivatives require additional permission and may be subject to an additional fee. Please apply to Journalpermissions@springernature.com/bookpermissions@springernature.com for these rights.

8. The Licensor's permission must be acknowledged next to the licensed material in print. In electronic form, this acknowledgement must be visible at the same time as the figures/tables/illustrations or abstract, and must be hyperlinked to the journal/book's homepage. Our required acknowledgement format is in the Appendix below.
9. Use of the material for incidental promotional use, minor editing privileges (this does not include cropping, adapting, omitting material or any other changes that affect the meaning, intention or moral rights of the author) and copies for the disabled are permitted under this licence.
10. Minor adaptations of single figures (changes of format, colour and style) do not require the Licensor's approval. However, the adaptation should be credited as shown in Appendix below.

Appendix — Acknowledgements:

For Journal Content:

Reprinted by permission from [**the Licensor**]: [**Journal Publisher** (e.g. Nature/Springer/Palgrave)] [**JOURNAL NAME**] [**REFERENCE CITATION**(Article name, Author(s) Name), [**COPYRIGHT**] (year of publication)

For Advance Online Publication papers:

Reprinted by permission from [**the Licensor**]: [**Journal Publisher** (e.g. Nature/Springer/Palgrave)] [**JOURNAL NAME**] [**REFERENCE CITATION**(Article name, Author(s) Name), [**COPYRIGHT**] (year of publication), advance online publication, day month year (doi: 10.1038/sj.[**JOURNAL ACRONYM**].)

For Adaptations/Translations:

Adapted/Translated by permission from [**the Licensor**]: [**Journal Publisher** (e.g. Nature/Springer/Palgrave)] [**JOURNAL NAME**] [**REFERENCE CITATION**(Article name, Author(s) Name), [**COPYRIGHT**] (year of publication)

Note: For any republication from the British Journal of Cancer, the following credit line style applies:

Reprinted/adapted/translated by permission from [**the Licensor**]: on behalf of Cancer Research UK: : [**Journal Publisher** (e.g. Nature/Springer/Palgrave)] [**JOURNAL NAME**] [**REFERENCE CITATION** (Article name, Author(s) Name), [**COPYRIGHT**] (year of publication)

For Advance Online Publication papers:

Reprinted by permission from The [**the Licensor**]: on behalf of Cancer Research UK: [**Journal Publisher** (e.g. Nature/Springer/Palgrave)] [**JOURNAL NAME**] [**REFERENCE CITATION** (Article name, Author(s) Name), [**COPYRIGHT**] (year of publication), advance online publication, day month year (doi: 10.1038/sj.[**JOURNAL ACRONYM**])

For Book content:

Reprinted/adapted by permission from [**the Licensor**]: [**Book Publisher** (e.g. Palgrave Macmillan, Springer etc) [**Book Title**] by [**Book author(s)**] [**COPYRIGHT**] (year of publication)

Other Conditions:

Questions? customercare@copyright.com or +1-855-239-3415 (toll free in the US) or +1-978-646-2777.

**SPRINGER NATURE LICENSE
TERMS AND CONDITIONS**

Oct 17, 2018

This Agreement between INSERM U1192, Universite de Lille -- Khalil Mallah ("You") and Springer Nature ("Springer Nature") consists of your license details and the terms and conditions provided by Springer Nature and Copyright Clearance Center.

License Number	4451380105768
License date	Oct 17, 2018
Licensed Content Publisher	Springer Nature
Licensed Content Publication	Nature
Licensed Content Title	Neuroscience: Glia — more than just brain glue
Licensed Content Author	Nicola J. Allen, Ben A. Barres
Licensed Content Date	Feb 4, 2009
Licensed Content Volume	457
Licensed Content Issue	7230
Type of Use	Thesis/Dissertation
Requestor type	academic/university or research institute
Format	print and electronic
Portion	figures/tables/illustrations
Number of figures/tables/illustrations	2
High-res required	no
Will you be translating?	no
Circulation/distribution	<501
Author of this Springer Nature content	no
Title	In Depth Systemic Biology Analysis of Central Nervous System Injuries
Institution name	Inserm U1192-Universite de Lille
Expected presentation date	Oct 2018
Portions	Figure 1 and Figure 2
Requestor Location	INSERM U1192, Universite de Lille Cité Scientifique, Bât SN3, 1er étage Villeneuve D'Ascq, 59650 France Attn: Khalil Mallah

Billing Type Invoice
Billing Address INSERM U1192, Universite de Lille
Cité Scientifique, Bât SN3, 1er étage
Villeneuve D'Ascq, France 59650
Attn: Khalil Mallah
Total 0.00 EUR
Terms and Conditions

Springer Nature Terms and Conditions for RightsLink Permissions
Springer Nature Customer Service Centre GmbH (the Licensor) hereby grants you a non-exclusive, world-wide licence to reproduce the material and for the purpose and requirements specified in the attached copy of your order form, and for no other use, subject to the conditions below:

1. The Licensor warrants that it has, to the best of its knowledge, the rights to license reuse of this material. However, you should ensure that the material you are requesting is original to the Licensor and does not carry the copyright of another entity (as credited in the published version).

If the credit line on any part of the material you have requested indicates that it was reprinted or adapted with permission from another source, then you should also seek permission from that source to reuse the material.

2. Where **print only** permission has been granted for a fee, separate permission must be obtained for any additional electronic re-use.
3. Permission granted **free of charge** for material in print is also usually granted for any electronic version of that work, provided that the material is incidental to your work as a whole and that the electronic version is essentially equivalent to, or substitutes for, the print version.
4. A licence for 'post on a website' is valid for 12 months from the licence date. This licence does not cover use of full text articles on websites.
5. Where '**reuse in a dissertation/thesis**' has been selected the following terms apply: Print rights of the final author's accepted manuscript (for clarity, NOT the published version) for up to 100 copies, electronic rights for use only on a personal website or institutional repository as defined by the Sherpa guideline (www.sherpa.ac.uk/romeo/).
6. Permission granted for books and journals is granted for the lifetime of the first edition and does not apply to second and subsequent editions (except where the first edition permission was granted free of charge or for signatories to the STM Permissions Guidelines <http://www.stm-assoc.org/copyright-legal-affairs/permissions/permissions-guidelines/>), and does not apply for editions in other languages unless additional translation rights have been granted separately in the licence.
7. Rights for additional components such as custom editions and derivatives require additional permission and may be subject to an additional fee. Please apply to Journalpermissions@springernature.com/bookpermissions@springernature.com for these rights.

8. The Licensor's permission must be acknowledged next to the licensed material in print. In electronic form, this acknowledgement must be visible at the same time as the figures/tables/illustrations or abstract, and must be hyperlinked to the journal/book's homepage. Our required acknowledgement format is in the Appendix below.
9. Use of the material for incidental promotional use, minor editing privileges (this does not include cropping, adapting, omitting material or any other changes that affect the meaning, intention or moral rights of the author) and copies for the disabled are permitted under this licence.
10. Minor adaptations of single figures (changes of format, colour and style) do not require the Licensor's approval. However, the adaptation should be credited as shown in Appendix below.

Appendix — Acknowledgements:

For Journal Content:

Reprinted by permission from [**the Licensor**]: [**Journal Publisher** (e.g. Nature/Springer/Palgrave)] [**JOURNAL NAME**] [**REFERENCE CITATION**(Article name, Author(s) Name), [**COPYRIGHT**] (year of publication)

For Advance Online Publication papers:

Reprinted by permission from [**the Licensor**]: [**Journal Publisher** (e.g. Nature/Springer/Palgrave)] [**JOURNAL NAME**] [**REFERENCE CITATION**(Article name, Author(s) Name), [**COPYRIGHT**] (year of publication), advance online publication, day month year (doi: 10.1038/sj.[**JOURNAL ACRONYM**].)

For Adaptations/Translations:

Adapted/Translated by permission from [**the Licensor**]: [**Journal Publisher** (e.g. Nature/Springer/Palgrave)] [**JOURNAL NAME**] [**REFERENCE CITATION**(Article name, Author(s) Name), [**COPYRIGHT**] (year of publication)

Note: For any republication from the British Journal of Cancer, the following credit line style applies:

Reprinted/adapted/translated by permission from [**the Licensor**]: on behalf of Cancer Research UK: : [**Journal Publisher** (e.g. Nature/Springer/Palgrave)] [**JOURNAL NAME**] [**REFERENCE CITATION** (Article name, Author(s) Name), [**COPYRIGHT**] (year of publication)

For Advance Online Publication papers:

Reprinted by permission from The [**the Licensor**]: on behalf of Cancer Research UK: [**Journal Publisher** (e.g. Nature/Springer/Palgrave)] [**JOURNAL NAME**] [**REFERENCE CITATION** (Article name, Author(s) Name), [**COPYRIGHT**] (year of publication), advance online publication, day month year (doi: 10.1038/sj.[**JOURNAL ACRONYM**])

For Book content:

Reprinted/adapted by permission from [**the Licensor**]: [**Book Publisher** (e.g. Palgrave Macmillan, Springer etc) [**Book Title**] by [**Book author(s)**] [**COPYRIGHT**] (year of publication)

Other Conditions:

Questions? customercare@copyright.com or +1-855-239-3415 (toll free in the US) or +1-978-646-2777.



**SPRINGER NATURE LICENSE
TERMS AND CONDITIONS**

Oct 17, 2018

This Agreement between INSERM U1192, Universite de Lille -- Khalil Mallah ("You") and Springer Nature ("Springer Nature") consists of your license details and the terms and conditions provided by Springer Nature and Copyright Clearance Center.

License Number	4451380404920
License date	Oct 17, 2018
Licensed Content Publisher	Springer Nature
Licensed Content Publication	Spinal Cord
Licensed Content Title	Spinal cord injury models: a review
Licensed Content Author	T Cheriyan, D J Ryan, J H Weinreb, J Cheriyan, J C Paul et al.
Licensed Content Date	Jun 10, 2014
Licensed Content Volume	52
Licensed Content Issue	8
Type of Use	Thesis/Dissertation
Requestor type	academic/university or research institute
Format	print and electronic
Portion	figures/tables/illustrations
Number of figures/tables/illustrations	1
High-res required	no
Will you be translating?	no
Circulation/distribution	<501
Author of this Springer Nature content	no
Title	In Depth Systemic Biology Analysis of Central Nervous System Injuries
Institution name	Inserm U1192-Universite de Lille
Expected presentation date	Oct 2018
Portions	Figure 2
Requestor Location	INSERM U1192, Universite de Lille Cité Scientifique, Bât SN3, 1er étage Villeneuve D'Ascq, 59650

France
Attn: Khalil Mallah

Billing Type Invoice

Billing Address INSERM U1192, Universite de Lille
Cité Scientifique, Bât SN3, 1er étage

Villeneuve D'Ascq, France 59650
Attn: Khalil Mallah

Total 0.00 EUR

Terms and Conditions

Springer Nature Terms and Conditions for RightsLink Permissions
Springer Nature Customer Service Centre GmbH (the Licensor) hereby grants you a non-exclusive, world-wide licence to reproduce the material and for the purpose and requirements specified in the attached copy of your order form, and for no other use, subject to the conditions below:

1. The Licensor warrants that it has, to the best of its knowledge, the rights to license reuse of this material. However, you should ensure that the material you are requesting is original to the Licensor and does not carry the copyright of another entity (as credited in the published version).

If the credit line on any part of the material you have requested indicates that it was reprinted or adapted with permission from another source, then you should also seek permission from that source to reuse the material.

2. Where **print only** permission has been granted for a fee, separate permission must be obtained for any additional electronic re-use.
3. Permission granted **free of charge** for material in print is also usually granted for any electronic version of that work, provided that the material is incidental to your work as a whole and that the electronic version is essentially equivalent to, or substitutes for, the print version.
4. A licence for 'post on a website' is valid for 12 months from the licence date. This licence does not cover use of full text articles on websites.
5. Where '**reuse in a dissertation/thesis**' has been selected the following terms apply: Print rights of the final author's accepted manuscript (for clarity, NOT the published version) for up to 100 copies, electronic rights for use only on a personal website or institutional repository as defined by the Sherpa guideline (www.sherpa.ac.uk/romeo/).
6. Permission granted for books and journals is granted for the lifetime of the first edition and does not apply to second and subsequent editions (except where the first edition permission was granted free of charge or for signatories to the STM Permissions Guidelines <http://www.stm-assoc.org/copyright-legal-affairs/permissions/permissions-guidelines/>), and does not apply for editions in other languages unless additional translation rights have been granted separately in the licence.
7. Rights for additional components such as custom editions and derivatives require additional permission and may be subject to an additional fee. Please apply to

Journalpermissions@springernature.com/bookpermissions@springernature.com for these rights.

8. The Licensor's permission must be acknowledged next to the licensed material in print. In electronic form, this acknowledgement must be visible at the same time as the figures/tables/illustrations or abstract, and must be hyperlinked to the journal/book's homepage. Our required acknowledgement format is in the Appendix below.
9. Use of the material for incidental promotional use, minor editing privileges (this does not include cropping, adapting, omitting material or any other changes that affect the meaning, intention or moral rights of the author) and copies for the disabled are permitted under this licence.
10. Minor adaptations of single figures (changes of format, colour and style) do not require the Licensor's approval. However, the adaptation should be credited as shown in Appendix below.

Appendix — Acknowledgements:

For Journal Content:

Reprinted by permission from [**the Licensor**]: [**Journal Publisher** (e.g. Nature/Springer/Palgrave)] [**JOURNAL NAME**] [**REFERENCE CITATION**(Article name, Author(s) Name), [**COPYRIGHT**] (year of publication)

For Advance Online Publication papers:

Reprinted by permission from [**the Licensor**]: [**Journal Publisher** (e.g. Nature/Springer/Palgrave)] [**JOURNAL NAME**] [**REFERENCE CITATION**(Article name, Author(s) Name), [**COPYRIGHT**] (year of publication), advance online publication, day month year (doi: 10.1038/sj.[**JOURNAL ACRONYM**].)

For Adaptations/Translations:

Adapted/Translated by permission from [**the Licensor**]: [**Journal Publisher** (e.g. Nature/Springer/Palgrave)] [**JOURNAL NAME**] [**REFERENCE CITATION**(Article name, Author(s) Name), [**COPYRIGHT**] (year of publication)

Note: For any republication from the British Journal of Cancer, the following credit line style applies:

Reprinted/adapted/translated by permission from [**the Licensor**]: on behalf of Cancer Research UK: : [**Journal Publisher** (e.g. Nature/Springer/Palgrave)] [**JOURNAL NAME**] [**REFERENCE CITATION** (Article name, Author(s) Name), [**COPYRIGHT**] (year of publication)

For Advance Online Publication papers:

Reprinted by permission from The [**the Licensor**]: on behalf of Cancer Research UK: [**Journal Publisher** (e.g. Nature/Springer/Palgrave)] [**JOURNAL NAME**] [**REFERENCE CITATION** (Article name, Author(s) Name), [**COPYRIGHT**] (year of publication), advance online publication, day month year (doi: 10.1038/sj.[**JOURNAL ACRONYM**])

For Book content:

Reprinted/adapted by permission from [**the Licensor**]: [**Book Publisher** (e.g. Palgrave Macmillan, Springer etc) [**Book Title**] by [**Book author(s)**] [**COPYRIGHT**] (year of publication)

Other Conditions:

Version 1.1

Questions? customercare@copyright.com or +1-855-239-3415 (toll free in the US) or +1-978-646-2777.



SPRINGER NATURE LICENSE TERMS AND CONDITIONS

Oct 17, 2018

This Agreement between INSERM U1192, Universite de Lille -- Khalil Mallah ("You") and Springer Nature ("Springer Nature") consists of your license details and the terms and conditions provided by Springer Nature and Copyright Clearance Center.

License Number	4451380562447
License date	Oct 17, 2018
Licensed Content Publisher	Springer Nature
Licensed Content Publication	Nature Reviews Neuroscience
Licensed Content Title	Animal models of traumatic brain injury
Licensed Content Author	Ye Xiong, Asim Mahmood, Michael Chopp
Licensed Content Date	Jan 18, 2013
Licensed Content Volume	14
Licensed Content Issue	2
Type of Use	Thesis/Dissertation
Requestor type	academic/university or research institute
Format	print and electronic
Portion	figures/tables/illustrations
Number of figures/tables/illustrations	1
High-res required	no
Will you be translating?	no
Circulation/distribution	<501
Author of this Springer Nature content	no
Title	In Depth Systemic Biology Analysis of Central Nervous System Injuries
Institution name	Inserm U1192-Universite de Lille
Expected presentation date	Oct 2018
Portions	Figure 1
Requestor Location	INSERM U1192, Universite de Lille Cité Scientifique, Bât SN3, 1er étage Villeneuve D'Ascq, 59650

France
Attn: Khalil Mallah

Billing Type Invoice

Billing Address INSERM U1192, Universite de Lille
Cité Scientifique, Bât SN3, 1er étage

Villeneuve D'Ascq, France 59650
Attn: Khalil Mallah

Total 0.00 EUR

Terms and Conditions

Springer Nature Terms and Conditions for RightsLink Permissions
Springer Nature Customer Service Centre GmbH (the Licensor) hereby grants you a non-exclusive, world-wide licence to reproduce the material and for the purpose and requirements specified in the attached copy of your order form, and for no other use, subject to the conditions below:

1. The Licensor warrants that it has, to the best of its knowledge, the rights to license reuse of this material. However, you should ensure that the material you are requesting is original to the Licensor and does not carry the copyright of another entity (as credited in the published version).

If the credit line on any part of the material you have requested indicates that it was reprinted or adapted with permission from another source, then you should also seek permission from that source to reuse the material.

2. Where **print only** permission has been granted for a fee, separate permission must be obtained for any additional electronic re-use.
3. Permission granted **free of charge** for material in print is also usually granted for any electronic version of that work, provided that the material is incidental to your work as a whole and that the electronic version is essentially equivalent to, or substitutes for, the print version.
4. A licence for 'post on a website' is valid for 12 months from the licence date. This licence does not cover use of full text articles on websites.
5. Where '**reuse in a dissertation/thesis**' has been selected the following terms apply: Print rights of the final author's accepted manuscript (for clarity, NOT the published version) for up to 100 copies, electronic rights for use only on a personal website or institutional repository as defined by the Sherpa guideline (www.sherpa.ac.uk/romeo/).
6. Permission granted for books and journals is granted for the lifetime of the first edition and does not apply to second and subsequent editions (except where the first edition permission was granted free of charge or for signatories to the STM Permissions Guidelines <http://www.stm-assoc.org/copyright-legal-affairs/permissions/permissions-guidelines/>), and does not apply for editions in other languages unless additional translation rights have been granted separately in the licence.
7. Rights for additional components such as custom editions and derivatives require additional permission and may be subject to an additional fee. Please apply to

Journalpermissions@springernature.com/bookpermissions@springernature.com for these rights.

8. The Licensor's permission must be acknowledged next to the licensed material in print. In electronic form, this acknowledgement must be visible at the same time as the figures/tables/illustrations or abstract, and must be hyperlinked to the journal/book's homepage. Our required acknowledgement format is in the Appendix below.
9. Use of the material for incidental promotional use, minor editing privileges (this does not include cropping, adapting, omitting material or any other changes that affect the meaning, intention or moral rights of the author) and copies for the disabled are permitted under this licence.
10. Minor adaptations of single figures (changes of format, colour and style) do not require the Licensor's approval. However, the adaptation should be credited as shown in Appendix below.

Appendix — Acknowledgements:

For Journal Content:

Reprinted by permission from [**the Licensor**]: [**Journal Publisher** (e.g. Nature/Springer/Palgrave)] [**JOURNAL NAME**] [**REFERENCE CITATION**(Article name, Author(s) Name), [**COPYRIGHT**] (year of publication)

For Advance Online Publication papers:

Reprinted by permission from [**the Licensor**]: [**Journal Publisher** (e.g. Nature/Springer/Palgrave)] [**JOURNAL NAME**] [**REFERENCE CITATION**(Article name, Author(s) Name), [**COPYRIGHT**] (year of publication), advance online publication, day month year (doi: 10.1038/sj.[**JOURNAL ACRONYM**].)

For Adaptations/Translations:

Adapted/Translated by permission from [**the Licensor**]: [**Journal Publisher** (e.g. Nature/Springer/Palgrave)] [**JOURNAL NAME**] [**REFERENCE CITATION**(Article name, Author(s) Name), [**COPYRIGHT**] (year of publication)

Note: For any republication from the British Journal of Cancer, the following credit line style applies:

Reprinted/adapted/translated by permission from [**the Licensor**]: on behalf of Cancer Research UK: : [**Journal Publisher** (e.g. Nature/Springer/Palgrave)] [**JOURNAL NAME**] [**REFERENCE CITATION** (Article name, Author(s) Name), [**COPYRIGHT**] (year of publication)

For Advance Online Publication papers:

Reprinted by permission from The [**the Licensor**]: on behalf of Cancer Research UK: [**Journal Publisher** (e.g. Nature/Springer/Palgrave)] [**JOURNAL NAME**] [**REFERENCE CITATION** (Article name, Author(s) Name), [**COPYRIGHT**] (year of publication), advance online publication, day month year (doi: 10.1038/sj.[**JOURNAL ACRONYM**])

For Book content:

Reprinted/adapted by permission from [**the Licensor**]: [**Book Publisher** (e.g. Palgrave Macmillan, Springer etc) [**Book Title**] by [**Book author(s)**] [**COPYRIGHT**] (year of publication)

Other Conditions:

Version 1.1

Questions? customercare@copyright.com or +1-855-239-3415 (toll free in the US) or +1-978-646-2777.



**SPRINGER NATURE LICENSE
TERMS AND CONDITIONS**

Oct 17, 2018

This Agreement between INSERM U1192, Universite de Lille -- Khalil Mallah ("You") and Springer Nature ("Springer Nature") consists of your license details and the terms and conditions provided by Springer Nature and Copyright Clearance Center.

License Number	4451400599286
License date	Oct 17, 2018
Licensed Content Publisher	Springer Nature
Licensed Content Publication	Phytochemistry Reviews
Licensed Content Title	The potential of mass spectrometry imaging in plant metabolomics: a review
Licensed Content Author	Heino M. Heyman, Ian A. Dubery
Licensed Content Date	Jan 1, 2015
Licensed Content Volume	15
Licensed Content Issue	2
Type of Use	Thesis/Dissertation
Requestor type	academic/university or research institute
Format	print and electronic
Portion	figures/tables/illustrations
Number of figures/tables/illustrations	1
Will you be translating?	no
Circulation/distribution	<501
Author of this Springer Nature content	no
Title	In Depth Systemic Biology Analysis of Central Nervous System Injuries
Institution name	Inserm U1192-Universite de Lille
Expected presentation date	Oct 2018
Portions	Figure 2
Requestor Location	INSERM U1192, Universite de Lille Cit� Scientifique, B�t SN3, 1er �tage Villeneuve D'Ascq, 59650 France Attn: Khalil Mallah

Billing Type Invoice
Billing Address INSERM U1192, Universite de Lille
Cité Scientifique, Bât SN3, 1er étage

Villeneuve D'Ascq, France 59650
Attn: Khalil Mallah
Total 0.00 EUR

Terms and Conditions

Springer Nature Terms and Conditions for RightsLink Permissions
Springer Nature Customer Service Centre GmbH (the Licensor) hereby grants you a non-exclusive, world-wide licence to reproduce the material and for the purpose and requirements specified in the attached copy of your order form, and for no other use, subject to the conditions below:

1. The Licensor warrants that it has, to the best of its knowledge, the rights to license reuse of this material. However, you should ensure that the material you are requesting is original to the Licensor and does not carry the copyright of another entity (as credited in the published version).

If the credit line on any part of the material you have requested indicates that it was reprinted or adapted with permission from another source, then you should also seek permission from that source to reuse the material.

2. Where **print only** permission has been granted for a fee, separate permission must be obtained for any additional electronic re-use.
3. Permission granted **free of charge** for material in print is also usually granted for any electronic version of that work, provided that the material is incidental to your work as a whole and that the electronic version is essentially equivalent to, or substitutes for, the print version.
4. A licence for 'post on a website' is valid for 12 months from the licence date. This licence does not cover use of full text articles on websites.
5. Where '**reuse in a dissertation/thesis**' has been selected the following terms apply: Print rights of the final author's accepted manuscript (for clarity, NOT the published version) for up to 100 copies, electronic rights for use only on a personal website or institutional repository as defined by the Sherpa guideline (www.sherpa.ac.uk/romeo/).
6. Permission granted for books and journals is granted for the lifetime of the first edition and does not apply to second and subsequent editions (except where the first edition permission was granted free of charge or for signatories to the STM Permissions Guidelines <http://www.stm-assoc.org/copyright-legal-affairs/permissions/permissions-guidelines/>), and does not apply for editions in other languages unless additional translation rights have been granted separately in the licence.
7. Rights for additional components such as custom editions and derivatives require additional permission and may be subject to an additional fee. Please apply to Journalpermissions@springernature.com/bookpermissions@springernature.com for these rights.

8. The Licensor's permission must be acknowledged next to the licensed material in print. In electronic form, this acknowledgement must be visible at the same time as the figures/tables/illustrations or abstract, and must be hyperlinked to the journal/book's homepage. Our required acknowledgement format is in the Appendix below.
9. Use of the material for incidental promotional use, minor editing privileges (this does not include cropping, adapting, omitting material or any other changes that affect the meaning, intention or moral rights of the author) and copies for the disabled are permitted under this licence.
10. Minor adaptations of single figures (changes of format, colour and style) do not require the Licensor's approval. However, the adaptation should be credited as shown in Appendix below.

Appendix — Acknowledgements:

For Journal Content:

Reprinted by permission from [**the Licensor**]: [**Journal Publisher** (e.g. Nature/Springer/Palgrave)] [**JOURNAL NAME**] [**REFERENCE CITATION**(Article name, Author(s) Name), [**COPYRIGHT**] (year of publication)

For Advance Online Publication papers:

Reprinted by permission from [**the Licensor**]: [**Journal Publisher** (e.g. Nature/Springer/Palgrave)] [**JOURNAL NAME**] [**REFERENCE CITATION**(Article name, Author(s) Name), [**COPYRIGHT**] (year of publication), advance online publication, day month year (doi: 10.1038/sj.[**JOURNAL ACRONYM**].)

For Adaptations/Translations:

Adapted/Translated by permission from [**the Licensor**]: [**Journal Publisher** (e.g. Nature/Springer/Palgrave)] [**JOURNAL NAME**] [**REFERENCE CITATION**(Article name, Author(s) Name), [**COPYRIGHT**] (year of publication)

Note: For any republication from the British Journal of Cancer, the following credit line style applies:

Reprinted/adapted/translated by permission from [**the Licensor**]: on behalf of Cancer Research UK: : [**Journal Publisher** (e.g. Nature/Springer/Palgrave)] [**JOURNAL NAME**] [**REFERENCE CITATION** (Article name, Author(s) Name), [**COPYRIGHT**] (year of publication)

For Advance Online Publication papers:

Reprinted by permission from The [**the Licensor**]: on behalf of Cancer Research UK: [**Journal Publisher** (e.g. Nature/Springer/Palgrave)] [**JOURNAL NAME**] [**REFERENCE CITATION** (Article name, Author(s) Name), [**COPYRIGHT**] (year of publication), advance online publication, day month year (doi: 10.1038/sj.[**JOURNAL ACRONYM**])

For Book content:

Reprinted/adapted by permission from [**the Licensor**]: [**Book Publisher** (e.g. Palgrave Macmillan, Springer etc) [**Book Title**] by [**Book author(s)**] [**COPYRIGHT**] (year of publication)

Other Conditions:

Version 1.1

Questions? customercare@copyright.com or +1-855-239-3415 (toll free in the US) or +1-978-646-2777.

**THE AMERICAN ASSOCIATION FOR THE ADVANCEMENT OF SCIENCE LICENSE
TERMS AND CONDITIONS**

Oct 17, 2018

This Agreement between INSERM U1192, Universite de Lille -- Khalil Mallah ("You") and The American Association for the Advancement of Science ("The American Association for the Advancement of Science") consists of your license details and the terms and conditions provided by The American Association for the Advancement of Science and Copyright Clearance Center.

License Number	4451400821936
License date	Oct 17, 2018
Licensed Content Publisher	The American Association for the Advancement of Science
Licensed Content Publication	Science
Licensed Content Title	Mass Spectrometry Sampling Under Ambient Conditions with Desorption Electrospray Ionization
Licensed Content Author	Zoltán Takáts,Justin M. Wiseman,Bogdan Gologan,R. Graham Cooks
Licensed Content Date	Oct 15, 2004
Licensed Content Volume	306
Licensed Content Issue	5695
Volume number	306
Issue number	5695
Type of Use	Thesis / Dissertation
Requestor type	Scientist/individual at a research institution
Format	Print and electronic
Portion	Figure
Number of figures/tables	1
Order reference number	
Title of your thesis / dissertation	In Depth Systemic Biology Analysis of Central Nervous System Injuries
Expected completion date	Oct 2018
Estimated size(pages)	300
Requestor Location	INSERM U1192, Universite de Lille Cité Scientifique, Bât SN3, 1er étage

Villeneuve D'Ascq, 59650
France
Attn: Khalil Mallah

Billing Type Invoice
Billing Address INSERM U1192, Universite de Lille
Cité Scientifique, Bât SN3, 1er étage

Villeneuve D'Ascq, France 59650
Attn: Khalil Mallah

Total 0.00 EUR

Terms and Conditions

American Association for the Advancement of Science TERMS AND CONDITIONS
Regarding your request, we are pleased to grant you non-exclusive, non-transferable permission, to republish the AAAS material identified above in your work identified above, subject to the terms and conditions herein. We must be contacted for permission for any uses other than those specifically identified in your request above.

The following credit line must be printed along with the AAAS material: "From [Full Reference Citation]. Reprinted with permission from AAAS."

All required credit lines and notices must be visible any time a user accesses any part of the AAAS material and must appear on any printed copies and authorized user might make.

This permission does not apply to figures / photos / artwork or any other content or materials included in your work that are credited to non-AAAS sources. If the requested material is sourced to or references non-AAAS sources, you must obtain authorization from that source as well before using that material. You agree to hold harmless and indemnify AAAS against any claims arising from your use of any content in your work that is credited to non-AAAS sources.

If the AAAS material covered by this permission was published in Science during the years 1974 - 1994, you must also obtain permission from the author, who may grant or withhold permission, and who may or may not charge a fee if permission is granted. See original article for author's address. This condition does not apply to news articles.

The AAAS material may not be modified or altered except that figures and tables may be modified with permission from the author. Author permission for any such changes must be secured prior to your use.

Whenever possible, we ask that electronic uses of the AAAS material permitted herein include a hyperlink to the original work on AAAS's website (hyperlink may be embedded in the reference citation).

AAAS material reproduced in your work identified herein must not account for more than 30% of the total contents of that work.

AAAS must publish the full paper prior to use of any text.

AAAS material must not imply any endorsement by the American Association for the Advancement of Science.

This permission is not valid for the use of the AAAS and/or Science logos.

AAAS makes no representations or warranties as to the accuracy of any information contained in the AAAS material covered by this permission, including any warranties of merchantability or fitness for a particular purpose.

If permission fees for this use are waived, please note that AAAS reserves the right to charge for reproduction of this material in the future.

Permission is not valid unless payment is received within sixty (60) days of the issuance of this permission. If payment is not received within this time period then all rights granted herein shall be revoked and this permission will be considered null and void.

In the event of breach of any of the terms and conditions herein or any of CCC's Billing and Payment terms and conditions, all rights granted herein shall be revoked and this permission will be considered null and void.

AAAS reserves the right to terminate this permission and all rights granted herein at its discretion, for any purpose, at any time. In the event that AAAS elects to terminate this permission, you will have no further right to publish, publicly perform, publicly display, distribute or otherwise use any matter in which the AAAS content had been included, and all fees paid hereunder shall be fully refunded to you. Notification of termination will be sent to the contact information as supplied by you during the request process and termination shall be immediate upon sending the notice. Neither AAAS nor CCC shall be liable for any costs, expenses, or damages you may incur as a result of the termination of this permission, beyond the refund noted above.

This Permission may not be amended except by written document signed by both parties. The terms above are applicable to all permissions granted for the use of AAAS material. Below you will find additional conditions that apply to your particular type of use.

FOR A THESIS OR DISSERTATION

If you are using figure(s)/table(s), permission is granted for use in print and electronic versions of your dissertation or thesis. A full text article may be used in print versions only of a dissertation or thesis.

Permission covers the distribution of your dissertation or thesis on demand by ProQuest / UMI, provided the AAAS material covered by this permission remains in situ.

If you are an Original Author on the AAAS article being reproduced, please refer to your License to Publish for rules on reproducing your paper in a dissertation or thesis.

FOR JOURNALS:

Permission covers both print and electronic versions of your journal article, however the AAAS material may not be used in any manner other than within the context of your article.

FOR BOOKS/TEXTBOOKS:

If this license is to reuse figures/tables, then permission is granted for non-exclusive world rights in all languages in both print and electronic formats (electronic formats are defined below).

If this license is to reuse a text excerpt or a full text article, then permission is granted for non-exclusive world rights in English only. You have the option of securing either print or electronic rights or both, but electronic rights are not automatically granted and do garner additional fees. Permission for translations of text excerpts or full text articles into other languages must be obtained separately.

Licenses granted for use of AAAS material in electronic format books/textbooks are valid only in cases where the electronic version is equivalent to or substitutes for the print version of the book/textbook. The AAAS material reproduced as permitted herein must remain in situ and must not be exploited separately (for example, if permission covers the use of a full text article, the article may not be offered for access or for purchase as a stand-alone unit), except in the case of permitted textbook companions as noted below.

You must include the following notice in any electronic versions, either adjacent to the reprinted AAAS material or in the terms and conditions for use of your electronic products: "Readers may view, browse, and/or download material for temporary copying purposes only, provided these uses are for noncommercial personal purposes. Except as provided by law, this material may not be further reproduced, distributed, transmitted, modified, adapted, performed, displayed, published, or sold in whole or in part, without prior written permission from the publisher."

If your book is an academic textbook, permission covers the following companions to your textbook, provided such companions are distributed only in conjunction with your textbook at no additional cost to the user:

- Password-protected website
- Instructor's image CD/DVD and/or PowerPoint resource
- Student CD/DVD

All companions must contain instructions to users that the AAAS material may be used for non-commercial, classroom purposes only. Any other uses require the prior written permission from AAAS.

If your license is for the use of AAAS Figures/Tables, then the electronic rights granted herein permit use of the Licensed Material in any Custom Databases that you distribute the electronic versions of your textbook through, so long as the Licensed Material remains within the context of a chapter of the title identified in your request and cannot be downloaded by a user as an independent image file.

Rights also extend to copies/files of your Work (as described above) that you are required to provide for use by the visually and/or print disabled in compliance with state and federal laws.

This permission only covers a single edition of your work as identified in your request.

FOR NEWSLETTERS:

Permission covers print and/or electronic versions, provided the AAAS material reproduced as permitted herein remains in situ and is not exploited separately (for example, if permission covers the use of a full text article, the article may not be offered for access or for purchase as a stand-alone unit)

FOR ANNUAL REPORTS:

Permission covers print and electronic versions provided the AAAS material reproduced as permitted herein remains in situ and is not exploited separately (for example, if permission covers the use of a full text article, the article may not be offered for access or for purchase as a stand-alone unit)

FOR PROMOTIONAL/MARKETING USES:

Permission covers the use of AAAS material in promotional or marketing pieces such as information packets, media kits, product slide kits, brochures, or flyers limited to a single print run. The AAAS Material may not be used in any manner which implies endorsement or promotion by the American Association for the Advancement of Science (AAAS) or Science of any product or service. AAAS does not permit the reproduction of its name, logo or text on promotional literature.

If permission to use a full text article is permitted, The Science article covered by this permission must not be altered in any way. No additional printing may be set onto an article copy other than the copyright credit line required above. Any alterations must be

approved in advance and in writing by AAAS. This includes, but is not limited to, the placement of sponsorship identifiers, trademarks, logos, rubber stamping or self-adhesive stickers onto the article copies.

Additionally, article copies must be a freestanding part of any information package (i.e. media kit) into which they are inserted. They may not be physically attached to anything, such as an advertising insert, or have anything attached to them, such as a sample product. Article copies must be easily removable from any kits or informational packages in which they are used. The only exception is that article copies may be inserted into three-ring binders.

FOR CORPORATE INTERNAL USE:

The AAAS material covered by this permission may not be altered in any way. No additional printing may be set onto an article copy other than the required credit line. Any alterations must be approved in advance and in writing by AAAS. This includes, but is not limited to the placement of sponsorship identifiers, trademarks, logos, rubber stamping or self-adhesive stickers onto article copies.

If you are making article copies, copies are restricted to the number indicated in your request and must be distributed only to internal employees for internal use.

If you are using AAAS Material in Presentation Slides, the required credit line must be visible on the slide where the AAAS material will be reprinted

If you are using AAAS Material on a CD, DVD, Flash Drive, or the World Wide Web, you must include the following notice in any electronic versions, either adjacent to the reprinted AAAS material or in the terms and conditions for use of your electronic products: "Readers may view, browse, and/or download material for temporary copying purposes only, provided these uses are for noncommercial personal purposes. Except as provided by law, this material may not be further reproduced, distributed, transmitted, modified, adapted, performed, displayed, published, or sold in whole or in part, without prior written permission from the publisher." Access to any such CD, DVD, Flash Drive or Web page must be restricted to your organization's employees only.

FOR CME COURSE and SCIENTIFIC SOCIETY MEETINGS:

Permission is restricted to the particular Course, Seminar, Conference, or Meeting indicated in your request. If this license covers a text excerpt or a Full Text Article, access to the reprinted AAAS material must be restricted to attendees of your event only (if you have been granted electronic rights for use of a full text article on your website, your website must be password protected, or access restricted so that only attendees can access the content on your site).

If you are using AAAS Material on a CD, DVD, Flash Drive, or the World Wide Web, you must include the following notice in any electronic versions, either adjacent to the reprinted AAAS material or in the terms and conditions for use of your electronic products: "Readers may view, browse, and/or download material for temporary copying purposes only, provided these uses are for noncommercial personal purposes. Except as provided by law, this material may not be further reproduced, distributed, transmitted, modified, adapted, performed, displayed, published, or sold in whole or in part, without prior written permission from the publisher."

FOR POLICY REPORTS:

These rights are granted only to non-profit organizations and/or government agencies. Permission covers print and electronic versions of a report, provided the required credit

line appears in both versions and provided the AAAS material reproduced as permitted herein remains in situ and is not exploited separately.

FOR CLASSROOM PHOTOCOPIES:

Permission covers distribution in print copy format only. Article copies must be freestanding and not part of a course pack. They may not be physically attached to anything or have anything attached to them.

FOR COURSEPACKS OR COURSE WEBSITES:

These rights cover use of the AAAS material in one class at one institution. Permission is valid only for a single semester after which the AAAS material must be removed from the Electronic Course website, unless new permission is obtained for an additional semester. If the material is to be distributed online, access must be restricted to students and instructors enrolled in that particular course by some means of password or access control.

FOR WEBSITES:

You must include the following notice in any electronic versions, either adjacent to the reprinted AAAS material or in the terms and conditions for use of your electronic products: "Readers may view, browse, and/or download material for temporary copying purposes only, provided these uses are for noncommercial personal purposes. Except as provided by law, this material may not be further reproduced, distributed, transmitted, modified, adapted, performed, displayed, published, or sold in whole or in part, without prior written permission from the publisher."

Permissions for the use of Full Text articles on third party websites are granted on a case by case basis and only in cases where access to the AAAS Material is restricted by some means of password or access control. Alternately, an E-Print may be purchased through our reprints department (brocheleau@rockwaterinc.com).

REGARDING FULL TEXT ARTICLE USE ON THE WORLD WIDE WEB IF YOU ARE AN 'ORIGINAL AUTHOR' OF A SCIENCE PAPER

If you chose "Original Author" as the Requestor Type, you are warranting that you are one of authors listed on the License Agreement as a "Licensed content author" or that you are acting on that author's behalf to use the Licensed content in a new work that one of the authors listed on the License Agreement as a "Licensed content author" has written.

Original Authors may post the 'Accepted Version' of their full text article on their personal or on their University website and not on any other website. The 'Accepted Version' is the version of the paper accepted for publication by AAAS including changes resulting from peer review but prior to AAAS's copy editing and production (in other words not the AAAS published version).

FOR MOVIES / FILM / TELEVISION:

Permission is granted to use, record, film, photograph, and/or tape the AAAS material in connection with your program/film and in any medium your program/film may be shown or heard, including but not limited to broadcast and cable television, radio, print, world wide web, and videocassette.

The required credit line should run in the program/film's end credits.

FOR MUSEUM EXHIBITIONS:

Permission is granted to use the AAAS material as part of a single exhibition for the duration of that exhibit. Permission for use of the material in promotional materials for the exhibit must be cleared separately with AAAS (please contact us at permissions@aaas.org).

FOR TRANSLATIONS:

Translation rights apply only to the language identified in your request summary above. The following disclaimer must appear with your translation, on the first page of the article, after the credit line: "This translation is not an official translation by AAAS staff, nor is it endorsed by AAAS as accurate. In crucial matters, please refer to the official English-language version originally published by AAAS."

FOR USE ON A COVER:

Permission is granted to use the AAAS material on the cover of a journal issue, newsletter issue, book, textbook, or annual report in print and electronic formats provided the AAAS material reproduced as permitted herein remains in situ and is not exploited separately. By using the AAAS Material identified in your request, you agree to abide by all the terms and conditions herein.

Questions about these terms can be directed to the AAAS Permissions department permissions@aaas.org.

Other Terms and Conditions:

v 2

Questions? customercare@copyright.com or +1-855-239-3415 (toll free in the US) or +1-978-646-2777.

